Textron Aviation
Raytheon Missile Systems
AIAA Foundation

The 2017 AIAA/Textron Aviation/Raytheon Missile Systems Design/Build/Fly Competition Flyoff was held at TIMPA Field in Tucson, AZ on the weekend of April 20-23, 2017. This was the 21st year for the competition. A total of 138 entries were received with a new requirement this year to submit a proposal with the entry. The 138 proposals were judged and 104 teams were invited to submit a formal report for the next phase of the competition. 95 teams submitted design reports to be judged, and 73 teams attended the flyoff (14 international). About 750 students, faculty, and guests were present. The weather was hot but allowed for non-stop flying. Of the record 310 official flight attempts, 153 resulted in a successful score with 52 teams achieving a successful flight score and 34 teams successfully completing all three missions. The quality of the teams, their readiness to compete, and the execution of the flights continues to improve each year.

The contest theme this year was a Tube Launched UAV. The UAV had to fit inside a launch tube and be removed with all flight surfaces and features moved to the locked, flight condition in less than 5 minutes. The first mission was a Demonstration Flight with no payload for three laps. Prior to attempting the second mission, each team was required to successfully complete the first mission and a ground mission. The ground mission consisted of three drops from 12 inches with the UAV stored inside the launch tube. The tube and airplane must survive the drops without damage and the UAV must be capable of flight. The second mission was a Speed Flight with a payload consisting of 3 regulation hockey pucks with the time to fly three laps as the score. The third mission was a Range Flight where each team determined the number of hockey pucks to carry as payload with the score being the product of the number of pucks carried times the number of laps flown in 5 minutes. As usual, the total score is the product of the total flight score and design report score. More details on the mission requirements can be found at the competition website: http://www.aiaadbf.org .

First Place went to the University of Southern California, Second Place went to Georgia Institute of Technology and Third Place went to the University of Ljubljana. A full listing of the results is included below. The Best Paper Award, sponsored by the Design Engineering TC for the highest report score, went to Veermata Jijabai Technological Institute with a score of 96.03.

We owe our thanks for the success of the DBF competition to the efforts of many volunteers from Textron Aviation, Raytheon Missile Systems, and the AIAA sponsoring technical committees: Applied Aerodynamics, Aircraft Design, Flight Test, and Design Engineering. These volunteers collectively set the rules for the contest, publicize the event, gather entries, judge the written reports, and organize the flyoff. Thanks also go to the Premier Sponsors: Raytheon Missile Systems and Textron Aviation, and also to the AIAA Foundation for their financial support as well as our Gold sponsors this year - Aurora Flight Sciences, Esteco, General Atomics, Lockheed Martin, Northrop Grumman and SpaceX. Special thanks go to Raytheon Missile Systems for hosting the flyoff this year.

Finally, this event would not be nearly as successful without the hard work and enthusiasm from all the students and advisors. If it weren't for you, we wouldn't keep doing it.

Russ Althof
For the DBF Organizing Committee

VEERMATA JIJABAI TECHNOLOGICAL INSTITUTE

TEAM VAYUPUTRAS

AIAA Design/Build/Fly 2016-17 Design Report

TABLE OF CONTENTS:

ACRONYMS, ABBREVIATIONS AND SYMBOLS:

α - Angle of Attack

α_{clmax} - Stall angle of attack

AR - Aspect Ratio

AUW - All Up Weight

AVL - Athena Vortex Lattice

b - Span

C.G. - Centre of Gravity

C_D - Aircraft Drag Coefficient

C_d - Airfoil Section Drag Coefficient

C_{DO} - Parasite Drag Coefficient

C_L - Aircraft Lift Coefficient

C_l - Airfoil Section Lift Coefficient

c_{lmax} - 2-Dimensional Maximum Lift Coefficient

C_{Lmax} - Wing Maximum Lift Coefficient

C_m - Co-efficient of pitching moment

C_P - Co-efficient of power

D - Diameter of propeller

DBF - Design/ Build/ Fly

ESC - Electronic Speed Controller

EW - Empty Weight

FOM - Figure of Merit

FOS - Factor of Safety

ID - Inner Diameter of Tube

Kv - Motor speed constant

LiPo - Lithium Polymer

M1 - Mission One

M2 - Mission Two

M3 - Mission Three

M.A.C. - Mean Aerodynamic Chord

N - RPM of motor

N.P. - Neutral Point

NiCd - Nickel Cadmium

NiMH - Nickel-Metal Hydride

OD - Outer Diameter of Tube

RAC - Rated Aircraft Cost

Re - Reynolds Number

r_x - Turn radius

S - Planform Area

S.M. - Static Margin

S_{wet} - Wetted Surface Area

TFS - Total Flight Score

T/W - Thrust-to-weight ratio

TMS - Total Mission Score

V_{cruise} - Cruise Velocity

V_{wind} - Wind Speed

β - Sideslip angle

ρ - Density of air

1. EXECUTIVE SUMMARY:

This report documents the design process and progress made towards the AIAA D/B/F Competition 2017 by Team Vayuputras of VJTI, India. This year's theme was a 'Tube-launched UAV'. It required us to design and manufacture a UAV that can be stowed inside a cylindrical tube of given specifications using captive, self-locking mechanisms. The UAV must complete three hand-launched missions that test speed, range, endurance and payload capacity and maximize the total score in the process. The tube acts as the storage container for the aircraft. In addition, the tube has to sustain three drops to clear the ground mission, while carrying the aircraft with maximum payload.

1.1 DESIGN SUMMARY:

The design phase began with the identification of key mission requirements and constraints. Through score analysis, the team determined the most influential parameters on the Total Flight Score and concluded that a winning aircraft concept would be one built with the lightest possible empty weight and that fits into a tube of the smallest possible diameter and length. Several solution concepts were then compared using Figures of Merit to yield an aircraft with a folding and rotating wing, an extendable tail boom, and a folding horizontal tail. Feasible mechanisms were built for each of these and tested on the prototypes. A battery pack was sized to provide enough power and energy for all missions while minimizing weight. Aerodynamics, propulsion and stability analyses ran in an iterative loop to optimize and improve the design at each stage. Built-up balsa techniques were used for the fabrication of the structural components. A stringer and former assembly covered with Monokote constituted a light tube that was capable of withstanding the three drops in the ground mission. Flight testing followed the manufacturing of each prototype. It was used to gather valuable data on mission performance as well as feedback from the pilot regarding flying and handling qualities.

1.2 MISSION REQUIREMENTS AND DESIGN PARAMETERS:

The translation of key mission requirements into design parameters and features is summarised below:

1.2.1 Empty Weight:

The empty weight of the aircraft and the tube has a significant influence on the total score. The aircraft and tube were designed to be as light as possible without compromising the ability to complete all flight missions and the ground mission respectively.

The propulsion package optimisation and testing resulted in the selection of a T-Motor MT2216 spinning an APC 11×8F propeller, powered by 12 Elite 1500 mAh 2/3 AA batteries. This selection ensures a low propulsion weight contribution in the empty weight. Judicious use of material and an efficient built-up structure was a key feature in weight reduction.

1.2.2 Tube Diameter:

The aircraft is required to be stored in a cylindrical tube. The tube diameter is the most important factor in the RAC, featuring in the form of the circumference ($\pi \times D$). Any increase in the diameter would also warrant an increase in tube length, which has to be at least 4 times the diameter. The team realised that rotation of the wing to align it with the fuselage was a pre-requisite in reducing the diameter, and thus the final inner

diameter would be decided by the following factors: the wing chord, the span of the horizontal and vertical stabilizer, landing gear height and the propeller diameter.

Accordingly, a folding propeller (11×8F) was used for all missions and a mechanism was built for folding the horizontal tail when storing the aircraft in the tube. Use of a compressible wire skid at the rear helped absorb impact energy and protect the HT sub-assembly.

1.2.3 Payload Requirement:

Two of the three missions require the aircraft to carry a payload. Mission 2 (M2) requires a payload of three ice hockey pucks to be carried internally and the number of pucks for M3 will be a team-specified quantity. Flapped windows on either side of the fuselage provided easy access for loading/unloading the internal payload.

1.2.4 Hand Launch Requirement:

Aerodynamic performance requirements, including stall velocity, were adjusted since a ground take-off run is not permitted this year. The light, compact design required by other constraints helped the team achieve successful, consistent hand launches with the selected profile and wing size.

1.3 SYSTEM PERFORMANCE AND CAPABILITIES:

The final solution concept was a conventional high-wing configuration with a single motor tractor, equipped with mechanisms for wing rotation, folding of wing and horizontal tail and extension of the tail boom. The performance capabilities of the aircraft have been listed below:

1) Successful hand launches with an all-up weight of 1.2 kg for M2 and 1.37 kg for M3.
2) Launch speed of up to 10 m/s.
3) Maximum airspeed of 20-23 m/s for all 3 missions.
4) Able to fit in a tube with outer diameter of 0.16 m and a length of 0.72 m.
5) Flight time of 130s in M2.
6) Capable of carrying 4 pucks and flying 6 laps of the course in M3.
7) Estimated RAC of 90 lb-in and a Total Mission Score of 6.88.

Figure 1.3: Aircraft in flight

2. MANAGEMENT SUMMARY:

2.1 TEAM ORGANIZATION:

Team Vayuputras consists of seven undergraduate student members, organised into four sub-teams: Aerodynamics and Stability, Propulsion and Flight Performance, Structures and Manufacturing, Mechanisms and Testing. The hierarchy shown below (Figure 2.1) only serves as an outline, as all team members collaborated extensively to learn the interrelation between various disciplines and obtain solutions through a wealth of fresh ideas. The entire team participated in the manufacturing, testing operations and the documentation of the design. Good co-ordination and communication ensured that no formal team leader was required for overall management. The team reported its progress to the Faculty Advisor through weekly meetings.
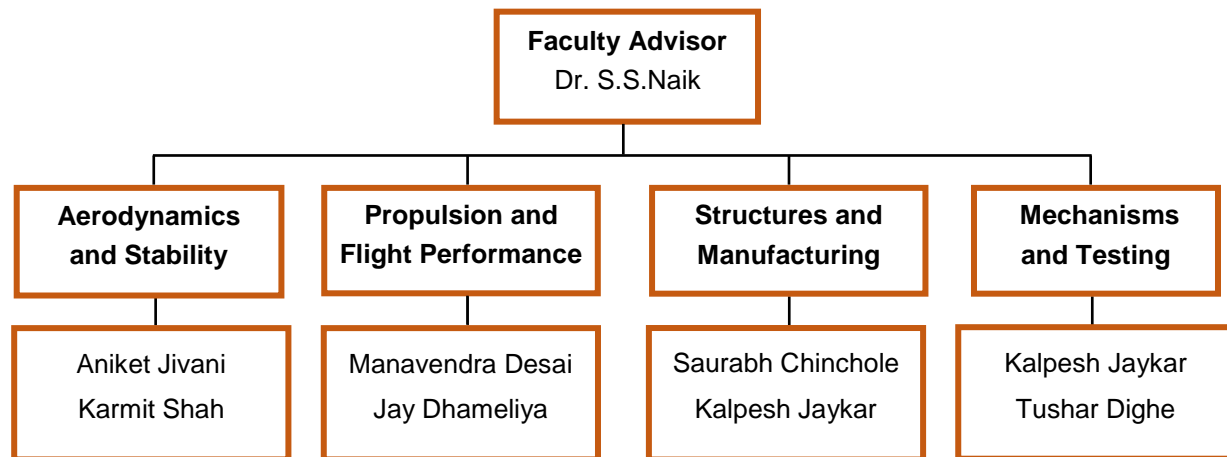
Figure 2.1: Team organization chart

2.1.1 Aerodynamics and Stability:

The sub-team computed the flight characteristics and designed the lifting surfaces. This team was also responsible for empennage and control surface design to achieve certain control and stability standards. The software used for computing aerodynamic characteristics were XFLR5 [1], based on the XFoil code developed by M.Drela and H.Youngren and AVL [2], a Vortex Lattice Method (VLM) solver.

2.1.2 Propulsion and Flight Performance:

The sub-team analyzed and tested the propulsion system to find the best motor, propeller, and battery combination for the aircraft. It also prepared the mission model to predict performance parameters of the aircraft for each mission, using MATLAB [3].

2.1.3 Structures and Manufacturing:

The sub-team was responsible for the structural design and fabrication of the various aircraft components and the tube. It experimented with new manufacturing methods in order to decrease the overall weight while maintaining structural integrity.

2.1.4 Mechanisms and Testing:

This sub-team worked in close coordination with structures and is tasked with the development and testing of various mechanisms required to stow the aircraft in the tube.

2.2 MILESTONE CHART:

The team prepared a design timeline stretching from the date of publication of the problem statement till the date of the fly-off. Certain deadlines were set to ensure that an appropriate amount of time is allotted for each task. In the milestone chart given below, the team's expected and actual progress has been depicted. Important dates have been marked as well.
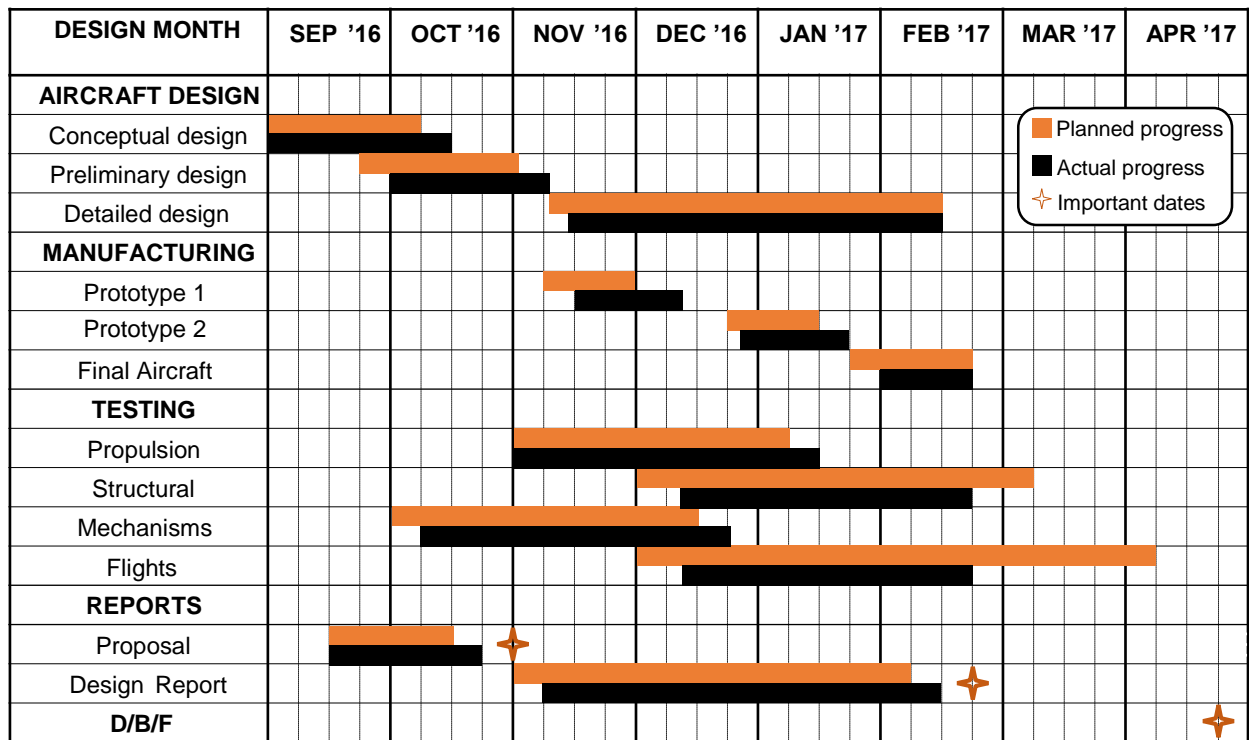
DESIGN MONTH	SEP '16	OCT '16	NOV '16	DEC '16	JAN '17	FEB '17	MAR '17	APR '17
AIRCRAFT DESIGN								
Conceptual design								
Preliminary design								
Detailed design								
MANUFACTURING								
Prototype 1								
Prototype 2								
Final Aircraft								
TESTING								
Propulsion								
Structural								
Mechanisms								
Flights								
REPORTS								
Proposal								
Design Report								
D/B/F								

Legend: Planned progress · Actual progress · ☆ Important dates

Figure 2.2: Milestone chart showing planned and actual execution of objectives

3. CONCEPTUAL DESIGN:

3.1 MISSION REQUIREMENTS AND SCORING SUMMARY:

The AIAA 2016-17 Design/Build/Fly consists of three flight missions, one ground mission and a design report. Of these, the flight missions and the report contribute to the score. The total score is given by the following equation:

$$\text{Total Flight Score} = \frac{\text{Design Report Score x Total Mission Score}}{\text{Rated Aircraft Cost (RAC)}} \qquad (3.1)$$

where Total Mission Score (TMS) is the sum of the scores of flying missions 1, 2 and 3.

$$\text{TMS = M1 + M2 + M3} \qquad (3.2)$$

Rated Aircraft Cost (RAC) is calculated using empty weight (EW), tube weight (TW) as well as the length (L) and circumference (C) of the tube as seen in equation (3.3):

$$\text{RAC = (EW + TW) x (L + C)} \qquad (3.3)$$

All flight missions are flown along the same distance and pattern per lap. For the flight missions, the individual portions of the flight pattern seen in Figure 3.1 are as follows:

1. Successful hand launch from the starting line
2. Climb to Safe Altitude, 500 ft. Upwind
3. 180º U-turn
4. 1000 ft. Downwind
5. 360º Turn Along the Backstretch
6. 180º U-turn
7. Final 500 ft. upwind
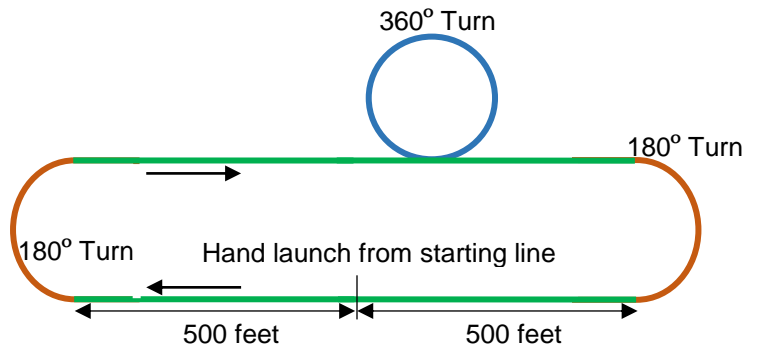8. Successful landing (after final lap)

Figure 3.1: Competition Flight Path

Accounting for the three turns, each lap is approximately 750 m long. In order to achieve a successful mission score, the aircraft must leave the launcher's hand, cross the start/finish line, fly the required number of laps in the defined pattern and complete a successful landing.

3.1.1 Mission 1 (Demonstration Flight):

The aircraft must complete three laps of the course within a five-minute flight window, without carrying any payload. The time starts when the aircraft leaves the launcher's hand, and the aircraft must cross the start/finish line in the air for a complete lap.

Scoring: $$M1=1.0 \tag{3.4}$$

3.1.2 Mission 2 (Speed Flight):

For the speed flight, the aircraft has to fly three laps carrying three regulation ice hockey pucks internally as the payload. This is a timed mission, and the timer stops when the aircraft crosses the start/finish line in the air at the end of the third lap. The scoring is relative, and is normalised by the fastest time to complete three laps by any team (equation 3.5). The mission must be completed within a five-minute window.

Scoring: $$M2 = 2 \times \left(\frac{\text{Flight Time}_{minimum}}{\text{Flight Time}} \right) \tag{3.5}$$

3.1.3 Mission 3 (Range Flight):

The aircraft must fly laps of the course while carrying a team-selected quantity of ice hockey pucks stored internally, within five minutes. The product of the number of complete laps flown times the number of ice hockey pucks carried is normalised by the maximum product of these quantities obtained by any team to yield the score, as seen in equation 3.6.

Scoring: $$M3 = 4 \times \left(\frac{N\_(\text{Laps x Pucks})}{N\_(\text{Laps x Pucks})_{maximum}} \right) + 2 \tag{3.6}$$

For mission 2 and 3, the UAV will be brought to the staging box inside its launch tube with their respective payloads already installed. Both payload missions have a greater weightage than M1.

3.1.4 Ground Mission:

The UAV has to be sealed inside the launch tube with maximum payload, followed by a series of drops onto a hard surface. One drop will be conducted with the long axis of the tube parallel to the landing surface in any orientation about the long axis, while the other two drops are on each end of the tube (long axis perpendicular). The UAV then must come out as a single assembly and be transitioned to the flight condition by movement or rotation of its surfaces. The tube or UAV should not sustain major damage as a result of the drops. All flight controls and subsystems, including propulsion, must be functional upon removal from the tube.

This is not a scoring mission, and must be successfully attempted either before or after flight mission 1.

3.1.5 Design Constraints:

The competition rules specify constraints on the aircraft storage, its propulsion system and the payload:

Storage: The aircraft must completely fit inside a right-circular cylindrical launch tube of constant cross-section. The length-to-diameter ratio of the tube is a minimum of four. All aircraft features must move or rotate to the "flight-ready" condition upon removal from the tube by use of captive, self-locking mechanisms. Features may be moved manually. The aircraft should be removed from the ends of the tube only. The tube should not have cut-outs or holes to access the aircraft.

Propulsion system: The rules require the use of NiMH or NiCd batteries which have lower power density compared to widely used LiPo batteries. There is no restriction on battery weight this year, or the number of cells and capacity. All components of the propulsion system must be commercially available. An arming system must be mounted on the outside of the aircraft.

Payload: The ice hockey puck payload for missions 2 and 3 must be stored within the aircraft. The dimensions of the same govern the fuselage shape and dimensions.

3.2 SENSITIVITY ANALYSIS:

A score sensitivity analysis was performed in MATLAB [3] to ascertain which parameter/s influenced the total score the most. The analysis examines an ideal situation where other parameters remain constant while one of them is varied or perturbed to observe the corresponding change on the score. The total score is computed using equations 3.1 to 3.6.

The input parameters to be varied independently are the tube diameter, the tube length, the number of laps flown and the number of pucks carried in M3. Tube length was taken to be four times its diameter for the analysis. The tube dimensions and weight were considered to be unaffected by the cell count and laps completed in M3 since they will not significantly change its volume. Past experience proved to be helpful in setting a reference value for the structural weight of the plane.

The graph plotted below (Figure 3.2) depicts percentage change in Total Flight Score against percentage change in each input parameter. A set of baseline values (indicated by 0% Change in Input Parameter and 0% Change in TFS on the graph) was used. The figure shows this analysis for a baseline of 3 pucks, 6 laps, 10 cells and an outer diameter of 0.16 m. M1 is assumed to be successful in the sensitivity (score=1.0) and the constant value of the score means it is not relevant to the score analysis like M2 and M3.
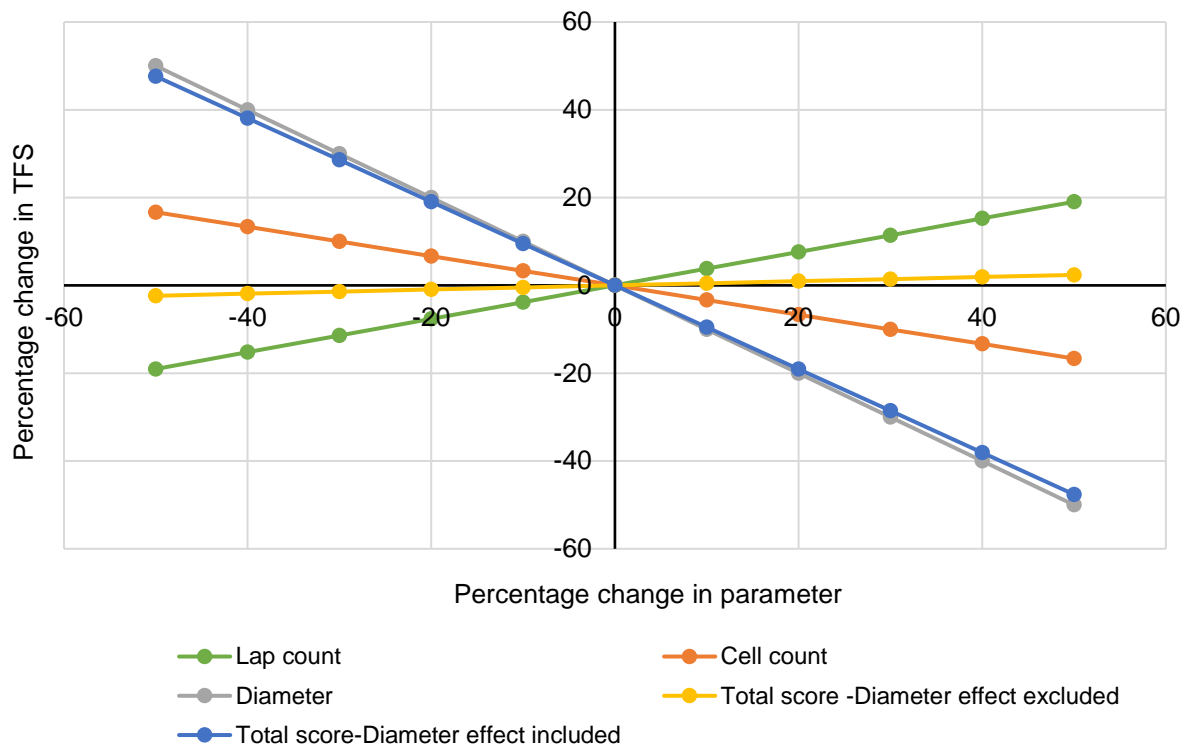
Figure 3.2: Score Sensitivity

The scoring in missions two and three also depends on the performance of other teams. This required us to assume values for their flight time, lap count and number of pucks. It was assumed that $N\_$ (Laps x Pucks)$_{maximum}$= 36 (6 laps and 6 pucks) and that our M2 flight time will be one and a half times more than the smallest recorded M2 time.

From the above graph, it is clear that the trend of change in total score follows that of the tube diameter very closely. Hence, the tube diameter is by far the most significant variable in the entire scoring equation.

Score analysis conclusions:

1) The team concluded that a minimum value of RAC would contribute to a better score rather than a significantly higher number of laps flown or pucks carried for M3. Therefore, the team chose to optimize M2 first and select the lightest propulsion system for carrying three pucks and completing three laps. Later, the number of laps and pucks would be increased for M3, with the aim of increasing total score. Another optimization cycle would follow for M3.

2) RAC itself is affected most by the tube dimensions and weight. Therefore, the team decided to pursue the following objective: the overall aircraft structure and stowing mechanisms introduced must result in a tube of the least diameter possible.

Thus, the score sensitivity helped narrow down a wide design space and enabled selection of a baseline configuration. This would be followed by further refinements, calculations and analysis.

3.3 TRANSLATION OF MISSION REQUIREMENTS INTO DESIGN REQUIREMENTS:

The competition rules and the scoring equation were translated into qualitative design metrics that could be used to evaluate and select the conceptual aircraft configuration.

Empty weight: Lighter aircraft would be more competitive as it would lead to a decrease in RAC. This requires an efficient structure and appropriate material selection.

Hand launch: Hand launch of the fully-loaded aircraft requires sufficient static thrust during launch, and a low stall speed, coupled with an ergonomic design that permits good hand grip and propeller clearance for the thrower.

Ground Mission: The tube had to be sized and designed around the aircraft. Apart from being strong enough to withstand three drops in different orientations, it had to be as compact as possible since the score is dramatically sensitive to the tube diameter. This conclusion inspired many of the proposed configurations and motivated the decisions taken regarding the concept aircraft and its various mechanisms. The tube dimensions and material were finalized thereafter.

Payload: The fuselage had to be built around the payload, and the internal bays had to be easily accessible for loading/ unloading the pucks for missions 2 and 3.

Flight Speed: The aircraft must have a high cruise speed to fly three laps in the minimum possible time in M2. A propulsion system designed to produce high propulsive power for high airspeeds had to be selected.

3.4 COMPONENT WEIGHTING AND SELECTION PROCESS:

Figures of Merit (FOM) were created based on the most important configuration factors that were determined from sensitivity analysis and the qualitative translation of mission requirements into key design requirements. The general FOMs considered for important configurations are given below. These were given different weightage based on their importance for a particular configuration to be selected. The scoring is done as follows: -1 is detrimental, 0 is neutral, and 1 is positive. The assigned values were multiplied by their respective weightage and the total score was calculated. The configuration yielding the highest total score is the design chosen for the aircraft. The common FOMs considered were:

Drag: Minimizing the wetted area results in less drag, and therefore a higher top speed when trying to minimize flight time in M2 and fly more laps in M3.

Empty Weight: Empty weight is an important parameter in RAC, as explained previously. A lighter aircraft would give a better score so it was taken under consideration.

Effect on tube dimensions: Each configuration was evaluated along with mechanisms necessary to fit it into a tube. The one which can be fitted in a tube of minimum diameter is the preferred configuration. This is the most important FOM.

Manufacturability and Reparability: This is an important consideration of the skills, materials, and time needed to assemble and repair the aircraft. The final configuration must be quickly and easily reproducible with suitable modifications after testing of prototype models.

Ease of Hand Launch: It is a common FOM since the aircraft must be safely and successfully launched for all missions.

3.4.1 Aircraft Configuration:

The team examined 3 basic configurations: conventional, biplane and flying wing for the aircraft**.**

FOM	Weightage	Conventional	Biplane	Flying Wing
Drag	15	0	-1	1
Empty Weight	20	0	-1	1
Stability	15	1	1	-1
Effect on tube dimensions	30	1	0	1
Manufacturability	20	1	0	0
Total	**100**	**65**	**-20**	**50**

Table 3.4.1: Aircraft Configuration Figure of Merit Table

The biplane configuration offers less span requirement for generating lift in the same wing area. But it had the highest drag and structural weight compared to the other two configurations. Also, mounting and rotating mechanisms would be difficult to install and access for this configuration. A flying wing offers a lightweight design and less wetted area than other configurations, so drag is greatly reduced. The payload is compact, and the aircraft could also be stowed in a small tube with appropriate mechanisms. However, the conventional configuration offers an advantage, not just in terms of stability but also manufacturability and reparability, which is an important parameter. Hence, a conventional configuration was chosen for the aircraft with two mechanisms, for rotation of the wing about a centre pivot to align it along the length of the tube, and outboard folding wing sections to reduce the minimum tube length required.

3.4.2 Wing Placement:

The different placement options considered for the wing position were: the high, mid and low winger. The mid-wing configuration makes the aircraft too heavy since the wing root would require reinforcement at the intersection of the fuselage. Also, the wing would be made in two parts and wing rotation to align it along the length of the tube would no longer be feasible or easy. Hence it was eliminated. High winger has the least weight and was preferred over the low winger due to its inherent roll stability and ease in mounting and rotation.

3.4.3 Propulsion Configuration:

For selection of the propulsion system, apart from the previously explained FOMs, benefit of propwash was also considered

Benefit of Propwash: The flow, downstream of the propeller plane, can offer significant aerodynamic advantages. It can raise the local lift coefficients and hence improve the aerodynamic efficiency [4].

Moreover, it can ensure an attached flow over the wings and hence lower the stall speed. Since it significantly affects the aircraft performance, it is considered as an additional figure of merit.
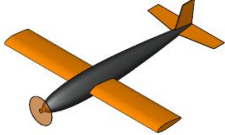
FOM	Weightage	Single Tractor	Double Tractor	Single Pusher
Total weight	20	1	0	1
Ease of hand launch	15	0	1	-1
Installed drag	10	0	-1	1
Benefit of AS	20	0	1	-1
Effect on tube dimensions	35	1	0	1
Total	**100**	**55**	**25**	**20**

Table 3.4.3: Propulsion Configuration Figure of Merit Table

The selection of the propulsion system configuration determines how efficiently the stored energy on-board an aircraft can be used. The single pusher configuration has less efficiency compared to the tractor configuration. Also, when the aircraft is hand launched, a pusher propeller is likely to strike the hand of the thrower without provision of specific safeguards.

For a single tractor configuration, keeping the tube diameter to a minimum required one of the following: using a propeller of considerably smaller diameter, designing a mechanism to rotate the motor mount, or use of a folding propeller. For the dual tractor, the propeller blades could be aligned along the length of the wing, eliminating the problem altogether.

Further studies showed a slight increase in tube diameter for the double tractor system, considering the entire assembly of the propeller, adapter and spinner cap. The team believed that the need to reduce the diameter and enhance the score greatly justified the use of a single tractor, with either a low diameter or a folding propeller used to avoid the complexity of adding another mechanism. It also offers less weight penalty as compared to the dual tractor system.

3.4.4 Fuselage Configuration:

As already seen, the scores are most sensitive to the tube dimensions. Hence, stowing the fuselage and boom assembly allows a major reduction in the tube length. The pod and stick configuration best suited this requirement by permitting retraction and extension of the boom.

FOM	Weightage	Conventional	Pod and Stick
Ease of stowing	10	-1	1
Weight	8	0	0
Manufacturability	7	1	0
Reparability	6	0	1
Experience	4	1	1
Drag	3	0	0
Total	**38**	**1**	**20**

Table 3.4.4: Fuselage Configuration Figure of Merit Table

3.4.5 Tail Configuration:

The following empennage configurations were analyzed for the aircraft: conventional, V-tail, T-tail, and box tail. The most crucial design factor for the empennage was the span of the horizontal and vertical stabilizers. The tails need to provide good stability characteristics while meeting geometric constraints of the tube. The conventional tail configuration has superior stability characteristics, offers large control surfaces and does not pose significant manufacturability or weight concerns.

However, it would have to be folded like the wing sections to fit within a particular diameter. The same would be true for a T-tail and V-tail configuration. Rather than adding another mechanism, the tails could be split up into multiple smaller surfaces that form a box tail empennage. The team believed that the objective of reduction in tube dimensions was achieved by using a box tail, but the size of the surfaces required for the box to be as effective as a conventional tail negated this benefit. Therefore, a conventional configuration was chosen, to be constructed with the appropriate folding mechanism. Care had to be taken so that the surface remained rigid and was not subjected to flutter when locked in the flight condition.

FOM	Weightage	Conventional	T-tail	V-tail	Box Tail
Stability and control	30	1	1	-1	0
Weight	15	1	-1	0	0
Drag	10	0	0	1	0
Manufacturability	10	1	0	-1	0
Effect on tube dimensions	35	0	0	-1	1
Total	**100**	**55**	**15**	**-65**	**35**

Table 3.4.5: Tail Configuration Figure of Merit Table

3.4.6 Landing Gear Configuration:

As shown below, two basic landing gear configurations were shortlisted. The tail skid configuration consists of a compressible wire bent to shape and attached below the HT. There is no main landing gear, and the fuselage base is designed to bear the brunt of the landing. Keeping the importance of the hand launch in a good take-off, use of only a tail skid was more ergonomic. Also, a tail dragger configuration (main gear and auxiliary gear with wheels), is more likely to cause a tube diameter increment due to the height it adds.

FOM	Weightage	Tail Skid	Tail Dragger
Effect on tube dimensions	20	1	0
Ease of hand launch	15	1	0
Drag	10	0	0
Weight	5	0	-1
Total	**50**	**35**	**-5**

Table 3.4.6: Landing Gear Configuration Figure of Merit Table

3.5 FINAL CONCEPTUAL DESIGN CONFIGURATION:
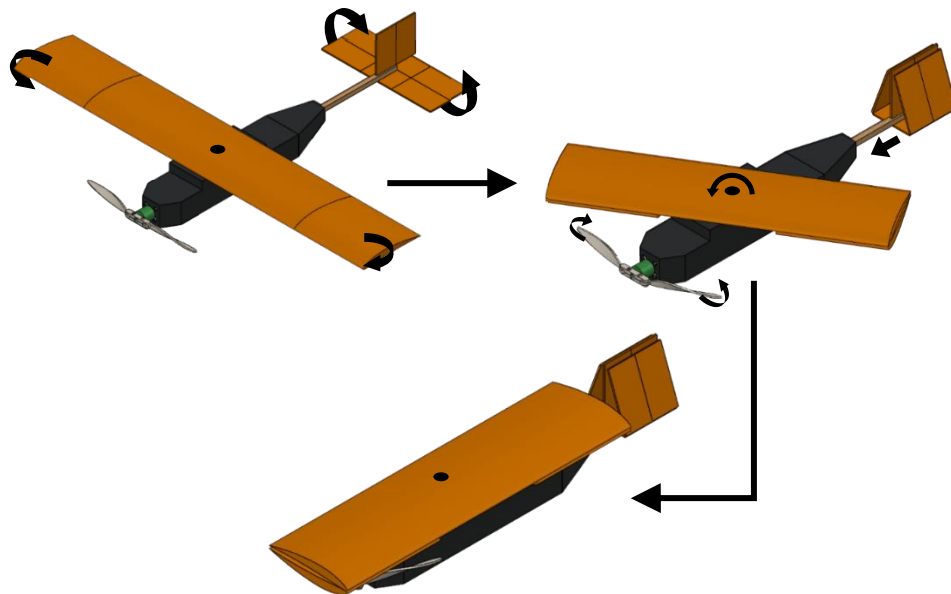
Figure 3.5: Concept sketches of the aircraft

The final conceptual design configuration is a conventional high-winger aircraft with a single tractor propulsion system, a conventional tail and a rear wire skid as the landing gear. All of the team's configuration and mechanism choices were made on the basis of maximizing score by successfully completing all three missions of the competition, having the lowest possible RAC and producing a practical, easy to materialize airplane that can be hand-launched. Combined with the sensitivity analysis, the configuration's design point was set at 0.7 kg empty weight, and a payload of four pucks while flying at least six complete laps for mission 3. The design point was chosen based on the team's realistic estimate of the

configuration's implementation. Figure 3.5 displays a concept sketch of the proposed design in the flight-ready condition, gradually transitioning into the stowed condition.

4. PRELIMINARY DESIGN:

4.1 DESIGN AND ANALYSIS METHODOLOGY:

Having finished the conceptual design phase for the aircraft, the team ventured into the preliminary design cycle. Initial sizing for the aircraft was done on the basis of the constraints provided in the problem statement and the score sensitivity analysis performed by the team.
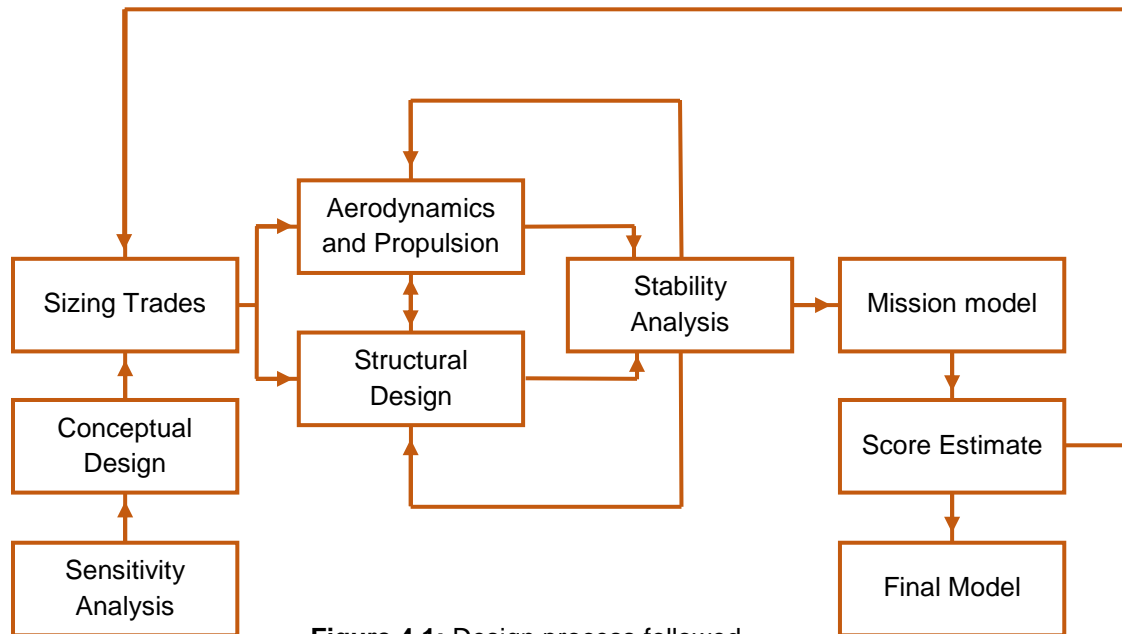
Figure 4.1: Design process followed

Multidisciplinary iterations were performed to determine aerodynamic characteristics, lifting surface dimensions and the required propulsion system specifications. Stability and control calculations followed for sizing of the empennage and fixing the control surface areas. Simultaneously, in-house testing began on the mechanisms that would need to be implemented for stowing the aircraft within a launch tube. Potential structural designs for the fuselage and options for the tube material were identified. All these processes ran in an iterative loop, though they are described sequentially in the sections ahead. After this, a mission model was prepared, to theoretically test the aircraft performance. Based on the mission model, a scoring estimate was made. In order to improvise on this score, all processes, sizing onwards were repeated. Once an optimal score was obtained, the final model was fixed. The tube was then designed around the aircraft.

4.2 SIZING TRADES:

The past entries of Team Vayuputras, in 2014 and 2016 were somewhat conservative with respect to weight, sizing and subsequent propulsion system selection. The resulting RAC was large compared to that of the top-tier contenders. To avoid a similar design approach, structural safety factors and weight

estimations were modified. Also, analysis of conditions at the competition site helped optimizing the selected propulsion system and made the aircraft more competitive.

4.2.1 FLYING CONDITIONS:

Weather conditions in Tucson, Arizona for the competition weekend from 2010 to 2016 were obtained from www.wunderground.com [6]. Figure 4.2.1 shows the recorded wind speed, averaged and plotted for each hour. Based on this, the team considered it prudent to design for a maximum head wind of 4 m/s for cruise conditions and the case of no headwind for hand launch conditions.
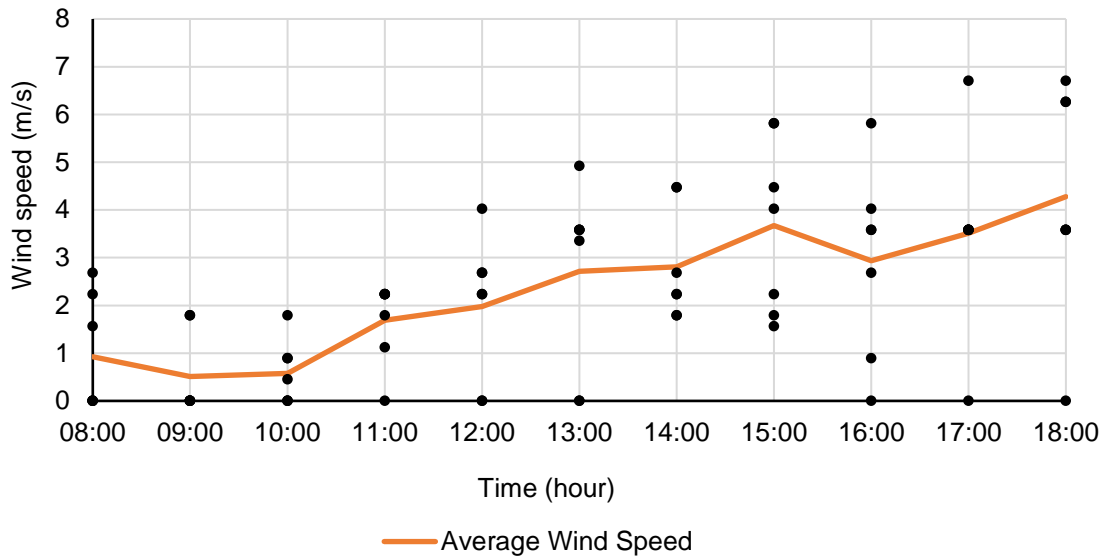
Figure 4.2.1: Average wind speed data from 2010 to 2016 at Tucson, AZ

4.2.2 HAND LAUNCH STUDY:

An important design consideration this year is the requirement of hand-launching the aircraft for all three missions. While the team had some experience building aircraft that could be safely hand-launched, the effect of throw velocity on the launch and the trajectory of the aircraft post-launch had never been evaluated. This is important since the aircraft must fly at the throwing speed i.e. its stall speed has to be equal to or less than the throwing velocity. Therefore, an aircraft was loaded up to 1.4 kg (approximate Mission 3 AUW) and was launched by different throwers. The launch was recorded between two fixed points and the average velocity of launch was calculated from the frames of the footage. After repeated throws, it was concluded that the aircraft could be thrown at 10 m/s for all missions. Preliminary calculations for the wing area followed from this result.

4.2.3 WING AREA TRADE STUDY:

A graph was plotted depicting variation of stall speed with increase in wing area (Figure 4.2.3), for different mission weights. Since the launch must result in a successful flight for the heaviest mission i.e. M3, the wing area was located by projecting the value of 10 m/s on the 1.4 kg line. The corresponding value of 0.135 m^2 was used for the first iteration in the preliminary design cycle.
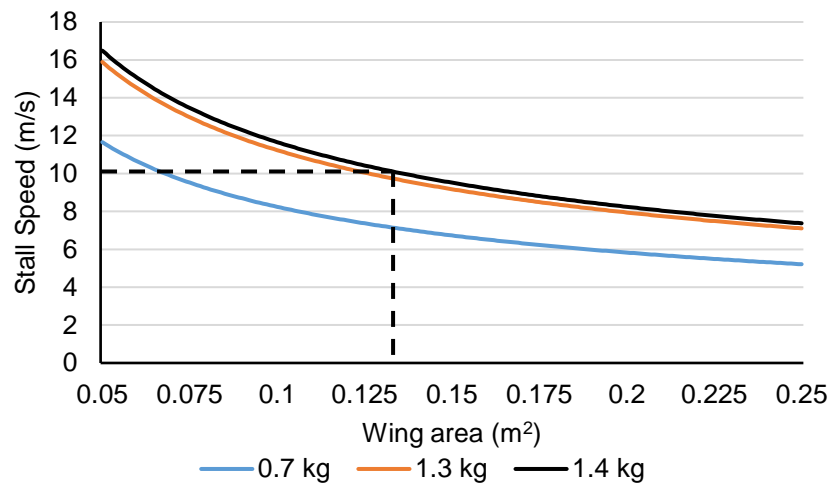
Figure 4.2.3: Stall speed v/s wing area

4.3 MISSION MODEL:

In order to simulate the performance of each design and to carry out comparison between different designs, the Mission Model was developed. The Mission Model, a virtual model of the mission task matrix was a series of MATLAB [3] programs that simulate the different scenarios experienced by an aircraft performing the mission matrix. It measured the aircraft performance in terms of various parameters for comparison.
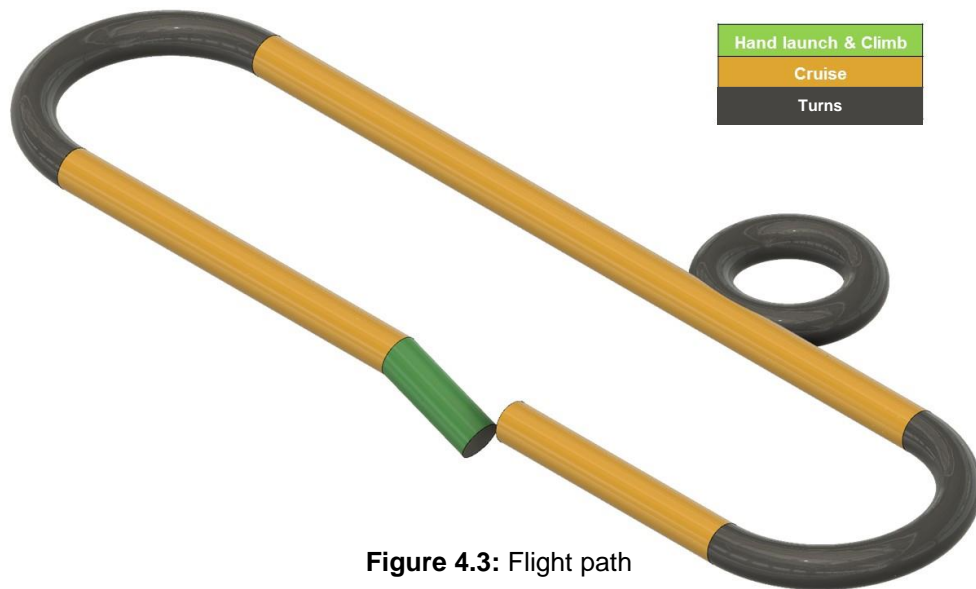

Figure 4.3: Flight path

Accordingly, the Mission Model consisted of the following simulations:

4.3.1 Take-off (Hand Launch):

When releasing the aircraft from the thrower's hand at full throttle, initial groundspeed was approximated as 10 m/s.

4.3.2 Climb:

The climb characteristics of the aircraft were estimated by modelling climb in a quasi-steady form. For an aircraft climbing at a constant power setting, the climb rate equation is given as:

$$\frac{dh}{dt} = V \times \left(\frac{T(V)-D(V)}{W}\right) \tag{4.1}$$

4.3.3 Cruise:

The cruise portion is divided into 4 segments on the basis of the parts of the track- Upwind Leg, Downwind Leg 1, Downwind Leg 2, Upwind Leg 2. This is used to calculate the lap times as well as the battery capacity required. The cruise programme was run for a no-wind condition as well as a high wind condition (4 m/s). A technique similar to finite element method was used for the stages up to cruise analysis. Velocity and power consumption of the aircraft was considered to be constant for a time step Δt. The products of instantaneous power with the corresponding time step were summed up to give the overall energy consumption.

$$\text{Energy (E)} = \sum \left(\text{Drag}(V) \times V + \rho \times N^3 \times D^5 \times C_p\right) \times \Delta t \tag{4.2}$$

4.3.4 Turn:

Wings of an aircraft are subjected to G-loading during turns. Lift greater than the weight of the aircraft is generated by the wings in order to provide the required centripetal acceleration.

Turn analysis requires aircraft velocity as an input. For a varying radius, it provides the total load acting on the wing. The performance of the aircraft during turns determines the operating range of velocities and turn radii for which the aircraft can execute turns safely without suffering aerodynamic stall or structural failure. This was done by iteratively calculating the G loading for different velocities and different turn radii and ensuring that the loading doesn't exceed the maximum Lift or the maximum allowable structural load. A G-factor of 2.5g was concluded to be limiting.

$$F_x = \frac{m \times V^2}{r_x} \qquad\qquad F_y = W \qquad\qquad \overline{F_t} = \overline{F_x} + \overline{F_y} \tag{4.3) to (4.5}$$

$$\text{G - Factor} = \frac{F_t}{m*g} \tag{4.6}$$

Where F_x = x-component of lift, F_y = y-component of lift, r_x = turn radius

4.3.5 Uncertainties:

1) The mission model assumed that the battery characteristics remain constant throughout the flight. In reality NiMH batteries do not have a constant discharge curve.

2) Ensuring constant power to the propeller was not always possible in practice as APC propeller data [5] is provided in discrete levels of RPM and not power. Linear interpolation was used to estimate data in between RPMs.

3) Crosswinds were neglected in the wind regime.

The mission model so developed was detailed to a considerable level. This ensured that the same model was used extensively for selection of the propulsion system as well as for detailed designing of the lifting surfaces.

4.3.6 Factors considered during simulations:

1) All aerodynamic coefficients at different Reynolds numbers were easily imported using the results of Constant Lift Analysis that is available in the XFoil software XFLR5 [1]. Data from XFLR5 could be seamlessly imported to the mission model on MATLAB [3].

2) All propulsion data such as thrust provided by the propeller and the electrical power consumed was referenced from APC propeller database. An attempt was made to make all cruise simulations at the maximum power that could be provided by the battery, hence simulating a full throttle condition, for a duration of up to five minutes.

3) Headwinds and tailwinds were incorporated into the mission model, on the basis of the site analysis in section 4.2.

4.4 AIRCRAFT AERODYNAMIC AND STABILITY CHARACTERISTICS:

4.4.1 AIRFOIL SELECTION:

Amongst various kinds of characteristics that an airfoil imparts to the nature of the flight regime, cruise performance was considered as the most significant. The range of Reynolds numbers used for analysis was based on the estimates of the aircraft cruise speed. The airfoils were analyzed up to a Reynolds
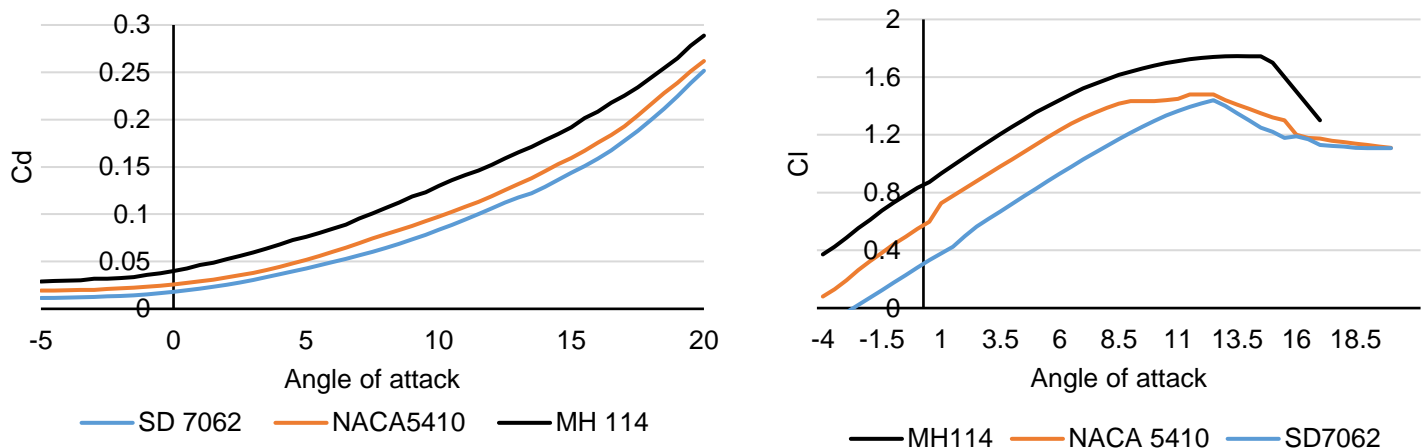
Figure 4.4.1: Airfoil Characteristics

number of 2,00,000 for the aircraft. The other influential parameters were Stall Angle ($α_{clmax}$) and the Maximum Cl (c_{lmax}) value. Airfoil analysis was carried out on XFLR5 [1]. They were evaluated on their basic characteristics with respect to lift and drag. The airfoils MH114, SD7062 and NACA 5410 were shortlisted for the aircraft. An initial study of airfoil polars showed that both stall characteristics and Lift-to-Drag ratio were optimised for airfoils having 10%-11% thickness. Both MH114 and NACA 5410 showed favourable lift and stall characteristics, whereas the SD7062 owing to its lesser camber offered lower lift. MH114 and NACA 5410 showed a gradual stall pattern while the SD7062 suffers a sharper stall. The SD7062 was eliminated for inferior performance, but selection of a foil from MH114 and NACA 5410 posed a difficult choice. The highly cambered and sharp trailing edge of the MH114 poses difficulties in manufacturing.

Therefore, the NACA 5410 was chosen. The thickness of the chosen foil was sufficient to house the buckles for the folding mechanism.

The stall characteristics were studied and it was determined that the NACA 5410 could easily delay stall at higher angles thus keeping the stall speed to a lower value. A sufficiently higher maximum lift coefficient ensured that the aircraft could sustain sharp turns and an added possibility of successful hand launch and landing under adverse wind conditions with the NACA 5410 being the wing profile.

4.4.2 LIFTING SURFACE ANALYSIS:

The aircraft wing area selection was carried out by Vortex Lattice Method (Ring Vortex) analysis performed in XFLR5 [1]. The selected airfoil and wing area are responsible for creating the complete lifting surface characteristics. The lifting surface characteristics, in terms of operating range of Coefficient of Lift and C_l/C_d,
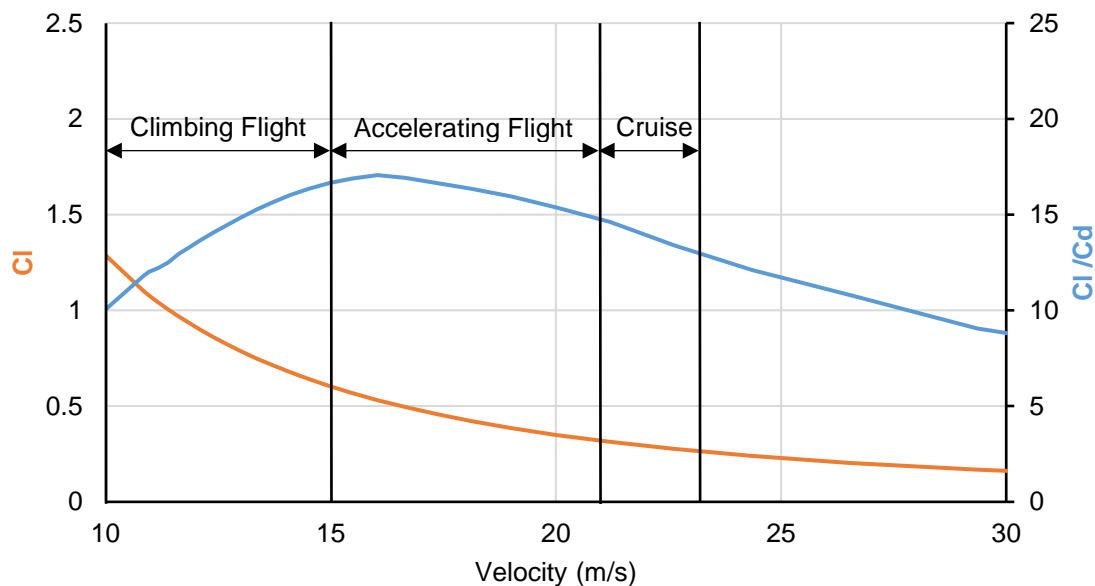
Figure 4.4.2: Lifting characteristics of the wing from XFLR5

define the flight behaviour of the aircraft. The aircraft was designed so that the maximum

Cl/Cd was achieved during that phase of flight wherein the aircraft is accelerating to cruise speed. This was done to optimise acceleration performance so that the aircraft is able to achieve cruise speed faster.

4.4.3 DRAG BUILD-UP:

With the wing, tail and fuselage sized, a more accurate drag model of the aircraft was created. This model was used to finalize the propulsion system as well as accurately profile the missions. Using methods described by Hoerner [8], the complete drag profile was compiled using basic equations for skin friction, form factor, and wetted area. Figure 4.4.3 lists the drag build-up of the aircraft components for mission 2. Wing zero-lift drag has the highest contribution, with the fuselage being the second-highest.
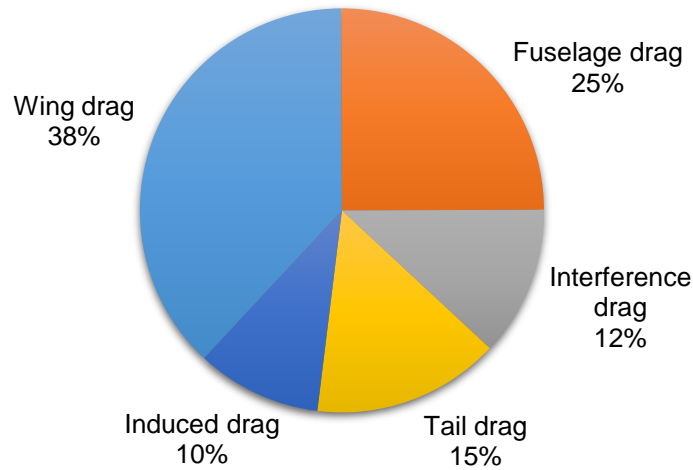
Figure 4.4.3: Total drag build-up of the aircraft

4.4.4 STABILITY CHARACTERISTICS:

Static Stability:

Initial stability and control analysis was performed to ensure a statically stable aircraft and an acceptable static margin. Static margin (S.M.) is the distance between the aircraft centre of gravity and neutral point relative to the wing chord.

$$\% \text{ S.M.} = \frac{X_{np}-X_{cg}}{\text{M.A.C.}} \times 100 \qquad (4.3)$$

It is mandatory for the static margin to be positive, for positive static stability. However, a very high static margin would lead to sluggish response and hamper the maneuverability of the aircraft. Keeping these in mind, a static margin of 12% was selected for all three missions. This value makes the plane more responsive to elevator deflections, saving weight in servos. The variables associated with longitudinal static stability have been listed in the table below:

C.G.	60 mm
N.P.	78 mm
Horizontal Tail Area	28000 mm^2
S.M.	12%

Table 4.4.4: Longitudinal Stability Characteristics

All the distances have been measured aft of the leading edge of the wing. By creating a simple Cm v/s α plot for the C.G. placed at the centre of pressure of the lifting surfaces and at the computed Neutral Point, the static stability of the aircraft was established over a range of angle of attack.
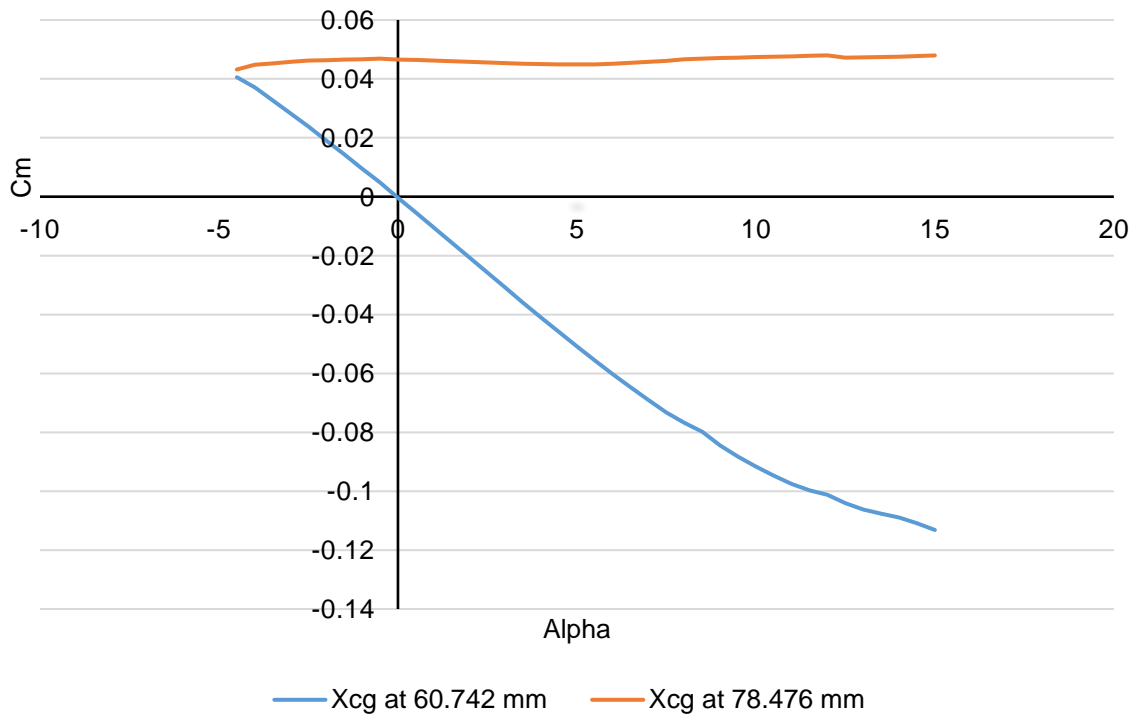
Figure 4.4.4 (a): Cm vs alpha

It can be observed that the graph has sufficient negative slope in the first case, which implies a good amount of longitudinal static stability.

Dynamic Stability:

Once the static stability had been established, an analysis on dynamic stability was also performed. The mass moments of inertia for the aircraft were calculated using the DS SolidWorks [9] CAD model and was used as input for the dynamic stability analysis. The root locus graphs were then plotted for all five modes of motion i.e. Short Period, Dutch Roll, Roll Damping, Spiral and Phugoid.
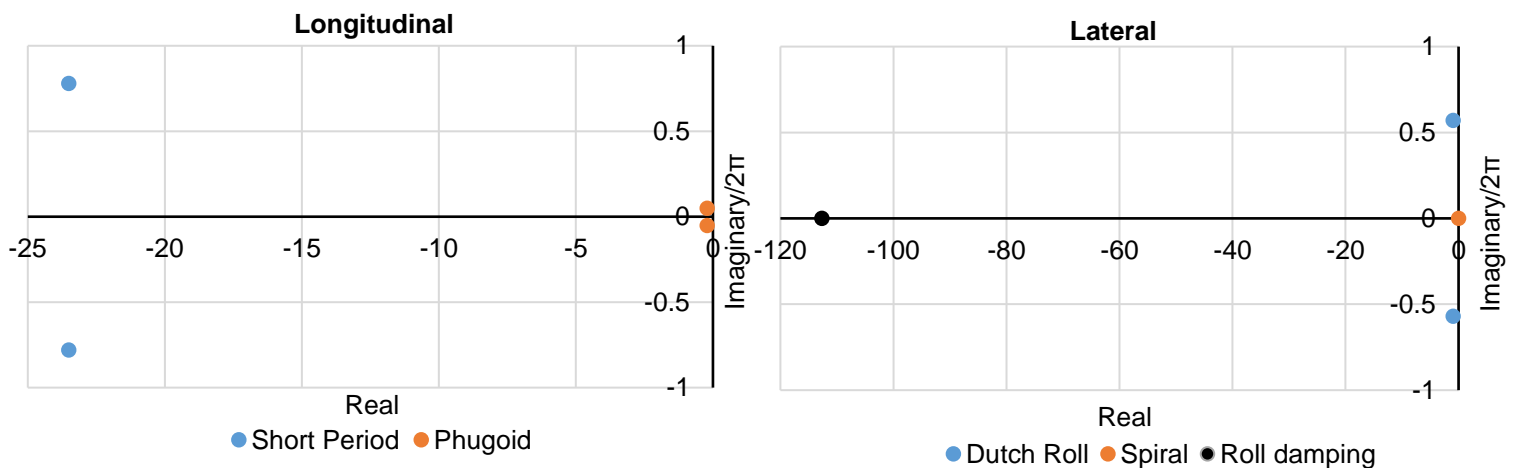
Figure 4.4.4 (b): Dynamic Stability Characteristics

It is observed that all modes for the aircraft, except spiral, lie to the left of the imaginary axis, which is the

criterion for positive dynamic stability. As far as the spiral mode is concerned, it was found that it satisfies the level one handling qualities [10], and hence will be easy for the pilot to correct.

<u>**Control Surface Sizing:**</u>

In every aircraft, along with stability, controllability is a must. Hence, it is essential that the control surfaces are sized appropriately to provide the required moment. The aircraft comprises only of primary control surfaces and was sized by the method elaborated below:

Ailerons: Aileron sizing and positioning were done by an iterative process. It was initiated by selecting minimum dimensions and outboard positions that fall under the thumb rules depending on the aircraft's lateral controllability requirement explained in Sadraey [10]. The chosen size was then used to calculate the roll rate of the aircraft considering parameters like the moment of inertia of the entire aircraft about the longitudinal axis, aileron effectiveness, aerodynamic and mass balancing. This roll rate was then compared to a particular range of roll rates corresponding to aircraft mentioned in [10] and checked for its acceptability. If the values were not acceptable, the entire process was repeated.

Elevator: For convenience, the elevator span was kept the same as the horizontal stabilizer span, and the chord was kept as the only variable. It has been stated that if the elevator chord is kept above 50% of the horizontal tail chord [10], flow separation at the tail is likely to occur. However, too small a chord (around 15%) would result in not enough moment being produced when the elevator is deflected. Finally, the elevator chord was conservatively sized at 50% of the stabilizer chord since some portion of the elevator would prove to be ineffective because of the presence of the folding mechanism parts near the root. Later XFLR5 [1] was used to verify that this elevator area was sufficient to assist the aircraft during hand launch and to maintain longitudinal trim.

Rudder: A rectangular rudder having the same span as the stabilizer and just enough area as per the thumb rules mentioned in [10] was selected. The underside of the rudder was given a swept cut in order to permit upward elevator deflection.

In addition, a control analysis was done using AVL [2] by inputting standard roll, pitch and yaw rates along with the flight conditions. It was verified that the required control surface deflections for the rudder or elevator were up to or less than 20°, which is the maximum deflection to provide an adequate safety margin from stalling the surface. No extreme deflections were required for any of the cases analyzed.

4.5 PROPULSION SYSTEM SELECTION:

The flight performance of the aircraft is dependent on the power output of the propulsion system. Considering this, the motor, battery and propeller selection was done to create a powerful yet efficient propulsion system.

4.5.1 BATTERIES:

Initially, a decision was made regarding the type of batteries that could be used in the competition: NiCd and NiMH. NiCds offered a lower internal resistance, beneficial for limiting the voltage drop with higher current draws. However, NiMHs offered superior energy density and were less prone to memory effect. Hence, they were the chosen battery type. From table 4.5.1, the Elite 1500 shows maximum power density and is an obvious choice over the Elite 2100.

The KAN 700 shows decent power density with a low maximum current and can be used only for motors that are rated at low currents. The selection of the battery pack depended not only on the characteristics of the cells themselves but also their compatibility with the motors powered by them.

The decision for the number of cells for the battery pack of the aircraft was made on the basis of the available power. Through appropriate use of the mission model it was concluded that increasing the power output was beneficial up to 220W and beyond that the benefits of additional power were lesser as compared to the corresponding weight penalty. Moreover, the number of cells for a battery pack was also limited by the voltage rating of motors available. Since most lightweight motors and speed controllers are rated for less than 25V, it imposed a limitation on the number of cells that could be put together in series.

Battery	Capacity (mAh)	Max Current (A)	Internal resistance (Ω)	Cell weight (g)	Power Density for 10 cells (W/g)
Elite 2100	2100	21A	0.02	32	0.6813
Elite 1500	1500	16A	0.02	23	0.9826
KAN 700	700	17A	0.048	13	0.8269

Table 4.5.1: Comparison of battery cells

Most manufacturers consider a voltage greater than 25.2 V (LiPo 6s, NiMH 17 Cells) as a High Voltage rating and hence for voltage protection both the cost as well as weight of these motors is considerably higher.

The cells' actual usable capacity decreases in accordance with Peukert's law [11]. It is therefore important to limit the continuous current draw from the battery to the maximum discharge rating specified by the manufacturer. Considering voltage drop during operations, a maximum nominal voltage of 16.8V (fully charged, 14- cell pack) was considered as safe for the operation of the motors under consideration. A 10-cell pack was made for testing battery performance. Finally, endurance was tested at different discharge rates (detailed in section 7.3.1) to find the maximum allowable current draw from any pack.

4.5.2 MOTOR AND PROPELLER SELECTION:

In order to reduce the battery weight, high-efficiency motors were selected, such that a greater fraction of the input power was available for use by the propellers. Also, due to a limit on the C-rating, which is 10C for the selected Elite batteries, it had to be ensured that these motors give high efficiency at or below 16A. Based on this requirement, a number of motors from manufacturers like Hacker, Scorpion, Cobra and Tiger were evaluated.

Next, motors which could operate within the designed working range of approximately 220W were shortlisted. The selections were further narrowed to a Kv range of 800-1400 RPM/volt. Higher Kv rating enables us to drive the propeller at lower voltages, leading to higher current draws for the required power output. On the other hand, lower Kv rating can drive the propeller at low currents, but at the cost of more battery cells and a heavier propulsion system.

Propeller performance is an important component of the propulsion system, determining the capabilities of the aircraft such as the cruise velocity. To aid tube diameter minimization, it is practical to use foldable propellers. It also avoids installation of an extra mechanism that would have been required for stowing the motor mount, if an electric propeller of the same diameter were to be used. It is important to note that such propellers are available only in select diameter and pitch combinations. Hence, there was a small pool of foldable propellers to look into.
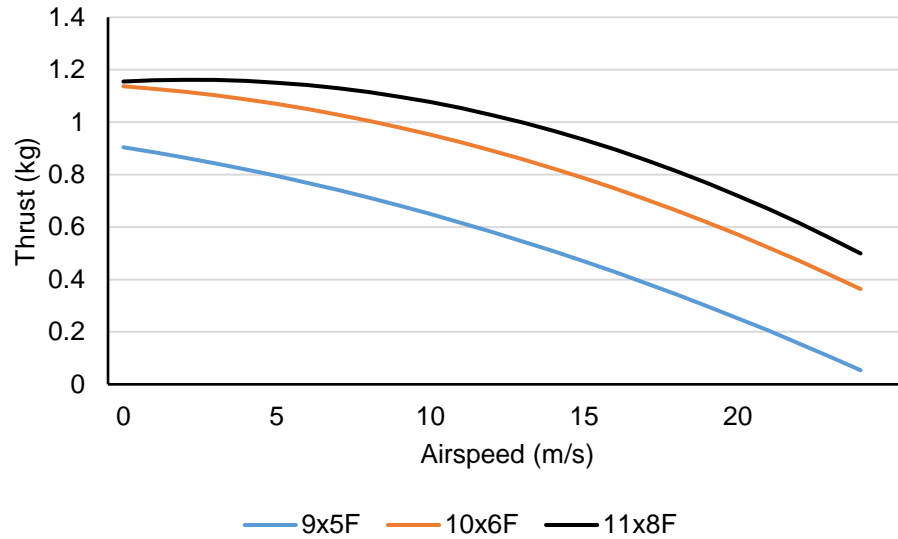
Figure 4.5.2: Comparison of folding propellers

From the figure, it is clear that the folding propeller 9x5F offers least thrust over the entire velocity profile of the aircraft. It experiences a steeper drop in thrust, as compared to propeller 11x8F and 10x6F. Also, keeping the importance of sufficiently high thrust during a hand launch, propeller 9x5F was incompetent and hence rejected. Thus, propellers 10x6F and 11x8F were shortlisted for each combination.

Finally, out of the different motor/battery/propeller combinations created, the lightest combinations were chosen. These were purchased for further testing, and the results were compared (section 5.3.8). The combinations are listed in table 4.5.

Propulsion System	Motor	Propeller	Battery	Cell Count	System weight (g)
PS1	Cobra C2213/18 1350Kv	APC 10×6F	Elite 1500 mAh 2/3 AA	10	324
PS2	T-Motor MT2216 1100Kv	APC 11×8F		12	381
PS3	T-Motor MT2216 800Kv	APC 11×8F		14	427

Table 4.5.2: Selected propulsion systems

4.6 MISSION PERFORMANCE ESTIMATES:

The velocity profiles for M1, M2 and M3, calculated from the mission model are shown in Figure 4.6 (a), (b) and (c) respectively for a single lap. These have been calculated considering effect of wind, with a headwind of 4 m/s incorporated for all missions. Table 4.6 lists the time taken for each flight segment, for the first lap.
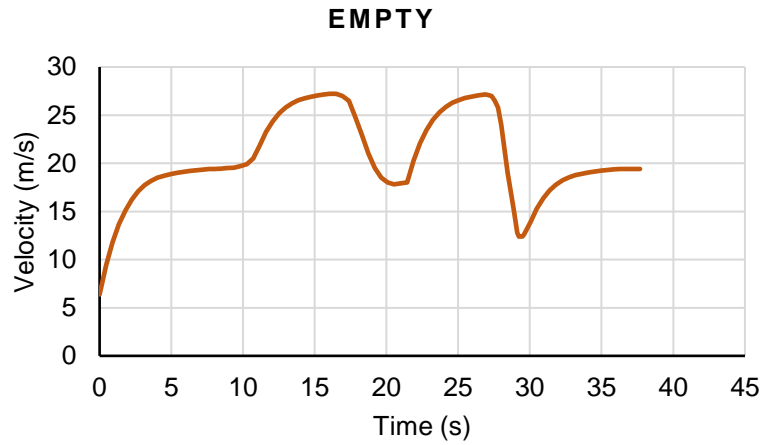
EMPTY

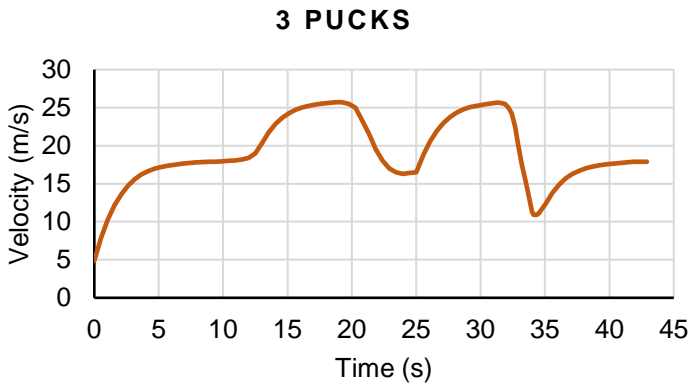**Figure 4.6 (a):** Mission 1 Velocity Profile

3 PUCKS

Figure 4.6 (b): Mission 2 Velocity Profile

4 PUCKS
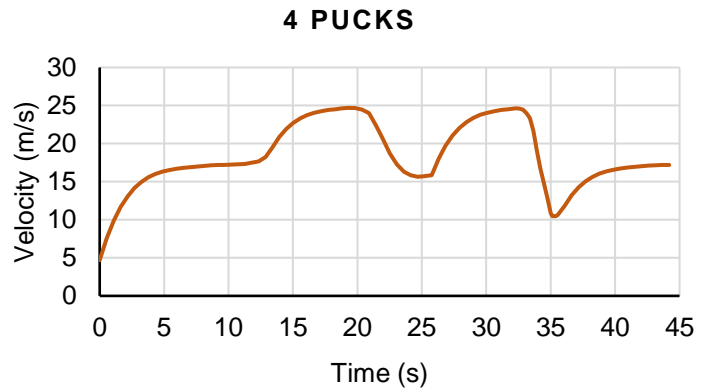
Figure 4.6 (c): Mission 3 Velocity profile

Flight Segment	Time taken (s)		
	M1	M2	M3
500 Feet Upwind	9.1	10.6	10.9
Turn 1 (180º)	2	2.5	2.7
500 Feet Downwind	5.7	6.8	7
Turn 2 (360º)	4	5	5.3
500 Feet Downwind	6.9	7.5	7.7
Turn 3 (180º)	2	2.5	2.7
500 Feet Upwind	6.9	8	8.2
TOTAL	**36.6**	**42.9**	**44.5**

Table 4.6: Predicted time for flight segments (first lap)

5. DETAIL DESIGN:

After the preliminary design, the theoretical parameters were converted to physical design parameters with pragmatic considerations. The structural capabilities, system integration, weight and balance, flight and mission performance of the model have been considered keeping the tube diameter and weight as important factors, as inferred from the sensitivity analysis. The overall dimensions of the aircraft remained unchanged from the preliminary design stage. The wing and control surface chords were chosen to allow sufficient thickness for the structure and installation of the mechanisms for folding and rotation.

5.1 DIMENSIONAL PARAMETERS OF FINAL DESIGN:

Wing		Horizontal Stabilizer		Vertical Stabilizer	
Airfoil	NACA 5410	Airfoil	Flat Plate	Airfoil	Flat Plate
Span	0.90 m	Span	0.28 m	Height	0.11m
M.A.C.	0.15 m	M.A.C.	0.10 m	M.A.C.	0.10m
Incidence Angle	0°	Incidence Angle	0°	Incidence Angle	0°
Ailerons		Elevator		Rudder	
Semi-Span	0.232 m	Span	0.28 m	Height	0.11 m
M.A.C.	0.03 m	M.A.C.	0.10 m	Area	0.0044 m^2
Deflection	± 30°	Deflection	± 30°	Deflection	± 30°

Fuselage		Tube	
Retracted length	0.52 m	Length	0.72 m
Extended length	0.64 m	OD	0.16 m
Width	0.085 m	Thickness	0.01 m
Height	0.07 m	Weight	0.15 kg

Table 5.1: System Dimensional Parameters

5.2 STRUCTURAL CHARACTERISTICS AND PARAMETERS:

The aircraft allows for stowage inside a tube through hinged folding sections of lifting surfaces, wing rotation and an extendable tail while still maintaining features that provide the structural integrity required for this competition. Keeping the mission profiles in mind, loading conditions for the aircraft and the tube were listed as follows:

Aerodynamic loads – Forces of lift and drag will tend to bend and twist the wing and control surfaces.

Motor loads – Thrust produced by the propeller and reaction torque of the motor will respectively pull and twist the fuselage. Sustained vibrations of an operating motor will also be experienced by the fuselage.

Impact loads – These come into play when the aircraft lands and the tube is dropped during the ground mission.
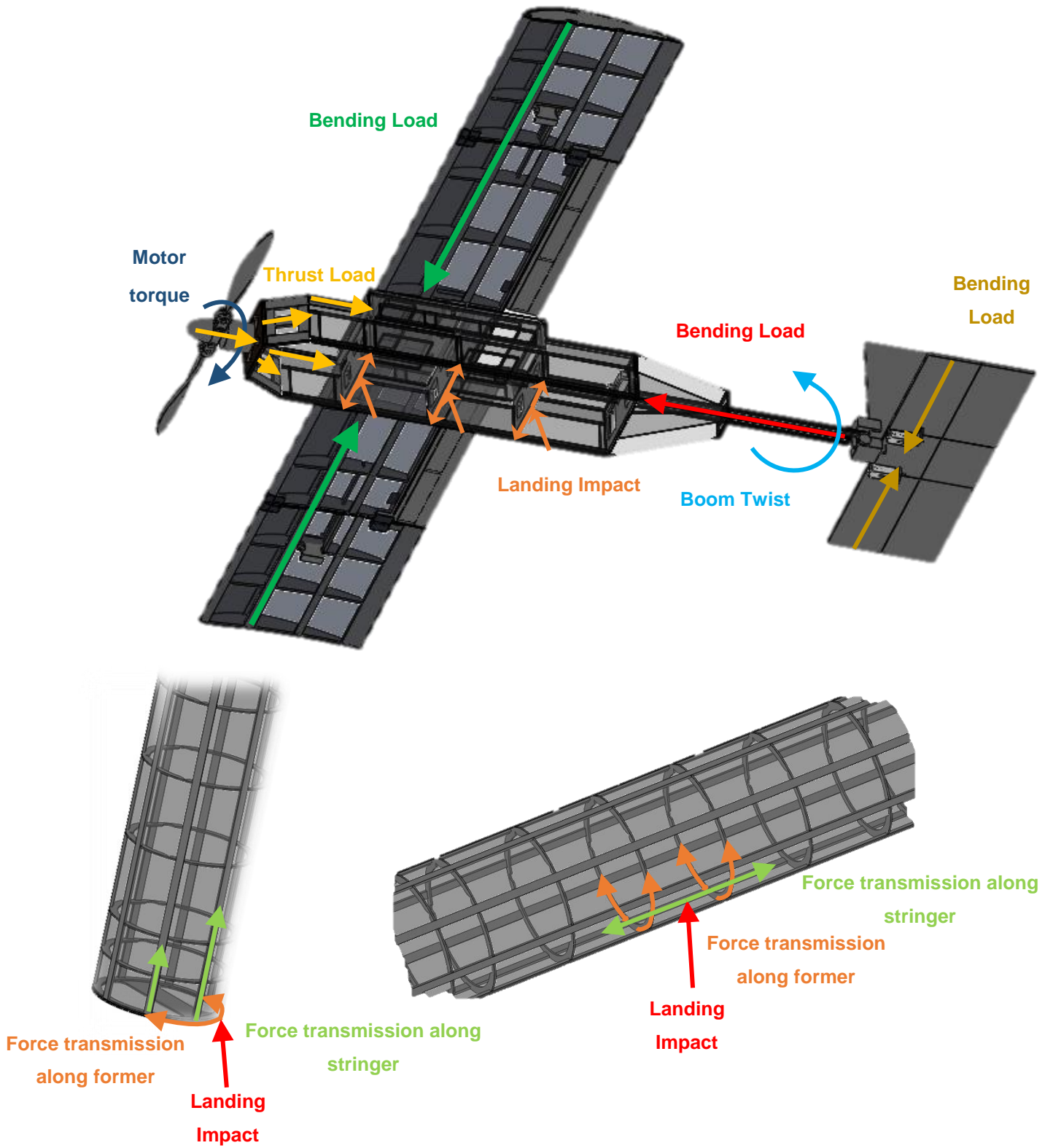
Figure 5.2: Load path diagrams for the aircraft and the tube

5.2.1 OPERATING REGION FOR THE AIRCRAFT:

A more practical operating envelope of the aircraft will be dictated by its structural and aerodynamic limits. Constraints are imposed by aerodynamic stall and the ultimate strength of balsa. Also, from previous experience of competitive flying, the aircraft is expected to have a turn radius of not more than 30 metres. Accounting for variations in the ultimate strength of balsa used, the airplane was designed to withstand a 2.5G loading (corresponding to a 60-degree bank angle (for sustained level turns) at a maximum all up weight of 1.4 kg (occurring in mission 3). Combining these parameters, the region for safe operation of the aircraft is obtained by constructing a V-n diagram as shown below:
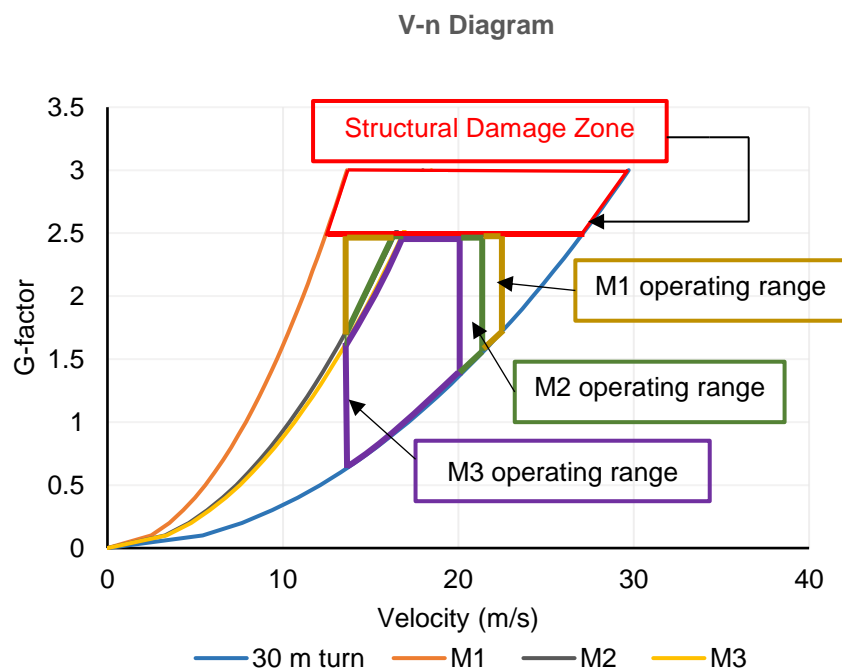
Figure 5.2.1: G-Factor vs. Velocity for the aircraft

Each mission line corresponds to its aerodynamic stall line. The 30 m turn line refers to a turn radius of 30 meters.

5.3 SYSTEM AND SUBSYSTEM DESIGN/ SELECTION/ INTEGRATION:

The following system and subsystem components were analysed in greater detail to finalize the design of the following: fuselage and boom, payload, wing folding sections, landing gear, motors, batteries and other electronics.

Based on the load paths, the design was made in a way that ensured efficient load transmission to stiffer structural members. Balsa was chosen for most structural parts, owing to its light weight, strength and high workability. Aero-ply was used only in critical areas for enhanced strength and stiffness.

5.3.1 Self-Locking Mechanisms:

Buckle:
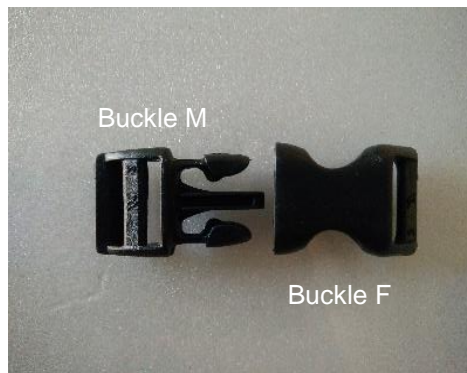
Figure 5.3.1 (a): Buckle parts

These are contoured side-release buckles. They are lightweight, strong and easy to operate. Each comprises of a male part (Buckle M) that fits into a female (Buckle F) part. The buckles have been used to mechanize wing folding.

Nut-Spring-Bolt:

A centre bolt serves as the pivot for wing rotation. A nut on this bolt restricts vertical motion of the wing. Bolts on either side consist of a nut-guarded spring, which help in locking the wing and restrict all planar motions by slipping into holes cut into a wing seat in the flight condition. While stowing the aircraft in the tube, spring compression enables the side bolts to be lifted out of these holes and the wing to be rotated.
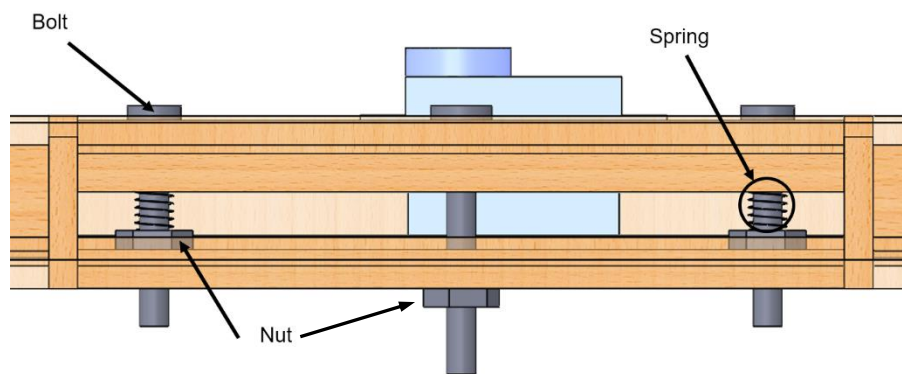
Figure 5.3.1 (b): Nut-bolt-spring mechanism

Spring-operated latch:

A quick-release latch was assembled using a spring operated steel spoke that moves in a 3D printed guide. An extension connected to the rod enables it to be translated easily and bring about spring compression at the time of stowing the HT and the boom.
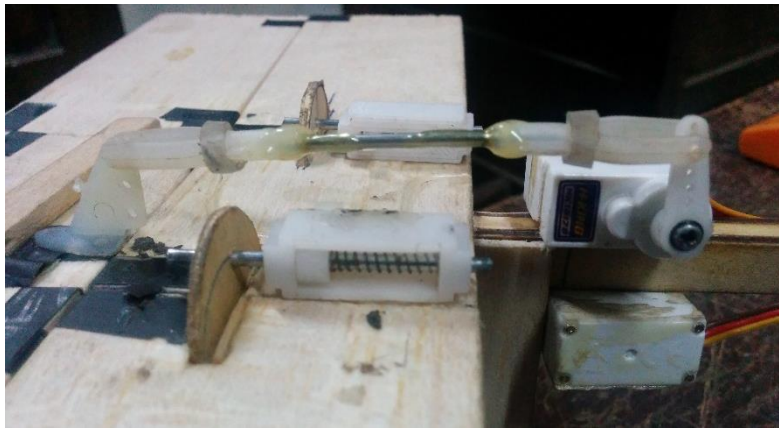
Figure 5.3.1 (c): Spring-operated latch mechanism for HT

5.3.2 Fuselage – cum – payload bay:

In order to minimize tube diameter, the four pucks were placed inline. The fuselage was now designed around this volume. A 4mm base and 3mm side walls –all made of hard balsa - interlocked with slotted

Figure 5.3.2: Fuselage under construction

aero-ply bulkheads to increase overall rigidity. A battery and wing seat were fit in a similar way. A hexagonal balsa ring connected the motor mount, the inclined walls and the side walls to the first bulkhead for increased support. The taper helped reduce profile drag of the fuselage and created space for folding the propeller when the aircraft was inserted into the tube. Coroplast (corrugated plastic) flapped windows in the side walls facilitate easy loading of the pucks. The first puck is loaded from the top through a separate flap. Another flap at the rear closes the fuselage once all electrical connections are made. The three side-windows were cut alternately on either side to avoid having all the discontinuities in the Monokote covering on only one side wall.

5.3.3 Payload:

A 170g regulation ice hockey puck served the purpose of the payload. Each puck was secured to the fuselage base using double-sided tape. Chequered tape was then used to seal the coroplast flaps.

Figure 5.3.3: Payload securing

5.3.4 Wing:

The wing followed a conventional balsa rib and spar structure. The resulting 'I' section provided high resistance to wing flexing. A 1.5 mm balsa skin sheet was added in the leading section to make application of a covering film more effective, hence gaining more strength and shape. The ailerons were placed inboard to ease wing folding and keep the servo count to one. This servo was placed on an aero-ply plate, which also seated a nut-spring-bolt mechanism for wing rotation. Aero-ply plates were placed at the bottom of the centre section. This provided a flat surface for wing rotation and also guided and held the

bolts into holes drilled in the wing seat.
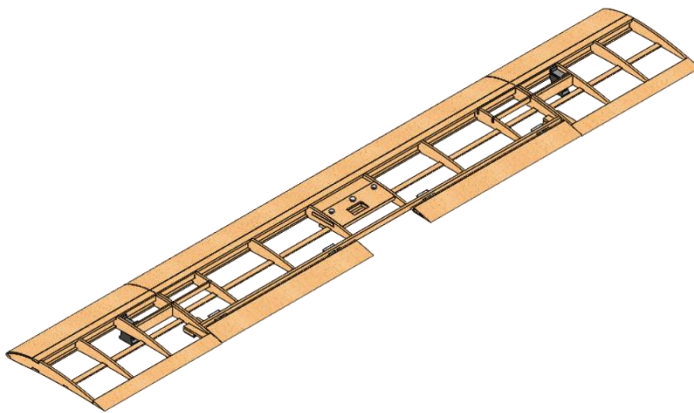
Figure 5.3.4 (a): Wing CAD

Figure 5.3.4 (b): The wing, rotated and folded

Both folding sections have aero-ply jaws for holding Buckle M. Buckle F was stuck to an adjacent rib. Light plastic hinges were screwed into balsa stalks glued to adjacent ribs. This facilitated easy folding of the wing.

5.3.5 Empennage:

The horizontal tail (HT) and vertical tail (VT) were made of flat 3mm balsa plates that follow a conventional

configuration. Both were connected to a retractable boom. This allowed us to keep the tube length to a minimum. Grain orientation of balsa was kept along the span for increased strength against flexing. The HT folds on itself, enabling it to fit in the tube. While bringing the stowed plane into flight ready condition, the
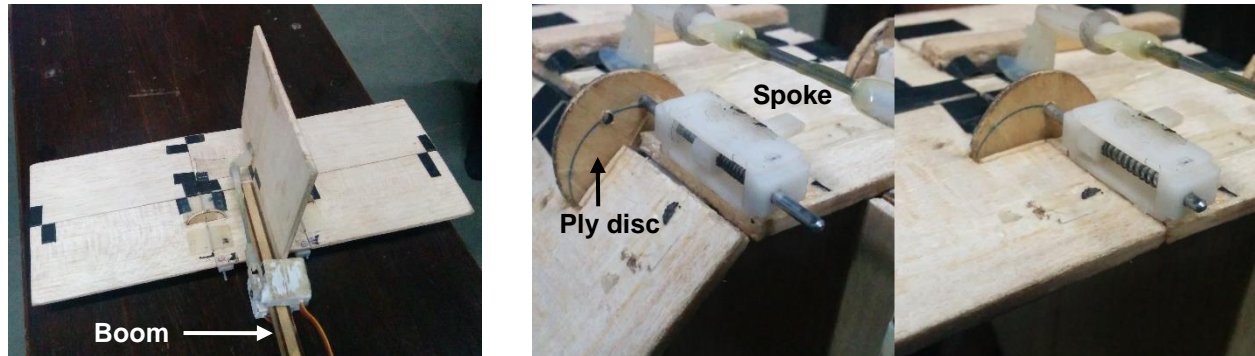
Figure 5.3.5: The HT, VT and HT folding mechanism

HT is folded back. The spring-operated steel spoke slides along the boom and a ply disc fit on the HT, till it slips into appropriately drilled holes and self-locks. A similar mechanism has been used to lock the boom in the fully extended condition.

5.3.6 Landing Gear:
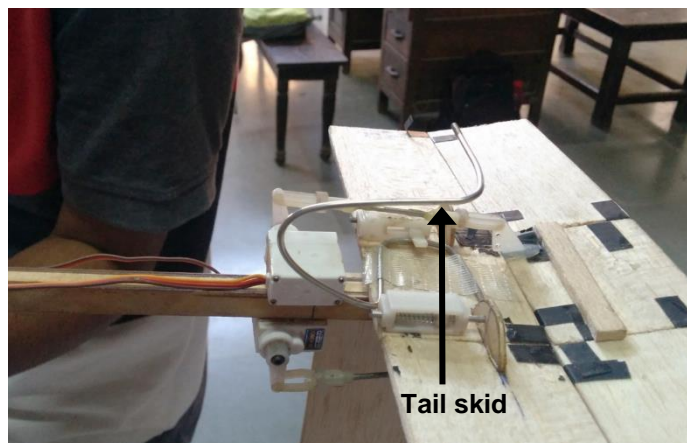
Figure 5.3.6: Tail landing gear

A 3mm steel spoke was bent to a shape as shown and connected to prevent the tail striking the ground at the time of landing. Sufficient line contact was provided on the horizontal stabilizer for distributed load transmission. A horizontal 'U' allows more efficient shock absorption.

5.3.7 The Tube:

The tube is a simple stringer and former design. 3mm hard balsa stringers fit into slots made on 2mm aero-ply formers. Slots have also been made for ushering wing, fuselage and VT insertion into the tube. Starting from one end of the tube, successive formers have been placed with their fibre lines at increasing angles of 45°. In effect, fibre strength has been provided all around the tube. Since the CG of the aircraft does not coincide with the CG of the tube, the tube will rotate when dropped in all throws. When the tube is dropped, the rims of the tube will always be the first parts to sustain the impact on account of rotation when in air.

Hence, end formers were placed closer to the lids for increased load transmission. The lids are connected to the tube using chequered tape. Styrofoam is placed on the inner side of the lids to restrict aircraft motion in the tube and cushion the drop. A Monokote covering film has been applied to make the tube water tight and provide increased strength for the drop.
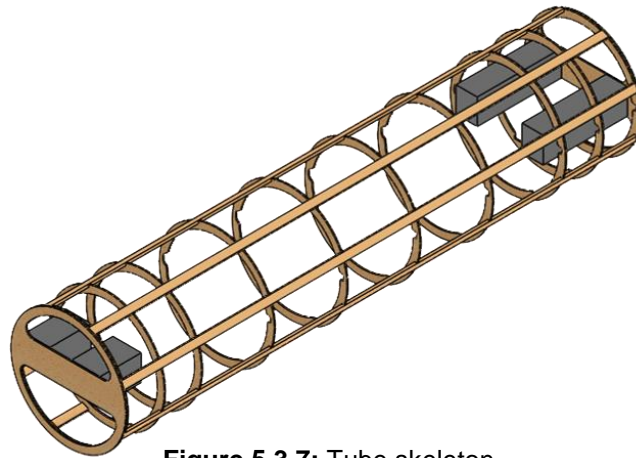

Figure 5.3.7: Tube skeleton

5.3.8 Propulsion system:

As described in section 4.5, three propulsion systems were selected for testing. Their flight performance was characterized by comparing the thrust available for each system and determining the maximum airspeed by the intersection of these curves with the drag curve for steady-level flight. Available thrust data was obtained from the APC database [5].

PS1 (Cobra C2213/18 1350Kv, APC 10x6F, 10S) was the lightest propulsion system, but it fell short of the estimated performance in terms of maximum speed. PS2 (T-Motor MT2216 1100Kv, APC 11×8F, 12S) and PS3 (T-Motor MT2216 800Kv, APC 11×8F, 14S) have almost similar performance post 15 m/s, but PS2 is 2 cells lighter and is thus the preferred choice.
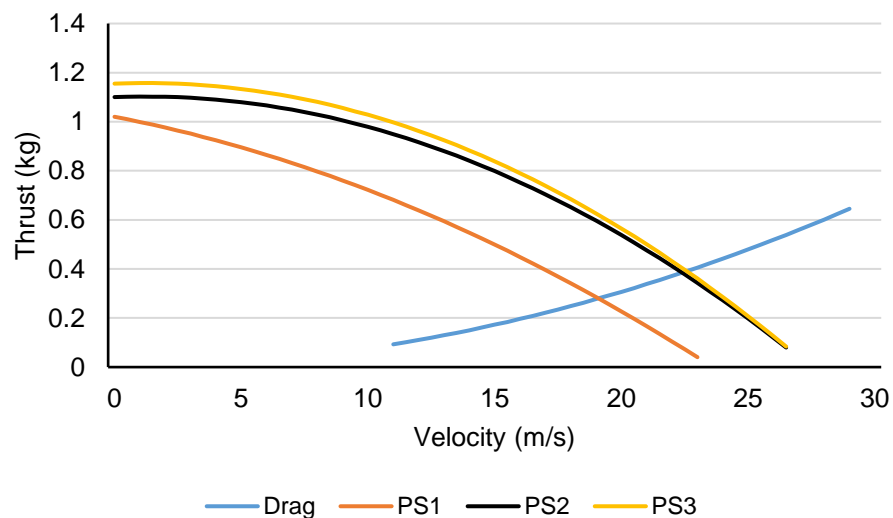
Figure 5.3.8: Comparison of propulsion systems

5.3.9 ESC Selection:

The ESC selection was primarily driven by the maximum current and voltage of the battery. The weight and programmability were secondary parameters. All the ESCs satisfying the voltage and current requirements were shortlisted. The ESCs were checked for their programmability to switch from default high cut-off voltage (LiPo mode) to low cut-off voltage (NiMH mode). Finally, the Turnigy Plush Opto (without Battery Eliminator Circuits) 30A ESCs which were found to have minimum weights were chosen. As the receiver has its separate battery, the Battery Eliminator Circuit was not required in the ESC, which further supported this selection.

5.3.10 Servo selection:

The servo selection was primarily driven by the required torque calculations. Weight and precision were the other requirements. The following equation was used:

$$\textbf{Servo Torque(oz-in)} = (8.5 \times 10^{-6}) \times C^2 \times V^2 \times L \times \sin(S_1) \times \frac{\tan(S_1)}{\tan(S_2)} \qquad (5.3)$$

Where C=control surface chord in cm; V=Speed in mph; L=Control Surface length in cm; S_1=Maximum control surface deflection in degrees; S_2=Maximum servo deflection in degrees.

After these calculations, the servos having sufficient control power and the lightest weight possible were shortlisted. Finally, HK15178 Digital Micro Servos were selected because they provided the required torque in the smallest volume and lightest assembly. The selected electronic components are tabulated in table 5.3.10 below:

Motor		Battery- Main and receiver		
Make	T-Motor MT2216	Make	ELITE 1500	KAN
Kv rating	1100	Size	2/3 AA	AAA
Maximum Continuous Power	380W	mAh	1500	700
Maximum Continuous Current	25A	Configuration	12S	4S
Weight	76g	Weight	230g	50g

Transmitter and Receiver		Servo		Electronic Speed Controller	
Make	Avionic RCB 6i	Make	HK15178	Make	Turnigy
Bandwidth	2.4 GHz	Torque	1.2kg-cm	Current Rating	30A
No. of Channels	6	Operating Voltage	4.8V	Voltage Rating	8.4V-25.2V
Rx Weight	15g	Servo Weight	9g	Weight	18g

Table 5.3.10 (a) and (b): Specifications of selected electronic components

5.3.11 Aircraft insertion into the tube:

The buckles are released from underneath the wing. The outboard sections of the wing fold under the respective inboard sections. Then the nut-bolt-spring mechanism comes into play and allows the wing to be rotated. Once the wing is made parallel to the fuselage, the boom – empennage system is retracted. This is achieved by operating the spring-loaded latch mechanism. Finally, the propeller is folded against the fuselage side walls. The plane in this stowed condition is then inserted into the tube. Suitably shaped slots have been made in the tube formers to facilitate comfortable insertion of the VT, the wing and ailerons.

Figure 5.3.11: Aircraft insertion into the tube

5.4 WEIGHT AND BALANCE FOR FINAL DESIGN:

The weight-and-balance chart enables correct location of the centre of gravity (C.G) of the aircraft. This is an important aspect of stability and flight control. Table 5.4 shows a list of all components, their weights and their C.G. locations along the x-axis. Weights of the structural components were estimated with the help of the CAD model and later confirmed with the physical vehicle. The x-axis was measured positive aft of the leading edge of the wing. The predicted C.G. locations from the CAD model are shown in Figure 5.4.
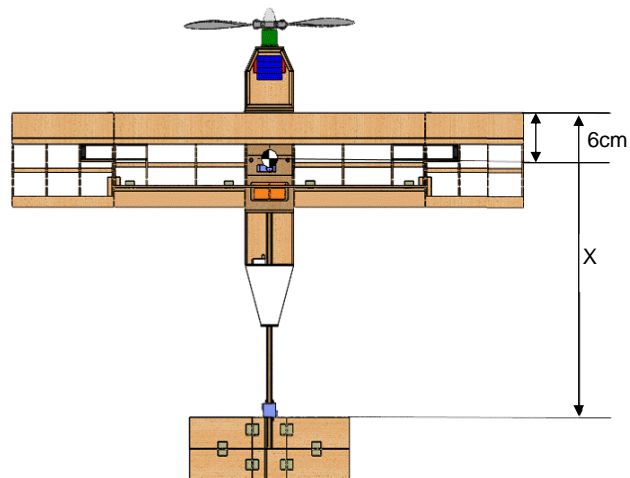
Figure 5.4: C.G. Location

Components	Weight (g)	CG Position (X-axis) (cm)	Moment (g-cm)
Wing	75	6.88	516
Fuselage	130	8.71	1132.3
Boom Rod	15	32.82	492.3
Empennage	11	52.94	582.34
Elevator Servo	9	47.17	424.53
Rudder Servo	9	47.11	423.99
Motor	76	-12.11	-920.36
Propeller	38	-14	-532
Receiver	15	16.5	247.5
Arming Plug	15	1.26	18.9
ESC	18	-5	-90
Receiver Battery	50	-5	-250
Aircraft Total	**461**	**4.44**	**2045.5**
Mission 1			
Aircraft Total	461	4.44	2045.5
Battery	230	9.14	2102.2
AUW	**691**	**6.00**	**4147.7**
Mission 2			
Aircraft Total	461	4.44	2045.5
Battery	230	8.8	2024
Payload (Puck x3)	510	6.15	3138.2
AUW	**1201**	**6.00**	**7207.7**
Mission 3			
Aircraft Total	461	4.44	2045.5
Battery	230	4.67	1074.1
Payload (Puck x 4)	680	7.51	5106.8
AUW	**1371**	**6.00**	**8226.4**

Table 5.4: Weight and Balance Chart

5.5 FLIGHT AND MISSION PERFORMANCE:

The final mission performance estimates were determined from the mission model for the selected propulsion system. These have been listed in tables 5.5 (a) and 5.5 (b). Lap times were calculated using the lap trajectories shown in figure 4.6. The projected mission scores have also been tabulated. It is noted that the analysis is likely optimistic, and true lap times would be verified after flight testing.

Parameter	Mission 1	Mission 2	Mission 3
C_{Lmax}	1.342		
$C_{Lcruise}$	0.396		
V_{cruise}	23	21	20
V_{stall}	9	9.7	10
RPM	8800	8800	8800
(T/W)cruise	0.51	0.31	0.27
Power Consumption (W)	190	216	225

Table 5.5 (a): Flight Performance Characteristics

Mission Parameter	Mission 1	Mission 2	Mission 3
Laps flown	3	3	6
Total time flown (s)	110	130	270
All-up weight (g)	691	1201	1371
Current draw (A)	15	17	17
Static thrust (g)	1100	1100	1100
Mission Score	1	1.3986	4.4
Estimated RAC	90.06	90.06	90.06

Table 5.5 (b): Mission Performance Characteristics

The mission and flight performance parameters underwent changes from their initial estimates made during the preliminary design stage. Some of the parameters changed insignificantly whereas there were corrections made to other performance estimates. A change was observed in the power input requirement of the propulsion system. An overestimated 220W of power consumption in the preliminary stage was corrected to 200W.

5.6 DRAWING PACKAGE:

The following six pages constitute the drawing package of the aircraft. The first sheet has the three-view diagram of the aircraft with relevant dimensions. The second sheet shows the structural arrangement of all major components. The third sheet displays the sub-systems layout and location. The fourth sheet shows detail views of all the mechanisms used. The fifth sheet has the three-view diagram of the tube with relevant dimensions. The sixth sheet displays the payload arrangement for the internal payloads i.e. the ice hockey pucks and illustrates the transition of the aircraft from flight condition to the stowed condition followed by insertion into the tube.
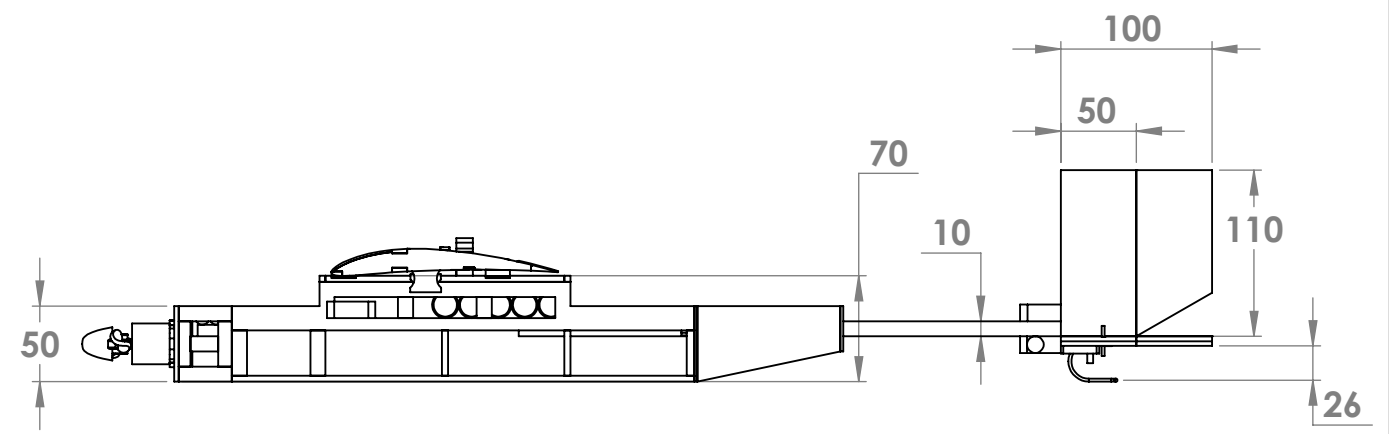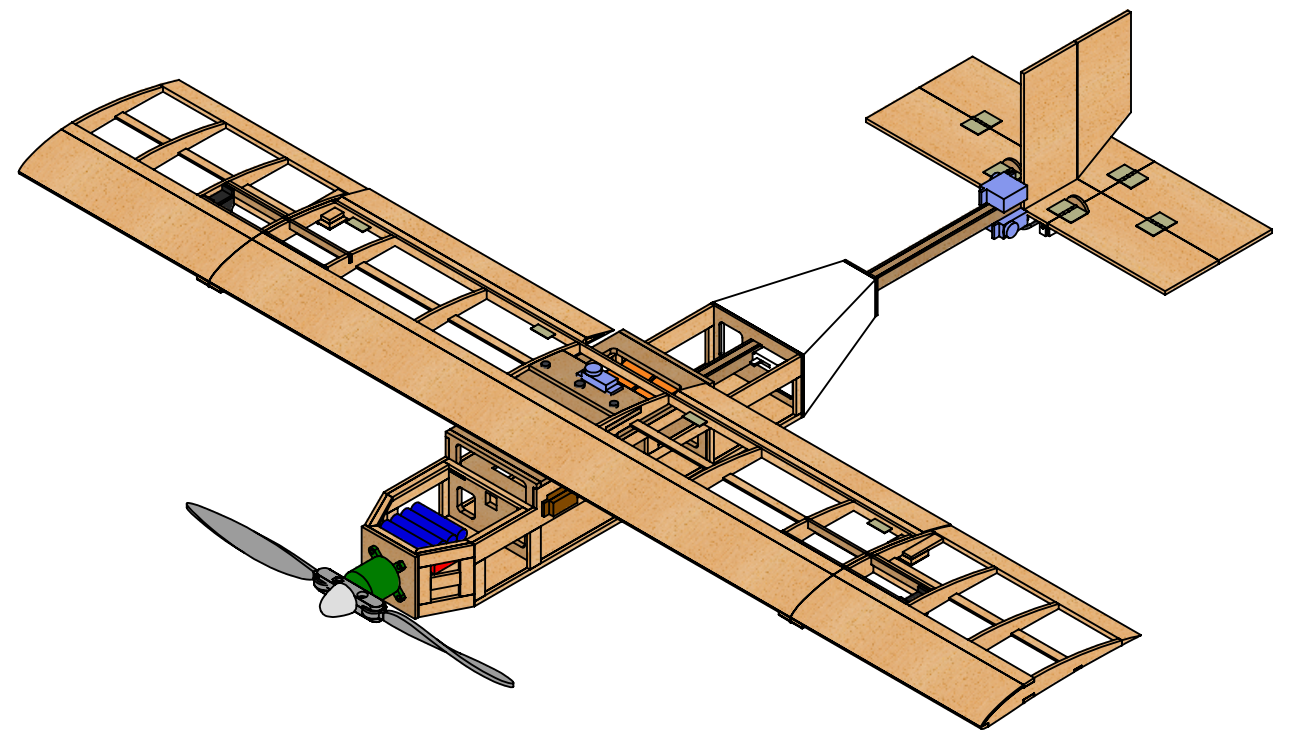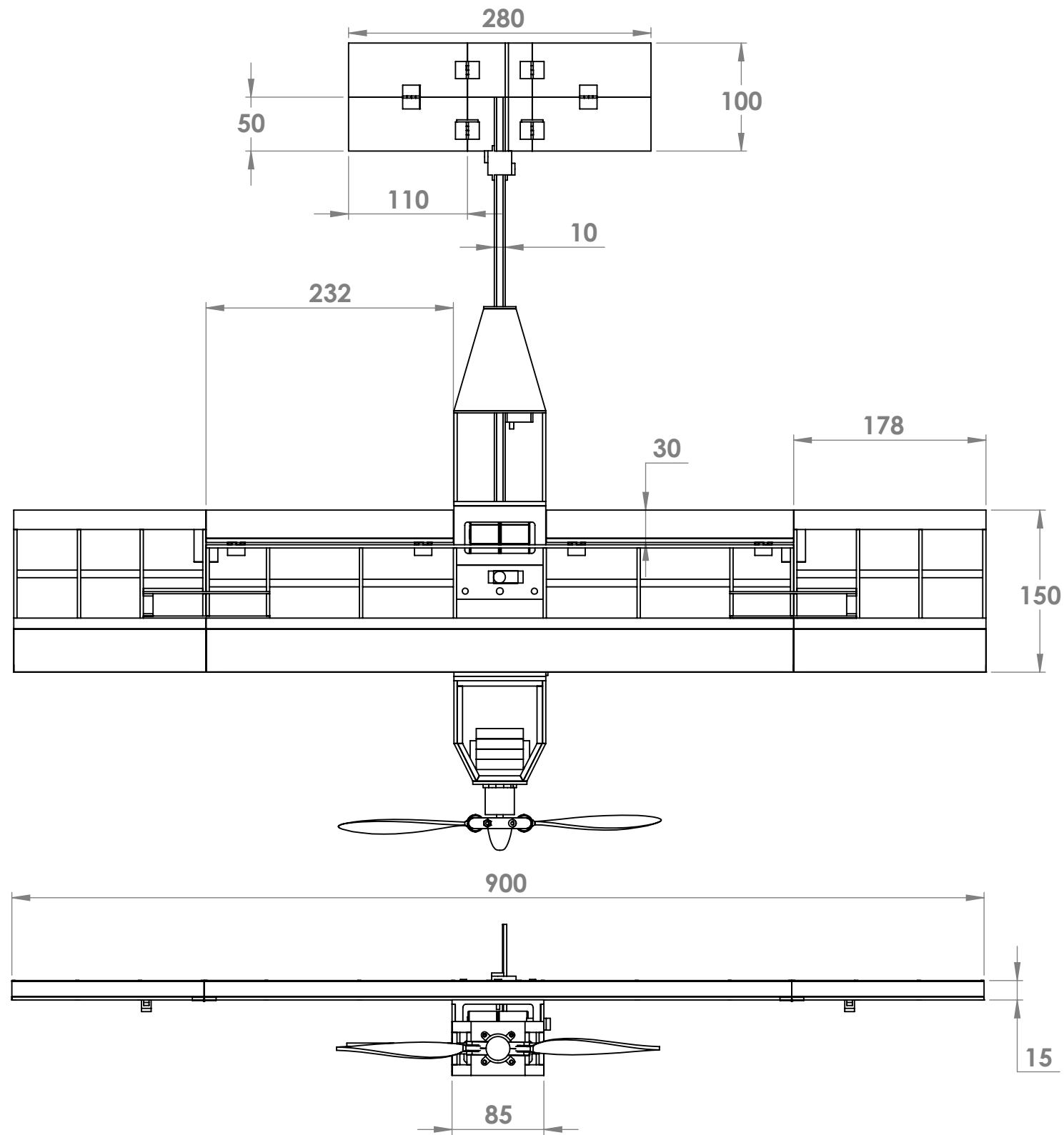
NOTE: Covering film and payload flaps removed for greater clarity.

VEERMATA JIJABAI TECHNOLOGICAL INSTITUTE
CESSNA-RAYTHEON-AIAA DESIGN/BUILD/FLY 2017

| SIZE **B**	Comment: All dimensions are in mm	**AIRCRAFT THREE VIEW DRAWING**
PROPRIETARY AND CONFIDENTIAL THE INFORMATION CONTAINED IN THIS DRAWING IS THE SOLE PROPERTY OF TEAM VAYUPUTRAS, VJTI. ANY REPRODUCTION IN PART OR AS A WHOLE WITHOUT THE WRITTEN PERMISSION OF TEAM VAYUPUTRAS, VJTI IS PROHIBITED.		SCALE 1:5
	13-02-2017	SHEET 1 OF 6

PARTS LIST

ITEM	PART NAME	MATERIAL	QTY
1	Motor Mount	Aero Ply	1
2	Inclined Wall Assembly	Balsa	2
3	Side Wall Assembly	Balsa	2
4	Bulkhead	Aero Ply	4
5	Wing Mounting Plate	Aero Ply	1
6	Battery Seat	Aero Ply	1
7	Fuselage Base	Balsa	1
8	Fairing	Foam	1
9	Boom Rod	Aero Ply	1
10	Horizontal Tail	Balsa	1
11	Vertical Tail	Balsa	1
12	Rib	Balsa	16
13	Leading Edge Spar	Balsa	3
14	Main Spar	Balsa	6
15	Trailing Edge Spar	Balsa	3
16	Torsion Webbing	Balsa	15
17	Sheeting	Balsa	3
18	Aileron	Balsa	2
19	Jaw	Aero Ply	4
20	Landing Gear	Stainless Steel	1
21	Guide for Spring Loaded Latch	PLA	3
22	Side Release Buckle	Acetal Polymer	2
23	Wing Rotation Bolt	Stainless Steel	1
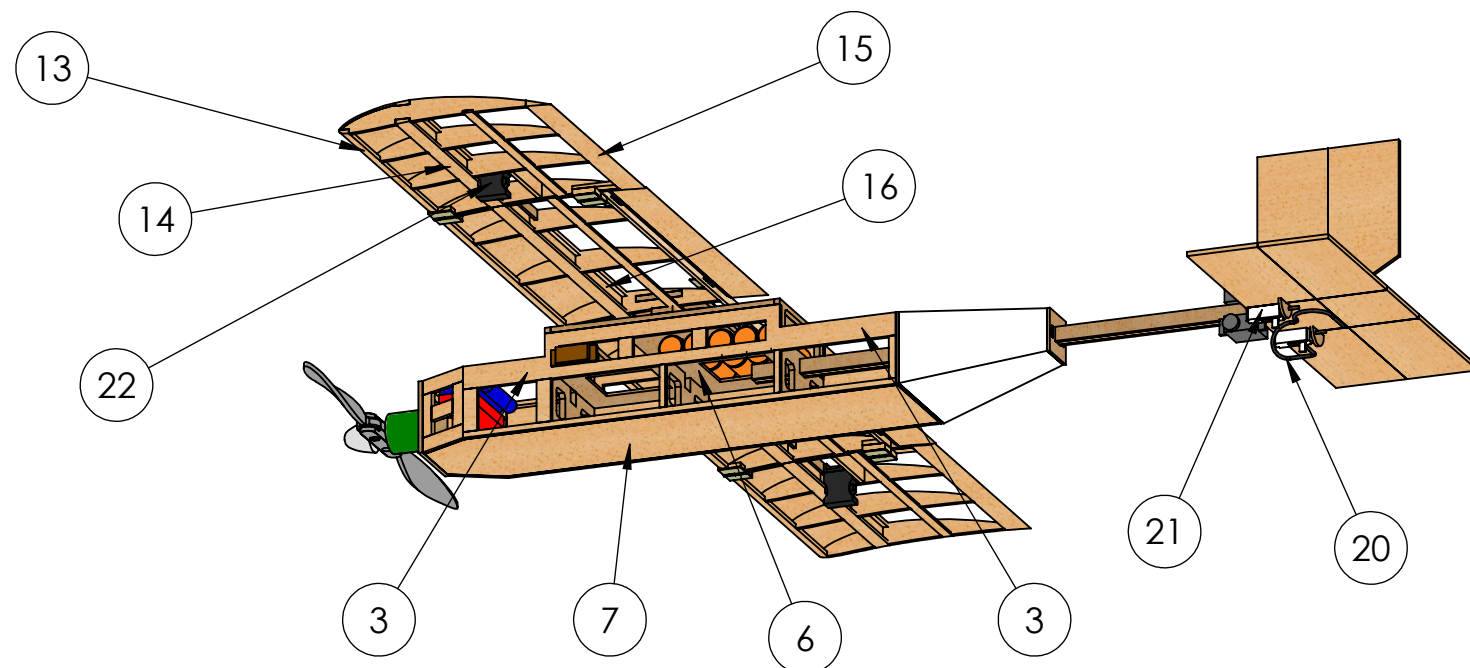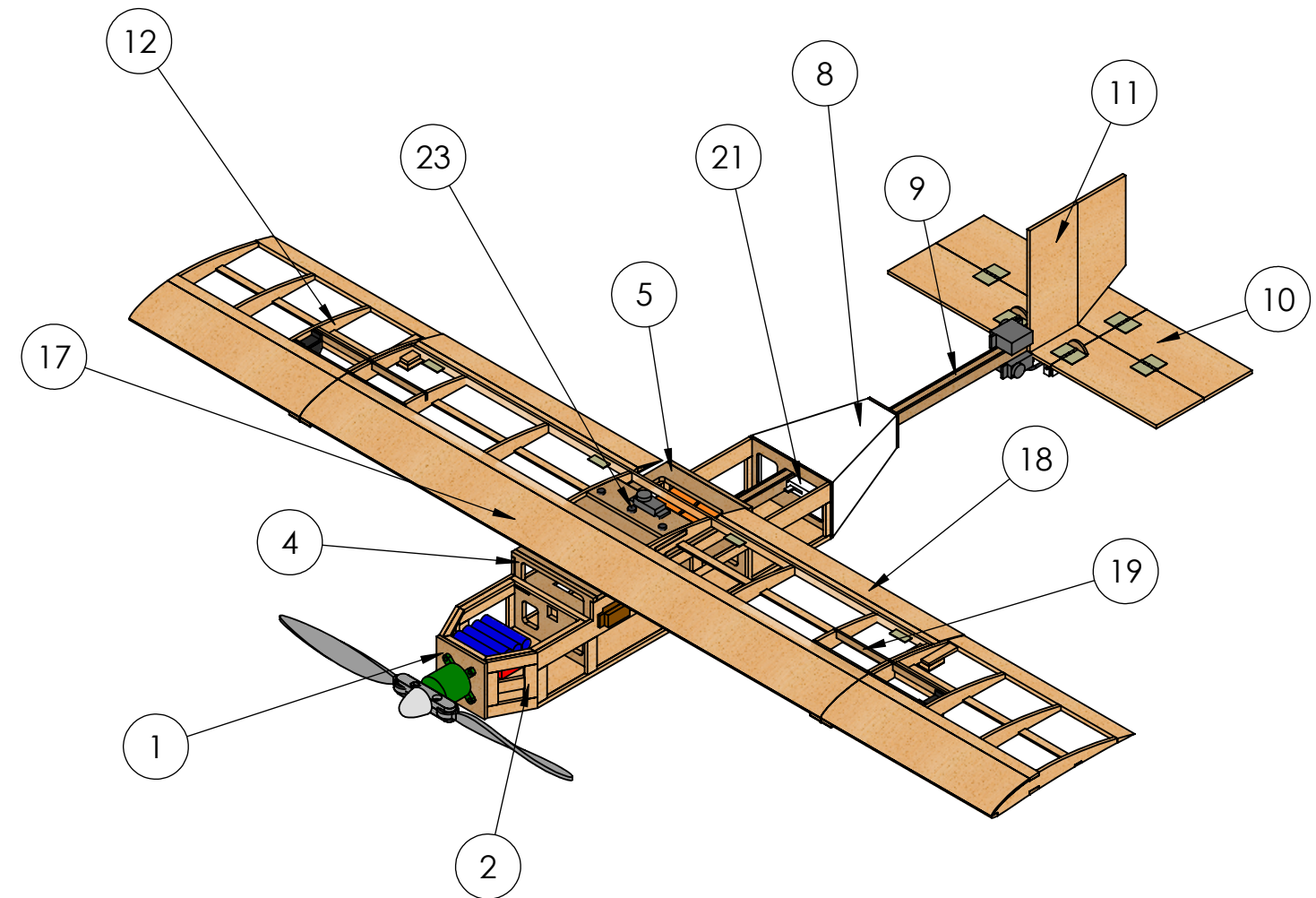
NOTE: Covering film and payload flaps removed to show the structure.

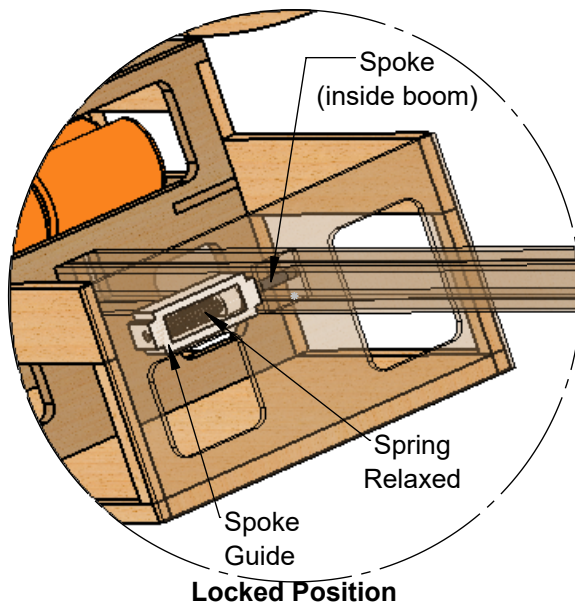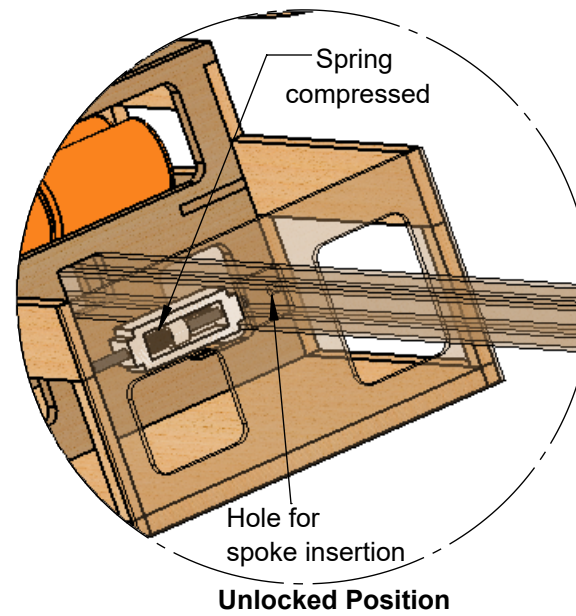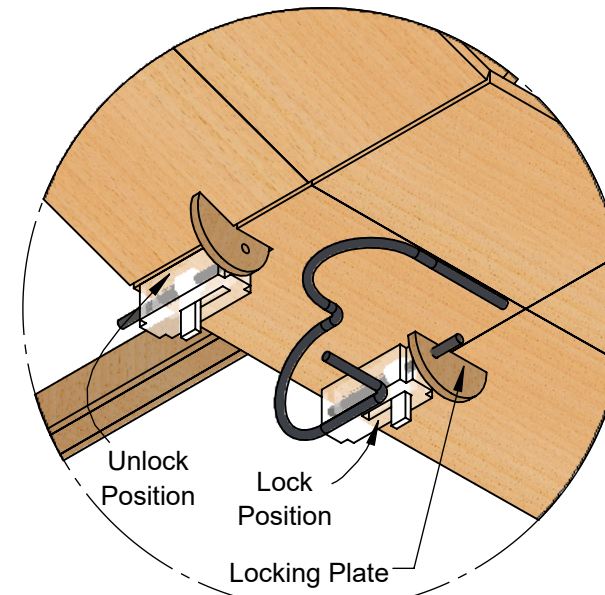**VEERMATA JIJABAI TECHNOLOGICAL INSTITUTE**
CESSNA-RAYTHEON-AIAA DESIGN/BUILD/FLY 2017

SIZE
B

STRUCTURAL VIEW DRAWING

SCALE 1:5

13-02-2017   SHEET 2 OF 6

SYSTEMS LIST

ITEM NO.	COMPONENT	DESCRIPTION	QTY
1	Propeller Adapter	M4 Adapter	1
2	Propeller Blade	APC 11X8F	2
3	Propeller Hub	LPFH3	1
4	ESC	Turnigy 30A	1
5	Motor	MT2216 1100Kv	1
6	Receiver Battery	4 KAN 700 mAh cells	1
7	Arming Plug	K - Nureka	1
8	Elevator Servo	HobbyKing	1
9	Rudder Servo	HobbyKing	1
10	Aileron Servo	HobbyKing	1
11	Battery	12 ELITE 1500 mAh cells	1
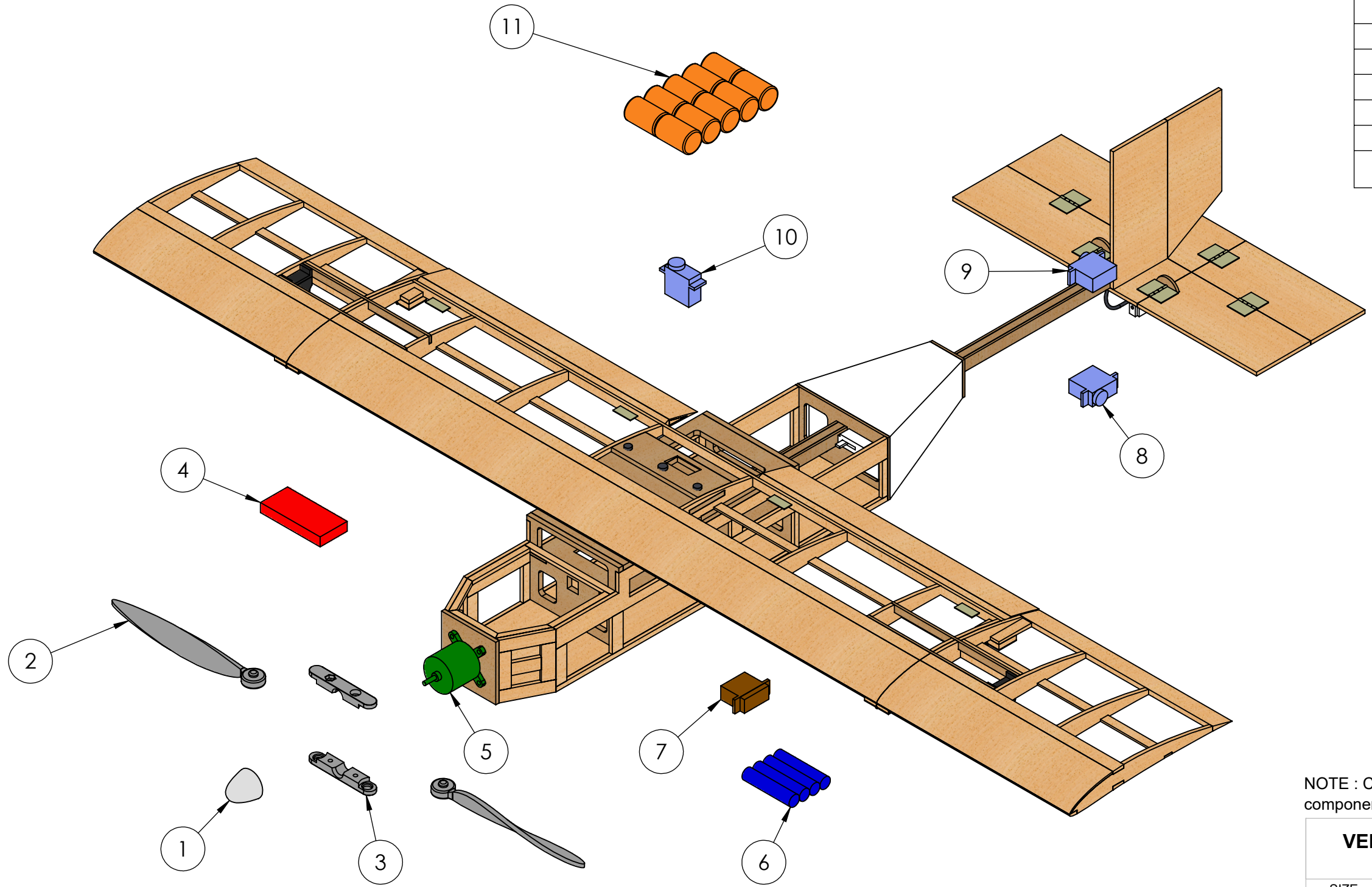
NOTE : Covering film and paylod flaps removed to show sub-system components.

VEERMATA JIJABAI TECHNOLOGICAL INSTITUTE
CESSNA-RAYTHEON-AIAA DESIGN/BUILD/FLY 2017

SIZE
B

AIRCRAFT SUBSYSTEM DRAWING

SCALE 1:3

13-02-2017   SHEET 3 OF 6

Wing Rotation Mechanism

Spring Loaded Bolt

Pivoting Bolt

DETAIL A
SCALE 1 : 1.5

Boom Locking Mechanism
SCALE 1:1.5

Spoke (inside boom)

Spring Relaxed

Spoke Guide

Locked Position

Spring compressed

Hole for spoke insertion

Unlocked Position

HT Folding Mechanism
SCALE 1:1.5

Unlock Position

Lock Position

Locking Plate

Wing Front View
SCALE 1:6

A

Wing Folding Mechanism
SCALE 1:3

Hinge

Buckle F

Jaw

Buckle M

Wing Rotation Mechanism

HT Folding Mechanism

Boom Locking Mechanism

Wing Folding Mechanism

SCALE 1:5

NOTE: Some Components have not been shown for greater clarity.

VEERMATA JIJABAI TECHNOLOGICAL INSTITUTE
CESSNA-RAYTHEON-AIAA DESIGN/BUILD/FLY 2017

SIZE
B

MECHANISMS FOR STOWED POSITION

SCALE VARIES

13-02-2017   SHEET 4 OF 6

PARTS LIST

ITEM	PART NAME	MATERIAL	QTY
1	Lid	Aero Ply	2
2	Stringer	Balsa	8
3	Former	Aero Ply	10
4	Packing	Styrofoam	4

720

⌀160
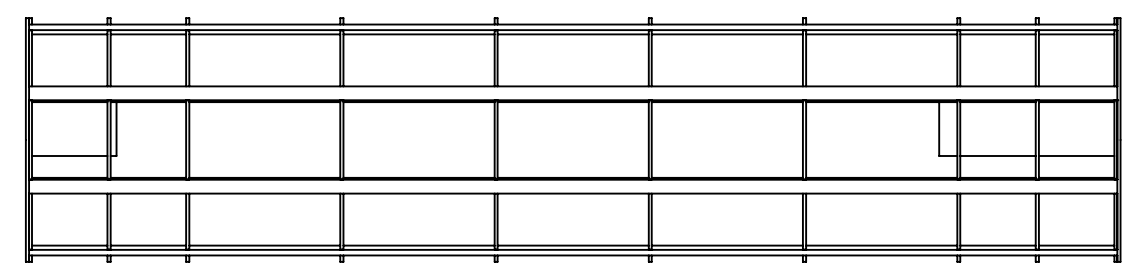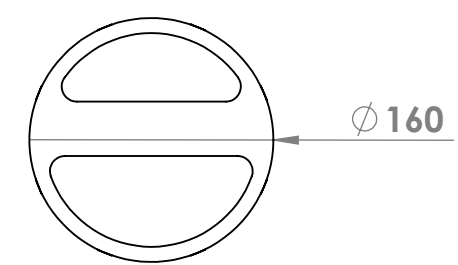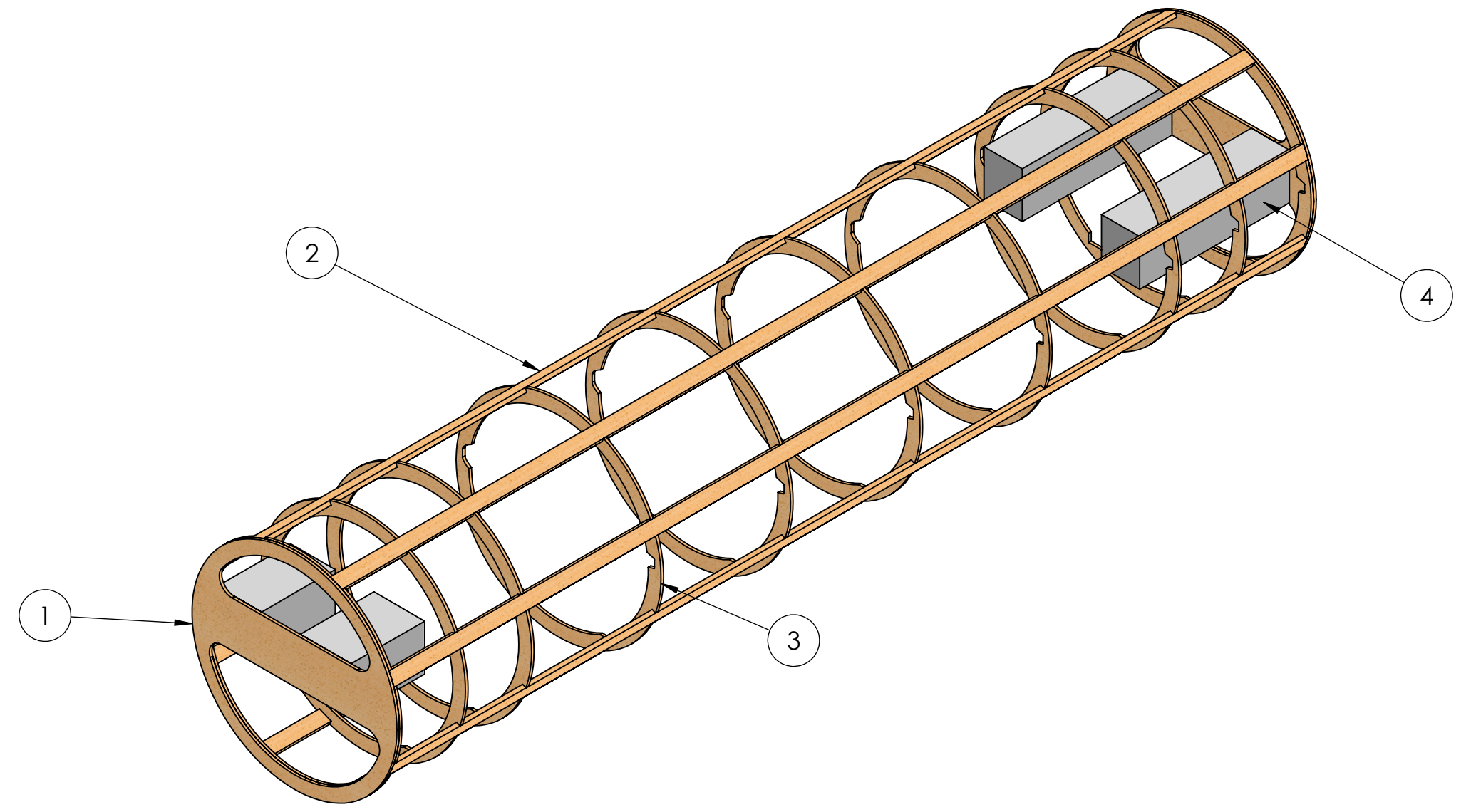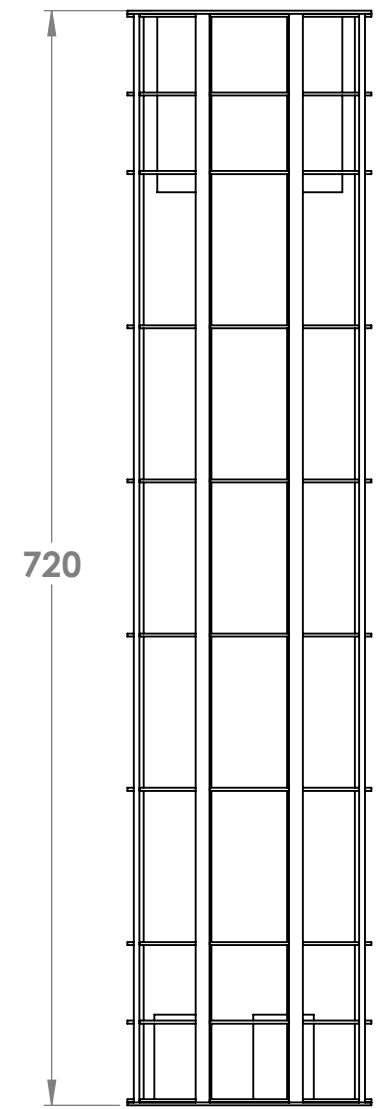
NOTE: Covering film has not been shown for greater clarity.

VEERMATA JIJABAI TECHNOLOGICAL INSTITUTE
CESSNA-RAYTHEON-AIAA DESIGN/BUILD/FLY 2017

SIZE **B**	Comment: All dimensions are in mm	**TUBE THREE VIEW AND STRUCTURAL VIEW DRAWING**

SCALE 1:5

13-02-2017 | SHEET 5 OF 6

Coroplast flaps x5

Puck x4

Payload accomodation
SCALE 1:5

$\varnothing 76.20$

25.40

Aircraft Insertion

Lid x2

Styrofoam packing on lids

Former

Stringer

Wing Folding

Wing Rotation

Boom Retraction

HT and Propeller Folding

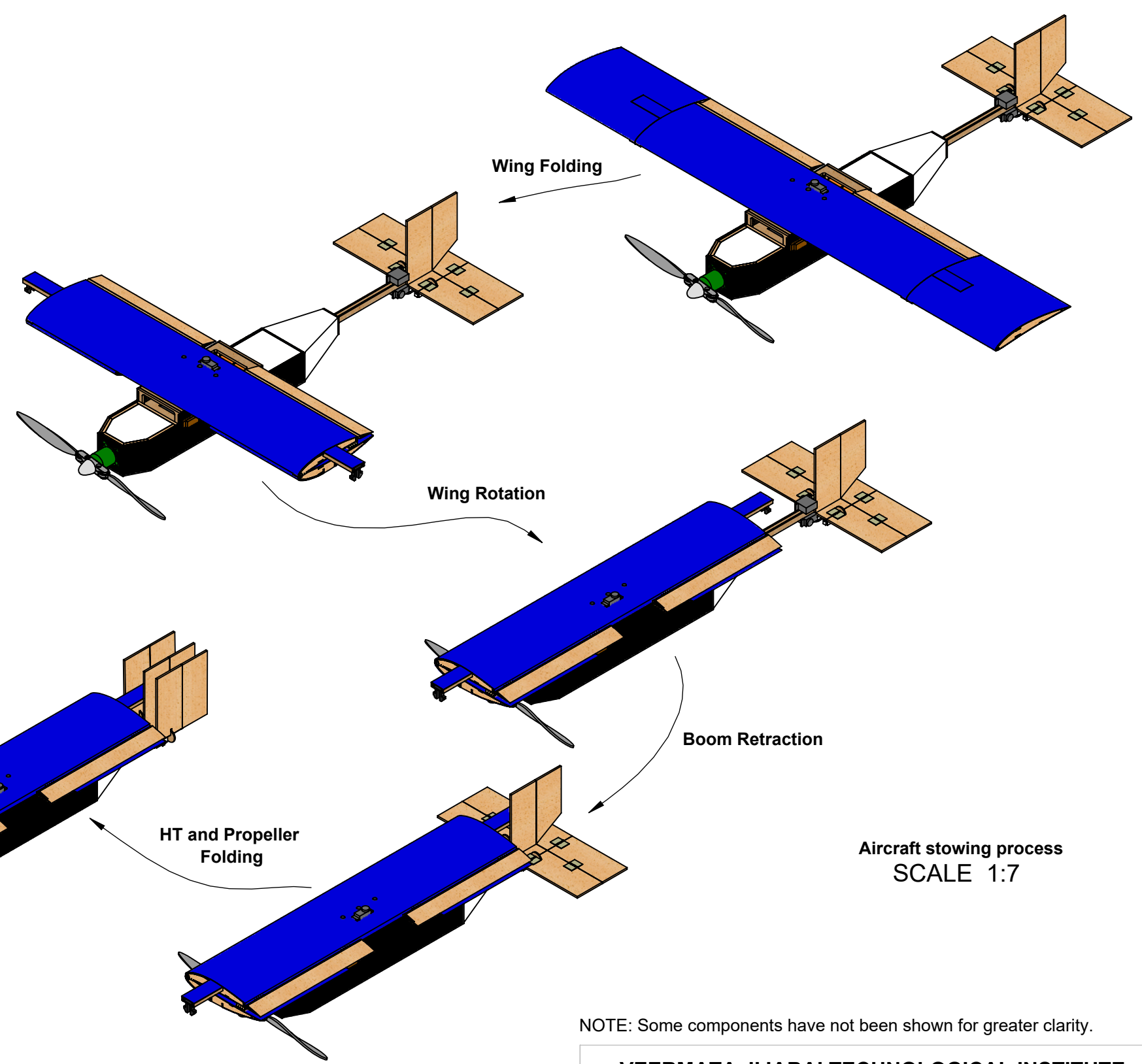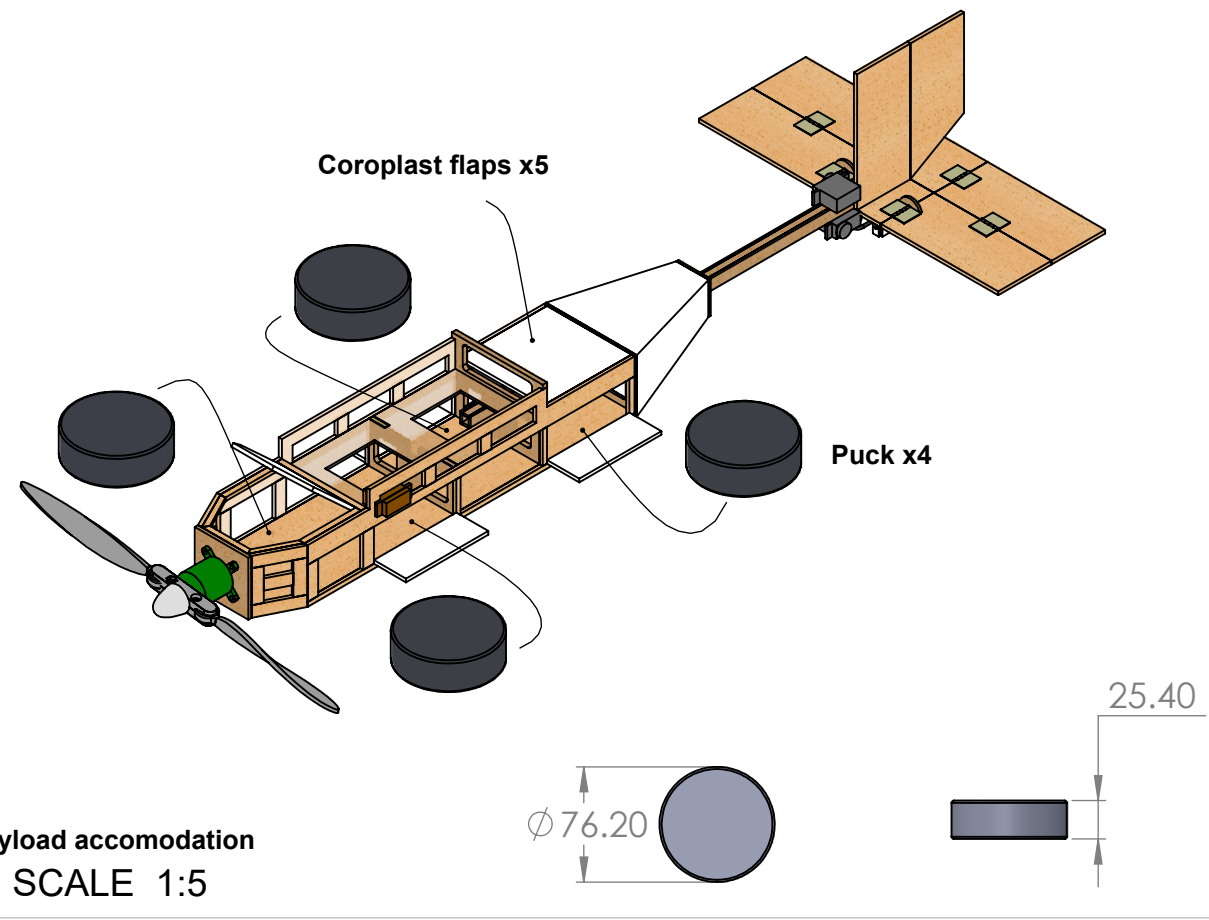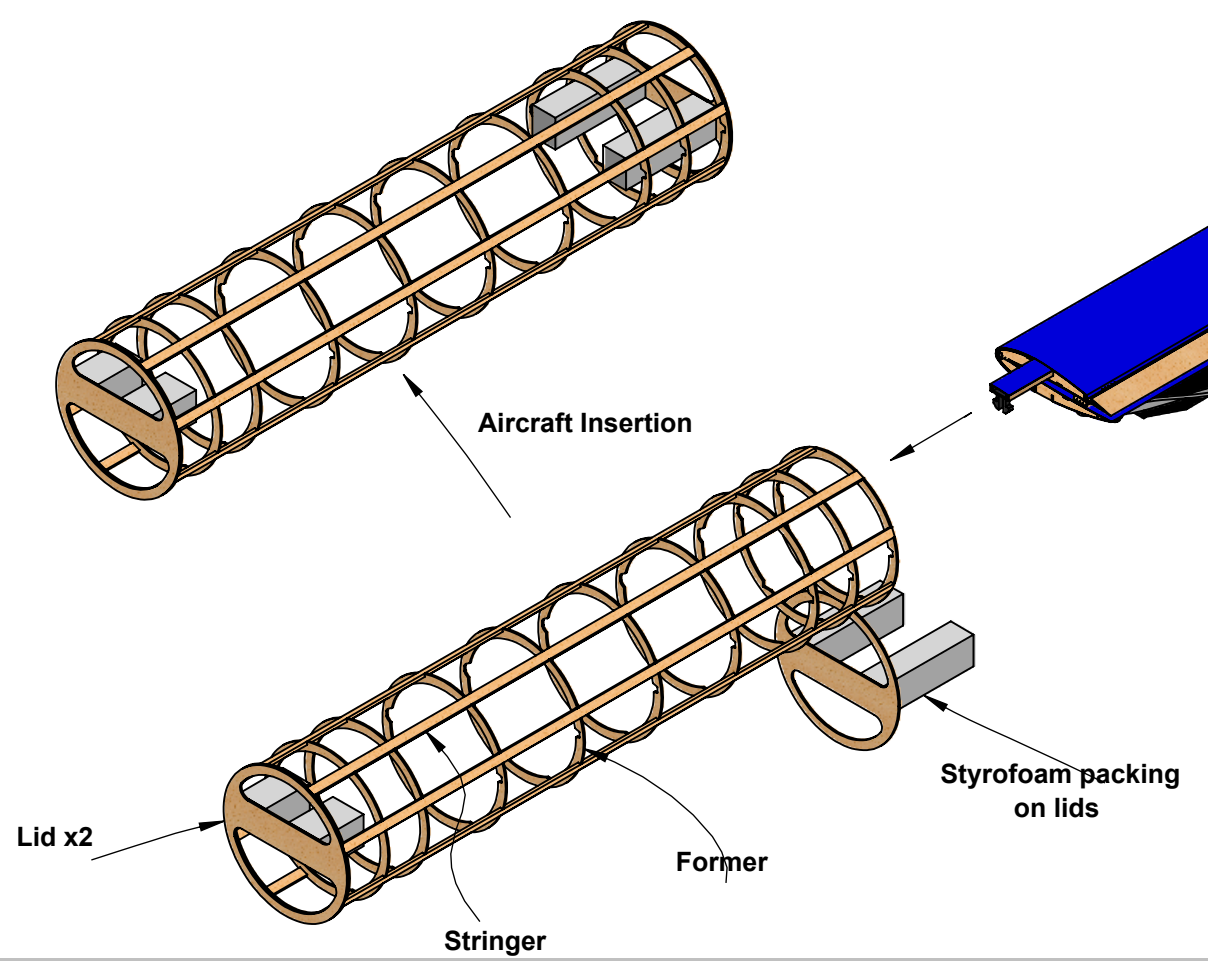**Aircraft stowing process**
SCALE 1:7

NOTE: Some components have not been shown for greater clarity.

VEERMATA JIJABAI TECHNOLOGICAL INSTITUTE CESSNA-RAYTHEON-AIAA DESIGN/BUILD/FLY 2017	
SIZE **B**	Comment: All dimensions are in mm	**PAYLOAD AND STOWED AIRCRAFT INSERTION DRAWING**

SCALE VARIES

13-02-2017   SHEET 6 OF 6

6. MANUFACTURING PLAN AND PROCESSES:

The team aimed at fabricating a competitive aircraft and a sufficiently strong tube. The final manufacturing process selected represented the best combination of weight, reparability, ease of manufacturing, team experience with the process, and cost.

6.1 PROCESS INVESTIGATION METHOD:

The team had greater experience building balsa wood aircrafts. However, there were other feasible manufacturing processes that could be superior, given that we were building a tube for the first time. These processes were put up against the built up balsa technique using Figures of Merit considering the below listed parameters:

Strength and Weight – A light build always helps in enhancing performance. As it features in the RAC, minimizing the weight will only increase the expected scores. The tube must sustain three drops in the ground mission while the aircraft fuselage base must bear the brunt of the landing.

Reparability – With omnipresent possibilities of an accident or crash, the ease with which repairs can be made must be accounted for.

Manufacturability - The process must allow easy transformation of the on-paper design into high performing models.

Experience – It holds the key to ensure accurate reproduction of plans. However, the team's curiosity did not inhibit it from looking for new techniques and methodologies.

Cost and Availability– The team had limited resources to work with and hence it was considered as a necessary parameter. Given the team's focus on performing well, it was not a dominant factor.

The following processes were looked at for the respective components:

6.1.1 Wing:

FOM	Weightage	Balsa build	Solid foam and composite
Weight	10	1	0
Strength	9	1	1
Manufacturability	8	1	1
Reparability	6	1	0
Experience	4	1	0
Cost and Availability	2	0	1
Total	**39**	**37**	**19**

Table 6.1.1: Wing manufacturing FOM chart

(i) Solid Foam with Composites and Ply Reinforcements: Solid foam is cut into the wing shape using a CNC (Computer Numerically Controlled) router or a hot wire. The wing is then sanded to correct all the defects. Next, the structure is reinforced using carbon fibre rods as the main load-bearing member.

(ii) Balsa and Aero-Ply structure: The ribs and spars are laser cut and assembled on a graph paper

layout for precise and accurate results. Torsional webbings are later inserted. The ailerons are made of trailing rib sections covered with 1 mm balsa skin sheets. Monokote is used as the covering film for providing shape and strength. Cyanoacrylate is used as an adhesive.

6.1.2 Fuselage and Boom:

(i) <u>Moulded composite structure:</u> The fuselage is moulded into shape using a forming process while the boom is made of carbon fibre.

(ii) <u>Balsa and Aero-Ply structure</u>: All parts are laser cut and assembled on a graph paper for a precise and accurate build. Aero-Ply is used only in high stress concentration areas. An aft fairing is built out of depron. The adhesives used are cyanoacrylate and epoxy resin.

FOM	Weightage	Balsa build	Moulded composite
Weight	10	1	0
Strength	9	1	1
Manufacturability	8	1	1
Reparability	6	1	0
Experience	4	1	0
Cost and Availability	2	0	0
Total	**39**	**37**	**17**

Table 6.1.2: Fuselage and Boom manufacturing FOM chart

6.1.3 Tube:

(i) <u>Moulded composite structure:</u> The tube is moulded into shape using fibreglass while the lids are made of plastic. Weight reduction slots are cut along the curved surface. Finally, a Monokote covering film is applied to make the tube water tight.

(ii) <u>Balsa and Aero-Ply structure:</u> This follows a basic aero-ply former and balsa stringer assembly. Styrofoam will be used only in selected areas as packing material to cushion the impact sustained when the tube is dropped. Monokote is applied as a covering film for providing shape and strength. The adhesive used is cyanoacrylate.

FOM	Weightage	Balsa build	Moulded composite
Weight	10	1	0
Strength	9	1	1
Manufacturability	8	1	1
Reparability	6	1	0
Experience	4	1	0
Cost and Availability	2	0	-1
Total	**39**	**37**	**15**

Table 6.1.3: Tube manufacturing FOM chart

From the above FOM charts it is evident that a tube and aircraft built out of balsa and aero-ply is most preferred. This choice will give us a structure with a higher strength to weight ratio. The wealth of experience the team possesses in using these materials would also help in their procurement, handling and repair.

6.2 MATERIAL AND PROCESS SELECTION FOR MAJOR COMPONENTS:

The basic balsa and aero-ply structure was optimized further with the intention of making it as compact as possible, as light as possible and have easy incorporation of the mechanisms, all without compromising its structural integrity. The techniques utilized have been summarized below:

Material distribution for the aircraft and tube	
Manufacturing Component	**Material**
Principal material	Balsa wood and aero-ply
Strengthening material	Aero-ply
Packing material	Styrofoam
Adhesive	Cyanoacrylate and epoxy-resin
Covering Film	Monokote

Table 6.2: Built-up balsa manufacturing technique

Selective Use of Materials: Balsa wood varies significantly in density and strength. Hence, all balsa sheets were segregated on the basis of weight and only the lightest and the hardest were laser-cut for component manufacturing. Tube packing was accomplished using Styrofoam, and the fairing was fabricated from light-weight Depron.

A jigsaw assembly: Balsa side walls were first glued to a balsa base. Aero-ply bulkheads, battery seat and wing seat were provided with notches. This allowed quick assembly and support for the side walls.
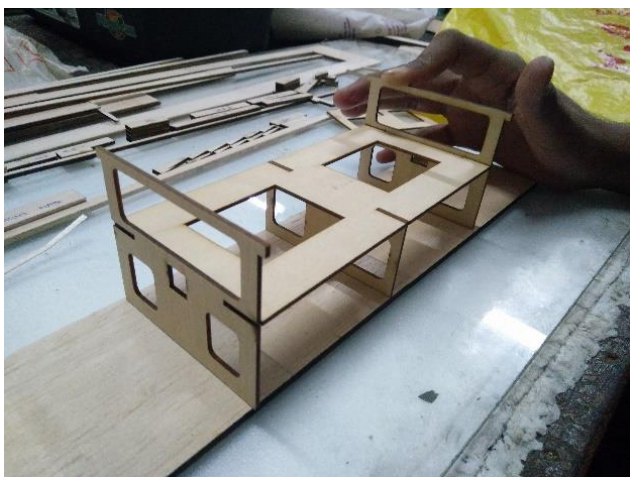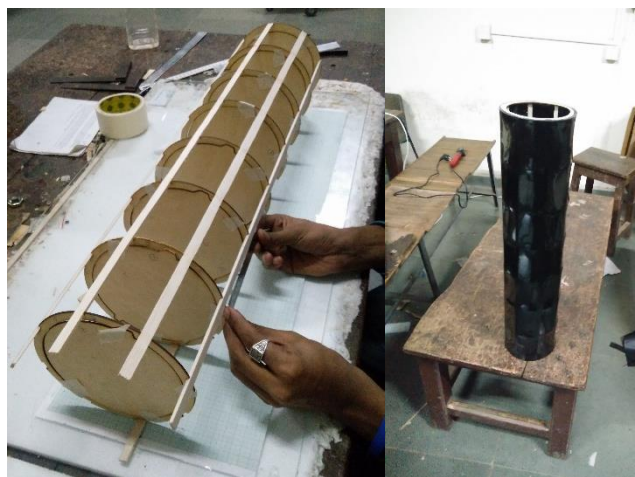

Figure 6.2 (a): Assembly of fuselage parts

Figure 6.2 (b): Tube assembly, and after coating

In the tube, balsa stringers were glued into slotted aero-ply formers using cyanoacrylate. Appropriate cuts were also made in the formers for smooth insertion of the wing and fuselage. Monokote was later used as a covering film. This added torsional and flexural rigidity and made the tube water tight.

Aero-ply reinforcement: Every component made from aero-ply comprised two of its 2mm sheets glued in orthogonal directions. As a result, directional dependence of stiffness and strength was greatly reduced. In the tube, each former was placed with its fibre lines at a relative angle of 45^0. There being ten such formers – the tube gained all-round strength.

Figure 6.2 (c): Weight reduction slots

Weight reduction slots: Lightening holes were made in all bulkheads, the battery seat and the wing seat. This helped in shedding material mass without losing strength and also provided paths for wires connecting the electronic components.

3-D Printing: The guides for the spring-loaded latch were made using additive manufacturing techniques. This allowed quick fabrication of a light custom component.
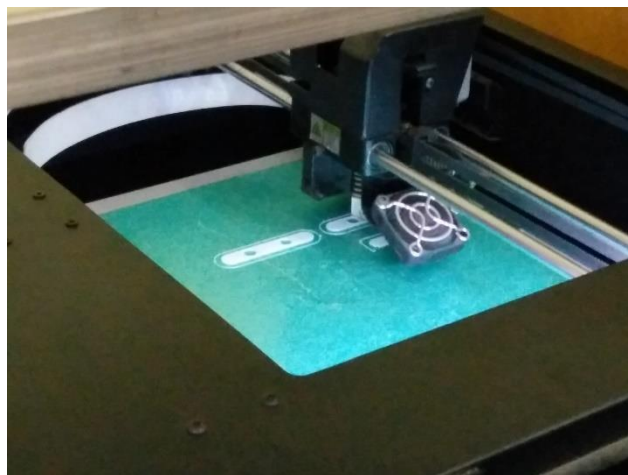

Figure 6.2 (d): 3D Printing of mechanism parts

6.3 MANUFACTURING MILESTONE CHART:

The team prepared a separate schedule for manufacturing to ensure that construction of the aircraft and the tube proceeded sequentially and in a systematic manner. Certain deadlines were set to ensure that an

appropriate amount of time is allotted for each task. In the milestone chart shown below, the team's expected and actual progress has been depicted.
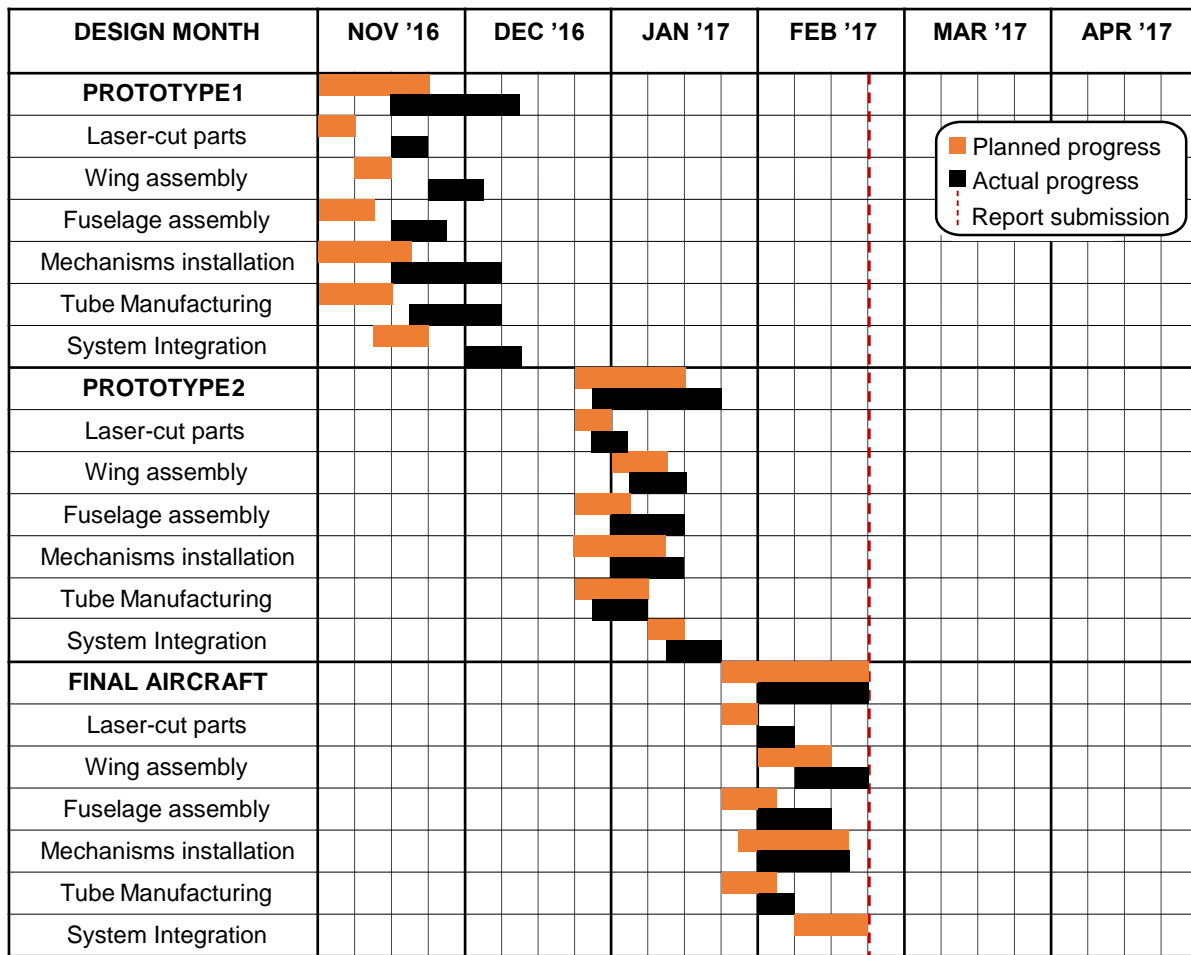
DESIGN MONTH	NOV '16	DEC '16	JAN '17	FEB '17	MAR '17	APR '17
PROTOTYPE1						
Laser-cut parts						
Wing assembly						
Fuselage assembly						
Mechanisms installation						
Tube Manufacturing						
System Integration						
PROTOTYPE2						
Laser-cut parts						
Wing assembly						
Fuselage assembly						
Mechanisms installation						
Tube Manufacturing						
System Integration						
FINAL AIRCRAFT						
Laser-cut parts						
Wing assembly						
Fuselage assembly						
Mechanisms installation						
Tube Manufacturing						
System Integration						

Legend: ■ Planned progress (orange) ■ Actual progress (black) ┊ Report submission

Figure 6.3: Manufacturing Milestone Chart

7. TESTING PLAN:

7.1 TESTING OBJECTIVES AND SCHEDULE:

A comprehensive test plan was prepared for the following purposes:

1) Validating and improving choices made in structural design and overall propulsion.

2) Improving flight qualities and performance through flight testing of each prototype.

3) Testing the reliability and ease of operation of various mechanisms by simulating the ground mission in the prototyping stage.

4) Integration of the tube and aircraft designs.

Results from testing highlighted areas of improvement and direction for the final design. The testing was divided into three main sections:

7.1.1 Propulsion:

This involved testing of different combinations of motor, propeller and battery under static and dynamic conditions.

7.1.2 Structural:

Structural testing of all major components was carried out. The ground mission was also simulated in a series of drops of the tube carrying the aircraft.

7.1.3 Mechanisms:

The various mechanisms that were implemented: wing rotation, extension of the tail boom, folding of wing sections and HT were operated and checked in the lab as well as under flight conditions.

The auxiliary electronics i.e. the servos, the receiver battery and the arming plug were also tested. The testing schedule is shown in figure 7.1. It depicts planned and actual progress till the date of report submission.
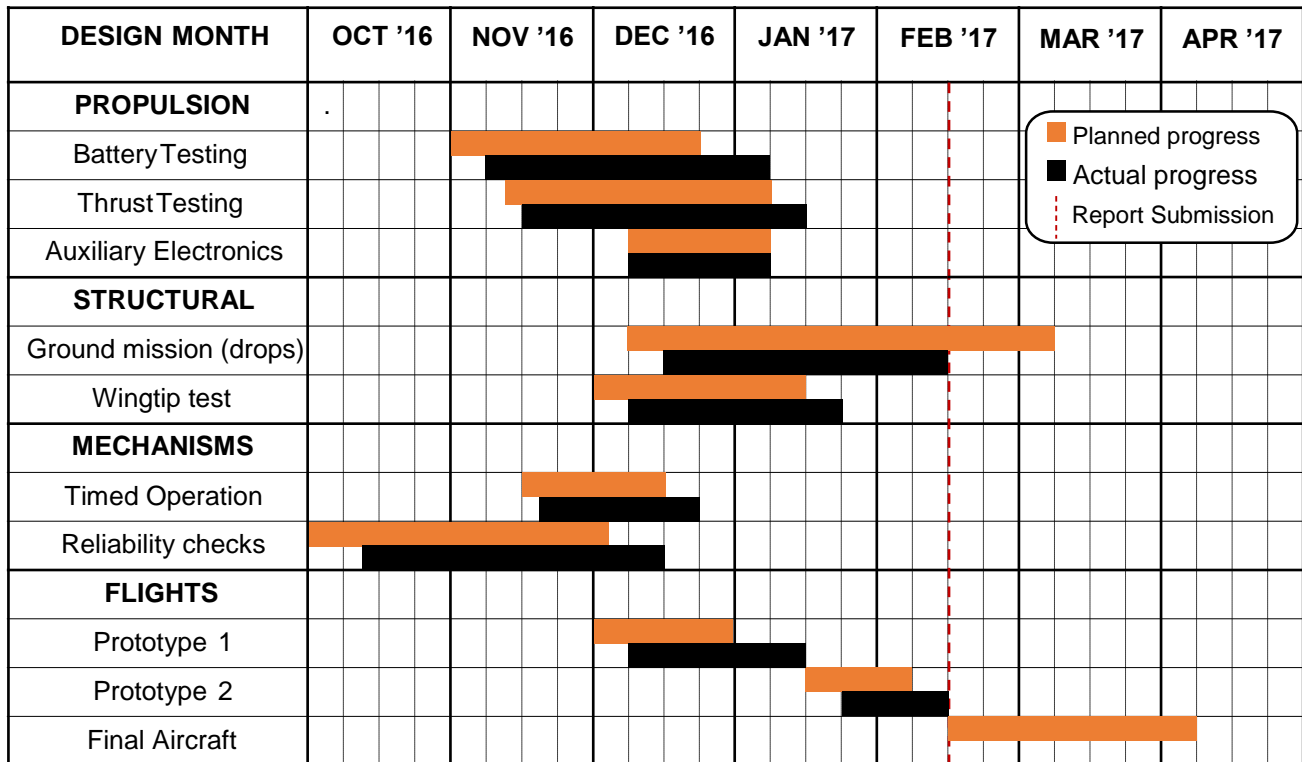
DESIGN MONTH	OCT '16	NOV '16	DEC '16	JAN '17	FEB '17	MAR '17	APR '17
PROPULSION							
Battery Testing							
Thrust Testing							
Auxiliary Electronics							
STRUCTURAL							
Ground mission (drops)							
Wingtip test							
MECHANISMS							
Timed Operation							
Reliability checks							
FLIGHTS							
Prototype 1							
Prototype 2							
Final Aircraft							

Figure 7.1: Testing Schedule Milestone Chart

7.2 STRUCTURAL TESTING:

7.2.1 Wing:

The wing spars were made discontinuous in order to allow wing folding. Thus, it was all the more important to simulate in-flight loading conditions on the wing to check integrity of the buckle mechanism and the wing as a whole.

Wing loading test:

The wing was progressively loaded from 0.7 kg to 3.5 kg. Support was provided only in the centre section. Sand bags were used as weights here. The deflection of the leading edge of the wing was measured for each trial and load at failure was noted.

Figure 7.2.1 (a): Wing loading test

Wing tip test:

In its maximum all up weight condition (mission 3 payload), the aircraft was lifted by the wing tips alone. This helped evaluate its structural performance against the greatest loading it may experience during the flight missions. One such test is shown in the figure below:
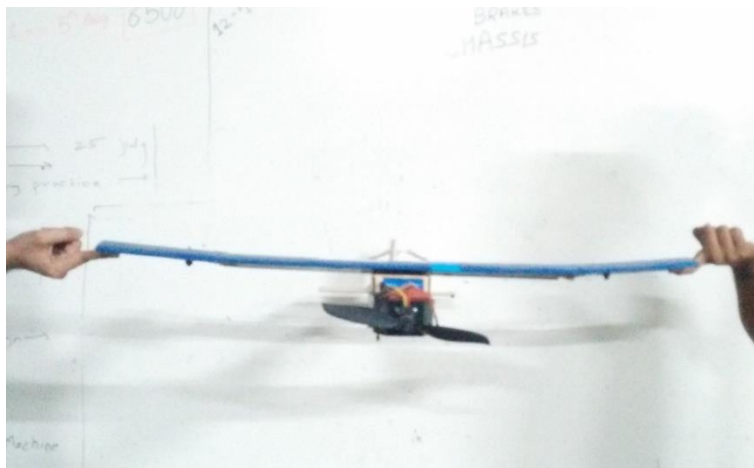
Figure 7.2.1 (b): Wing tip test

7.2.2 Tail Boom:

The tail skid will transmit an impact load to the HT at the time of landing. Hence, a significant moment will act on the boom, causing it to bend at the last bulkhead. To determine its failure point, a destructive test was conducted by securing one end of the boom and applying a measured moment from the free end.

7.2.3 Tube:

The aircraft was loaded to its maximum all up weight and loaded into the tube. The ground mission was then replicated and the number of drops before failure were noted. For the first few drops, no packing material was placed inside the tube to ascertain the exact locations where damage is likely to occur and

position the packing accordingly. The time required for removal of aircraft and transitioning it to flight-ready condition was also noted.

The structural testing for both the wing and the tube was conducted on their respective prototypes. Based on the results of these, the final structure of each was decided.

7.3 PROPULSION SYSTEM TESTING:

7.3.1 BATTERY TESTING:

OBJECTIVE:

To test the ideal discharge rate of the assembled battery packs keeping the endurance requirement in mind and verify the constant voltage per cell that can be provided by the battery after the initial drop.

The batteries were initially cycled through charging and discharging at constant current (0.3-0.5 A) to ensure they were at their optimum capacity. Fully charged battery packs were then discharged under load. The current draw was monitored through a wattmeter and the voltage readings were recorded at 10 second intervals. By altering the throttle setting on the transmitter in each run, the procedure was repeated at other constant discharge rates. This testing regime was executed for a number of times till a significant decrease in the battery voltage was observed and hence a specific limit was set on the number of charge-discharge cycles that the battery could sustain. Accordingly, backup battery packs were made.

7.3.2 THRUST TESTING:

Motor and propeller combinations shortlisted for the competition plane were tested with their respective battery packs. These were tested to get static thrust values for each mission. The thrust testing was carried out on a rig specially constructed for the purpose, as shown in figure 7.3.2. The motor was mounted on a rigid aluminium frame. Weights were loaded in the compartment below and the apparatus was placed on a weighing machine to record thrust. The wattmeter connected between the battery and ESC recorded power.
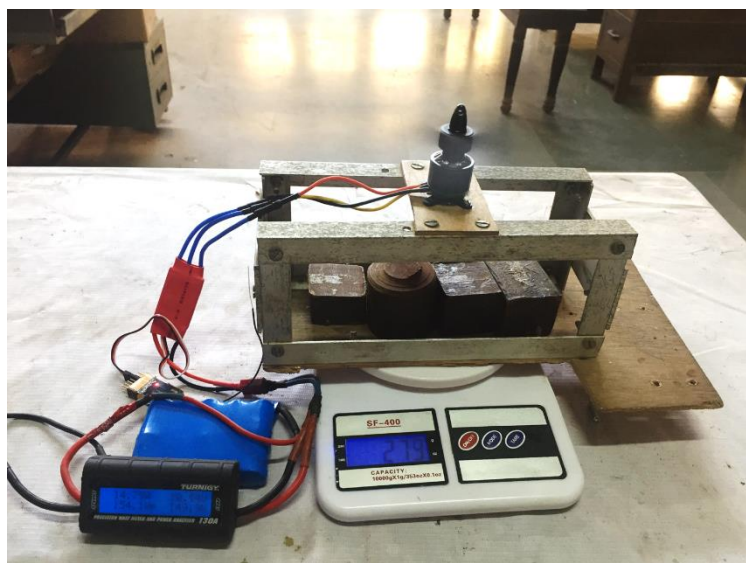

Figure 7.3.2: The thrust testing rig in operation

The data obtained was compared with the predictions of the APC database [5]. The results of the static thrust tests and the selected combination are detailed in section 8.1.

7.4 AUXILIARY ELECTRONICS TESTING:

7.4.1 RECEIVER BATTERY:

A receiver pack was sized to provide necessary voltage and capacity to the electronics systems for the duration of the missions, including preparation time before the flight. The selected receiver battery was tested during flights and also by actuating all the servos controlled by the receiver all at the same time for the entire estimated flight time.

7.4.2 ARMING PLUG:

Arming plugs of appropriate current rating were tested to ensure that they would not fail during the duration of the flight. To simulate the load on the arming plug in flight, it was attached to the static thrust test rig consisting of the selected battery, motor, propeller, and speed controller to ensure competition conditions were replicated as accurately as possible.

7.5 FLIGHT TESTING AND CHECKLISTS:

Initial flight testing started with basic maneuvers without payload to determine actual flying and handling qualities. The testing slowly progressed to heavier all-up weights and entire mission simulations. The flights in the scheduled time period were conducted with a view to accomplish the following objectives:

Test	Objective
Hand launch	Record velocity of hand launch and observe the trajectory of the aircraft post-launch
Wing	Ensure wing strength is sufficient for in-flight loads
Mechanisms	Check reliability of buckles, latches, bolts and the rigidity of surfaces equipped with mechanisms
Stability	Ensure tail surfaces are adequately sized to meet minimum stability criteria
Tail Boom	Check torsional and axial strength for tail forces
Landing	Verify aircraft can withstand forces of hard belly landing carrying full payload
Motor/Battery/Propeller	Optimize propulsion system for all mission profiles

Table 7.5 (a): Flight Test Sequence

The pre-flight checklist shown in table 7.5 (b) was made to ensure a primary level of safety for the aircraft as well as the pilots and the crowd in the vicinity. The checklist has been formed after years of field experience and witnessing a variety of pre-flight and in flight failures that could be avoided by a thorough inspection before the flight.

Date:___/__/____	Pilot:_____	Flight Number:___
General System Checks		

☐ Inspect for visual damage	☐ Payload secured
☐ Verify CG location within designed limits	☐ Propeller fastened to shaft
☐ Check wing, empennage & motor mounts	☐ Electronics secured
☐ Wing mounting bolt tightened	☐ Wing buckles fastened

Avionics and Propulsion

☐ Check main battery voltage	☐ Failsafe engaged	☐ Direction of propeller rotation
☐ Check receiver connections	☐ Check receiver battery voltage	

Control surfaces

☐ Deflection of control surfaces	☐ Control surface linkages	☐ Servo deflections
☐ Correct control surface movement	☐ Trimming and neutral setting of surfaces	

Weather

Wind speed:_____	Location:_____	Temperature:_____

Final Inspection

☐ Check for clear flight line	☐ Control surface check by pilot	☐ Pilot and thrower ready

Table 7.5 (b): Pre-flight checklist

8. PERFORMANCE RESULTS:

8.1 COMPONENT AND KEY SUBSYSTEM PERFORMANCE:

8.1.1 STRUCTURAL PERFORMANCE:

1) WING TESTING RESULTS:
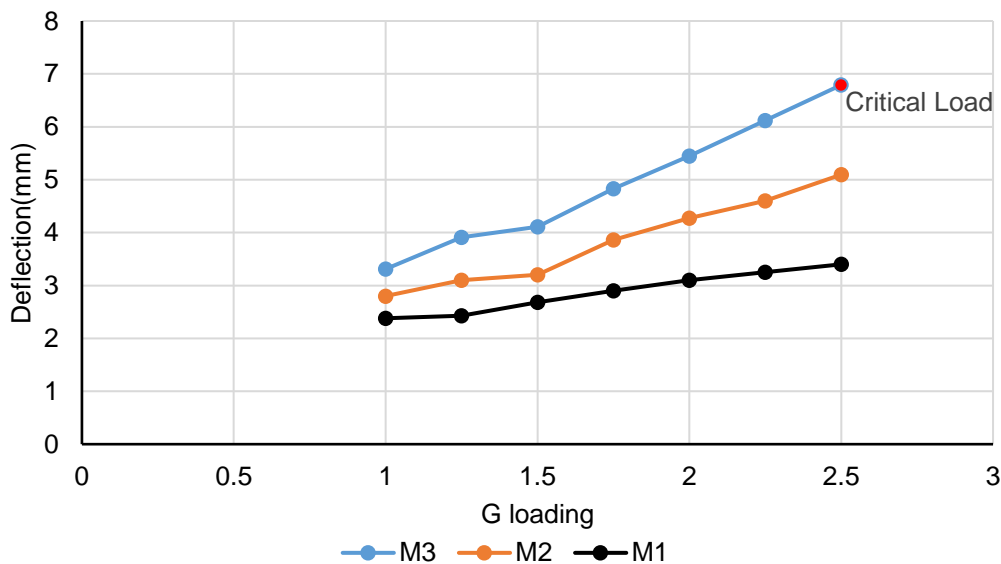
Figure 8.1.1 (a): Wing loading results

The wing failed in bending once the load exceeded 2.5 G with respect to the third mission, in which maximum stresses are expected to occur. The wing achieved its target G-loading, hence there was no need to resize the spar dimensions.

2) TUBE DROP RESULTS:

The footage of the tube drops confirmed that the tube rotates during the horizontal and vertical drops as it falls. Minor cracks started appearing on the tube only after a complete iteration of the ground mission was completed. Styrofoam packing was added only at the critical positions. This ensured that a light tube was made which served its purpose without being overdesigned.
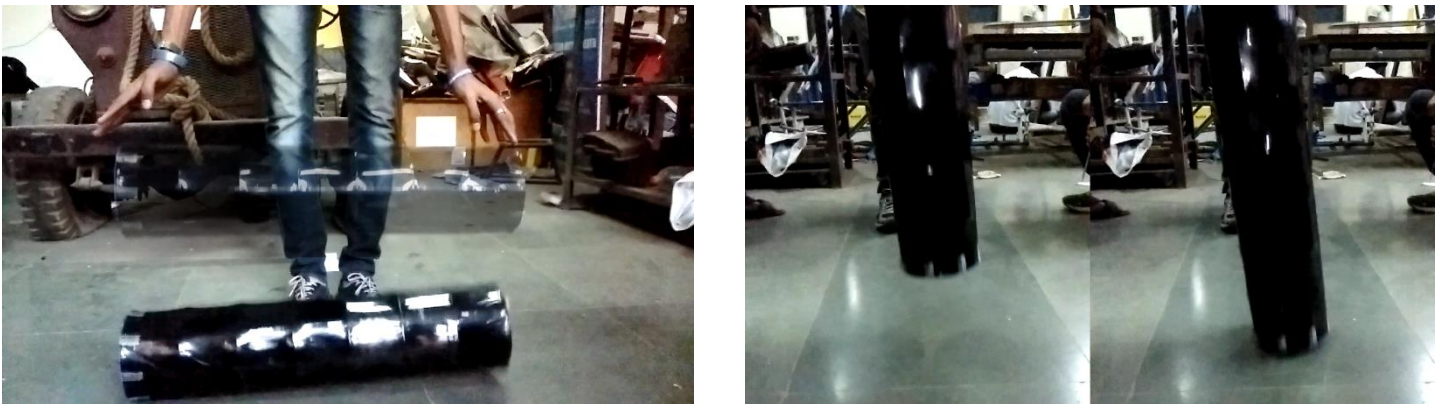
Figure 8.1.1 (b): Tube drops, horizontal and vertical

Post the drops, the aircraft was removed from the tube and transitioned to the flight-ready condition by a single team member. In each case, this was completed well within five minutes. This confirmed that the mechanisms on-board the aircraft were reliable and could be easily operated under all conditions. The ground mission was then repeated a number of times to increase the familiarity of the assembly crew member with the system.

3) TAIL BOOM BENDING RESULTS:

The boom failed only after a weight of more than 1.4 kg was applied at the free end. This was considered satisfactory given that on landing, the wire skid deforms first, absorbs a significant fraction of the impact load and then transmits the rest to the boom.
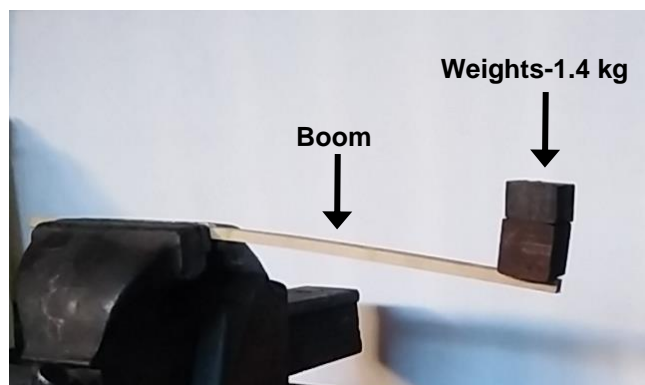

Figure 8.1.1 (c): Boom bending test

8.1.2 BATTERY AND PROPULSION PERFORMANCE:

For testing the batteries as described in section 7.3, a 10 cell Elite 1500 mAh pack was discharged at 5C, 10C and 12.5C. At 5C, after the initial drop, the nominal voltage of 1.2V per cell could be maintained as seen from the graph, but the effective available power was not sufficient considering the requirement of the aircraft. At 12.5C (20A), the available power was sufficient. However, the endurance of the pack was below the maximum five-minute requirement imposed by the team. Finally, at 10C i.e. a continuous draw of 16A, the power requirement was satisfied and the endurance was well over five minutes, making it the ideal discharge rate for the chosen pack.
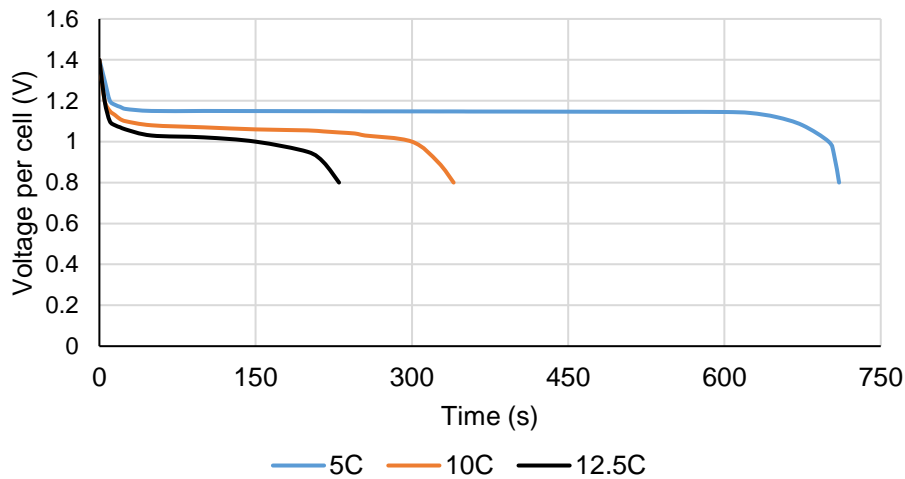
Figure 8.1.2 (a): Cell discharge characteristics

Overall System Performance: Static Thrust testing for the combinations shortlisted in preliminary design was carried out and the results were plotted as seen in Figure 8.1.2 (b). Each combination produced slightly lower thrust than that predicted by the APC database [5]. The results differed because of the drag produced by the airflow interaction with the fixture on which the motor-propeller system was mounted.
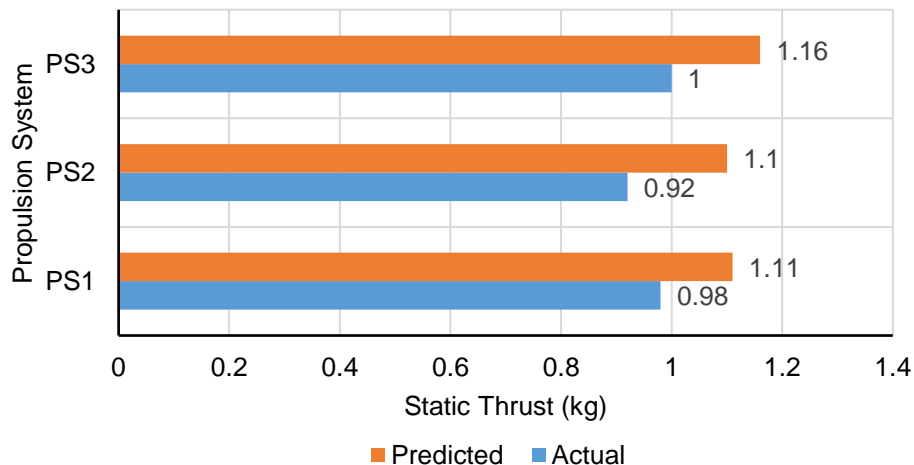

Figure 8.1.2 (b): Comparison of static thrust for different propulsion systems

8.2 FLIGHT PERFORMANCE AND RESULTS:

Flight Testing is the moment of confirmation of all theoretically obtained results and a materialisation of the design that was once conceptualised, then detailed and fabricated.

Initial Flight Testing:

Mission 1 was tested first due to its least weight. This mission proved that when flown at various speeds and bank angles the main concerns were structural integrity and stability rather than propulsion system. Several test flights followed for the other missions. Some of the issues encountered, and the solutions developed to these based on team deliberations and pilot feedback are listed in Table 8.2 (a). Problems encountered in the ground mission are also listed.

Serious issue, may require change of aircraft/tube definition	Moderate issue, can be solved by altering a few parameters	No issues encountered, results meet expectations

Testing Parameter	Issue	Corrections
Hand launch	The plane dipped significantly just after launch and crashed on a few occasions.	Launch velocity was increased by adopting a 'running' hand launch style.
Stability and Control	Misalignment of the folding sections of the wing with the main section caused undesirable pitch-up moments after hand launch.	Each folding section was manufactured and coated separately, and ensuring correct alignment while hinging.
	The pilot found the aircraft to be tail-heavy during most of the initial flights.	The calculations for the CG location were revised and it was shifted forward by 0.5 cm. The front portion of the fuselage was extended to increase the moment-arm of the motor weight and make C.G. balancing easier.
	The inboard ailerons were ineffective while turning at low speeds.	The span of the ailerons was increased by 5 cm outwards and it was resolved satisfactorily.
Flight velocity	The aircraft was able to achieve its design speed.	---

Climb characteristics	The aircraft was quickly able to climb to a high altitude.	---
Landing	The motor mount broke off from the inclined wall at the joint.	The angle of the inclined wall was reduced to increase contact with the motor mount surface and the fuselage base.
Tube drops	During the vertical drops of the first prototype of the tube, three stringers near the end cap facing the floor buckled and cracked.	Formers were added between the last two formers before the lids to strengthen the stringers.
	The wing jaw used for locking the folding section broke when the tube landed vertically.	Styrofoam was added on the inner side of the lid in order to absorb the impact of the drop.

Table 8.2 (a): Evaluation from test flights

Detailed Flight Testing:

In detailed flight testing, a variety of aircraft parameters were tested simultaneously using a Data Acquisition System placed on board the aircraft during the flights of the prototype models. The expected values and the actual ones are compared in table 8.2 (b).

Parameter	Estimated value	Actual value
Battery	Elite 1500 mAh	
Maximum voltage	18V	17.8V
Maximum continuous current	16A	16A
Average internal resistance	0.02Ω	0.023Ω

Parameter	Upwind velocity (m/s)		Downwind velocity (m/s)		Flight Time (s)	
	Expected	Actual	Expected	Actual	Expected	Actual
Mission 1	19.5	22.6	27.2	24	110	120
Mission 2	18.2	21	25.7	23.1	130	145
Mission 3	17.4	20.4	24.6	21.6	270	284

Table 8.2 (b): Compilation of actual and expected parameters

The actual groundspeeds deviated from the calculated speeds by almost the same amount, for both the upwind and downwind legs. It was reasoned that the calculations accounted for a wind speed of 4 m/s while the speed during actual testing was as low as 1 m/s. Discrepancies in the flight time can be attributed to

deviation of the actual path flown from the expected course and any uncertainties in the mission model predictions.

At the time of submission of the Design Report, there have been twenty-one flight attempts on two prototypes, with the suggested corrections incorporated in the later flights. The aircraft and the tube will be prepared for the final phase of flight testing, which will go on till both are well-optimised. The aircraft has been deemed stable and airworthy after the flights. The team is confident that the configuration it has developed is highly competitive, and is poised for success in Tucson.

Figure 8.2: Aircraft being hand-launched

9. REFERENCES:

[1] Deperrois, Andre, "XFLR5 v6.13". XFLR5 is an open source software that makes use of the XFoil code written by M. Drela and H. Youngren and the Miarex solver by Matthieu Scherrer.

[2] Drela, Mark and H. Youngren. "Athena© Vortex Lattice Program." 23 Aug. 2010. <http://web.mit.edu/drela/Public/web/avl/>, a VLM solver.

[3] MATLAB (Matrix Laboratory) is a numerical computing environment and fourth-generation programming language. It is a proprietary programming language developed by MathWorks.

[4] Propeller Wing Aerodynamic Interference-Delft University of Technology, Faculty of Aerospace Engineering.

[5] APC Propeller Performance Database [online]. <https://www.apcprop.com>

[6] 'Weather Underground' <https://www.wunderground.com>, commercial weather information service.

[7] Anderson, J.D., "Introduction to Flight", 3rd ed., McGraw Hill Book Company, 1989.

[8] Hoerner, Sighard F., "Fluid-Dynamic Drag", 1965, Great Britain.

[9] Dassault Systemès SolidWorks, solid modelling computer-aided design and computer-aided engineering computer program

[10] Sadraey, M.H., "Aircraft Design: A Systems Engineering Approach", Wiley Publications, 2013.

[11] Chan, C. C., Guoliang Wu, Rengui Lu, and Chunbo Zhu, 'Apply a Piece-wise Peukert's Equation with Temperature Correction Factor to NiMH Battery State of Charge Estimation', *Journal of Asian Electric Vehicles*, Volume 8, Number 2, December 2010.

Table of Contents

ACRONYMS, ABBREVIATIONS, AND SYMBOLS

η_{Motor}	Mechanical Efficiency of the motor
η_{Prop}	Aerodynamic Efficiency of the propeller
τ	Time constant
ω_d	Damped frequency (rad/s)
ω_n	Natural frequency (rad/s)
ζ	Damping coefficient
AIAA	American Institute of Aeronautics and Astronautics
AR	Aspect Ratio
AVL	Athena Vortex Lattice
b	Wingspan
c	Wing chord
C_d, C_D	Drag coefficient (2D, 3D)
C_{D0}	Parasite drag coefficient
C_{D_i}	Induced Drag coefficient
CG	Center of Gravity
C_l, C_L	Coefficient of lift (2D, 3D)
$C_{L_{MAX}}$	Maximum 3D lift coefficient
C_{m_α}	Moment coefficient
C_P	Coefficient of power
C_T	Coefficient of thrust
DAQ	Data Acquisition Board
DBF	Design/Build/Fly
D_{Tube}	Outer diameter of tube
e	Oswald efficiency factor
ESC	Electronic Speed Controller
EW_{Plane}	Empty weight of the aircraft
FEA	Finite Element Analysis
FoM	Figures of Merit
I_{MAX}	Maximum current allowable for a mission
L/D	Lift-to-drag ratio
$(L/D)_{cruise}$	Lift-to-drag ratio in cruise
$(L/D)_{max}$	Maximum lift-to-drag ratio
L_{Tube}	Axial length of the tube
M_1	Mission 1 Flight Score
M_2	Mission 2 Flight Score
M_3	Mission 3 Flight Score

MAC	Mean Aerodynamic Chord (ft, m)
MDO	Multidisciplinary design optimization
n_{cells}	Number of battery cells flown
NiCd	Nickel-Cadmium
NiMH	Nickel-Metal Hydride
N_{Laps}	M_3: Completed laps in 5 min.
N_{Pucks}	Number of pucks flown for M_3
PF	Payload Fraction
P_{OUT}	Power output of propulsion system
RAC	Rated Aircraft Cost
Re_c	Reynolds number over wing chord
Re_{cruise}	Cruise Reynolds number
S	Wing planform area
SM	Static Margin
T_{BEST}	Fastest successful time for M_2
T_{USC}	USC time for M_2
UAV	Unmanned Aerial Vehicle
USC	University of Southern California
V	Voltage
V_{cruise}	Cruise Velocity
V_{launch}	Launch velocity
V_{stall}	Stall velocity
V_∞	Free-stream velocity of air
W/S	Wing loading
$W_{Battery}$	Total weight of battery
$W_{Payload}$	Total weight of all payloads
$W_{Structure}$	Structural weight of the aircraft
W_{Total}	Total takeoff weight of aircraft
W_{Tube}	Empty weight of the tube

1.0 EXECUTIVE SUMMARY

The objective of the 2016-2017 American Institute of Aeronautics and Astronautics (AIAA) Design/Build/Fly (DBF) contest is to simulate the design of a tube-launched UAV that transitions from a stowed configuration and self-locks into a flight configuration prior to completing three hand-launched flight missions in Tucson, AZ. In addition to designing the competition aircraft, the team must also design a launch tube to store the aircraft in its stowed configuration and protect the aircraft in the ground mission. The payloads for this year's contest are regulation-sized hockey pucks (3 in. diameter, 6 oz. weight).

The first flight mission, a display flight, consists of flying three competition laps with no payloads in five minutes or less. The second flight mission, a speed flight, requires the plane to fly three competition laps with three payloads as fast as possible. The third flight mission, an endurance flight, consists of flying as many laps as possible within five minutes while carrying a team-specified number of payloads. The ground mission consists of three drop tests with the aircraft fully loaded and stowed in the launch tube. The fully loaded tube is dropped three times, once on each end cap and once horizontally, all from a height of 12 in (0.3 m). Although the performance in the ground mission does not directly affect the total score, the tube dimensions and weight heavily affect the rated aircraft cost (RAC), which negatively affects total score.

After analyzing the flight mission scoring and aircraft contribution to RAC, it was determined that minimizing the dimensions and weight of both the aircraft and launch tube without sacrificing in-flight performance was critical to this year's design. Performance trade studies indicated that flying with the minimum number of allowable payloads (3) for the endurance flight would score highest. Furthermore, structural analysis indicated that a lightweight nonstructural launch tube could be designed to efficiently transfer ground mission impact loads to the aircraft's primary structure, thereby minimizing the rated aircraft cost.

A monoplane configuration was identified as the highest scoring configuration because it stored most conveniently within the launch tube and its design simplicity allowed the team to devote energy to the design of lightweight captive mechanical mechanisms that stowed flight surfaces and components while minimizing the negative effect on RAC. Wing and tail loads were carried through spars constructed of balsa shear webbing and carbon spar caps. A lightweight spar coupler transferred flight loads to the fuselage in the flight condition but allowed the spars to rotate and offset on top of the fuselage in the stowed configuration. The team built an abrasion-resistant fuselage from Kevlar and inlaid foam stringers that transferred flight and landing loads between two bulkheads and the motor mount. A V-tail was selected as the empennage configuration due to its simple method of stowing beneath the wings along the length of the fuselage. The wing area and tail sizing was first done analytically and then validated empirically through extensive hand launch testing that characterized the launch conditions and refined launch technique. All payloads were located forward of the wing and secured to the primary bulkhead using lightweight fishing line.

The University of Southern California's aircraft, *Starscream* (Figure 1), is designed to maximize score by combining high-speed flight performance with innovative folding mechanisms that allow for a compact

stowed configuration and minimalistic tube design. *Starscream* will take off at 50 ft/s (15 m/s) and rapidly climb to cruise altitude and velocity for all missions. With a top flight speed of 88 ft/s (27 m/s), Starscream will complete three laps for Mission 2 in 106 s at a total weight of 2.4 lb (1.1 kg). With three payloads and an optimally efficient flight speed of 81 ft/s (25 m/s) *Starscream* will complete eight laps for a maximum product of laps and pucks of 24. *Starscream* fits inside a tube that has a diameter of 4.5 in (0.11 m). and a length of 17.9 in. (0.5 m), that weighs 0.1 lb (0.05 kg) and yields an RAC of 52.6.
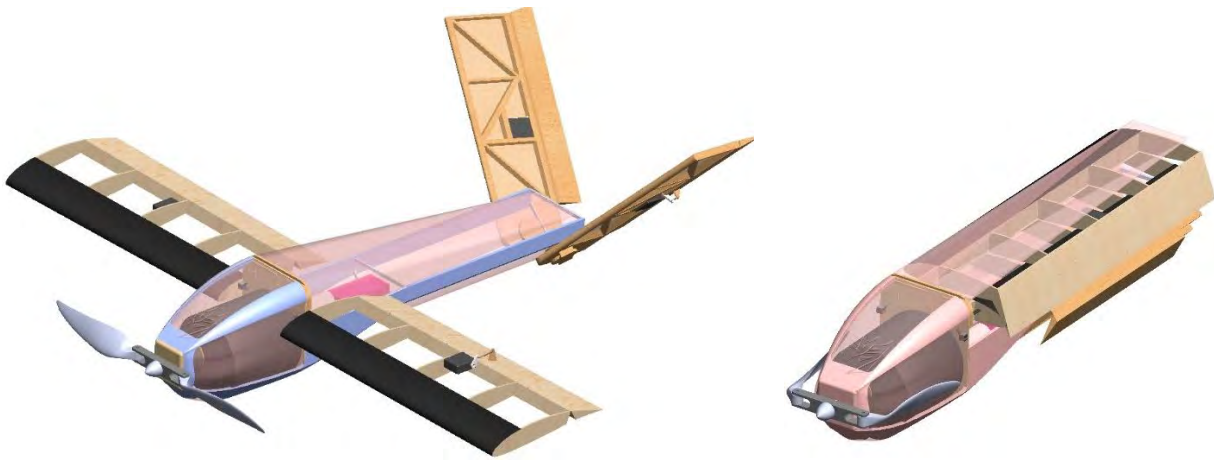
Figure 1: *Starscream* in flight (left) and stowed (right) configuration

2.0 MANAGEMENT SUMMARY

The 2016 – 2017 AeroDesign Team of USC consists of 45 students that participate on an extracurricular basis. Five team members are seniors and the remainder are juniors and underclassmen. The team is entirely student-led but receives guidance and suggestions from industry advisors, USC alumni, and faculty members at weekly meetings and design reviews.

2.1 TEAM ORGANIZATION

The AeroDesign Team of USC employs the matrix structure of leadership in order to simulate the management hierarchy employed at most aerospace firms. The team leadership for the 2016-2017 competition is shown in Figure 2.
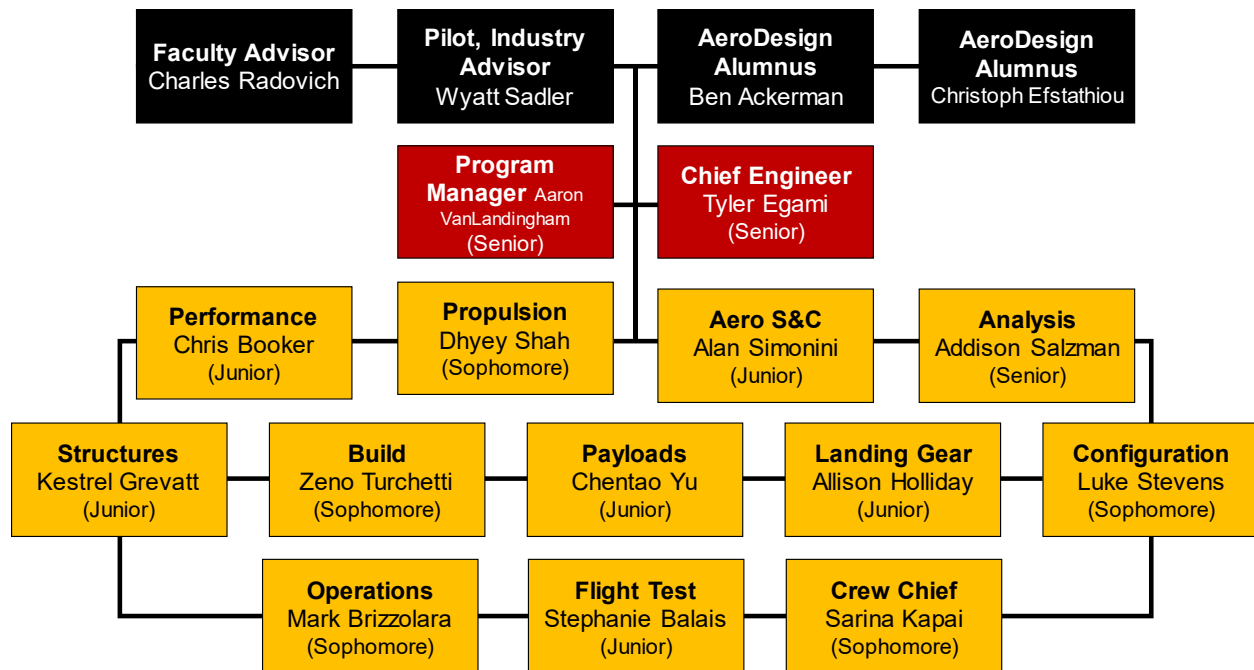
Figure 2: Organization chart of the USC AeroDesign Team

Team leaders, as shown in red, receive suggestions from team advisors (**black**) and coordinate the design effort among sub-team leaders (gold). The Chief Engineer and Program Manager divide tasks such that the Chief Engineer supervises design, build, and test efforts while the Program Manager sets major milestones, ensures adherence to the master schedule and works with the Operations Manager to obtain funding and manage team logistics

2.2 MILESTONE CHART

The Program Manager maintains a Gantt chart with planned and actual schedule, shown in Figure 3. The schedule helps assess how long a task should take, determine required resources, and plan task dependencies. Unplanned tasks, (indicated by ***) were required in December and January as a result of complexity associated with a hand launch aircraft. The manufacturing schedule set at the beginning of the year was adjusted accordingly as shown by "Actual Timing". Note that actual timing is not shown for future tasks.
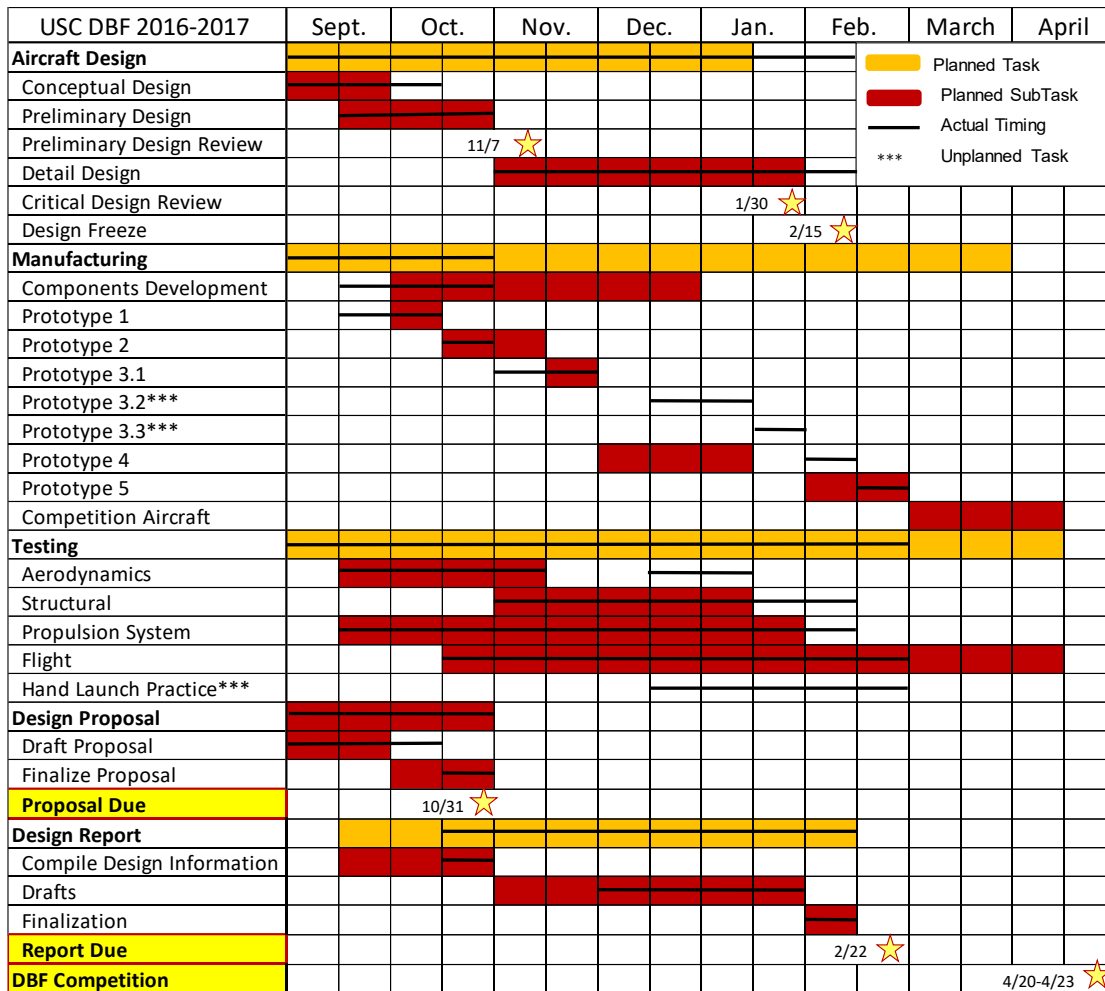
USC DBF 2016-2017	Sept.	Oct.	Nov.	Dec.	Jan.	Feb.	March	April
Aircraft Design								
Conceptual Design								
Preliminary Design								
Preliminary Design Review			11/7 ★					
Detail Design								
Critical Design Review					1/30 ★			
Design Freeze						2/15 ★		
Manufacturing								
Components Development								
Prototype 1								
Prototype 2								
Prototype 3.1								
Prototype 3.2***								
Prototype 3.3***								
Prototype 4								
Prototype 5								
Competition Aircraft								
Testing								
Aerodynamics								
Structural								
Propulsion System								
Flight								
Hand Launch Practice***								
Design Proposal								
Draft Proposal								
Finalize Proposal								
Proposal Due		10/31 ★						
Design Report								
Compile Design Information								
Drafts								
Finalization								
Report Due						2/22 ★		
DBF Competition								4/20-4/23 ★

Legend:
- ▬ (yellow) Planned Task
- ▬ (red) Planned SubTask
- ─ Actual Timing
- *** Unplanned Task

Figure 3: Master Schedule showing the planned and actual timing of team processes

3.0 CONCEPTUAL DESIGN

In the conceptual design phase, the team analyzed the competition requirements and scoring equation to set design parameters for the competition year. Numerous aircraft configurations were evaluated in order to identify the highest scoring configuration. The end product of the conceptual design phase is presented in Section 3.5.

3.1 MISSION REQUIREMENTS

The rules for the 2016-2017 AIAA DBF contest simulate the design of a tube launched UAV. Although the aircraft is not required to launch directly from a tube, the objective is to design a UAV that completes a series of missions, and a tube that stores the UAV. The contest consists of three flight missions and a ground mission. The UAV will be optimized to fit inside the tube in its stowed configuration and transition to its flight configuration prior to completing three flight missions. Both the UAV and the tube will be designed to complete a ground mission, which does not factor into the scoring but must be completed after Mission 1 in order to attempt the remaining missions.

Each flight mission requires the aircraft be hand-launched upwind and then fly competition laps, consisting of two 1000 ft. (300 m) straightaways, two 180° turns, and one 360° turn in the opposite direction of the 180° turns. The competition lap requires that the aircraft make right-hand and left-hand turns and land within the bounds of the runway, thereby setting the bare minimum performance of the aircraft. A schematic of a competition lap is shown in Figure 4.
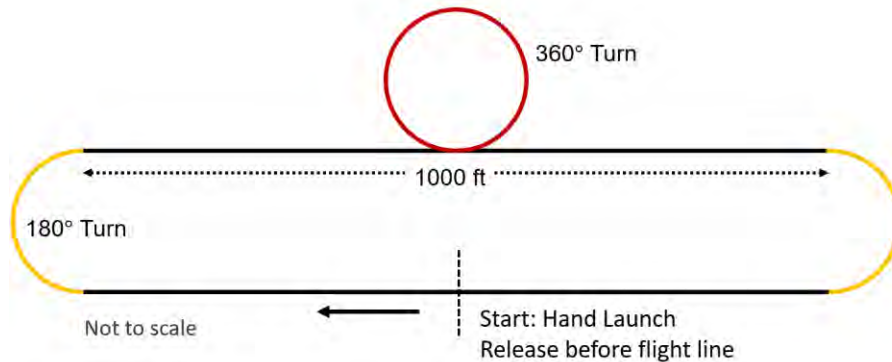

Figure 4: AIAA Competition Lap Layout

Prior to each flight, the aircraft must arrive at the flight line in the stowed configuration inside the launch tube. Once at the flight line, the flight crew will have five minutes to remove the aircraft from the launch tube and transition to the flight configuration.

3.1.1 SCORING SUMMARY

The overall score for the 2017 AIAA DBF contest is given by Eq. 1.

$$Total\ Score = \frac{Written\ Report\ Score \cdot Total\ Mission\ Score}{Rated\ Aircraft\ Cost}$$

Eq. 1

The *Written Report Score* is based on the quality of the design report, and the *Total Mission Score* is the sum of the scores of each flight mission given by Eq. 2.

$$Total\ Mission\ Score = M_1 + M_2 + M_3$$

Eq. 2

M_1, M_2, and M_3 denote the scores for Mission 1, Mission 2, and Mission 3, respectively. RAC is given by Eq. 3.

$$RAC = (EW_{Plane} + W_{Tube}) \cdot (L_{Tube} + \pi D_{Tube})$$

Eq. 3

The individual components of the RAC are defined as follows:

- *Empty Weight* (EW_{Plane}): Maximum aircraft empty weight recorded after each successful mission
- *Weight of Tube* (W_{Tube}): Tube weight recorded after a successful Ground Mission, including end cap(s) and all internal supports
- *Lenght of Tube* (L_{Tube}): Tube Length
- *Circumference of Tube* (πD_{Tube}): Tube circumference

3.1.2 MISSION SCORING

Flight Mission 1 – Display Flight

The objective of the Display Flight is to successfully complete three competition laps within a five-minute flight window without any payloads. Timing starts when the aircraft leaves the launcher's hand during the first attempted hand launch. M_1 is binary with $M_1 = 1.0$ for a successful mission and $M_1 = 0$ for an unsuccessful mission.

Flight Mission 2 – Speed Flight

The objective of the Speed Flight is to complete three laps as fast as possible and land with three regulation hockey pucks as the payload. Timing starts when the aircraft leaves the launcher's hand during the first attempted hand launch and stops when the aircraft passes over the start/finish line in the air at the end of the third lap. The score for this mission (M_2) is given by Eq. 4 where T_{BEST} is the fastest successful time of any team for M_2 and T_{USC} is the time USC takes to complete the mission.

$$M_2 = \left(\frac{T_{BEST}}{T_{USC}}\right) \cdot 2.0 \qquad\qquad \text{Eq. 4}$$

Flight Mission 3 – Range Flight

The objective of the Range Flight is to maximize the product of the number of complete laps (N_{Laps}) flown and number of pucks (N_{Pucks}) carried. The aircraft will carry a team-chosen number of hockey pucks and fly as many laps as possible within a 5-minute flight window. Timing starts when the aircraft leaves the launcher's hand during the first attempted hand launch. A lap is considered "complete" when the aircraft passes over the start/finish line in the air. Landing is not included in the flight window. A successful landing is required to complete a successful mission. Scoring for Mission 3 is given by Eq. 5.

$$M_3 = \frac{\left(N_{Laps}N_{Pucks}\right)_{USC}}{\left(N_{Laps}N_{Pucks}\right)_{BEST}} \cdot 4.0 + 2.0 \qquad\qquad \text{Eq. 5}$$

where $\left(N_{Laps}N_{Pucks}\right)_{USC}$ is the product of the number of laps and number of pucks flown by USC and $\left(N_{Laps}N_{Pucks}\right)_{BEST}$ is the maximum product of number of laps and number of pucks flown by any team.

Ground Mission – Drop Test

The Ground Mission must be completed prior to Mission 2. The objective of the ground mission is to survive a series of three drops from a minimum height of 12 in. (0.3 m) onto a hard surface. The UAV must be sealed inside the launch tube with the maximum payload determined during tech inspection. The three drops will consist of a flat drop with the tube's long axis parallel to the ground and two end drops, one for each end of the tube, with the tube's long axis perpendicular to the ground. M_G does not factor into the total mission score but must be completed successfully before attempting M_2. In order to be considered a

successful drop, the launch tube cannot sustain any major damage as a result of the drop test. Major damage could consist of cracks or perforations, dislodged end caps, or structural failures, but is ultimately up to the discretion of the mission official. After the successful completion of all three drops, the assembly crew will remove the plane from the launch tube and transition the aircraft to the flight condition. The pilot will verify all flight systems and the assembly crew will perform a wing tip test.

3.1.3 AIRCRAFT CONSTRAINTS

In addition to the flight missions described above, the final aircraft must meet the following requirements:

Stowed Configuration

1. All surfaces or aircraft features that are folded, rotated, stowed or otherwise moved to a condition for storage in the launch tube must be moved to the flight condition.
2. All surfaces or aircraft features must "move" to flight position using hinges, pivots, or other captive mechanical mechanisms. Surfaces or aircraft features cannot temporarily separate from the aircraft and use "lanyards" or similar devices to provide a connection to the aircraft with the operator controlling the path the surfaces or aircraft features takes from stowed to flight position.
3. All surfaces or aircraft features described above must securely lock in the flight condition without the use of tools or manual release or engagement of any locking features (in other words, all locking features must be self-locking).
4. All surfaces or aircraft features described above may be manually moved or rotated to the flight condition by hand. Spring loaded or self-deploying mechanisms are not required.

Propulsion

5. Batteries must be Nickel-Cadmium (NiCd) or Nickel-Metal Hydride (NiMH).

Payloads

6. All payloads must be stored internally.

Launch Tube

7. The launch tube must be a right circular cylinder of constant cross-section.
8. The launch tube length to diameter (L_{Tube}/D_{Tube}) ratio must be a minimum of 4.
9. The launch tube must be completely sealed in the storage and pre-flight condition.
10. No perforations, cut-outs or access holes are allowed.
11. The tube must have end caps that completely seal both ends of the tube, one or both of which must be removable by hand only for removing the UAV for flight – no tools or aids are allowed to remove the end cap(s).

3.2 DESIGN REQUIREMENTS

Design requirements were developed from the DBF scoring equations and competition guidelines in order to guide the design process. By analyzing the scoring equations, an aircraft configuration and competition approach was selected to maximize total score. Mission requirements and score equations were translated into design parameters, as shown in Table 1.

Table 1: Design parameters

Missions and RAC	Objective	Design Parameter
2 – Speed Flight	Maximize flight speed to minimize flight time for 3 laps	T_{USC}
3 – Endurance Flight	Balance flight speed and payload to maximize product of laps and pucks flown	$\left(N_{Laps}N_{Pucks}\right)_{USC}$
RAC	Minimize EW_{Plane} to minimize RAC	EW_{Plane}
RAC	Minimize tube length to minimize RAC	L_{Tube}
RAC	Minimize tube diameter to minimize RAC	D_{Tube}
RAC	Minimize tube weight to minimize RAC	W_{Tube}

3.2.1 FLIGHT SCORE SENSITIVITY ANALYSIS

The scoring equations, Eq. 1 - Eq. 5, were analyzed to set design objectives by identifying mission objectives and design parameters that were most important in maximizing score. Analysis began by estimating the top mission performance of any competitor in each of the three missions. Additionally, performance for a "baseline" competition aircraft, shown in Table 2, was estimated in order to provide for comparison. The assumptions guiding these estimates are detailed in the following paragraphs.

Table 2: Estimates for top performance(competitors) and baseline aircraft parameters(USC)

Top Mission Performances	Assumption
T_{BEST}	80 s
$\left(N_{Laps}N_{Pucks}\right)_{BEST}$	80

Design Parameter	Baseline Assumption
T_{USC}	100 s
$\left(N_{Laps}N_{Pucks}\right)_{USC}$	24
EW_{Plane}	1.125 lb (0.51 kg)
L_{Tube}	30 in (0.76 m)
D_{Tube}	5.5 in (0.13 m)
W_{Tube}	0.15 lb (0.07 kg)

Estimates for Top Mission Performance

Assumptions for the top mission performance of any competitor were made based on aircraft performance in previous competitions. In the 2014 AIAA DBF Ferry Flight, eight was the maximum number of laps completed in the 4-minute flight window [1]. Lap times between 26 and 27 s are assumed for M_2 based on the assumption that the actual lap times were slightly faster as a result of partial laps not counted toward the total lap count. Based on this, the best flight speed (T_{BEST}) was assumed to be 80 s. The assumptions for the quantity $\left(N_{Laps}N_{Pucks}\right)_{BEST}$ are that a team heavily optimized for M_3 could successfully fly sixteen pucks for five laps.

Assumptions for Baseline Performance

The baseline assumptions for the aircraft design parameters shown in Table 2 are estimates of the team's capability based on experience in previous competitions. For example, the USC entrant to the 2014 AIAA DBF contest, *Mischief*, completed 7 laps in 4 minutes for the Ferry Flight. It is assumed that actual lap times could be between 33 and 34 s, resulting in a baseline aircraft that could fly 8 laps in 5 minutes. With an assumed baseline of 3 payloads, the quantity $\left(N_{Laps}N_{Pucks}\right)_{USC}$ is 24. The baseline EW_{Plane} was determined by assuming a maximum of 3 payloads with a payload fraction, PF, of 50% according to Eq. 1.

$$PF = W_{Payload}/EW_{Plane}$$
<div align="right">Eq. 1</div>

PF = 50% is a realistic estimate based on past USC aircraft when taking into account the added weight required by folding mechanisms [1]. The assumptions for the dimensions of the tube, L_{Tube} and D_{Tube}, were derived from the relationships between aircraft configuration and tube geometry described in 3.2.2. As a preliminary estimate, W_{Tube} was calculated using the mass properties of a foam (0.035 oz/in^3, 7.6 kg/m^3) right cylinder with length, L_{Tube}, outer diameter D_{Tube} and wall thickness of 0.125 in (0.003 m). Each design parameter of the baseline aircraft was varied while keeping all remaining variables constant in order to determine its sensitivity on overall score. The results are plotted in Figure 5.
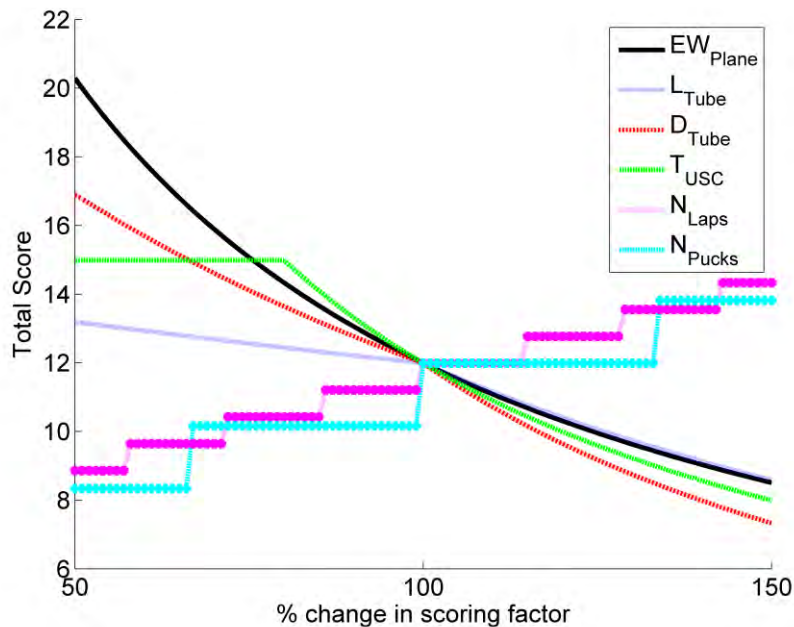
Figure 5: Score analysis indicating the impact of score parameters.

Score analysis indicates that minimizing the empty weight of the aircraft (EW_{Plane}), minimizing the tube dimensions (L_{Tube} and D_{Tube}), and minimizing the M_2 flight time (T_{USC}) have the greatest impact on the total competition score. Although Figure 5 indicates a positive trend with increasing N_{Laps} and N_{Pucks}, further analysis was required to fully capture the coupled effects of M_3 parameters on EW_{Plane}, D_{Tube} and Total Score.

3.2.2 INTEGRATED PERFORMANCE ANALYSIS

In order to determine the highest scoring aircraft size for M_3, the team developed a scoring model to calculate the flight score and identify the effects of trading the number of cells, n_{cells}, and pucks, N_{Pucks}, on the overall score.

Flight Score Calculation

The total weight of the aircraft (W_{Total}) was approximated as a function of the structural weight ($W_{Structure}$), payload weight ($W_{Payload}$) and battery weight ($W_{Battery}$) as shown in Eq. 6.

$$W_{Total} = W_{Structure} + W_{Payload} + W_{Battery} \qquad \text{Eq. 6}$$

Where $W_{Payload} = 6 \text{ oz.} \cdot N_{Pucks}$ and the structural weight, $W_{Structure}$, was approximated as a function of the total payload weight based on previous USC contest entrants. Battery weight was calculated as a function of n_{cells} at each design point according to Eq. 7. The 1500 mAh NiMH cells used in the conceptual analysis were selected based on their exceptional performance throughout the team's history when compared to other commercially available cells.

$$W_{Battery} = n_{cells} \cdot \left(0.05 \frac{lb}{cell} \right) \qquad \text{Eq. 7}$$

The wing area, S, was calculated from the assumption that lift equals aircraft weight at steady level flight for initial launch conditions according to Eq. 8, where the maximum 3D lift coefficient of the airfoil, $C_{L_{MAX}} = 1.1$, and the launch velocity, $V_{launch} = 50$ ft/s, was obtained through hand launch testing presented in 8.1.1.

$$S = \frac{W_{total}}{C_{L_{MAX}} \left(\frac{1}{2} \rho V_{launch}^2 \right)} \qquad \text{Eq. 8}$$

With the selected wing area, the team set two constraints on the wing geometry to determine the aspect ratio, $AR = b^2/S$. The maximum aspect ratio, $AR = 8$, is a limitation based on the team's experience with flutter at higher aspect ratios. The minimum chord was calculated to keep the Reynolds number of the flow over the wing above, Re_c, above 125,000, an aerodynamic limit to avoid stall from flow separation at launch.

The propulsion system was modeled as a power plant of constant power out, P_{OUT}, as a function of n_{cells} and the maximum current allowable for each mission, I_{MAX}. The efficiency of the motor and propeller, η_{Motor} and η_{Prop}, account for mechanical and aerodynamic losses in the system as shown in Eq. 9 and Eq. 10.

$$P_{OUT,M1/M2} = \eta_{Motor.} \cdot \eta_{Prop} \cdot n_{cells} \cdot \left(1.2 \frac{V}{cell} \right) * I_{MAX,M2} \qquad \text{Eq. 9}$$

$$P_{OUT,M3} = \eta_{Motor.} \cdot \eta_{Prop} \cdot n_{cells} \cdot \left(1.2 \frac{V}{cell} \right) * I_{MAX,M3} \qquad \text{Eq. 10}$$

Battery testing determined the maximum allowable current draw from the baseline cells, $I_{MAX,M1/M2} = 28$ A. Battery testing, presented in 8.1.2 indicated that the 1500 mAh cells selected as a baseline for this trade

study could last just over five minutes at a cruise current of 13 A. $I_{MAX,M3} = 13$ A. The resulting P_{OUT} was used to solve for the cruise velocity, V_{cruise}, for each mission according to Eq. 11.

$$P_{OUT} = \frac{1}{2}\rho V_{cruise}^3 S C_{D0} + \frac{2W}{\rho V_{cruise} S \pi A R e}$$
Eq. 11

Rated Aircraft Cost Calculation

Tube dimensions were calculated assuming that tube diameter was driven by the arrangement of the wing chord and payload profile and that the length of the tube was driven by the aircraft's half span according to Eq. 12. The additional length specified in Eq. 12 allows for motor/payload placement in front of a wing hinge.

$$L_{Tube} = \frac{b}{2} + 5 \text{ in.}$$
Eq. 12

A MATLAB script optimized the arrangement of the aircraft components to determine D_{Tube} at each design point. L_{Tube} was checked to verify it satisfied the geometric constraint, $\frac{L_{Tube}}{D_{Tube}} \geq 4$, and was adjusted if it did not meet this requirement. EW_{Tube} was calculated from the tube volume assuming a wall thickness of 0.125 in. (0.003 m) and the density of white foam ($\rho = 1.2$ lb/ft^3, 16 kg/m^3). RAC was calculated from Eq. 3

Final Trade Study

The design parameters n_{cells} and N_{Pucks} were varied to identify trends in overall score. The results are summarized in Figure 6. As shown by the nearly vertical lines of constant score (constant color), increasing n_{cells} does not dramatically alter score. Total score was, however, sensitive to changes in N_{Pucks}, with $N_{Pucks} = 3$ yielding the highest score.
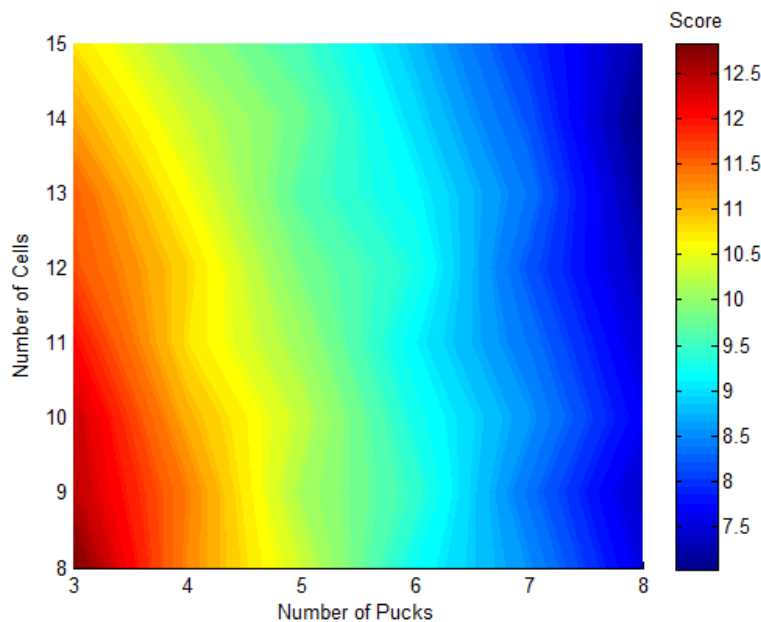
Figure 6: Trade study showing effect on Total Score as n_{cells} and N_{Pucks} are varied.

As a result of the conclusions drawn from the integrated performance analysis, the team moved forward designing a plane to carry a maximum payload of three hockey pucks.

3.2.3 GROUND MISSION ANALYSIS

Although the ground mission does not directly affect the scoring equation, the aircraft and tube structure required to withstand the 12 in. (0.3 m) drops could have a substantial effect on the RAC. Both end cap drops and horizontal drops apply loads to the aircraft that are directionally very different than the loads experienced in-flight. After comparing impact loads from a drop test to typical flight loads, the team concluded that the structural elements of the aircraft in the stowed configuration could be designed to withstand the impact sustained from the drops. Thus, the conceptual design was for a primarily nonstructural launch tube that would efficiently transfer impact loads to the primary structure of the aircraft.

3.3 CONFIGURATION SELECTION

3.3.1 CONFIGURATIONS CONSIDERED

A configuration down-select process was used to select a preliminary aircraft configuration. As a result of the competition rules, all conceptual designs considered both the sizing for the flight configuration and an evaluation of the motions required to transition from the flight condition to the stowed configuration. Four designs were selected for further analysis and are shown as conceptual sketches in Figure 7 - Figure 9.

The conventional configuration was evaluated for its simplicity and high flight speed when compared to other configurations with similar propulsion packages. The wing span and chord were identified as the driving dimensions of the tube for the conventional aircraft. The wing was placed centrally and folded span-wise as shown in Figure 7. The conventional configuration requires a folding mechanism that stows the empennage within the tube volume without adding too much diameter or length.
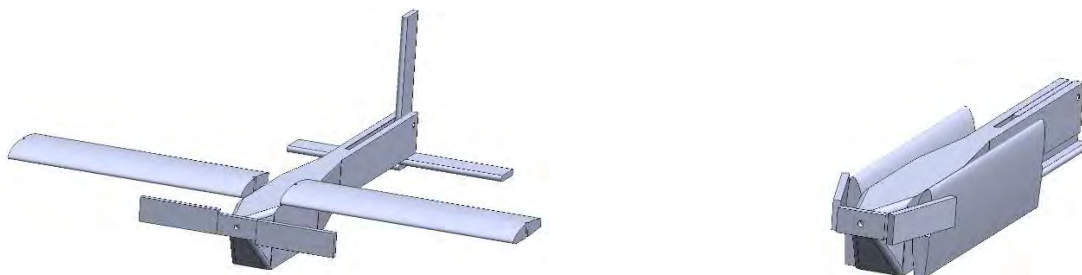
Figure 7: Sketch of the conventional aircraft in the flight (left) and stowed (right) configuration.

The flying wing configuration was evaluated as shown in Figure 8. A single hinge at the fuselage allows the wings to fold in line with the tube. With no tail, the flying wing would not require a folding mechanism for the empennage. Despite lower drag at cruise, the flying wing requires a larger wing area to achieve takeoff at the same launch velocity.
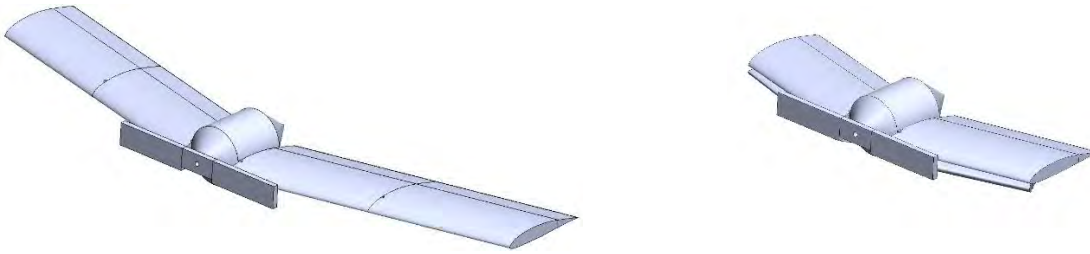
Figure 8: Sketch of the flying wing aircraft in the flight (left) and stowed (right) configuration.

The tandem wing configuration was evaluated as a result of its popularity within industry as the design for tube launched UAVs. This conceptual configuration was inspired by the AeroVironment Switchblade and consists of two lifting surfaces that hinge at the center and lay flat along the fuselage [2]. Two vertical fins provide the required aerodynamic stability and fold along the fuselage as shown in Figure 9. Further analysis identified numerous disadvantages to the tandem wing configuration at launch. Most notably, splitting the lifting area across two surfaces with reduced chord, at the scale and launch velocity of this hand-launched UAV, could produce a tendency to stall as a result of low Reynolds numbers ($Re_c \leq 200,000$) and high wing loading. With this configuration, the chord must increase such that the total wing area would be larger than the conventional configuration to prevent stall at launch.
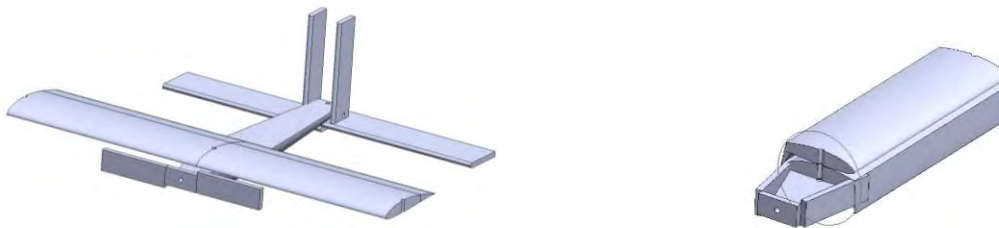
Figure 9: Sketch of the tandem wing aircraft in the flight (left) and stowed (right) configuration.

3.3.2 CONFIGURATION SELECTION PROCESS

The configuration downselect method uses a series of estimates and assumptions that quantitatively compare each of the above configurations across a range of design parameters. Figures of Merit (FoM) were derived from the design parameters as shown in Table 3. Each FoM was assigned a score factor and was used to identify the most competitive aircraft configuration.

Table 3: Figures of Merit (FoM) and corresponding design parameters.

Figures of Merit	Design Parameters	Score Factor
Wing Surface Area	L_{Tube}, D_{Tube}	0.30
Flight Speed	T_{USC}	0.25
Fold Complexity	EW_{Plane}	0.15
Build Complexity	EW_{Plane}	0.15
Launchability	D_{Tube}	0.15

The score factor for each FoM was derived qualitatively by looking at the comprehensive impact of the FoM on the overall score when compared to the other FoM. The score factors were weighted such that the sum of the score factors equaled one and are shown in the third column of Table 3. The next step was determining how each configuration scored for each FoM (independent of the other FoM). For each FoM a value was assigned from -1 to 1 indicating the expected performance of that particular aircraft configuration. A value of -1 indicates the design configuration (represented by the column) scored poorly for the FoM (represented by the row), while 1 meant it would do very well. As a result of the team's experience with building light-weight monoplanes, a monoplane was used as the baseline to which all other configurations were compared. Therefore, a value of 0 implied that the configuration scored as well as a monoplane for the given FoM. The final step was to multiply each configuration evaluation with the corresponding FoM Score Factor, and then sum the values for each configuration. The Total Score for each configuration, shown at the bottom of Table 4, provides the basis for the quantitative comparison, with the highest score being most favorable.

Table 4: Aircraft configuration downselect.

Figures of Merit (FoM)	Score Factor	Monoplane	Flying Wing	Tandem Wing
Wing Surface Area	0.30	0	-1	-1
Flight Speed	0.25	0	-1	0
Fold Complexity	0.15	0	1	1
Build Complexity	0.15	0	0	0
Launchability	0.15	0	0	-1
	Total Score	0	-0.4	-0.3

As shown in Table 4, despite the reductions in folding complexity, there were significant disadvantages to the Flying Wing and Tandem Wing configuration that would result in a larger tube and lower total score when compared to the Monoplane configuration. With the overall aircraft configuration selected, the team moved forward using the downselect process to select the folding method and empennage configuration.

3.4 CONFIGURATION REFINEMENT

Following the identification of the Monoplane as the highest scoring configuration, the team refined the conceptual design to account for the wing folding method, tail design and payload accommodations.

3.4.1 FOLDING APPROACH SELECTION

The team considered numerous approaches to stowing the wings in the launch tube prior to flight. Driving factors in the consideration of each approach were weight and the resultant tube dimensions. Although many configurations were considered, three were selected for further analysis. The three approaches selected, known as "Lock and Load", "McTwist", and "F-14", are presented below.

Lock and Load

The objective of "Lock and Load" was to align the curvature of the upper wing surface with the curvature of the tube by centering the fuselage with stowed wings on either side. The pucks were placed vertically in the fuselage. The wings rotate twice, 270° about the leading edge and 90° flush with the sides of the fuselage. A complex hinge joint is required to complete the design.
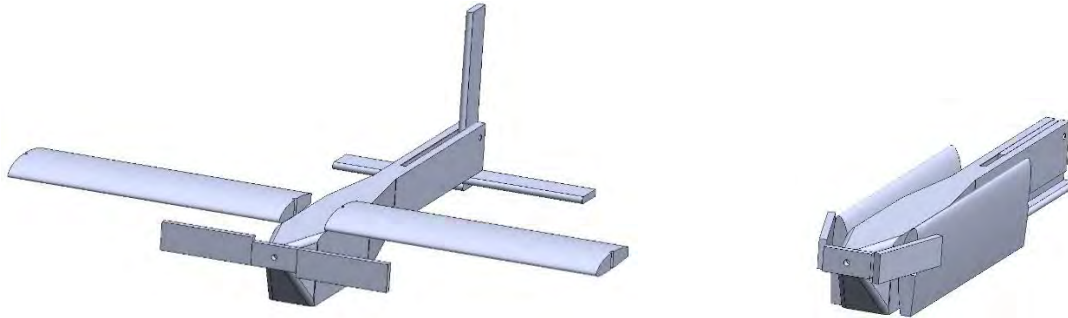
Figure 10: The "Lock and Load" technique in flight (left) and stowed (right) configuration.

McTwist

The "McTwist" is intended to reduce the build complexity of the hinge mechanism by preserving the structural integrity of the load bearing elements in the wing. This is accomplished with a single rotating hinge aft of the wing quarter chord with enough structure to counter the lift produced by the wings. Although these loads could likely be distributed throughout the fuselage, the magnitude of these loads might offset the weight benefits of having a single hinge.
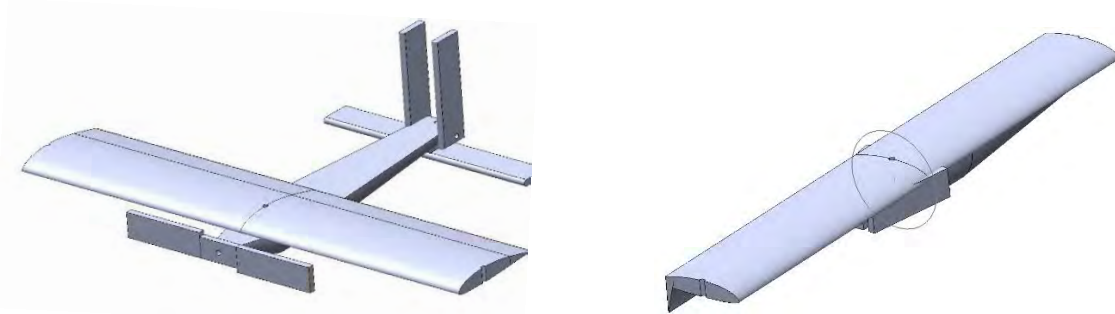
Figure 11: The "McTwist" configuration in flight (left) and stowed (right) configuration.

F-14

In the "F-14" configuration, the wing splits at the center and both halves of the span rotate rearward and sit on top of the fuselage. In this configuration, the wings would likely remain offset in the flight configuration or require an intricate folding mechanism that allows the wings to remain level in the flight configuration.
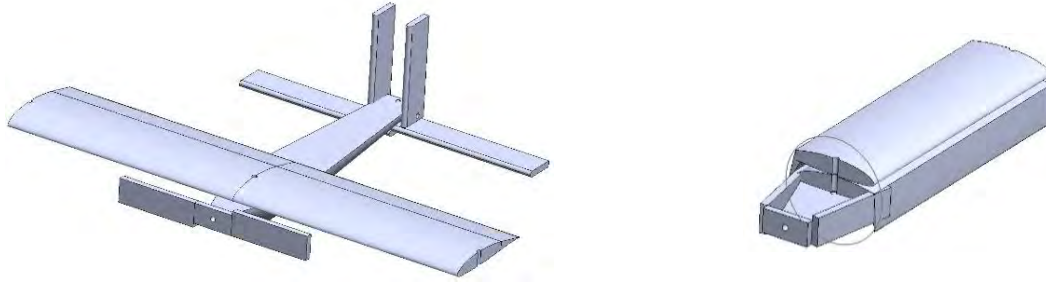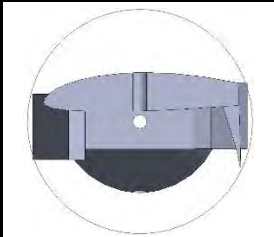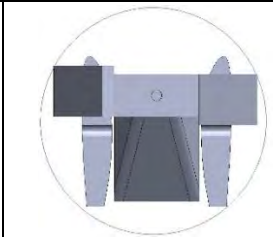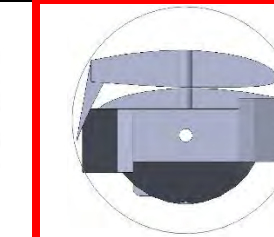
Figure 12: The 'F-14' in flight (left) and stowed (right) configuration

The tube dimensions impact the RAC through the quantity $(L_{Tube} + \pi D_{Tube})$. An approximation for this quantity was estimated for each folding method and the results were quantitatively compared in Table 5.

Table 5: Wing folding approach selection.

Configuration	McTwist	Lock and Load	F-14
Tube Diameter	5.5	5.5	5.5
Tube Length	27	22	22
$(L_{Tube} + \pi D_{Tube})$	44.3	39.3	39.3

As shown in Table 5, both the "Lock and Load" and "F-14" configuration were estimated to have approximately the same impact on the RAC. The team identified the hinge mechanism in the "Lock and Load" configuration as a high risk component because it required rotation in two planes. As the "F-14" configuration had a simpler mechanism and an equivalent estimation for $(L_{Tube} + \pi D_{Tube})$, the team moved forward with the "F-14" configuration as the approach to folding the wings into the stowed configuration.

3.4.2 TAIL CONFIGURATION
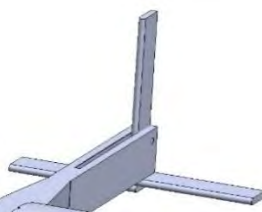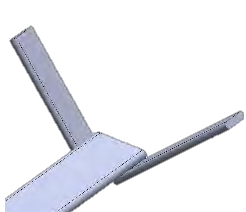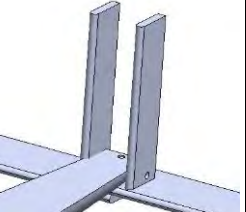
As a result of the aircraft configuration selected, an empennage was required to maintain stability. The main factors governing empennage selection were minimizing folded volume, minimizing weight, minimizing hinge complexity, maximizing stability, and minimizing drag. The following designs were compared, and a configuration downselect is shown in Table 6.

- Conventional: The conventional design requires at least three hinges and rotation about at least two axes. Pitch and yaw control are not coupled, allowing these to be sized independently.
- V-Tail: The stabilizers form a V-shape, which provides both pitch and yaw control using ruddervators, resulting in coupling between longitudinal and lateral-directional stability. Although

theoretically lower drag because of the reduced wetted area, the primary benefit of this configuration is the simplicity of rotating the surfaces flush with the fuselage. Two hinges are required about two separate axes.

- Split Tail: The split tail is similar to the conventional tail but has two fins that both provide yaw stability. The vertical stabilizers slide flush with the sides of the fuselage and the horizontal stabilizers fold underneath the fuselage. At least three rotations are required about two axes. The primary strength of this design is that the hinge mechanisms required are very simple and could be very lightweight.

Table 6: Empennage downselect table.

Figures of Merit	**Score Factor**	**Conventional**	**V-Tail**	**Split Tail**
Folded Volume	0.3	0	1	-1
Hinge Complexity	0.2	0	1	1
Weight	0.2	0	-1	1
Stability and Control	0.2	0	-1	-1
Drag	0.1	0	1	-1
Total	1	0	0.2	-0.2

From this down-select, the V-tail design was selected for the competition aircraft. The V-tail easily integrates with the fuselage and most efficiently occupies the tube volume beneath the aft section of the fuselage.

3.4.3 PAYLOADS

Three payload configurations were evaluated in the conceptual design phase. Each is configuration is shown relative to the oncoming velocity of air, V_∞

Vertically-Oriented Stack

In-Line

Combined
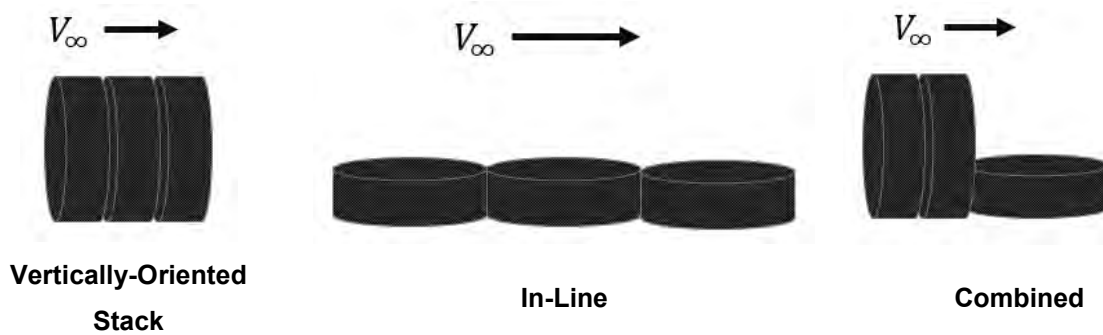
The first solution considered was to orient the face of the pucks toward the oncoming flow and place all of the payload forward of the center of gravity (CG). Orienting the pucks in this configuration minimized tube diameter required to house the payloads, allowed for an aerodynamic fuselage aft of the wing, and made it easy to place the CG for flight. The disadvantages for this configuration were that it required a significant amount of fuselage volume in front of the wing when compared to other configurations.

The second solution considered was to lay the pucks flat horizontally as shown in the "in-line" configuration. The benefits of this configuration were that it allowed the pucks to stow nicely underneath the wings and minimized the frontal area of the tube. Further analysis revealed that distributing the mass underneath the wing made CG placement difficult and required more length in the nose when compared with the vertically-oriented stack.

An intermediate solution considered was the "combined" configuration, which consisted of one puck stacked vertically and two flat horizontally in line with the fuselage and underneath the wings. While this configuration was promising, the orientation of the longest dimensions for the vertical and horizontal orientation required the largest tube diameter of the configurations considered.

As a result of the conceptual payload analysis, the team moved forward with the vertically oriented stack. The tube diameter required, ease of integration with the fuselage, and simplicity of placing the CG of the airplane made this the most ideal payload arrangement.

3.5 FINAL CONCEPTUAL DESIGN

The final configuration consists of a high wing conventional aircraft with a V-tail designed to carry three payloads as shown in Figure 13. The aircraft will be hand launched and skid on the bottom of the fuselage to remove the need for a landing gear. To transition to the stowed configuration, each tail surface rotates underneath the fuselage, wings rotate back in the "F-14" configuration, ailerons fold down and the folding propeller aligns with the tube wall. The tube is designed as a nonstructural element that transfers loads to the fuselage.
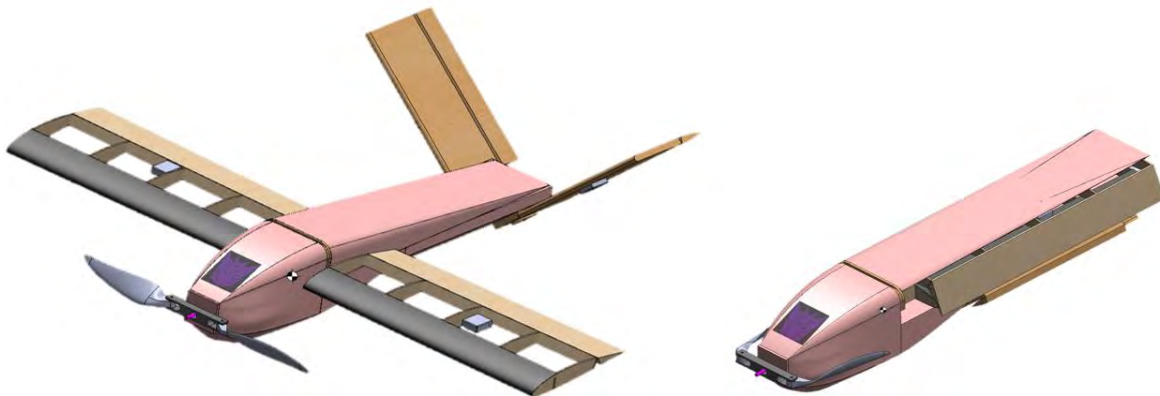
Figure 13: Final conceptual design in flight (left) and stowed (right) configuration

4.0 PRELIMINARY DESIGN

The team collaborated to design all aircraft components to meet the three design objectives: minimize tube diameter, reduce empty weight, and maximize speed for M_2. Numerous trade studies were conducted using software simulations and models to develop the optimum sizing for all components of the aircraft and launch tube. Computer models and lab mockups allowed for further development of the hinging mechanisms and structural elements critical to the success of the team's design.

4.1 DESIGN METHODOLOGY

The preliminary design was developed through an iterative and collaborative process that required the input of numerous captains and team members across all disciplines. The critical components in the preliminary design phase and their corresponding design requirements are described as follows:

Wings

- Wing planform area (S): The wing area produces the lift required to support the aircraft payload. This wing area is constrained by the launch velocity at takeoff. As the driving factor in the size of the launch tube, the wing area was minimized to reduce the tube dimensions and aircraft weight.

- Aspect Ratio (AR): High AR wings reduce induced drag, offering better takeoff and cruise performance than low AR wings. As a function of the wing chord, c, and wing span, b, the AR of the wing largely determines, L_{Tube} and D_{Tube}.

- Airfoil: The team used a custom airfoil designed to operate efficiently at low Reynolds numbers. The minimum allowable Reynolds number for this airfoil is $Re_c = 125,000$, based on wind tunnel data collected by the team in 2011 [3]. The airfoil is designed to generate the required lift at launch and then optimize for $(L/D)_{cruise}$ to improve lifting efficiency and minimize power required at cruise.

Propulsion

- Motor, propeller, and battery pack: The components were selected to meet the performance goals of the aircraft while minimizing overall package weight.

Launch Tube

- Ground Mission: All aspects of the tube are designed to minimize the rated aircraft cost and meet the requirements of the ground mission. The tube must maintain its shape during the drop test while transferring all loads to the structural elements of the aircraft without deforming or cracking.

4.2 MISSION MODEL

The Performance sub-team used multidisciplinary design optimization (MDO) methods to determine the highest scoring design. The MDO was implemented via PlaneTools, a package of simulation modules written by the team in MATLAB. PlaneTools simulated a full mission of the input aircraft by modeling four phases of the competition course: Takeoff, Climb, Cruise, and Turn [5], as shown in Figure 14 and detailed below:

1. Takeoff – Assumed to be performed at maximum throttle using no high-lift devices. Testing was performed to determine the design launch speed (50 ft/s, 15 m/s), concurrent with records of the team's last hand-launched plane and initial testing (8.1.1).
2. Climb – The aircraft was assumed to climb to 25 ft (7.6 m) above the 2643 ft (806 m) altitude (ground level) of Tucson, AZ. The rate of climb was calculated via the difference in thrust and drag on takeoff and multiplied by the proportion of the takeoff speed to the plane's weight.
3. Cruise – This phase of flight was assumed to be level, constant speed flight with equal thrust and drag. For each mission, an optimum cruise throttle setting was selected so the aircraft did not exceed its nominal battery capacity at the end of the mission.
4. Turn – A coordinated level turn with constant speed and radius was assumed for both types of turning maneuvers (two 180° turns and one 360° turn). The load factor on the aircraft structure was calculated based on predicted turn radius.
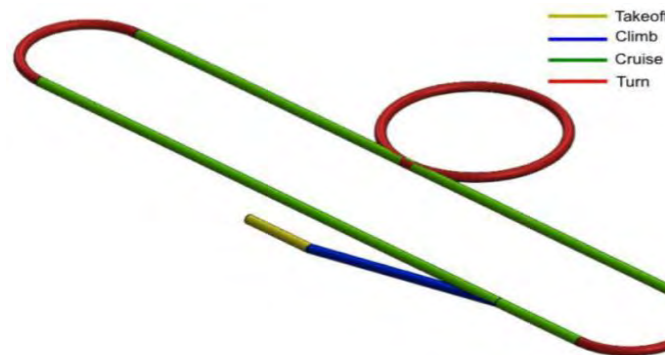
Figure 14: Flight model used in PlaneTools, indicating all phases of flight.

Fundamental aircraft and aerodynamic equations were used to calculate output parameters such as rate of climb, cruise conditions, and turn radius. The mission model also included the following uncertainties and assumptions:

- **Winds** – A headwind of 8 ft/s (2.4 m/s) was assumed for cruise based on historical weather patterns during competition weekend in Tucson, AZ [4]. For takeoff, a headwind of 0 ft/s (0 m/s) was assumed to ensure that throwing velocity would provide ample lift in still air.
- **Battery performance** – Battery resistance and capacity were based on in-lab bench tests and flight tests rather than manufacturer specs. Battery voltage was assumed to be constant throughout each flight.
- **Propeller performance** – The coefficients of thrust (C_T) and power (C_p) used in thrust calculations were based on values provided by the manufacturer and verified via static testing [5]
- **Tube** - The tube dimensions and weight were based on detailed configuration analysis which concluded the tube diameter was a function of the folded chord and the tube length was a function of the wing half-span. Both functions included constants which accounted for the pre-defined stowed wing offset and nose length, respectively.

The mission model neglected interference drag and compressibility. The propulsion model ignored variations in internal temperature, which affect the resistance and voltage of the system. From in-lab testing, it was determined that these parameters were very small perturbations on the overall mission and were neglected for simplicity.

The mission model is programmed within PlaneTools as a class with several operations to simulate missions on any user-defined aircraft. The role of the mission model in PlaneTools is represented by Figure 15. The simulations help determine the initial design parameters for the aircraft by selecting those that result in a higher flight score.

This object-oriented approach allowed the team to isolate each component of the aircraft and perform trade studies more effectively. Uncertainties are propagated throughout the mission model; uncertainty values are quantified based on results from laboratory testing and flight tests. Figure 15 depicts a simplified order of operations that PlaneTools utilizes in order to simulate the entire mission. Note that while this figure shows a linear progression to output values, iteration is used within the tool to ensure convergence.

Plane Components	Mission Model	Flight Attempt	Outputs
•Wing	•Altitude	•Takeoff	•Capacity Required
•Empennage	•Headwind	•Climb	•Turning Radius
•Fuselage	•Temperature	•Cruise	•Laps Flown
•Propeller	•Time Limit	•Turn	•Elapsed Time
•Battery	•Launch Velocity		
•Motor			
•Payloads			
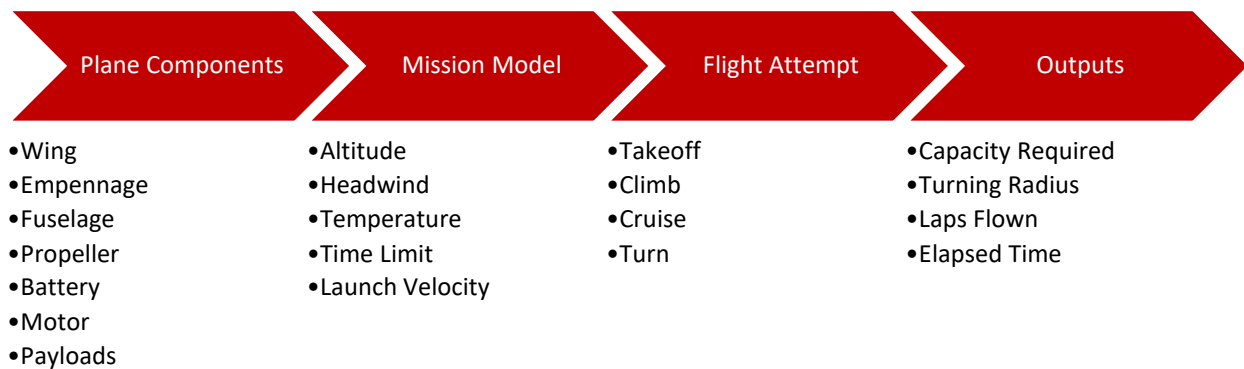
Figure 15: PlaneTools object model.

4.3 DESIGN TRADE STUDIES

4.3.1 WING GEOMETRY

A trade study determining the effect of variations in AR, b, and S on Total Score was performed. This was performed for multiple propulsion packages, consisting of different motors, battery cells (type and count), and propeller sizes. The analysis was performed with the M_2 flight as the constraint. Results of this trade study for the final propulsion package are shown in Figure 16, which presents the Total Score vs. wing geometry.
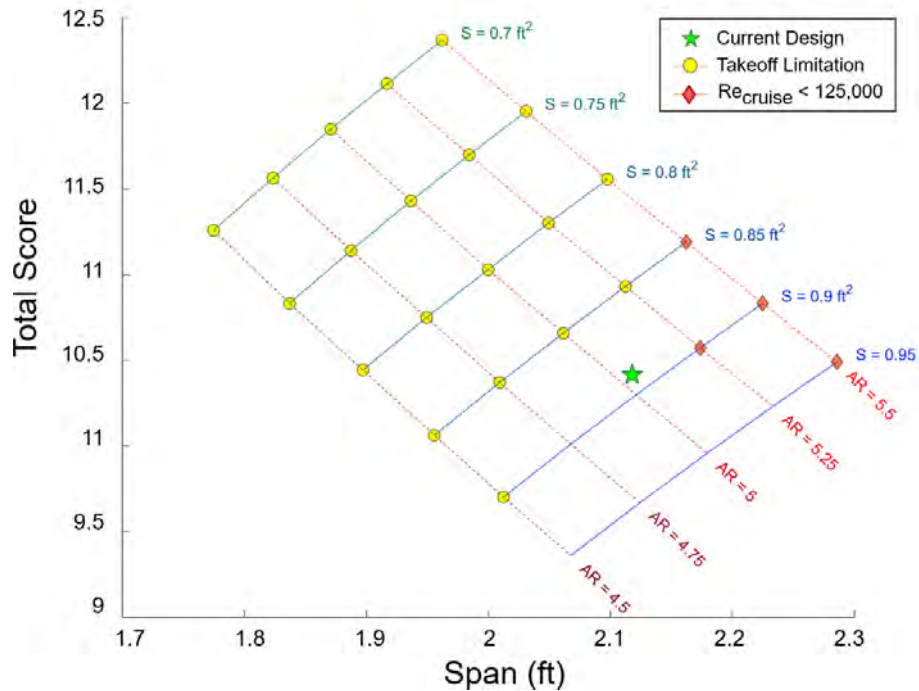
Figure 16: Carpet plot showing changes in total score with variations in wing AR, S, and b.

The optimal wing geometry maximizes score while still meeting the takeoff requirement that $V_{launch} \geq V_{stall}$. Figure 16 shows that increasing wing area decreases V_{stall} but decreases score by increasing structural weight and tube dimensions. Furthermore, increasing AR also decreases V_{stall} but decreases Re_{cruise} to a value where laminar separation may occur, indicated with diamond-shaped (red) markers. Simulations that failed to meet the takeoff limitation are denoted with a circular (yellow) marker. Therefore, the highest-scoring aircraft has a wing configuration indicated by the green star in Figure 16. This wing has $AR = 5.0$ and $S = 0.89$ ft^2 (0.083 m^2).

4.3.2 PROPULSION SIZING

The propulsion system was designed to maximize the number of laps flown for M_3 and to minimize the time required to complete three laps for M_2 while reducing weight. Sizing for M_3 proved to be the most restrictive as it consists of flying the maximum payload as well as flying as many laps as possible in five minutes.

As indicated by the integrated performance analysis in 3.2.2, increasing the number of cells flown did not correspond to the highest scoring configuration. As a result, the team targeted an electrical power loading of 50 W/lb, which is common for basic park flyers and resulted in a power requirement of 112 W for M_3 according to Eq. 13 [6].

$$2.25 \text{ lb} \cdot (50 \text{ W/lb}) = 112 \text{ W} \qquad \text{Eq. 13}$$

NiMH cells were chosen due to their higher energy density and lack of a memory effect when compared to NiCd cells. Elite 1500mAh 2/3A cells ($1.2\ V/cell$) were selected based on exceptional performance

throughout the team's history when compared to other commercially available cells. The electrical power output of the battery pack is shown in Eq. 14.

$$Power = Voltage * Current \qquad \text{Eq. 14}$$

Battery testing in Section 8.1.2 indicated that the maximum current allowable for a 5-minute flight time was 13 A. At this current draw, the propulsion sub-team observed an average voltage reduction of 10%, resulting in the power available calculation, Eq. 15.

$$Power = \left(0.9 \cdot 1.2 \frac{V}{cell} \cdot n_{cell}\right) \cdot 13 \text{ A} \qquad \text{Eq. 15}$$

By solving Eq. 15 for n_{cells} with a target electrical power of 120 W, the team determined that an 8 cell battery pack was optimal for M_3.

For M_2, increasing current resulted in faster flight speeds and lower total flight times. PlaneTools indicated that the current draw for M_2 was not constrained by flight time, but by the maximum allowable current output of the cell. Based on testing conducted in previous years, these cells were limited to 28 A before performance diminished significantly [7].

$$Power = \left(0.8 \cdot 1.2 \frac{V}{cell} \cdot 8 \text{ cells}\right) \cdot 28 \text{ A} = \ 215 \text{ W} \qquad \text{Eq. 16}$$

With a voltage knockdown of 20% at 28 A, the M_2 power output for is 215 W according to Eq. 16. The power loading for the 2.25 lb aircraft is 96 W/lb, which is consistent with traditional sport flying [6].

The team iterated through a motor library in PlaneTools in order to identify the optimal Kv for completing the mission with the above specifications. The highest scoring motor identified in PlaneTools was the 1400 Kv Scorpion SII 2212. Using the same method, the highest scoring folding propeller was identified in order to complete the preliminary propulsion package presented in Table 7. The team moved forward in the critical design phase to validate PlaneTools predictions and test individual components prior to flight tests.

Table 7: Preliminary design propulsion package for the aircraft.

Motor	Battery Pack	Propeller
Scorpion SII 2212 (1400 Kv)	8 x Elite 1500s (9.6 V)	AERONAUT 8x6 folding

4.4 AERODYNAMICS

The aircraft performance was optimized using a combination of Athena Vortex Lattice (AVL), a flight dynamic vortex lattice based analysis software, and XFOIL, an inviscid panel based airfoil analysis program.

4.4.1 AIRFOIL SELECTION

A comparison of simulated coefficients $C_{d,cruise}$, $C_{d,turn}$, and $C_{l,max}$ was made using XFOIL for several airfoils developed by members of the team, the best are shown in Figure 17.
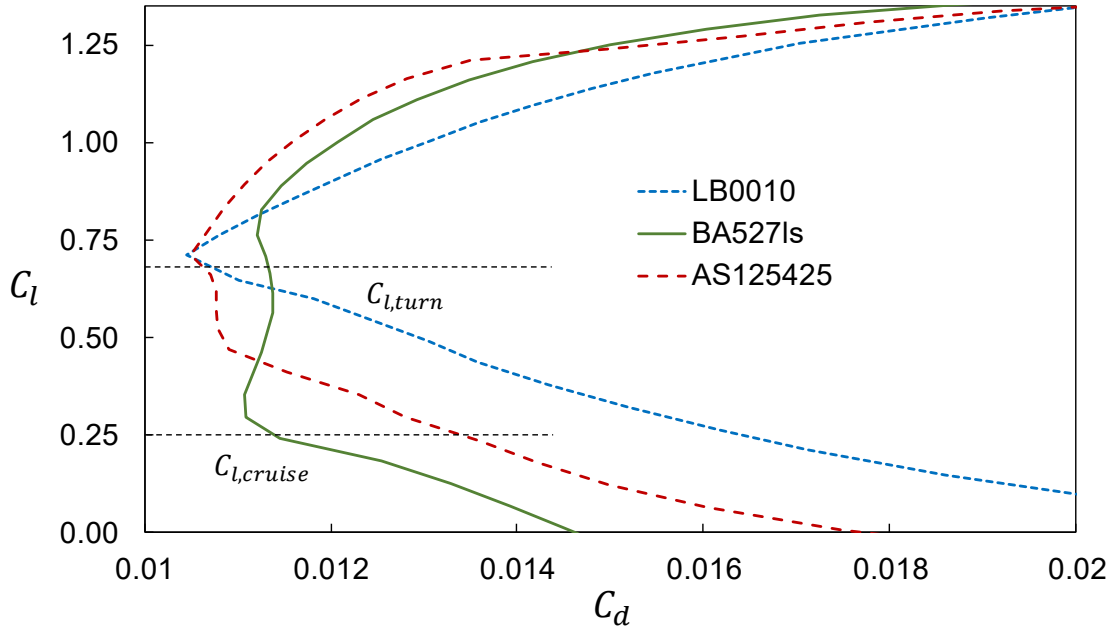
Figure 17: Polars for the LB0010, BA527ls, AS125425, analyzed in XFOIL at Re_c = 200,000.

The BA527ls airfoil was selected due to its low drag in cruise and comparable drag in turn. While the LB0010 produces a significantly higher max lift ($C_{l,max} = 1.7$) compared to that of the other two shown ($C_{l,max} = 1.5$), any resulting reduction in wing area is unable to justify the large drag penalty at cruise [8].

4.4.2 AERODYNAMIC COMPONENT ANALYSIS

The drag was estimated for the various aircraft components. Wing profile drag was estimated using XFLR. Induced and viscous drag for other components were estimated using flat plate approximations described by Hoerner [9] and Page [10]. Figure 18 shows the breakdown of s drag components for M_2 and M_3 cruise.
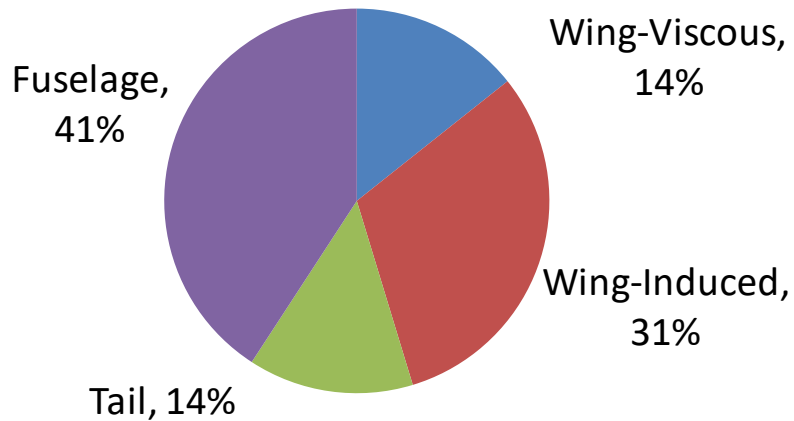
Figure 18: Drag break down for M_2 and M_3 cruise.

4.4.3 DRAG ANALYSIS

AVL was used to analyze the L/D vs C_L of the aircraft in M_2 and M_3 cruise, shown in Figure 19.
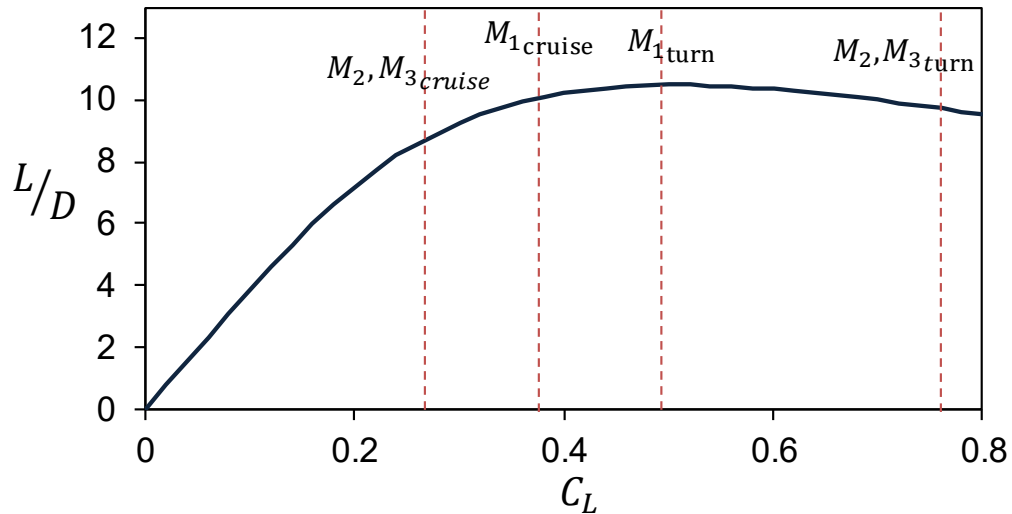
Figure 19: L/D **vs** C_L **for cruise and turn for all missions. Vertical lines indicate the** C_L **for each mission.**

$(L/D)_{max}$ is positioned evenly between the cruise and turn conditions for M_2 and M_3. This allows for relatively low drag in all phases of flight, especially if the aircraft is unable to reach full cruise speed between turns, which is likely to occur before and after the 360º turn.

The AVL solutions were used to perform Trefftz plane analysis to determine the aircraft angle of attack and trim elevator deflections. Acceptable bounds of $\pm 5°$ for α and $\pm 3°$ for tail deflection were set for low trim drag, to optimize for the speed-sensitive M_2 and M_3. From Table 8, it can be seen that these characteristics are within acceptable bounds.

Table 8: Trim deflections for cruise conditions.

	M_1 **Cruise**	M_2, M_3 **Cruise**
e	0.71	0.78
α [º]	-0.4	0.08
Elevator [º]	-1.5	-1.8
C_L	0.08	0.15
C_D	0.041	0.043
C_{D_i}	0.006	0.008
C_{D_0}	0.035	0.035

Figure 20 shows the Trefftz plot for M_2 and M_3, in which the plane is similarly loaded. The green curve denotes the lift coefficient normalized with respect to the wing chord. It can be seen that the lift distribution is positive along the entire span.

α = 0.0787 pb/2V = -0.0000 CL = 0.2732 Cl' = 0.0000
β = 0.0000 qc/2V = 0.0000 CY = 0.0000 Cm = 0.0000
M = 0.000 rb/2V = -0.0000 CD = 0.04270 Cn' = 0.0000
Aileron = 0.0000 CDi = 0.00737 e = 0.7521
elevator = -1.8086 CDp = 0.03500
rudder = 0.0000

AVL 3.35
Trefftz Plane
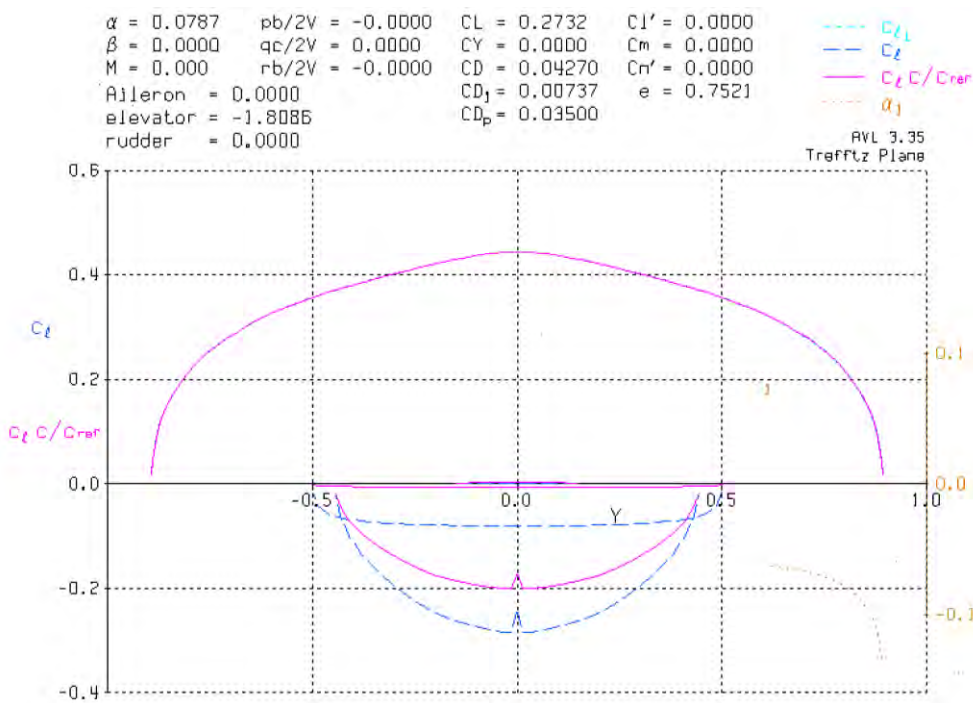
Figure 20: Trefftz Plane Plot.

4.5 STABILITY AND CONTROL

4.5.1 STATIC STABILITY ANALYSIS

Static stability was iteratively sized in AVL. Due to variance in the predicted CG location during the preliminary design phase, an acceptable CG range was selected for stable cruise in M_2 and M_3. The limits of such a range were selected as those producing a static margin of 15% and 35%, which occurred at 2% MAC and 25%. The tail arm and tail size were then iterated until the static stability derivatives satisfied Level 1 flying qualities as defined by MIL-F-8785C [11]. As shown in Table 9 and Table 10, C_{m_α}, C_{m_q}, C_{l_β}, C_{l_p}, and C_{n_r} are negative and C_{n_β} is positive, which are necessary conditions for static stability.

Table 9: Forward CG limit static stability derivatives for M_2 and M_3 calculated with AVL.

C_{L_α}	4.37	C_{m_α}	-1.58	C_{Y_β}	-0.64	$C_{Y_{\delta_r}}$	-0.01	C_{Y_p}	-0.034	C_{Y_r}	0.37
$C_{L_{\delta_e}}$	0.017	$C_{m_{\delta_e}}$	-0.035	C_{l_β}	-0.11	$C_{l_{\delta_r}}$	0	C_{l_p}	-0.38	C_{l_r}	0.17
C_{L_q}	9.93	C_{m_q}	-11.37	C_{n_β}	0.12	$C_{n_{\delta_r}}$	0	C_{n_p}	0.026	C_{n_r}	-0.23

Table 10: Aft CG limit static stability derivatives for M_2 and M_3 calculated with AVL.

C_{L_α}	4.37	C_{m_α}	-0.64	C_{Y_β}	-0.64	$C_{Y_{\delta_r}}$	-0.01	C_{Y_p}	-0.042	C_{Y_r}	0.32
$C_{L_{\delta_e}}$	0.017	$C_{m_{\delta_e}}$	-0.032	C_{l_β}	-0.11	$C_{l_{\delta_r}}$	0	C_{l_p}	-0.38	C_{l_r}	0.16
C_{L_q}	8.08	C_{m_q}	-9.01	C_{n_β}	0.089	$C_{n_{\delta_r}}$	0	C_{n_p}	0.025	C_{n_r}	-0.21

The static stability requirements were confirmed to be satisfied for each mission. It was confirmed that no combination of angle-of-attack and ruddervator deflection expected in-flight could cause the tail to stall.

4.5.2 DYNAMIC STABILITY ANALYSIS

The plane's dynamic stability characteristics were analyzed in a similar manner. Using the stability derivatives in Table 9 and Table 10 and the aircraft's mass moments of inertia, the characteristic values for each mode were calculated using AVL and derivations from Yechout [12]. Figure 21 shows the upper left quadrant of a root locus plot for the aircraft at cruise for M_2 and M_3. Short period (1), Dutch roll (2), roll (3), spiral (4), and phugoid (5) modes are plotted as damped frequency (ω_d) versus the damping coefficient and natural frequency ($-\zeta\omega_n$). Each of the five modes of motion was designed to be stable, indicated by negative real components in Figure 21.
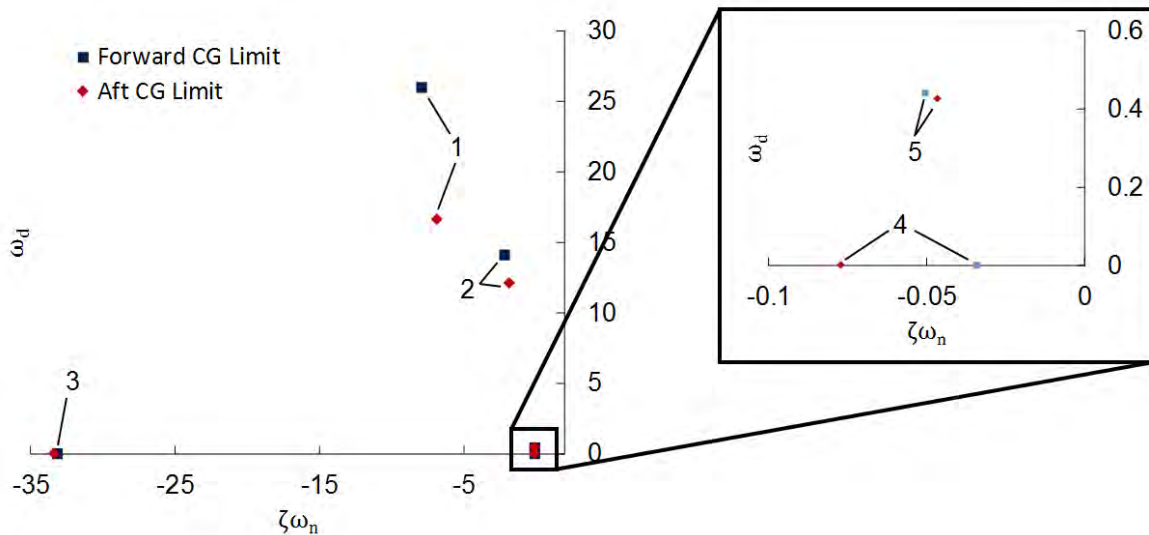
Figure 21: 5 modes of motion: (1) short period (2) Dutch roll (3) roll (4) spiral and (5) phugoid

The dynamic stability parameters for forward (CG$_1$) and aft (CG$_2$) limits of the CG are shown in Table 11.

Table 11: Dynamic Stability Parameters.

#	Mode	ζ		ω_d [rad/s]		$\zeta\omega_n$ [rad/s]		τ [s]	
		CG$_1$	CG$_2$	CG$_1$	CG$_2$	CG$_1$	CG$_2$	CG$_1$	CG$_2$
1	Short Period	0.45	0.42	26.00	16.62	-7.91	-6.81	0.13	0.15
2	Dutch Roll	0.20	0.12	14.12	12.12	-2.16	-1.86	0.46	0.54
3	Roll	-	-	-	-	-33.12	-33.35	0.03	0.03
4	Spiral	-	-	-	-	-0.03	-0.08	29.02	12.96
5	Phugoid	0.25	0.18	0.44	0.43	-0.05	-0.05	19.69	21.31

Military Specification MIL-F-8785C [11] was used to provide initial guidance for acceptable stability characteristics, which were modified based on pilot feedback during flight tests. While the damping

coefficients for Dutch roll and phugoid appear to low, pilot feedback at the Dec. 3 test flight confirmed that these quantities were acceptable. The plane was stable and responded as expected to all pilot inputs.

4.6 Transition to Stowed Configuration

Major design decisions were dependent on the successful implementation of wing and tail mechanisms that were sufficiently simple, reliable and lightweight. Preliminary design for these components was developed through a combination of CAD and lab mockups that served as proofs of concept.

4.6.1 Wing Hinge Mechanism

Following the survey of existing wing-folding mechanisms, many prototypes were built and tested to arrive at the preliminary design. The design consists of a structural coupler integrated with a bulkhead to flow loads from each half of the wing spar into the fuselage. Each spar contains a small metal rod that fits in a track to guide it from stowed to flight configuration. The wing halves are locked into place through the use of releasable zip ties. The zip ties were chosen for their reliability, accessibility and ease of operation, while satisfying the self-locking requirements set forth by the competition rules. The chosen design provides sufficient strength at considerably less weight than other options considered.
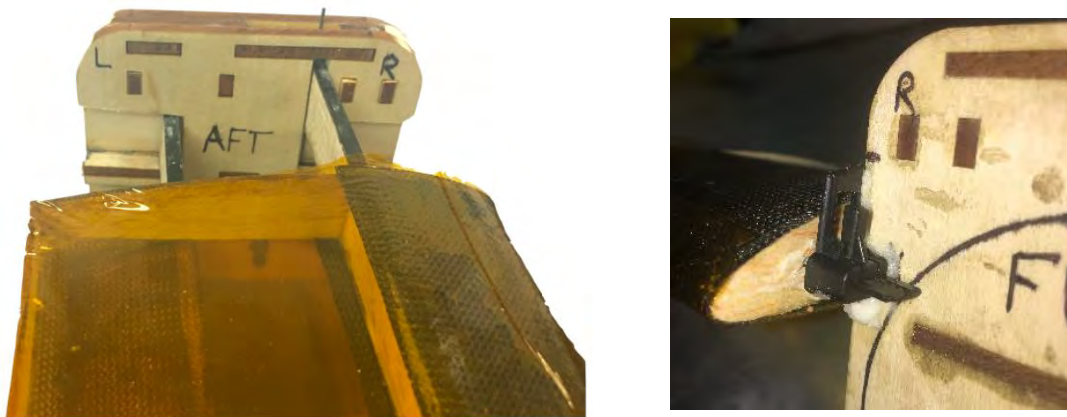
Figure 22: The spar coupler allows wings to offset in the stowed configuration (left) as shown.
Zip ties on the front of the spar coupler (right) secure the wings in the flight configuration.

4.6.2 Tail Hinge Mechanism

The choice of the V-tail provided a clear method of folding in order to provide the best use of space within the tube. Each side of the tail attached to the fuselage using a wooden dowel through its axis of rotation. When in stowed configuration, the tail provides a normal force against the locking mechanism in order to keep it in tension. When the tail is rotated into flight position, a flat plywood spring forces a square peg into a notch in the tail to lock the tail into flight configuration.

Figure 23: Preliminary design mockup of the empennage and locking mechanism.

4.7 PREDICTED AIRCRAFT PERFORMANCE

The performance of the preliminary designed aircraft, as predicted by PlaneTools, is listed in Table 12.

**Table 12: Preliminary design performance characteristics. Mission scores
are calculated using competitor assumptions in Table 2.**

Performance Parameter	M_1	M_2	M_3	M_G
$C_{L_{max}}$	1.2	1.2	1.2	
$C_{L_{cruise}}$	0.36	0.24	0.24	
e	0.80	0.80	0.80	
C_{D0}	0.034	0.034	0.034	
L/D$_{max}$	10.8	10.7	10.7	
L/D$_{cruise}$	3.0	5.0	5.0	
Rate of Climb	33 ft/s (10 m/s)	17 ft/s (5.2 m/s)	18 ft/s (5.4 m/s)	
W/S	1.3 lb/ft^2 (62 N/m^2)	2.6 lb/ft^2 (124 N/m^2)	2.6 lb/ft^2 (124 N/m^2)	
V_{cruise}	87 ft/s (27 m/s)	101 ft/s (31 m/s)	941 ft/s (29m/s)	
V_{stall}	32 ft/s (9.8 m/s)	44 ft/s (13 m/s)	44 ft/s (13 m/s)	
Gross Weight	1.13 lb (5.03N)	2.25 lb (10.06 N)	2.25 lb (10.06 N)	
Mission Score	1.0	1.51	2.96	2.0

5.0 DETAIL DESIGN

Detail design combines the theoretical sizing from conceptual and preliminary design with more detailed testing and analysis of individual components. Each sub-team considered the structural capabilities, subsystem design, weight, and mission performance in order to refine the dimensions of the competition aircraft.

5.1 DIMENSIONAL PARAMETERS TABLE

Table 13 lists the characteristic parameters for *Starscream*, USC's entrant into the 2017 DBF Competition. Each subsystem will be highlighted in the subsequent paragraphs.

Table 13: Characteristic parameters for *Starscream*.

Wing		Fuselage	
Airfoil	BA527ls	Total Length	1.5 ft (0.44 m)
Span	2.12 ft (0.65 m)	Nose Length	0.4 ft (0.12 m)
MAC	0.42 ft (0.13 m)	Tail Length	1.1 ft (0.32 m)
Planform Area	0.89 ft² (0.08 m²)	Width	0.3 ft (0.08 m)
AR	5.04	Height	0.3 ft (0.1 m)
Incidence Angle	0°		
Static Margin	35 %		
Controls		Motor	
Receiver	Futaba R7008SP	Model	Scorpion SII-2215
Servo	Diamond D47	Gearbox	Direct Drive
Battery Model	Elite 1500	Kv	1400
Internal Resistance	0.011 Ω	Power Rating	300 W
Cell Count	8	No-Load Current (I_0)	0.95 A
Pack Voltage	9.6 V	Internal Resistance	0.095 Ω
Pack Weight	0.27 lb (0.12 kg)	Weight	0.12 lb (0.055 kg)
Tail		Propeller	
Airfoil	Flat Plate	Mission 1	8" x 6"
Span	7.7 in (0.2 m)	Mission 2	9" x 7.5"
Chord	3.6 in (0.1 m)	Mission 3	8" x 6"
Planform Area	28 in² (0.02 m²)		
Incidence Angle	0°		
Tail Arm	0.8 ft (0.24 m)		
Spread Angle	90°		

5.2 STRUCTURAL CHARACTERISTICS AND CAPABILITIES

The aircraft structure was driven by the maximum load cases expected in the flight and ground missions. The wing was designed to withstand a 5g (11.25 lb, 5.1 kg) load case with a maximum weight of 2.25 lbs (1.02 kg), allowing for a $62°$ bank angle for sustained level turns. The Kevlar fuselage was designed to withstand in-flight and landing loads as well as to accommodate a firm grip during launch. Survivability of all components in the launch tube during the ground mission was a driving factor in the design and integration of each component.

5.3 SUB-SYSTEM DESIGN

5.3.1 WING

The wing design was driven by the wing geometry (4.3.1) and maximum aerodynamic loads. The spar coupler designed in 4.6.1 required that the spar split and allow for rotation to the stowed configuration. Although the primary flight loads were expected to transfer to the spar coupler, special care was taken to anticipate stress concentrations and account for the added complexity of splitting the spar across the coupler. The structure of the wing was sized using *SparSizer*, an excel tool made by former team advisor Mark Page. Trade studies were conducted with different materials and arrangements to identify the best solution. The spar was designed as an I-beam with carbon fiber caps and balsa wood shear web. Cap and shear web thickness were chosen to achieve a factor of safety of 1.5 at all points along the spar as shown in Figure 24.
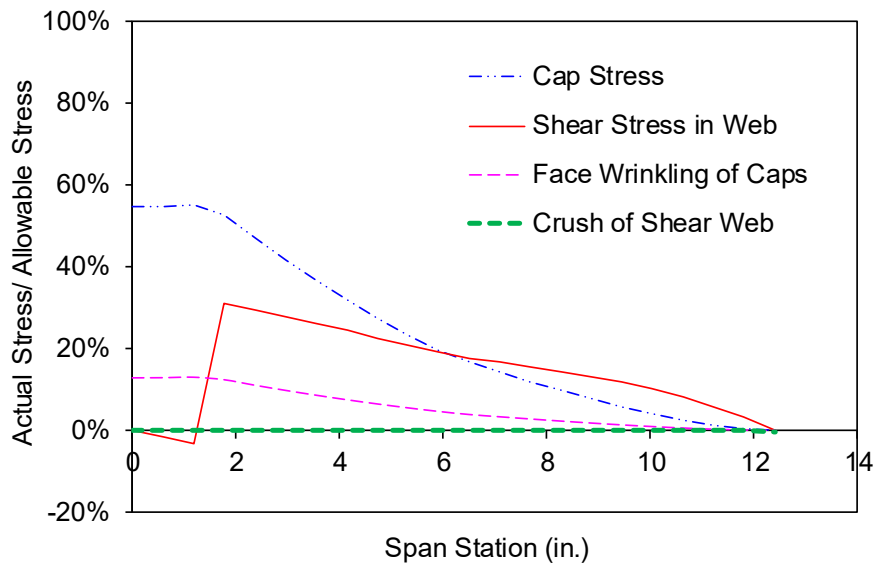
Figure 24: Percentage of allowable stress vs. the span of the wing.

5.3.2 WING HINGE MECHANISM

The wing folding mechanism was tested to ensure it could sustain the maximum 5g flight loads. Testing with Version 1 (V1) of the hinge mechanism, which consisted of unreinforced plywood identified stress risers and inconsistencies in build technique. Though failure occurred at an acceptably high load, the uncertainty in the measurements was determined to be unacceptable. V2 was designed to accommodate Kevlar strands that eliminated the stress riser and moved the failure point as shown in Figure 25.
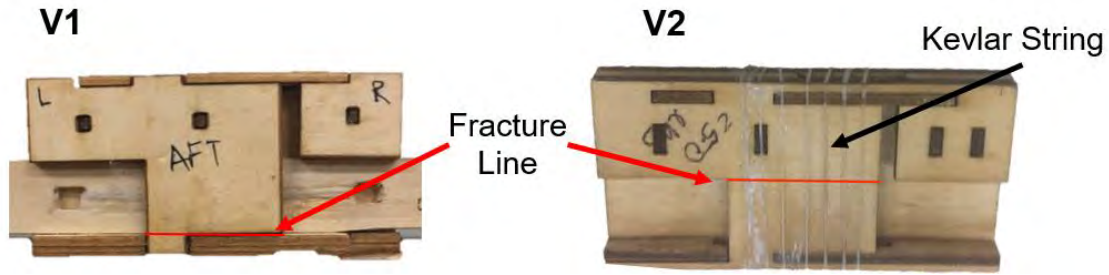
Figure 25: Comparison of changes between V1 and V2.

The results of mechanism structural testing are shown in Table 14.The redesigned part was shown to handle significantly higher loads with less variance in the failure point while only adding 0.03 oz. (0.9 g) to the weight of the part. As a result of this testing, the team moved forward implementing V2 into the aircraft.

Table 14: Results of structural testing (1g = 2.25 lb).

	V1 – Single Material	V2 – Added Kevlar Fibers
Mechanism Weight	0.29 ± 0.03 oz. (8.3 ± 0.8g)	0.32 ± 0.03 oz. (9.2 ± 0.8g)
Failure Point	12 ± 4 lb. (5 ± 2g)	52 ± 3 lb. (21 ± 1g)

5.3.3 TAIL

The V-tail folding mechanism was designed to provide a compact, lightweight and precise self-locking device to secure the stabilizers in flight position. The tail surfaces were designed as flat plates with a rounded leading edge and tapered trailing edge to simplify integration with the fuselage in the stowed configuration. The locking mechanism was designed with 1/16-in. (0.002 m) plywood as the locking arm. A balsa built up structure was selected for the tail design to minimize weight. Structural pieces of balsa fix the servos in place along the V-tail and allow for the proper deflections.
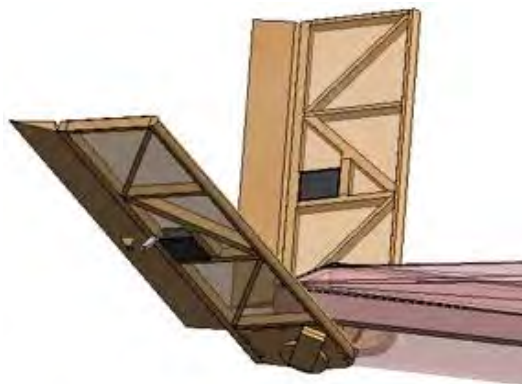
Figure 26: The tail locking mechanism and empennage assembly.

5.3.4 PAYLOAD RESTRAINTS

The payload restraints were designed to secure the three payloads for M_2, M_3 and M_G while minimizing the overall weight. The configuration of the payloads in the aircraft was determined by the conceptual analysis performed in 3.4.3. The team designed a support made from tensioned fishing line to fix all payloads to the forward bulkhead as shown in Figure 27.
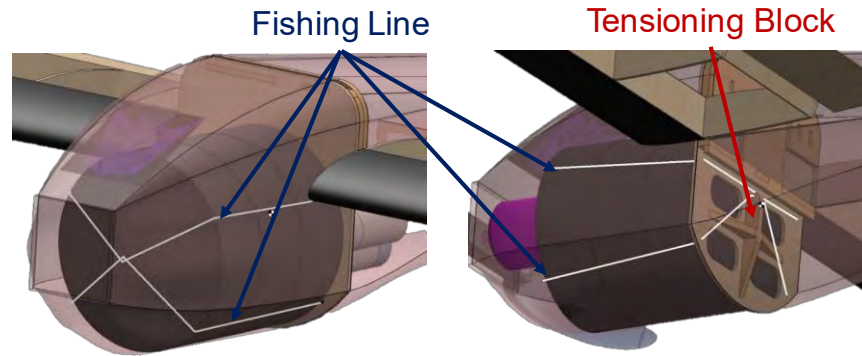
Figure 27: The pucks are fixed to a plywood bulkhead using fishing line and a tensioning block.

The fishing line design incorporates a tensioning block on the aft side of the bulkhead that allows the ground team to load the payload through access holes cut in the top of the fuselage. Once loaded, the team slides the line up the tensioning block and into a pre-fabricated slot. The fishing line 'bites' into the edges of the rubber hockey pucks and provides a secure fit that fully restricts the motion of the payloads.

5.3.5 FUSELAGE TYLER

The aircraft fuselage was designed to support aerodynamic, landing and ground mission loads. The monocoque fuselage consists of a load-bearing truss, manufactured with low-density foam sandwiched between 1.7 oz (48 g) Kevlar plies to increase the fuselage's stiffness and tensile strength. A forward bulkhead was included to integrate the wing folding mechanism with the fuselage and restrict the motion of the payloads. An aft-bulkhead takes ground loads in the event of a tail strike on landing and distributes loads for the end cap drop test. The truss design was based on load-path analysis that included supports for propulsion components, wing and tail integration, payloads, and continuous longitudinal structural members to absorb the impact of the end cap drops.
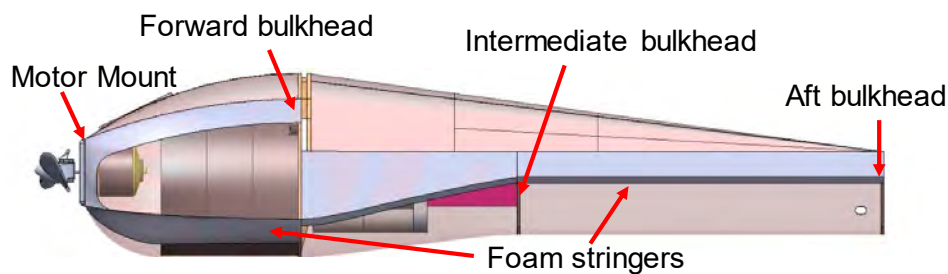
Figure 28: Side view of the fuselage with foam truss and bulkheads.

Finite Element Analysis (FEA) in Solidworks was used to inform the design of the fuselage for each load case [13]. Four load cases were created, one for the flight condition and one for each of the three drops of M_G. In the flight condition, the plane experiences an aerodynamic lifting force in the upward direction equivalent to the weight of the aircraft, 2.25 lb (1.0 kg). The tail exerts a net downward force of 0.3 lb (0.14 kg). The motor produces 1.6 lb (0.72 kg) of thrust and 0.2 lb-in (0.02 N-m) of torque. The resulting deflections and stresses on the model are shown in Figure 29.
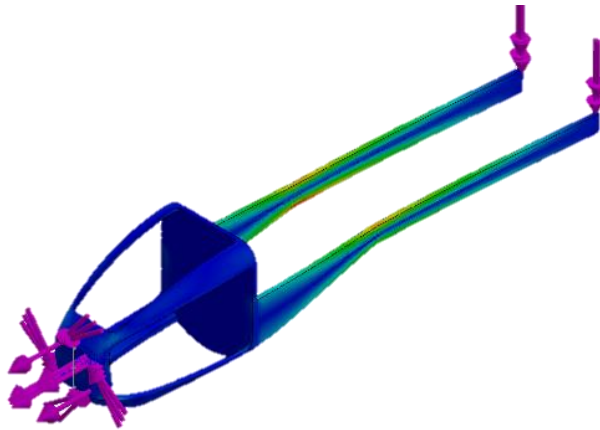
Figure 29: Truss structure analysis for flight loads.

These results indicate that the longitudinal members and junctions with the primary bulkhead exhibit the highest stresses. The intermediate bulkhead was placed at the location of maximum stress along the longitudinal member to provide increased strength. An iterative build and test method was implemented to further refine the design of the foam truss and to validate the results of the FEA model.

As a result of the complex set of contact points between the plane and the tube, the structures sub-team found that FEA did not fully capture the range of possible load paths for M_G. As a result of these conclusions, the sub-team quickly transitioned to repeated drop testing, shown in 7.2.3, as the primary method of validating the structural design for M_G.

5.3.6 PROPULSION SYSTEM

In the critical design phase the propulsion sub-team tested each component of the propulsion system to characterize and optimize the system as a whole. To validate the selection of the 1400 Kv Scorpion motor the team tested multiple motor configurations over a range of Kv ($1400 \leq Kv \leq 2100$). As a result of the testing performed in 8.1.2, the team confirmed that higher Kv motors required a higher current to produce the same thrust. Although lab testing could only be completed at static conditions, the assumed drop in current at dynamic conditions was not sufficient to meet the 13 A maximum current requirement at cruise. Flight testing confirmed these results and the team moved forward with the Scorpion SII 1400 Kv.

Multiple Electronic Speed Controllers (ESCs) were considered as shown in Table 15. The KISS ESC was selected because it was the lightest commercially available ESC that met the voltage and current requirements. The propulsion system components for each mission are shown in Table 16.

Table 15: Speed Controller comparison.

ESC	Max Burst Current	Max Cruise Current	Weight [g]
Turnigy Plush 30A	40 A	30 A	55
Castle Phoenix 35A	50	35 A	27
E-flite 30A	35 A	30 A	31
KISS 2-6S 30A	45A	30 A	25

Table 16: Propulsion Breakdown for each mission.

Propulsion Components	Mission 1		Mission 2		Mission 3	
	Description	Weight [g]	Description	Weight [g]	Description	Weight [g]
Motor	Scorpion S11 2212 (V2) 1400 Kv					58.0
Rx Pack	Varta 55608					20.0
ESC	KISS 30A					26.0
Rx	Futaba 617FS					9.1
Connections	Servo wire, electrical connections, solder					36.0
Propeller	CAM 8x6	27.8	CAM 9x7	27.8	CAM 8x6	27.8
Battery	Elite 1500s (8s)	186.8	Elite 1500s (8s)	186.8	Elite 1500s (8s)	186.8
Total (% EW)		343.7 (65%)		343.7 (65%)		343.7 (65%)

5.3.7 TUBE DESIGN

The tube was designed to minimize RAC by minimizing L_{Tube}, D_{Tube} and EW_{Tube}. Numerous lightweight materials were considered in designing the nonstructural tube. Built prototypes are compared in Table 17. The RAC estimate was calculated from Eq. 3 where EW_{Plane} is based on a 50% payload fraction according to Eq. 1 and the tube dimensions are estimates of those required to fit the preliminary design aircraft.

Table 17: Tube material down-select.

Material	Length	Inner Diameter	Thickness	Weight	RAC
Foam & Fiberglass	20 in (0.3 m)	4.75 (0.12 m)	0.16 (0.004 m)	0.11 (0.05 kg)	44.1
Mylar	20 (0.3 m)	4.75 (0.12 m)	0.24 (0.006 m)	0.09 (0.04 kg)	44.2
Depron	20 (0.3 m)	4.75 (0.12 m)	0.01 (0.0003 m)	0.24 (0.1 kg)	47.6

Both foam & fiberglass and Mylar scored higher than depron. Foam & fiberglass was selected because it was more supportive and scored slightly higher than Mylar. End caps were designed to keep the tube watertight during the vertical drop test. A plywood fitting on the end of the tube has a slot that allows a thin balsa plate to slide into place. A rubber O-ring seals the tube. The most difficult load case comes from the end drop with the plane on its nose. In order to properly transfer the loads to the plane and prevent the motor shaft from puncturing the tube, the end cap interfaces directly with the motor mount, as shown in Figure 30. Loads are passed through plywood blocks to the motor mount and directly into the primary fuselage structure.
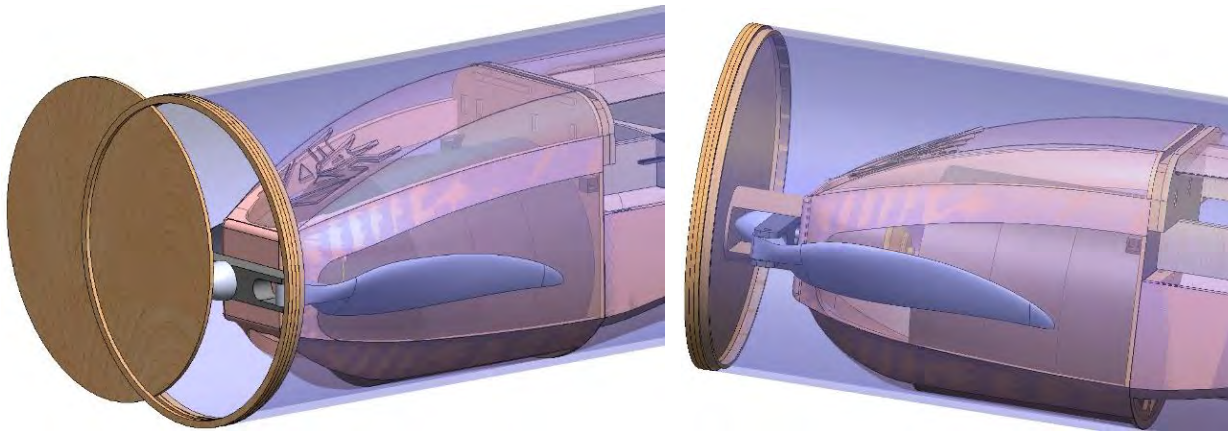
Figure 30: End cap design allows end cap drop loads to transfer directly to the motor mount.

5.4 WEIGHT AND MASS BALANCE

EW_{Plane} for M_1, M_2, and M_3 was 1.12 lb. (0.51 kg). It is expected that the added weight of epoxy for integration will push EW_{Plane} closer to 2.25 lb (1.02 kg), which is consistent with the team's weight targets in 3.2.2. The CG was kept within the design Static Margin for all three missions to ensure stable flight. In order to accommodate the shift in CG from the empty aircraft in M_1 to the loaded configuration in M_2, the flight batteries and ESC were shifted forward for these missions. The origin is located at the nose of the aircraft with the coordinate axis as shown in Figure 31. All CG distances shown in Table 18 are expressed in the airplane coordinate system.
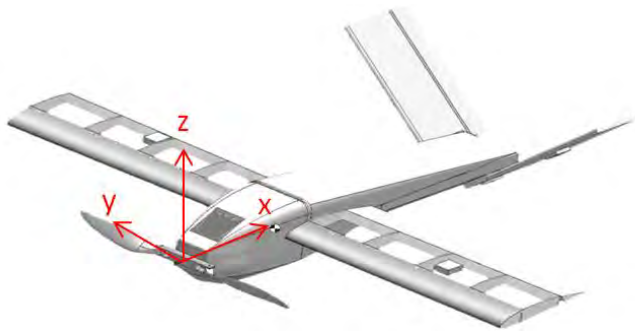
Figure 31: Starscream origin and coordinate directions.

Table 18: Weight and balance table for all missions.

Aircraft Component	Weight (lb)	Weight (kg)	X (in)	X (cm)	Y (in)	Y (cm)	Z (in)	Z (cm)
M_1	1.12	0.51	4.9	12.5	0.0	0.0	-0.7	-1.7
Fuselage	0.21	0.10	8.0	20.3	0	0	-0.5	-1.3
Wing	0.12	0.05	10.4	26.4	0	0	0.7	1.2
Motor	0.15	0.07	0.5	1.4	0	0	-0.4	-1.0
Propeller	0.06	0.03	0.3	0.8	1.1	2.7	-0.2	-0.6
Top Fairing	0.01	0.00	10.8	27.5	0	0	1.7	4.2
Flight Batteries	0.48	0.22	2.0	5.0	0	0	-0.9	-2.2
V-Tail (Left)	0.024	0.01	1.6	4.1	-1.1	-2.8	-1.2	-3.0
V-Tail (Right)	0.024	0.01	16.2	41.1	1.0	2.6	-1.1	-2.9
Bulkhead	0.04	0.02	4.7	11.9	0	0	-0.1	-0.3
M_2	2.20	1.00	4.9	12.5	0.0	0.0	-0.7	-1.7
Payload	1.08	0.49	3.1	8.0	0	0	-0.7	-1.8
Flight Batteries	0.48	0.22	6.1	15.4	0	0	-0.9	-2.2
M_3	2.20	1.00	4.9	12.5	0.0	0.0	-0.7	-1.7
Payload	1.08	0.49	3.1	8.0	0	0	-0.7	-1.8
Flight Batteries	0.48	0.22	6.1	15.4	0	0	-0.9	-2.2

5.5 FLIGHT AND MISSION PERFORMANCE

The expected flight performance of the final aircraft, as predicted by PlaneTools, is listed in Table 19.

Table 19: Predicted Aircraft Performance Parameters for each mission

Performance Parameter	M_1	M_2	M_3
$C_{L_{max}}$	1.2	1.2	1.2
$C_{L_{cruise}}$	0.08	0.15	0.15
e	0.80	0.80	0.80
C_{D0}	0.031	0.031	0.031
$(L/D)_{max}$	10.8	10.7	10.7
$(L/D)_{cruise}$	3.0	5.0	5.0
Rate of Climb	33 ft/s (10.0 m/s)	17 ft/s (5.2 m/s)	18 ft/s (5.2 m/s)
W/S	1.3 lb/ft² (62 N/m²)	2.6 lb/ft² (124 N/m²)	2.6 lb/ft² (124 N/m²)
Cruise Speed	87 ft/s (27 m/s)	101 ft/s (31 m/s)	94 ft/s (29 m/s)
Stall Speed	32 ft/s (9.8 m/s)	44 ft/s (13 m/s)	44 ft/s (13 m/s)
Empty Weight	1.14 lb (0.52 kg)	1.14 lb (0.52 kg)	1.14 lb (0.52 kg)
Battery Weight	0.41 lb (0.19 kg)	0.41 lb (0.19 kg)	0.41 lb (0.19 kg)

Based upon these performance parameters, the corresponding mission results and score parameters are listed in Table 20. M_1 scoring is binary, assumed to be 1.0 for a successful mission, and is therefore not listed below.

Table 20: Predicted score results based on mission configuration.

Score Parameter	M_2	M_3
$M_2{:}\,T_{USC}$	106 s	-
$M_3{:}\,N_{Pucks}$	-	3
$M_3{:}\,N_{Laps}$	-	8
$Total\ Mission\ Score$	14	
EW_{Plane}	1.14 lbs (0.52 kg)	
EW_{Tube}	0.11 lbs (0.05 kg)	
D_{Tube}	4.4" (11.1 cm)	
L_{Tube}	19.9" (50.5 cm)	
RAC	52.6	
$Total\ Score$	10.3	

5.6 DRAWING PACKAGE

The following drawing package includes a dimensional 3-view, structural arrangement, subassembly detail, mission configuration and locking mechanism detail drawings. All drawings were made using Solidworks [13].

SCALE 2:9

18.54

1.32

25.40

3.26

45°

7.70

⌀10.00

5.00

1.47

20.76°

3.55

3.86

SIZE
B

Aircraft 3-view

REV
C

Scale 1:6 | Drawing Package | 2/13/2017 | Page 1 OF 5

Structural Arrangement
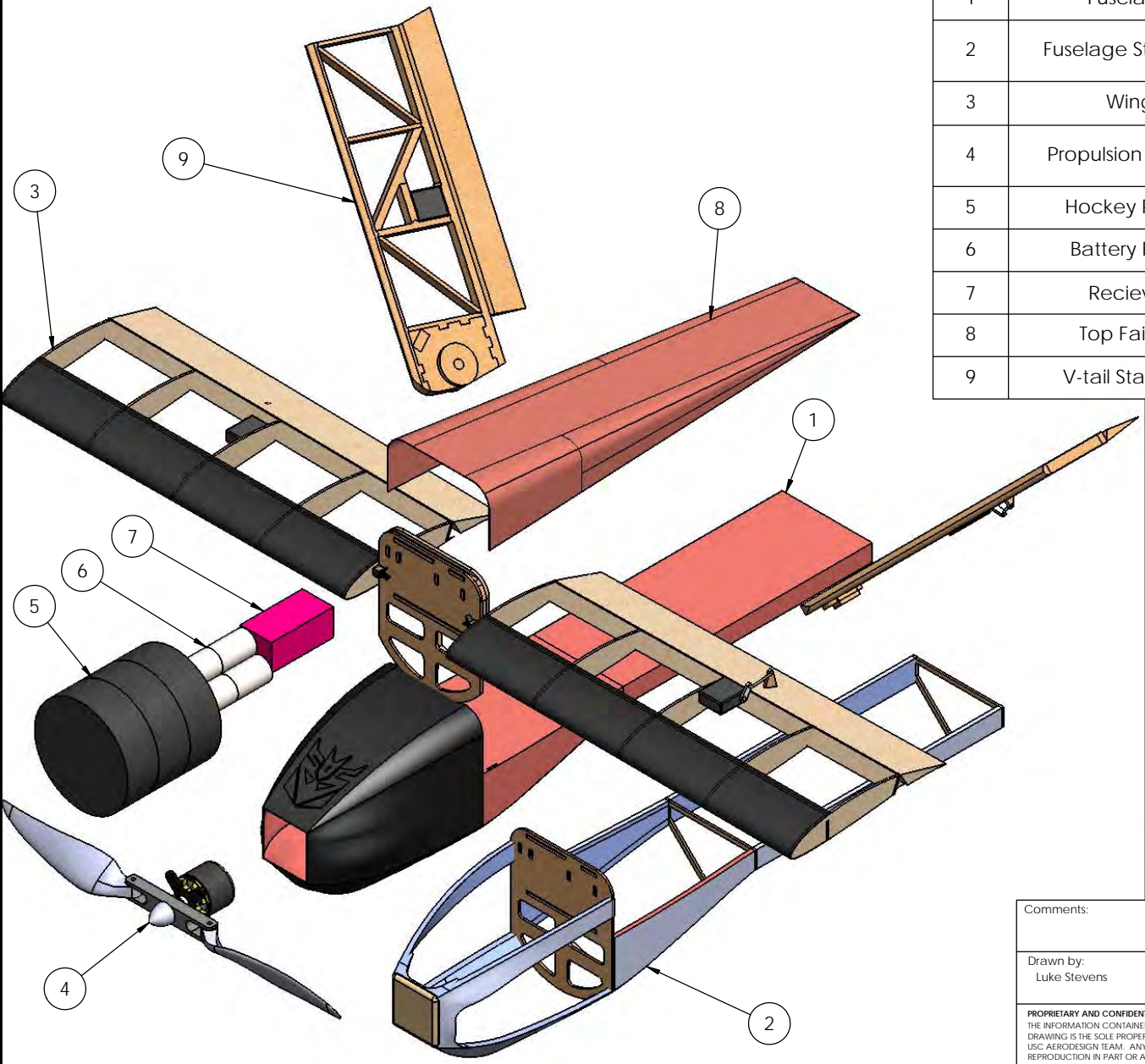
ITEM NO.	COMPONENT	DESCRIPTION	QTY.
1	Fuselage	Carbon Fiber and Kevlar Molded	1
2	Fuselage Structure	Plywood Bulkheads (x3), Plywood motor mount, Foam Stringers	1
3	Wing	Balsa Built-up, Carbon C-Box, So-Lite Covering	1
4	Propulsion System	Scorpion SII 2212-1400KV (V2); 8x6" Prop (M1, M3), 9x7" Prop (M2)	1
5	Hockey Puck		3
6	Battery Pack	8 x Elite 1500s	1
7	Reciever	Futaba R617FS 7 Ch. Reciever	1
8	Top Fairing	Kevlar Molded	1
9	V-tail Stabilizer	Balsa Truss, So-Lite Covering	2

Access Points

Battery, ESC, Reciever load through back hatch

Pucks load through front hatch

SCALE 4:9

V Tail Stabilizer

Solite (not shown) covers truss

ITEM NO.	DESCRIPTION	MATERIAL
1	Front Spar	1/4" Balsa
2	Cross Beams	1/4" Balsa
3	Aft Spar	1/4" Balsa
4	Ruddervater	1/4" Tapered Balsa
5	Servo	Dymond D47
6	Root Plate	1/4" Balsa
7	Washer	1/16" Plywood
8	Spring Plate	1/16" Plywood
9	Locking Block	3/8" Balsa
10	Dowel	1/4" Balsa Dowel

Washers distribute flight loads from stabilizer into fuselage

Wing

Kevlar string (not shown) is wrapped around the wing hub to better handle flight loads
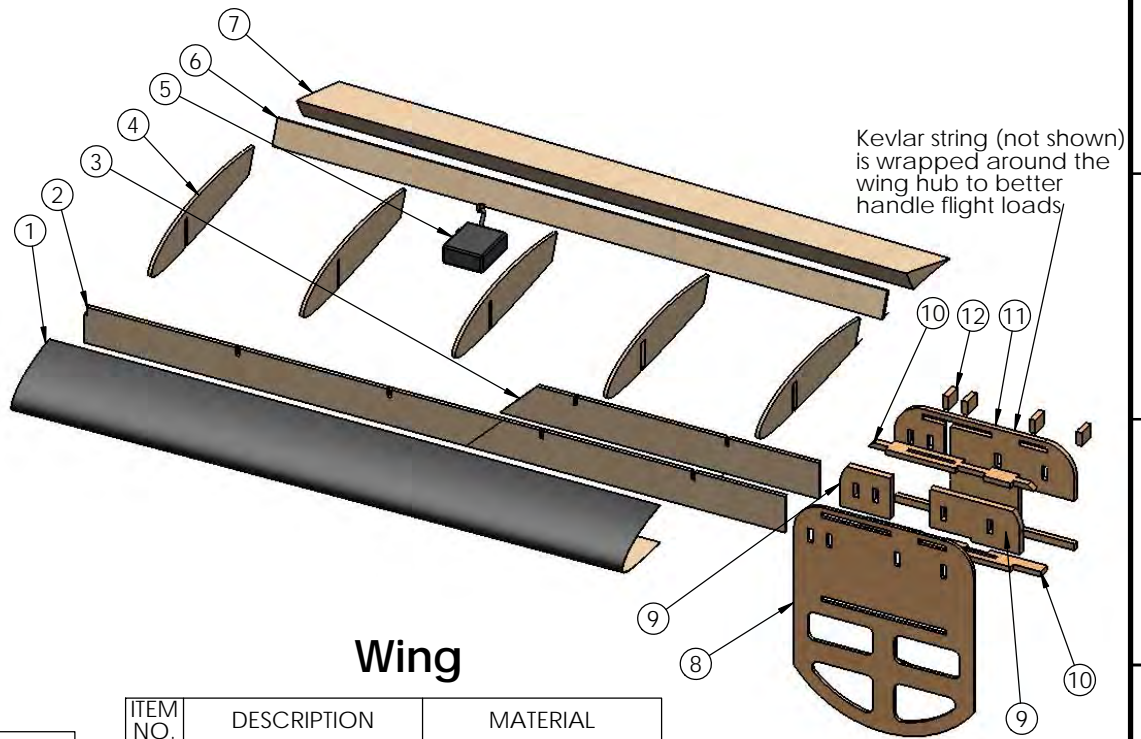
ITEM NO.	DESCRIPTION	MATERIAL
1	C-Box	45° Carbon
2	Front Spar (Long)	1/16" Balsa
3	Front Spar (Short)	1/16" Balsa
4	Ribs	1/16" Balsa
5	Servo	Dymond D47
6	Aft Spar	1/16" Balsa
7	Aileron	3/8" Balsa Tapered

Wing Hub

ITEM NO.	DESCRIPTION	MATERIAL
8	Front Bulkhead	1/8" Plywood
9	Spacer Plates	1/8" Balsa
10	Top/Bottom Plates	1/8" Balsa
11	Aft Plate	1/8" Balsa
12	Pins	1/8" Balsa

Payload/Bulkhead Integration

Fish wires hold pucks to bulkhead

Bulkhead integrates with the payload and wing spar

Hook to tension & release fish wire

SCALE 4:9

For Mission 1, battery pack (not shown) is moved to front of fuselage
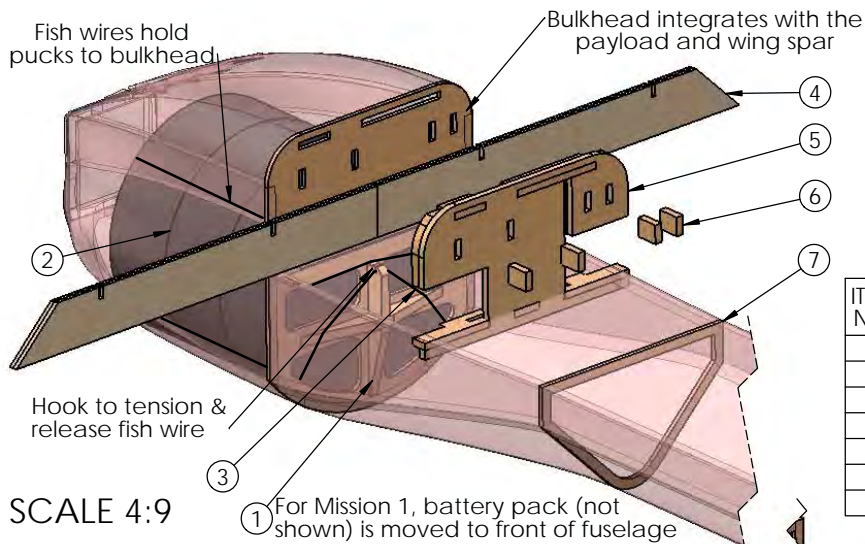
ITEM NO.	DESCRIPTION
1	Front Bulkhead
2	Hockey Pucks
3	Fish Wire
4	Wing Spar (Full)
5	Wing Hub
6	Pins
7	Rear Bulkhead

Comments:

Drawn by:
Luke Stevens

PROPRIETARY AND CONFIDENTIAL
THE INFORMATION CONTAINED IN THIS DRAWING IS THE SOLE PROPERTY OF USC AERODESIGN TEAM. ANY REPRODUCTION IN PART OR AS A WHOLE WITHOUT THE WRITTEN PERMISSION OF USC AERODESIGN TEAM IS PROHIBITED.

University of Southern California
Cessna - Raytheon - AIAA Design/Build/Fly 2017

StarSCream

SIZE **B**

Subassembly Structure Detail

REV **C**

Scale 1:3 | Drawing Package | 2/13/2017 | Page 3 OF 5
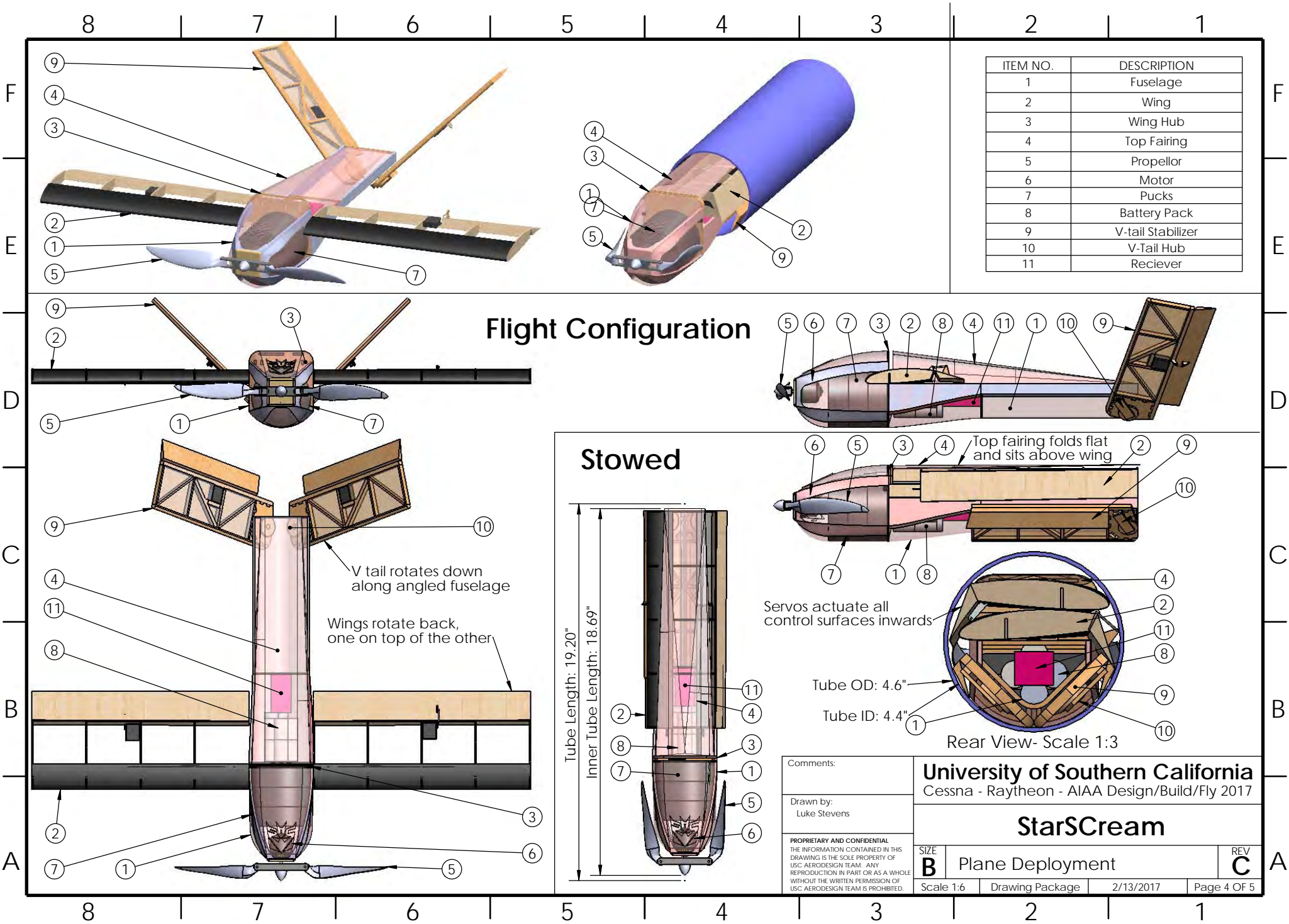
ITEM NO.	DESCRIPTION
1	Fuselage
2	Wing
3	Wing Hub
4	Top Fairing
5	Propellor
6	Motor
7	Pucks
8	Battery Pack
9	V-tail Stabilizer
10	V-Tail Hub
11	Reciever

Flight Configuration

Stowed

V tail rotates down along angled fuselage

Wings rotate back, one on top of the other

Top fairing folds flat and sits above wing

Servos actuate all control surfaces inwards

Tube Length: 19.20"
Inner Tube Length: 18.69"

Tube OD: 4.6"
Tube ID: 4.4"

Rear View- Scale 1:3

Comments:

Drawn by:
Luke Stevens

PROPRIETARY AND CONFIDENTIAL
THE INFORMATION CONTAINED IN THIS DRAWING IS THE SOLE PROPERTY OF USC AERODESIGN TEAM. ANY REPRODUCTION IN PART OR AS A WHOLE WITHOUT THE WRITTEN PERMISSION OF USC AERODESIGN TEAM IS PROHIBITED.

University of Southern California
Cessna - Raytheon - AIAA Design/Build/Fly 2017

StarSCream

Plane Deployment

SIZE B
REV C

Scale 1:6 | Drawing Package | 2/13/2017 | Page 4 OF 5

Wing Hub

Scale 1:3

Stowed position

Left wing rotates out, right wing moves down

Right wing rotates out

Rods can move along tracks

Spars rotate about attached metal rods

Zip tie in position for locking

Reusable zip tie lock

Scale 2:3

Both wings translate into flight position, zip tie locks
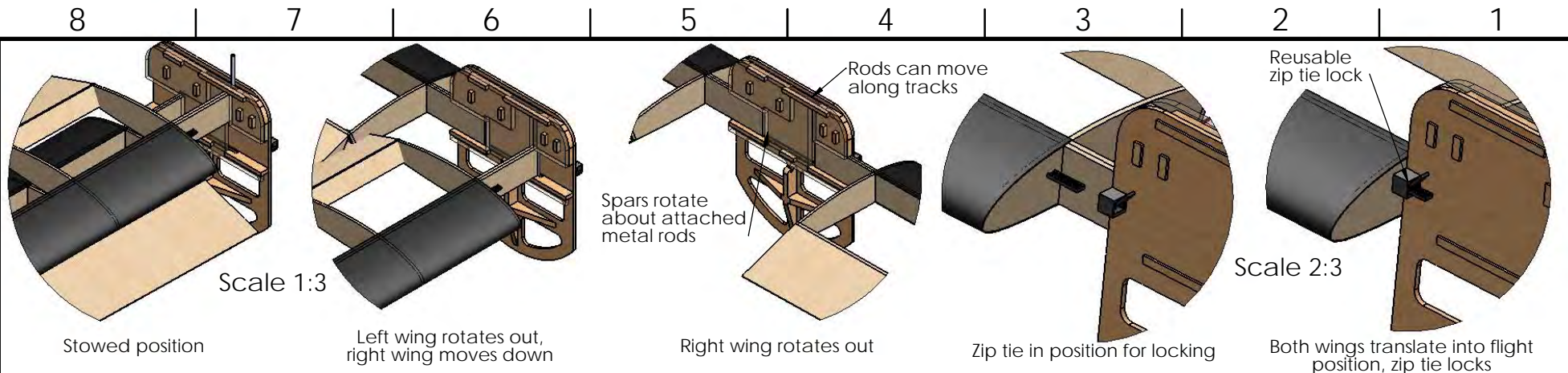
Tail Hub

Scale 1:3

Lock block

Spring plate
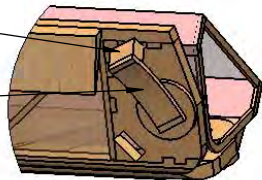
Stowed position: Spring plate flexed, lock block resting on stabilizer
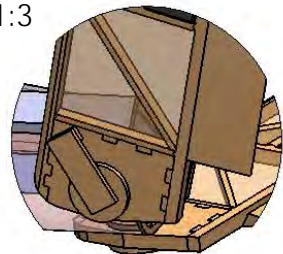
Flight position: Spring plate relaxed, lock block engaged

Top Fairing

Stowed Position: Sides are folded underneath top of fairing

A

Flight Position: Sides are folded out and lock into the fuselage

B

Scale 2:15
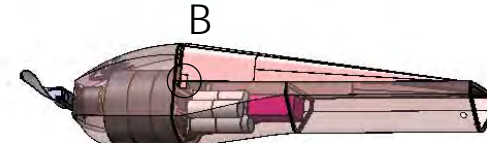
Plywood clip attached to fairing side
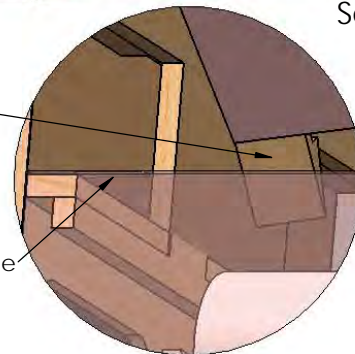
Slit in fuselage

Fuselage flexes to allow clip to engage
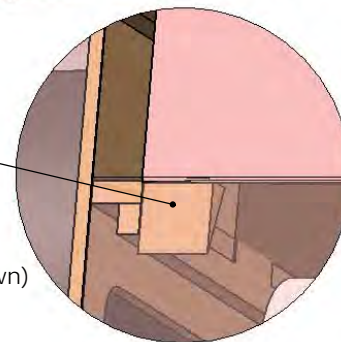
Multiple clips (not shown) placed on each side

DETAIL A

Scale 4:3

DETAIL B

Control Surfaces

Scale 1:1

Stowed Position

Servo rotates back

Servo rotates forward for normal flight operation
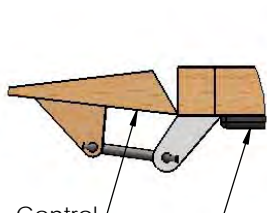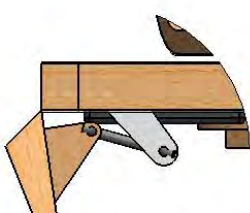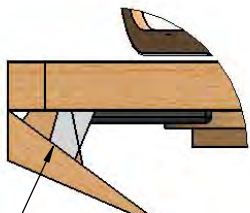
Small cuts to allow folding

Control surface

Servo

Note: The example used here is the ruddervater. The ailerons fold in similar (but not identical) ways. See previous drawings for reference.

Comments:

Drawn by:
Luke Stevens

University of Southern California
Cessna - Raytheon - AIAA Design/Build/Fly 2017

StarSCream

SIZE **B**

Locking Mechanisms Detail

REV **C**

Scale: See notes | Drawing Package | 2/13/2017 | Page 5 OF 5

6.0 MANUFACTURING PLAN

Numerous manufacturing processes were evaluated for each component including the wing, fuselage, hinge mechanism, and launch tube. The fabrication of each component was evaluated and selected as detailed in the following subsections.

6.1 MANUFACTURING PROCESSES INVESTIGATED

In order to identify the best manufacturing process for each aircraft component, the team first considered the pros and cons of each technique.

6.1.1 FOAM

Foam is an attractive building material because it is relatively cheap and can be easily shaped using a hotwire foam cutter and sanding. Although nonstructural foam elements can be very lightweight, foam is often heavier than balsa and composite structures. The team has extensive experience building with foam to validate the sizing of a prototype aircraft, but often shifts toward balsa or composites later in the year to minimize plane weight.

6.1.2 BALSA BUILD UP

Balsa is an attractive building material because of its low density. Well-designed balsa structures can often be lighter than composite structures for smaller aircraft, as demonstrated by the historical success of balsa aircraft in previous AIAA DBF competitions. Although the team's strongest skillset is working with foam and composites, the accessibility of CAD and laser cutters makes built up structures an attractive option.

6.1.3 3D PRINTING

Additive manufacturing allows for the design of complex forms that would otherwise be impossible to build. The team has access to a Markforged Mark Two 3D printer that can create high-precision parts reinforced with fiberglass, carbon fiber or Kevlar [14]. 3D printing can be used for rapid prototyping of complex mechanisms and reducing lead times in making molds for composites.

6.1.4 COMPOSITES

Composites are desirable because of their high strength to weight ratios. Additionally, composites are more durable than other build methods, more likely to bend than break, especially when compared with balsa structures. The team has a strong composite build skillset and has won competition through the innovative design of a foam-reinforced Kevlar fuselage in 2014 that was lighter than comparable balsa structures [7]. Building composites is expensive as a result of material costs and requires lead times upwards of six weeks to build molds and allow for fully cured parts.

6.2 MANUFACTURING PROCESSES SELECTED

6.2.1 WING AND TAIL STRUCTURE

The aircraft wing and tail structure was constructed using the balsa build-up method to minimize weight. As a result of the hinge mechanism, each half of the span was constructed individually and joined at the spar as shown. Ribs were cut with fitting slots, allowing for a consistent airfoil shape along the half-span. The balsa shear web was cut such that the grain ran at a positive and negative 45°. Shear webs and ribs were bonded with cyanoacrylate (CA) and the spar caps and carbon d-box were bonded with 15 min epoxy. The wing was covered with So-lite (not shown) in order to maintain the aerodynamic shape of the airfoil.
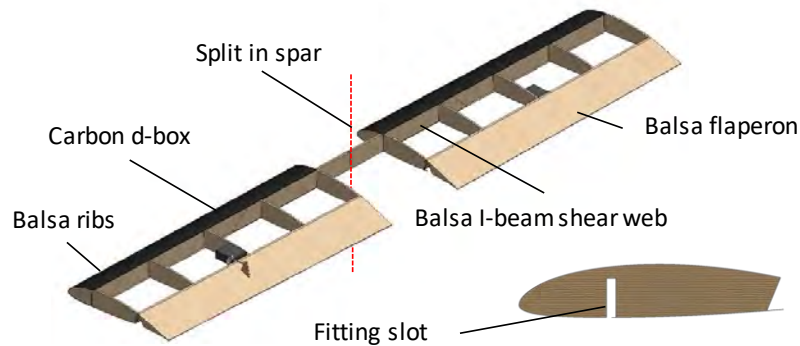
Figure 32: Detail design of the balsa wing structural arrangement.

6.2.2 HINGE MECHANISM

The spar coupler was laser cut from aircraft plywood. The pieces of the assembly were designed for ease-of-construction in order to minimize variation in build quality. Additionally, pieces were designed to integrate directly with the bulkhead, providing a lightweight solution for transferring flight and landing loads into the fuselage.

6.2.3 FUSELAGE STRUCTURE

The fuselage was constructed using a two-part mold process, with the foam truss and plywood motor mount integrated directly into the layup. The skin was made using an outer layer of Kevlar and an inner layer of fiberglass. All fibers were at an angle of 45° with respect to the length-wise axis of the fuselage. The plywood bulkheads were integrated after the completion of the layup process.

6.2.4 LAUNCH TUBE

The launch tube was constructed using a foam-fiberglass composite. Foam was cut to shape using a hot-wire. Fiberglass was laid up on the outer surface of the foam in a helical pattern and cured with epoxy resin. The inner foam mold was covered in Mylar before the whole arrangement was vacuum bagged. Once removed from the vacuum bag, tube ends were trimmed and the end cap interface was fixed to the tube using epoxy.

6.3 MANUFACTURING MILESTONES

A milestone chart was produced to stay on schedule and coordinate build between different sub-teams. Although the plan in Figure 33 only depicts the schedule for the competition aircraft, the same scheduling was implemented for the construction of the critical design aircraft. Lessons learned in the development of the critical design aircraft were incorporated into the schedule for competition build. As shown, build and assembly of the fuselage requires upwards of five weeks to produce a high quality part. Simultaneous lab testing was conducted on the wing, tail, and hinge mechanism, as detailed in 7.0, to ensure the aircraft would meet all load requirements once fully integrated.
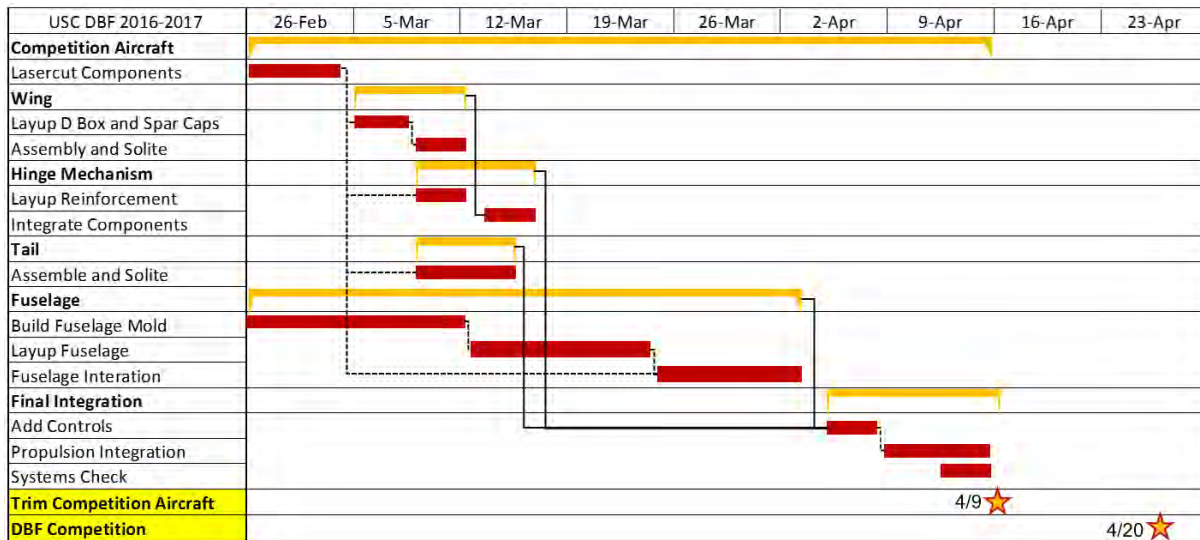
Figure 33: Aircraft manufacturing milestone chart showing planned timing of objectives

7.0 TESTING PLAN

A test plan was implemented to verify propulsion, aerodynamic performance, stability and control, and structural predictions. Experimental data was gathered both in the laboratory and at flight tests. Testing occurred at all stages in the development of the aircraft to validate predictions and inform future design decisions. The test schedule is presented in Figure 34 and explored in further detail in 7.1 through 7.4.
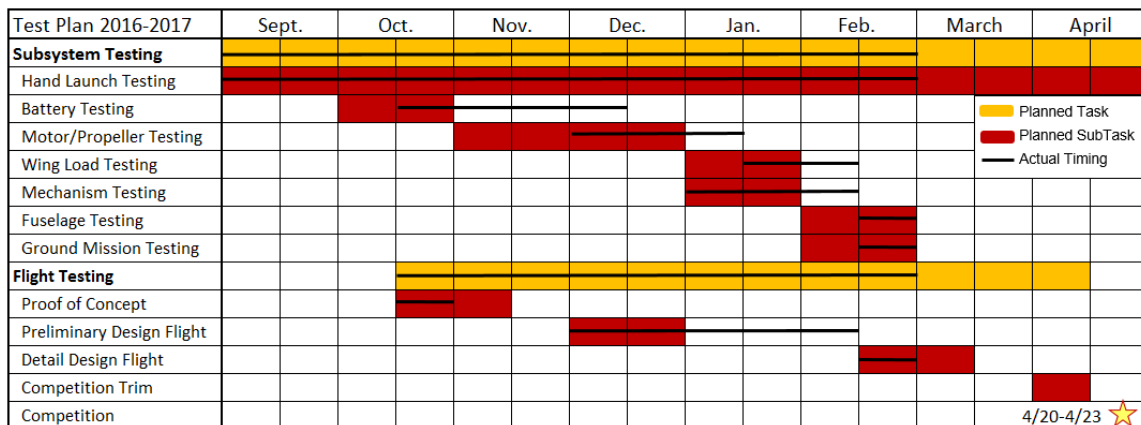
Figure 34: Testing Plan for the 2016-2017 competition year.

7.1 TEST OBJECTIVES

Overview

Tests for each sub-team were conducted to ensure that the designed components performed adequately to meet all competition and design requirements. The details of the test procedure and implications to the critical design are discussed in further detail in 7.2.

Propulsion

- Static thrust tests and flight tests were used to verify the expected performance of the propulsion system at both static and dynamic conditions
- Lab testing was conducted using a battery tester to characterize the discharge performance of assembled battery packs

Performance

- Flight tests were conducted to validate performance predictions provided by PlaneTools
- Hand launch trials were conducted to study different hand launch techniques and determine proper assumptions for the aircraft launch velocity at different weights

Aerodynamics

- Flight tests were used to confirm AVL and XFOIL predictions
- Pilot feedback was used to verify that the aircraft's handling qualities were acceptable

Payloads

- The ground crew executed Ground Mission simulations to verify efficacy of the payload restraints

Wing

- The aircraft was loaded to maximum takeoff weight and the wingtip test was performed to simulate technical inspection
- Failure points and deflections predicted in SparSizer were validated through wing loading tests
- The wing hinge mechanism was integrated into the wing and load testing was conducted to ensure that the mechanism could withstand flight loads

Fuselage

- Load testing was conducted to ensure the structure could withstand maximum design loads
- Drop tests were conducted to evaluate the survivability of the fuselage for the ground mission drops

Tube

- Drop tests were conducted with an airplane mockup to ensure that the aircraft would survive the ground mission drop tests inside the tube

7.2 SUBSYSTEM TESTING

7.2.1 PROPULSION TESTING

Propulsion testing consisted of characterizing the performance of the flight battery and validating propulsion predictions from PlaneTools to select the highest scoring motor. The objective of battery testing was to identify $I_{MAX,M3}$ for a 5-minute flight and $I_{MAX,M2}$, the maximum allowable current output of the cells. This testing was conducted with the West Mountain Radio Battery Tester, which logs the voltage throughout the discharge of cells at a user-specified current [15]. The propulsion sub-team built, charged, and discharged numerous battery packs at constant currents ranging from 10 to 20 A. Plots of voltage versus time allowed the team to determine the flight time for each package as shown in 8.1.2. The battery pack, power amplifier, and test unit setup for an 8-cell discharge is shown in Figure 35.
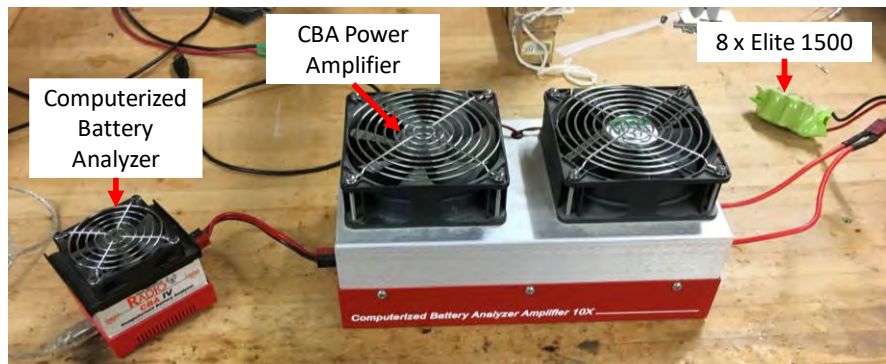
Figure 35: Experimental setup for a battery discharge test.

The objectives of motor testing were to compare actual propulsion system performance to theoretical predictions from PlaneTools. This was conducted using the RC Benchmark Dynamometer, which directly measures thrust, torque, voltage, current and RPM through an integrated Data Acquisition Board (DAQ) [16]. The team compared static current and static thrust of different motors, as shown in 8.1.2. Although testing with the dynamometer is restricted to static conditions, the team's experience has shown that for models with good agreement at static conditions, dynamic conditions (flight speed, current and RPM at cruise) similarly show good agreement (within 15%). The dynamometer setup is shown in Figure 36.
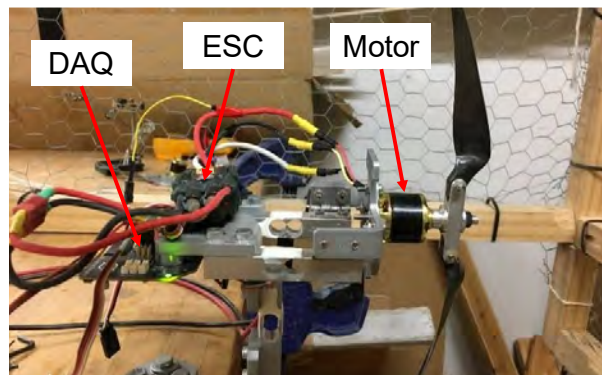
Figure 36: Experimental setup for a dynamometer thrust stand test.

7.2.2 STRUCTURAL TESTING

To validate the design of the wings and the integration with the hinge mechanism, the team conducted load testing that simulated the aerodynamic loads experienced in flight. Using a MATLAB program that calculated the mass distribution to mimic elliptical loading for a given load case, the team incrementally added weights to increase the g-loading experienced by the structural member. All components were tested to failure. Failure was defined as when the team observed excessive deflection, cracking, or crushing at any point along the wing. To ensure that the wing design would pass the pre-flight tech inspection, the team loaded the aircraft with the maximum payload (1.125 lb) and supported the aircraft at the wingtips. The two methods are shown in Figure 37.

Figure 37: Setup for elliptical flight load testing (left) and wingtip testing (right).

7.2.3 GROUND MISSION TESTING

Ground mission testing was conducted to ensure that all aircraft components and the launch tube could survive all three drops for the ground mission. The aircraft at its fully loaded weight was stowed into the tube and dropped from a height of 12 in. (0.3 m) as shown in Figure 38.

Figure 38: Drop testing was conducted with the fully loaded aircraft stowed inside the launch tube.

The team conducted hand launch testing to characterize launch conditions and refine launch technique. Multiple planes were built throughout the year without a propulsion system or electronics for launch testing. The aircraft was ballasted to the maximum takeoff weight such that the CG was at the appropriate location for flight. A launch was considered successful if the aircraft entered a stable unpowered glide without excessive displacements in roll, pitch, or yaw. Video analysis was used to measure launch velocity and initial aircraft displacements as shown in Figure 39. Using a reference distance and a known frame rate of the camera, the launch velocity was calculated, $V_{launch} = \Delta x/\Delta T$.
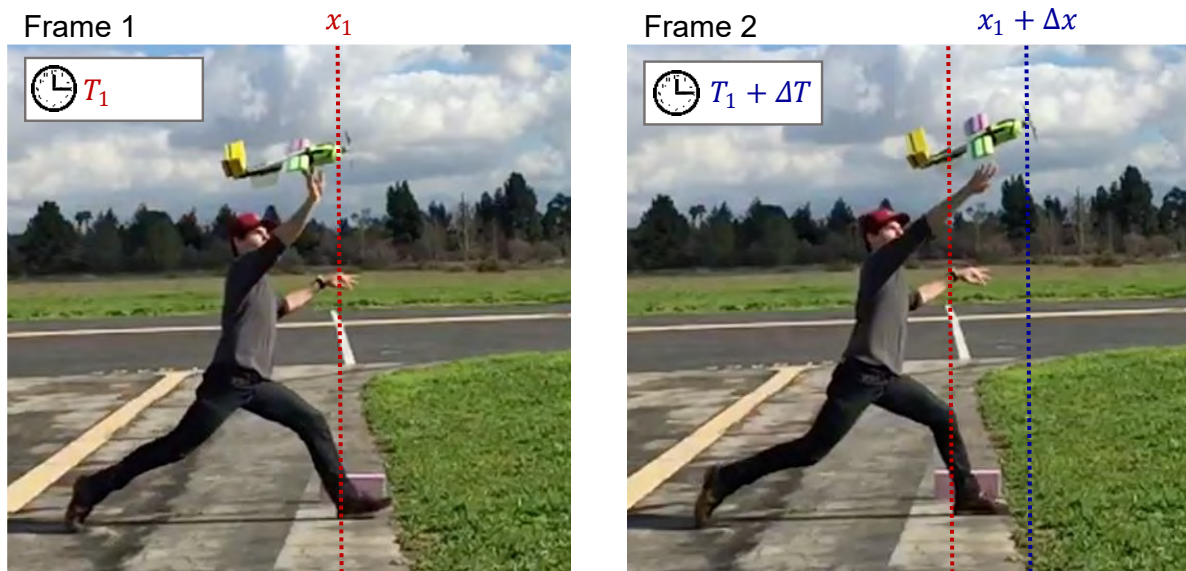
Figure 39: Video analysis method for a successful hand launch at test flight.
The pink foam block was used as a 12 in (0.3 m) reference distance.

7.3 Flight Test Schedule and Flight Plan

Flight testing was critical to the validation of the competition aircraft. Pilot feedback allows the team to determine aircraft stability, pilot workload and the corresponding flight performance at different throttle settings and control inputs. Propulsion data is collected through a data logging ESC that measures voltage, current, RPM and throttle position, which allows the team to compare flight data to PlaneTools predictions.

The flight test schedule and objectives are displayed in Table 21. Each flight test had explicit design objectives that were used to incrementally validate the effectiveness of all aircraft subsystems. Flight test objectives that were not met were reattempted in subsequent tests. Note that there are upcoming test flights planned to for February 26 and March 26.

Table 21: Flight Test Schedule.

Date	Location	Objectives
Nov. 13, 2016	Sepulveda Basin, Van Nuys, CA	Determine handling qualities of Preliminary Design
Dec. 3, 2016	Sepulveda Basin, Van Nuys, CA	Determine minimum wing area required at launch
Jan. 15, 2017	Sepulveda Basin, Van Nuys, CA	Validate propulsion system sizing
Jan 21, 2017	Sepulveda Basin, Van Nuys, CA	Validate propulsion system sizing
Feb. 4, 2017	Sepulveda Basin, Van Nuys, CA	Simulate all missions. Record lap times and performance data
Feb. 26, 2017	Sepulveda Basin, Van Nuys, CA	Test integrated competition aircraft. Refine propulsion. Record Lap times
Mar. 26, 2017	Sepulveda Basin, Van Nuys, CA	Trim competition aircraft

Each flight test was separated into specific objectives, which included the acceptance criteria to ensure all objectives were met. A sample plan from the Dec. 3, 2016 is shown in Table 22.

Table 22: December 3, 2016 flight test plan.

Flight #	Flight Name	Payloads	Objectives	Acceptance Criteria
3 December 2016				
1	Trim Flight	None	- Trim aircraft	- Aircraft trimmed for level flight
2	EW with Flaps	None	- Test flaps with no payload	- Identify flap effects
3	Speed Flight	50% PF	- Simulate M_2 - Obtain flight speeds at full throttle - Test flaps with payload	- Timed mission - Recorded flight speeds and lap times
4	Cut Span	50% PF	- Cut down wingspan to find optimal wing area for take-off	- Successful takeoff, cruise and landing

7.4 FLIGHT CHECKLISTS

The team adhered to a preflight checklist (Table 23) before each flight to ensure efficiency, proper data acquisition and team safety. It also serves as a final flight go or no-go evaluation criterion from the pilot. The on-site inspections checklist (Table 24), was used before and after each flight in order to ensure aircraft and crew safety. The inspection of each category of components allows for the systematic division of duties for aircraft inspection, note all discrepancies, and perform and verify maintenance if necessary.

Table 23: Pre-flight checklist.

Component	Task
Fuselage (internal)	☐ Secure and connect the fully charged battery ☐ Receiver has all connections plugged in and secured ☐ Load payloads (if applicable) ☐ CG aircraft
Fuselage (external)	☐ Close and secure all external hatches
Pilot's Checks	☐ Connect fuse ☐ Check all control systems with receiver ☐ Motor run-up/Go No-Go decision

Table 24: Aircraft inspection checklist.

Component	Items to Inspect	Discrepancies
Motor	☐ Motor mount and all fasteners ☐ Fuselage around motor mount is free of cracks or fractures ☐ Motor is free of damage to casing and debris ☐ Propeller is fastened to shaft property ☐ Propeller is free of damage	
Fuselage	☐ Battery is secured to fuselage and connected properly ☐ Speed-controller is secure and connected ☐ Receiver is secure and has all servos connected properly ☐ Servo wires are all secure ☐ Fuselage is secured and free of debris ☐ Fuse connectors secured (internal and external) ☐ Payload restraints secured and ready for loading (if applicable)	
Wings	☐ Wings are free of tears, cracks, and fractures ☐ Servo arms are secure with minimal play ☐ Control surfaces are secure and free of obstructions ☐ Fuselage around wing mount is free of cracks and fractures ☐ Wing is securely mounted to fuselage ☐ Hollow wings are properly sealed (Manufacturing plane only)	
Winglets	☐ Free of tears, cracks, and fractures ☐ Winglets are securely mounted to wing tips ☐ Check for possible damaged caused by landing gear	
Control Surface Check	☐ Control surfaces move freely without obstruction ☐ Check all servos are operating properly	

8.0 PERFORMANCE RESULTS

Predictions made during the Detail Design phase were compared to aircraft subsystem performance. Key subsystems were tested in lab and during flight tests to ensure each component performed as predicted.

8.1 DEMONSTRATED PERFORMANCE OF KEY SUBSYSTEMS

8.1.1 HAND LAUNCH

Characterizing the aircraft initial conditions at launch was critical to the success of this year's design and was conducted during the conceptual design phase in order to validate the assumptions made in 3.2.2 of V_{launch} = 50 ft/s. The team measured the launch velocity of multiple throwers with a ballasted aircraft across a range of weights in order to account for changes in W_{Total} that might occur throughout the year. The minimum weight (2.15 lb.) and maximum weight (3.4 lb.) planes thrown represent aircraft with a payload fraction of 52% and 33% respectively. Launch velocities were measured as described in 7.2.4 for four throwers (Liam, Alex, Jon, and Chris). As shown in Figure 40, the launch velocity for Liam and Alex intersects the target payload fraction (PF = 50%) at a launch velocity of 52 ft/s, which confirmed previous assumptions for V_{launch} = 50 ft/s.
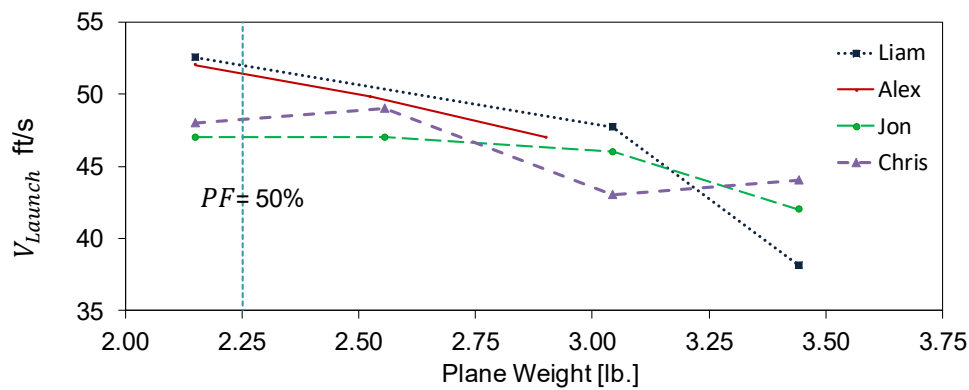
Figure 40: The results of the hand launch testing validated the assumption that V_{Launch} = 50 ft/s.

8.1.2 PROPULSION

Battery testing characterized the discharge performance of the Elite 1500 mAh cells. In order to maximize the number of laps flown for M_3, the team targeted a flight time of 5-minutes. As shown in Figure 41, the Elite 1500s maintain their voltage for just over 5-minutes when discharged at 13 A. The results of this testing defined I_{MAX,M_3} = 13 A and were incorporated into Eq. 10 of 3.2.2.
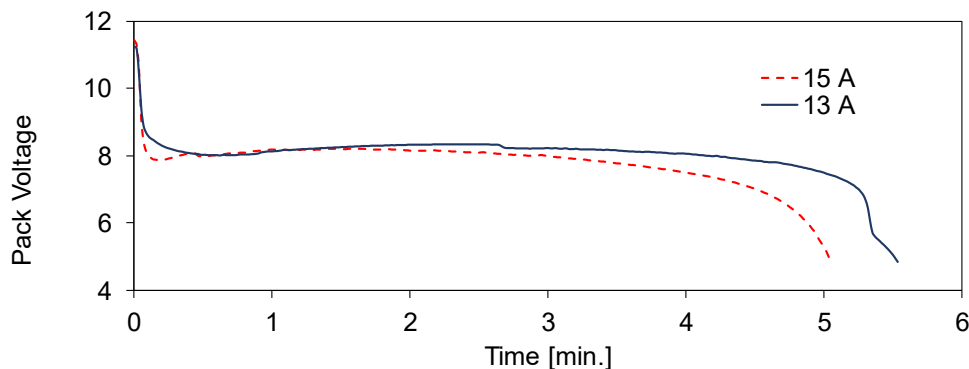
Figure 41: Discharge curves for 8 x Elite 1500s.

Based upon data collected at test flight and PlaneTools predictions, the team targeted a maximum static thrust of 1.6 lb. To validate the selection of the 1400 Kv Scorpion motor, the team tested motors over a range of Kv to show that the Scorpion motor would not exceed the cruise current limitation, $I_{MAX,M_3} = 13\ A$. As shown in Table 25, all motors produced the target 1.6 lb. of thrust. The higher Kv motors, however, required a much larger current to produce the same amount of thrust. Although the 1400 Kv Scorpion motor has a maximum current above 13 A, it is expected that the cruise current will drop below the 13 A maximum because at higher speed the motor produces the same power output at lower cruise currents.

Table 25: Critical design motor comparison.

	Hacker A20 12L	AXI Gold 2814/10	Scorpion SII 2212
Kv	2100	1640	1400
Maximum Thrust	1.6 lb (0.73 kg)	1.6 lb (0.73 kg)	1.6 lb (0.73 kg)
Maximum Current	32 A	24 A	18 A

In order to characterize the performance of the selected 1400 Kv Scorpion motor with different propellers, the team conducted static testing and compared measured thrust values to PlaneTools predictions. For all propellers tested, the measured thrust values were ~10% lower than the predicted static thrust. This knockdown was incorporated into PlaneTools and used to identify the highest scoring propeller for each Mission. With these changes implemented, PlaneTools identified the propellers in 5.3.6 for M_2 and M_3.
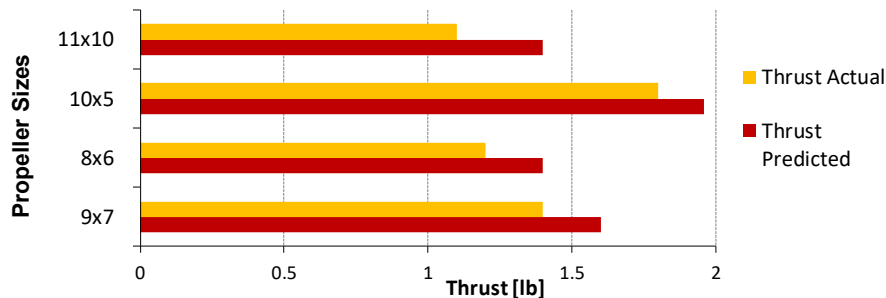
Figure 42: Comparison of predicted and actual static thrust values.

8.1.3 STRUCTURAL TESTS

The aircraft wing was subjected to an elliptical loading to mimic flight loads as described in 7.2.2. The results of load testing on the individual components and integrated system are summarized in Table 26. Since the wing folding subassembly was subject to excessive deformation rather than complete fracture, failure for this case was taken to be the load where maximum deflection of the wingtips exceeded 10% of the total wingspan.

Table 26: Load testing summary for individual components and wing folding subassembly. (1g = 2.25 lb)

	Wing (Full Span)	Wing Folding Subassembly
Maximum Load	9.2 ± 0.4g	21±1g

In order to evaluate how the tube transfers loads to the plane during the drop test, the tube was drop tested from 1 ft. (0.30 m) and 3 ft. (0.90 m) ($FS = 3$) with a fully weighted test mule with balsa wings, as shown in Figure 43. The tube survived all drop tests from both heights. In initial tests, the plane survived three drops in each orientation. Worst-case wing load testing was performed by removing a portion of the aft-fuselage so that the wing would incur the maximum possible load a drop could provide, as shown in Figure 43. From this testing, it was discovered that the balsa rib at the wingtip would break as a result of the bending moment from an end drop. Future iterations of the wing were designed to incorporate a balsa fillet at the trailing edge of the rib to aid in transferring the loads to the forward and aft spars.

Figure 43: Drop test mule, simulating weight of the aircraft on balsa wings. The failure in the balsa ribs resulting from the worst case loading led to improved load transfer in the balsa wings.

8.2 DEMONSTRATED FLIGHT PERFORMANCE OF COMPLETED AIRCRAFT

Several test flights were carried out to validate predictions of aircraft performance. The goal of these flights was to evaluate the performance and capabilities of the detail design aircraft. Table 27 summarizes the flights to date as well as future flight test plans.

Table 27: Aircraft Performance evaluation from test flights.

Date	Description	Problems	Solutions
Nov. 13	- Determine handling qualities	- Wingtip stall on landing	- Implement 2° of twist into wing
Dec. 3	- Determine Minimum wing area	- None	
Jan. 15	- Validate Propulsion	- Instability on launch when empty	- Improve throw technique - Re-evaluate tail sizing
Jan. 21	- Validate Propulsion	- Wingtip stall on takeoff	- Throw practice to increase throw speed
Feb. 4	- Simulate Missions	-Limited maneuverability on takeoff	- Move CG toward aft limit
Feb. 26	- Simulate M_3		
March 26	- Competition Trim		

As shown, two test flights were repeated (Jan. 15, Jan. 21) as a result of difficulty hand launching the aircraft. Considerable effort was devoted to characterizing the launch conditions and improving thrower

technique so that the team could sufficiently characterize the performance of the critical design and successfully complete all missions. The team successfully completed two of the three missions at its Feb. 4 test flight and the comparison of these flights to predictions are shown in Table 28.

Table 28: Comparison of predicted and flight-validated performance characteristics

	Parameter	Predicted	Flown	Δ %
M_1	Flight Speed	87 ft/s (26 m/s)	74 ft/s (50 m/s)	-15%
	Cruise Current	8 A	13 A	63%
M_2	Flight Speed	101 ft/s (69 m/s)	88 ft/s (26 m/s)	-15%
	Cruise Current	24 A	26 A	8%
	T_{USC}	106 s	121 s	14%
M_3	Flight Speed	82 ft/s (25 m/s)	--	--
	Cruise Current	13 A	--	--
	N_{Laps}	8	--	--
	N_{Pucks}	3	--	--

As shown above, actual flight speeds are -15% lower on average and cruise currents are consistently higher than predicted. The difference between predicted and actual cruise velocity can be attributed to several factors, including the lack of headwinds at the California test location and simplifying assumptions made in the model for propeller efficiency. These results were used to improve the fidelity of the computer model and refine theoretical predictions. The team has currently completed the aircraft for the Feb. 26 test flight, shown in Figure 45, and expects to complete all missions at this test flight.
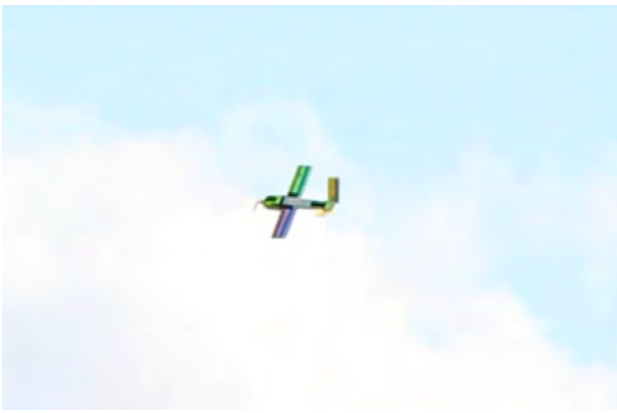
Figure 44: A successful flight test on February 4 at Sepulveda Basin, Van Nuys, CA

Figure 45: The critical design aircraft has been completed for the Feb. 26 test flight.

9.0 BIBLIOGRAPHY

[1]   USC AeroDesign Team, "Aircraft Design Report, 2015 AIAA DBF Competition," 2015.

[2]   Aerovironment, Inc., "Unmanned Aircraft Systems," 2016. [Online]. Available: https://www.avinc.com/uas/view/switchblade. [Accessed 17 September 2016].

[3]   USC AeroDesign Team, "Aircraft Design Report, 2011 AIAA DBF," 2011.

[4]   "Weather Underground," [Online]. Available: https://www.wunderground.com/. [Accessed 9 January 2017].

[5]   A. P. P. Data. [Online]. Available: http://www.apcprops.com. [Accessed 9 January 2017].

[6]   P. Carpenter, "R/C Airplane World," [Online]. Available: http://www.rc-airplane-world.com/watts-per-pound.html. [Accessed February 2017].

[7]   USC AeroDesign Team, "Aircraft Design Report, 2014 AIAA DBF Competition," Los Angeles, 2014.

[8]   M. Drela, "XFOIL," MIT, 2013. [Online]. Available: http://web.mit.edu/drela/Public/web/xfoil. [Accessed 13 Gebruary 2017].

[9]   S. Hoerner, "Fluid Dynamic Drag," Bakersfield, CA, 1965.

[10] M. Page, "Model Airplane Cook-book," 2008.

[11] MIL-F-8785C, Flying Qualities of Piloted Planes, Military Specification, 1980.

[12] T. Yechout, Introduction to Aircraft Flight Mechanics, Reston, VA: AIAA, 2014.

[13] Dassault Systems, "Solidworks," [Online]. Available: http://www.solidworks.com/. [Accessed 23 January 2016].

[14] Markforged, Inc., "THE MARK TWO," 2017. [Online]. Available: https://markforged.com/mark-two/. [Accessed 13 January 2017].

[15] West Mountain Radio, "CBA IV - Computerized Battery Analyzer," 2017. [Online]. Available: http://www.westmountainradio.com/product_info.php?products_id=cba4. [Accessed 20 January 2017].

[16] Tyto Robotics, "Dynamometer Series 1580," 2017. [Online]. Available: https://www.rcbenchmark.com/product/rcbenchmark_dynamometer/. [Accessed 20 January 2017].

[17] USC AeroDesign Team, "Aircraft Design Report, 2013 AIAA DBF Competition," 2013.

BUZZOOKA

AIAA DESIGN/BUILD/FLY
2016-2017
DESIGN REPORT

Georgia Institute of Technology

TABLE OF CONTENTS

LIST OF TABLES

TABLE OF FIGURES

ACRONYMS AND NOMENCLATURE

C.G.	Center of Gravity	e	Oswald Efficiency
RAC	Rated Aircraft Cost	P	Power
TFS	Total Flight Score	S	Area
GS	Ground Score	Kv	Motor Voltage Constant (V)
EW	Empty Weight	K_D	Wing Loading Dissipative Constant
TMS	Total Mission Score	K_T	Thrust Loading Dissipative Constant
M1	Mission One	K_A	Regressive Constant
M2	Mission Two	$\dot{x}$	Position Derivative with respect to time
M3	Mission Three	V	Velocity
FOM	Figures of Merit	$\dot{V}$	Velocity Derivative with respect to time
FS	Flight Score	m	Mass
TOFL	Takeoff Field Length	T	Thrust
s_g	Takeoff Roll Distance	D	Drag
NiCad	Nickel-Cadmium	$\bar{p}$	Dimensionless Rolling Rate
NiMH	Nickel-Metal Hydride	$\bar{q}$	Dimensionless Pitching Rate
AVL	Athena Vortex-Lattice	$\bar{r}$	Dimensionless Yawing Rate
$\widetilde{C}_L$	Airfoil Section Lift Coefficient	AR	Aspect Ratio
$\widetilde{C}_D$	Airfoil Section Drag Coefficient	R_e	Reynolds Number
$\widetilde{C}_m$	Airfoil Section Moment Coefficient	R_T	Taper Ratio
C_L	Aircraft Lift Coefficient	S_w	Wing Area (ft²)
C_D	Aircraft Drag Coefficient	T_S	Settling Time (s)
C_f	Skin Friction Coefficient	ρ	Density
C_Y	Aircraft Side Force Coefficient	T_d	Doubling Time (s)
C_n	Aircraft Yawing Moment Coefficient	W	Weight (lbs)
C_m	Aircraft Pitching Moment Coefficient	α	Angle of Attack (degrees)
C_l	Aircraft Rolling Moment Coefficient	β	Sideslip Angle (degrees)
$C_{D,i}$	Aircraft Induced Drag Coefficient	μ_r	Rolling Coefficient of Friction
$C_{D,0}$	Aircraft Zero-Lift Drag Coefficient	R_{ls}	Wing Sweep
L'	Wing Thickness Location Parameter	R_{wf}	Wing Fuselage Interference
MTOW	Maximum Takeoff Weight	V_{wind}	Wind Speed
Θ_{wind}	Wind Direction	$W_{battery}$	Battery Weight

1   EXECUTIVE SUMMARY

This report details the design, testing, and manufacturing of *Buzzooka*, Georgia Institute of Technology's entry in the 2016-2017 AIAA Design/Build/Fly (DBF) competition. The system consists of an aircraft and a tube which carries and protects the aircraft from impact loads. Together, the system is designed to complete the following tasks:

1. Empty flight
2. Loaded flight
3. Transformation from the carrying configuration to the ready to fly configuration
4. Survival of the tube and loaded aircraft in impact loads testing.

At the time of writing, there have been 28 test flights of the aircraft.

1.1   Design Process

Buzzooka is designed for victory. This is achieved through the development of a robust system capable of flying all missions reliably with minimum Rated Aircraft Cost (RAC). The conceptual design of a winning system involved converting the mission requirements and scoring criteria into a list of design metrics that were used to decide the preliminary configuration of the aircraft. Trade studies on wing loading and power were performed using historical data, and computer tools to estimate drag and lift. Battery and motor combinations were evaluated to achieve the required propulsion. Stability analysis was performed using a vortex lattice model to determine the size and placement of lifting surfaces. A detailed design with dimensions was created, then prototyped and flight tested to validate assumptions made during the design. For the tube, various designs were investigated using different materials and manufacturing processes. These designs were evaluated regarding their ability to protect the folded aircraft as well as for their dimensions and weights.

1.2   Key Mission Requirements and Design Features

Balancing key mission requirements was the basis for a successful system design. Design metrics were developed for each mission requirement and scoring element to maximize system performance and overall competition score.

Empty Weight: The aircraft's empty weight is a significant driver of total score. Empty weight is the weight of the airframe and propulsion system. Judicious use of composite materials was combined with a highly efficient built up structure and the lightest possible motor and battery to design an aircraft that was as minimalistic as possible without compromising the ability to complete all three flight missions.

Tube weight: The sum of the tube weight and empty weight of the aircraft is inversely proportional to the total score. Low tube weight was necessary for a high score. By maximizing the structural efficiency of an innovative composite design, a tube was created that was strong enough to fit mission requirements while being light enough to maximize score.

Tube Dimensions: The final flight score is inversely proportional to the sum of the tube length and circumference. In addition, the tube length must be at least four times the tube diameter. Therefore, maximizing score is dependent on reducing tube dimensions, especially the tube diameter. Minimization of wall thickness through the use of thin composite structures enabled the tube to have dimensions no larger than necessary to achieve the highest possible score.

1.3   System Performance Capabilities

All of the specific design features created to maximize the performance of the system can be summarized by the following performance capabilities:

- Empty Weight of 0.88 lbs and MTOW of 2.005 lbs
- Reliable hand launch
- Top speed of ~30 mph
- Compact storage in 4.25" diameter and 18.16" long tube
- Secure storage of payloads in M2 and M3
- Proven capability through 3 iterations and 28 test flights, as shown in Figure 1.1, below.
- Estimated RAC of 26.53 and flight score of 18.77.

Figure 1.1: Aircraft in flight

The final design is a hand launched Rogallo wing aircraft with one motor and a V-tail. The aircraft is designed to minimize weight and folded size while successfully carrying the required payload of three hockey pucks and flying three laps. The top speed of the aircraft was balanced against the stall speed to achieve the desired blend of reliability and scoring potential. The plane stores in a tube by folding the unique wing along the side of the fuselage with 3D printed hinges and joints. The team chose an ambitious design to maximize the total score.

2 MANAGEMENT

2.1 Team Organization

Buzzooka used a hierarchical structure to establish leadership amongst its senior members, with responsibilities flowing down to the team's newer members. This hierarchy served as an outline only, as all team members collaborated extensively to reach deadlines, share ideas, learn various disciplines, and produce a more successful aircraft. The work was divided during the design phase into CAD and Structures, Aerodynamics, Propulsion, Conceptual Design, and Manufacturing. During construction, testing, and report writing, all team members participated fully. Figure 2.1 shows the different positions and the roles within the team.
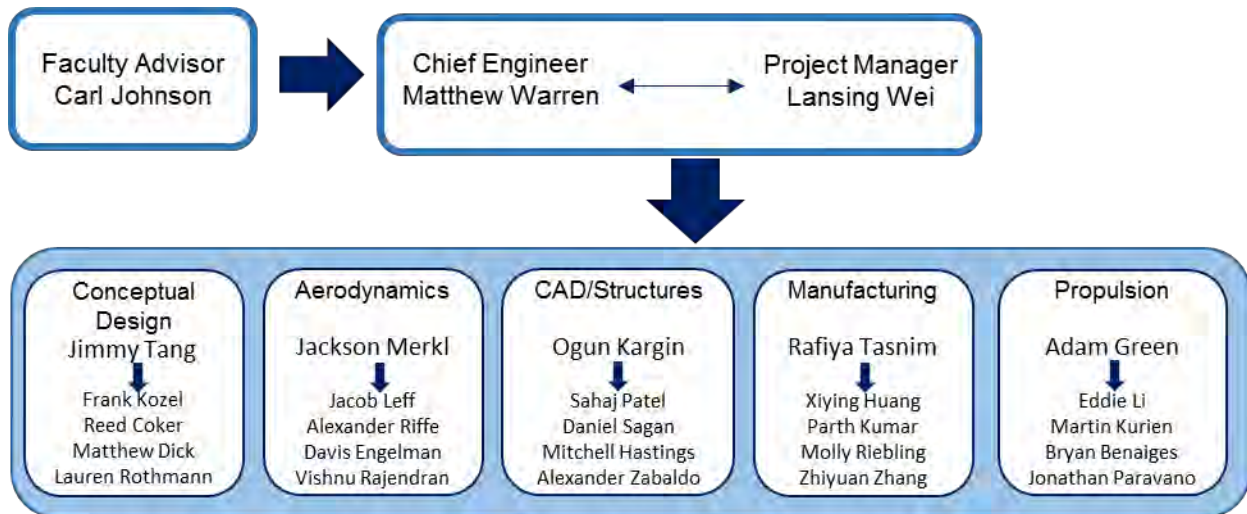

Figure 2.1: Team organization chart

2.2 Milestones

A milestone chart was established at the beginning of the design process to capture major deadlines and design and manufacturing goals. Progress was monitored by the team leaders to ensure all major milestones were met. The team worked throughout the entire academic year and established stringent deadlines early to ensure testing and flight experience before the competition in April. The team met frequently with the faculty advisor to discuss progress. The milestone chart is shown below in Figure 2.2, capturing planned and actual timing of major events.
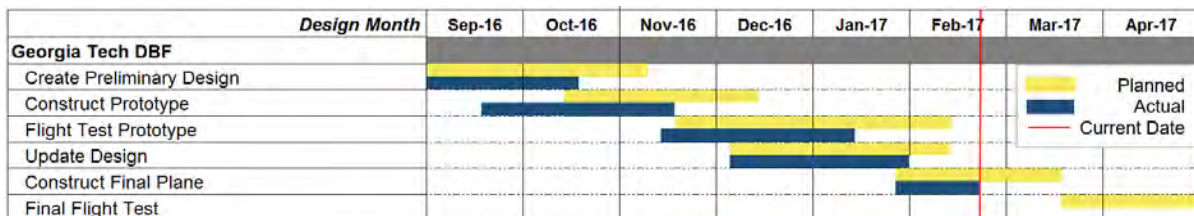

Figure 2.2: Aircraft design milestone chart showing planned and actual time ranges for objectives

3　CONCEPTUAL DESIGN

In this early phase of design, the team analyzed the competition rules to produce a feasible design that maximized score. The rules were distilled into design requirements and scoring factors. Quantitative analysis was performed to pinpoint key scoring drivers and constrain the design space. These scoring factors were then translated into Figures of Merit (FOM) and used to evaluate aircraft configurations and design decisions. This process in its entirety is presented in the following sections.

3.1　Mission Requirements

3.1.1　Mission and Score Summary

The AIAA Design/Build/Fly 2016/2017 competition consists of three flight missions, a ground mission, and a design report. The total score for each team is calculated using Equation 3.1, below.

$$Score = Written\ report\ score * TMS/RAC \qquad (3.1)$$

Equation 3.2 below breaks down the Total Mission Score (TMS). The TMS is the sum of the three mission flight scores. Equation 3.3 below breaks down the Rated Aircraft Cost (RAC). The RAC consists of the maximum empty weight of the aircraft recorded at competition (EW_{max}), unloaded tube weight (TW), tube length (L), and tube circumference (C).

$$Total\ mission\ score = M1 + M2 + M3 \qquad (3.2)$$

$$RAC = (EW_{max} + TW) * (L + C) \qquad (3.3)$$

Equations 3.1, 3.2, and 3.3 show that the tube dimensions and the combined weights of both the aircraft and the tube are the main score drivers. Increasing aircraft performance necessarily requires an increase in weight and size, and it was demonstrated during sensitivity analysis that the scoring equation is more sensitive to changes in RAC than the TMS. As a result, the team concluded that the main score drivers would be the tube dimensions and the combined weights.

All flight missions are flown along the same distance and pattern per lap. For flight missions, the individual portions of the flight pattern seen in Figure 3.1, below, are as follows:

1. Successful hand launch of aircraft
2. Climb to Safe Altitude
3. 180° U-turn, 500 ft. Upwind from the Start/Finish Line
4. 1000 ft. Downwind
5. 360° Turn Along the Backstretch
6. 180° U-turn
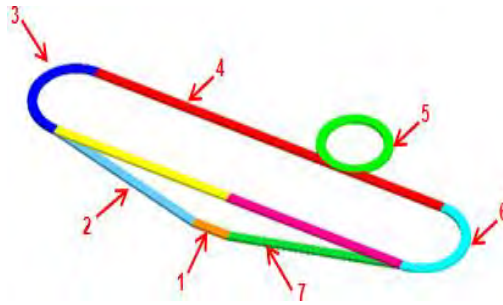7. 500 ft. Final with a Successful Landing

Figure 3.1: Competition flight course

Each lap is roughly 2500 ft. when accounting for the three turns involved. A complete lap is defined as crossing the start/finish line, completing the defined pattern, then crossing the start/finish line while still in the air. The required number of laps is defined by the mission. The ground mission may be completed either before or after the first flight mission.

Ground Mission: The ground mission must be successfully completed before attempting Mission 2, but can be performed before Mission 1. Three team members may participate in this mission: the assembly ground crew member, the observer, and the pilot. The aircraft is installed and sealed inside the launch tube with the maximum weight payload determined during tech inspection. A series of 3 drops from a minimum height of 12 inches are performed onto a hard surface. These drops are shown in Table 3.1, below.

Table 3.1: Drop breakdown for the Ground Mission

Test	Description
Drop 1	Flat drop; the launch tube long axis will be parallel to the landing surface; the mission official will select the orientation about the long axis for the drop
Drop 2	End drop; the launch tube long axis will be perpendicular to the landing surface
Drop 3	Same as Drop 2 on the opposite end

The assembly crew member will lift the launch tube to the required height, then release it on command. The mission official will confirm a good drop. A good drop as defined as any drop where the launch tube does not sustain major damage as a result of the drop tests. Major damage may be, but is not limited to, visible cracks or perforations (no longer meets the definition of water tight), external features moving or falling off, including end caps, and obvious signs that the structural integrity of the launch tube has been compromised.

After the three drops are completed, the assembly crew member will remove the aircraft from the launch tube. The aircraft must come out in one piece. Any dislodged items or damage to the aircraft will be a mission failure. The assembly crew member will transition the aircraft to the flight condition – manually rotate or move surfaces or features to the flight condition. The pilot will then verify all flight controls and subsystems are functional, including propulsion. The assembly crew member and one other crew member (pilot or observer) will conduct a wing tip test to ensure the structural integrity of the aircraft before flight.

The ground mission is considered successful if all the above conditions are met. Any failure to any of the above criteria will result in a failure for the ground mission.

Mission 1 Demonstration Flight: For this mission, the aircraft must achieve steady level flight at or before the start line. The team must complete three laps within a five-minute time window. Time starts when the aircraft leaves the launcher's hand and ends when the aircraft completes three laps. Points are awarded if the aircraft successfully lands. The scoring for M1 is shown in Table 3.2, below.

Table 3.2: Scoring breakdown for Mission 1

Mission	Description	Score
M1	Aircraft completes the mission	1.0
M1	Aircraft does not attempt or complete a successful flight	0.0

Mission 2 Speed Flight: For this mission, three hockey pucks are loaded into the aircraft. The team must complete three laps of the flight course within a five-minute time window. Time is started when the aircraft leaves the launcher's hand and ends when the aircraft completes three laps. Points are awarded based on Equation 3.4, as shown below, only if the aircraft successfully lands.

$$M2 = 2 * \frac{Time_{min}}{Time_{Buzz}}$$

(3.4)

Subscript "Buzz" refers to the time taken to fly three laps for *Buzzooka*, and subscript "min" refers to the fastest time achieved at the competition.

Mission 3 Range Flight: For this mission, a team-chosen number of hockey pucks is loaded into the aircraft. The aircraft must fly as many laps of the flight course as it can within a five-minute flight window. Time is started when the aircraft leaves the launcher's hand. After five minutes, the aircraft must land. The landing time is not part of the time window. A score is awarded based on Equation 3.5, as shown below, only if the aircraft successfully lands.

$$M3 = 4 * \frac{(Laps*Pucks)_{Buzz}}{(Laps*Pucks)_{max}} + 2$$

(3.5)

Subscript "Buzz" refers to the lap-pucks achieved by *Buzzooka*, and subscript "max" refers to the highest value of lap pucks achieved at the competition.

3.1.2   Aircraft and Launch Tube Constraints

Hand Launch: All aircraft must be hand launched. Hand launches must be accomplished by holding the fuselage. No wingtip or discus launches are allowed. No "hand launch assist" device (such as a spear-thrower or any type of arm extender) may be used.

Propulsion System: The aircraft must be propeller driven and electrically powered, with all components of the propulsion system commercially available. These include the motor, propeller, speed controllers, receivers, and batteries. The battery selection is limited to NiCad or NiMH, but may be of any cell count, voltage, or capacity. There is no limit to the weight of the battery packs. The entire propulsion

system must be armed by an external safety plug or fuse. The arming device must be mounted on the exterior of the aircraft and be accessible from behind in a tractor propeller configuration.

Payload: The aircraft payload for Mission 2 and Mission 3 is some number of regulation hockey pucks. Regulation hockey pucks are of diameter 3 inches, thickness 1 inch, and weight 6 ounces.

Launch Tube: The launch tube must be a right circular cylinder of constant cross-section with a length-to-diameter ratio of no less than 4. The launch tube must be completely sealed and airtight in the storage and pre-flight condition. No perforations, cut-outs, or access holes are allowed. The tube must open from one end with an end cap that is secured in place. If the cap is secured externally, the largest diameter measured will be used as the diameter of the tube.

Hinging: The aircraft must store completely within the launch tube. All surfaces or aircraft features that are folded, rotated, stowed or otherwise moved to a condition for storage in the launch tube must be moved to the flight condition using hinges, pivots, or other captive mechanical mechanisms. Surfaces or aircraft features cannot temporarily separate from the aircraft and use "lanyards" or similar devices. All features must securely lock in the flight condition without the use of tools or manual release or engagement of any locking features. All surfaces or aircraft features described above may be manually moved or rotated to the flight condition by hand. Spring loaded or self-deploying mechanisms are not required. Magnetic locks, springs, and friction fits are not considered sufficient to lock a feature.

3.1.3 Flight Score Sensitivity Analysis

A sensitivity analysis on the flight scoring drivers was performed to understand the design trades and mission objectives that maximize the total mission score (TMS) as divided by the rated aircraft cost (RAC). The scoring is a function of the RAC, top speed, and payload capacity of the aircraft. The RAC is a function of the aircraft empty weight and the weight and dimensions of the storage tube. This analysis was conducted for a conventional airplane design to examine the design space and determine the general scoring trends.

Empty Weight: Aircraft empty weight was divided into propulsion and structural components. The propulsion system weight is proportional to the number of battery cells used. Based on previous team experience, 1500 mAh NiMH cells were selected as representative batteries, weighing 0.05 lbs each. Based on testing of battery discharge rate, the maximum current draw is 20 amps. The electric motor weight was estimated at 0.5 lbs / kW from past experience, and speed controllers that met the pack voltage were cataloged. The propulsion weight assessment is summarized by Equations 3.6 and 3.7, below:

$$P_{electric} = n_{cells} \left(1.2 \frac{V}{cell} \times 20amps\right) \qquad (3.6)$$

$$W_{propulsion} = n_{cells} \left(0.05 \frac{lbs}{cell}\right) + P_{electric} \left(0.5 \frac{lbs}{kW}\right) + W_{ESC} \qquad (3.7)$$

Structural weight was estimated using the team's experience, with a baseline minimum weight which increases with wing area. The coefficients K_A and K_B in Equation 3.8, below, were adjusted to match past years' Design/Build/Fly planes, and Equation 3.9, below, summarizes the empty weight assessment:

$$W_{struct} = W_{baseline} + K_A\left(S_{wing} - S_{baseline}\right)^{K_B} \tag{3.8}$$

$$EW = W_{struct} + W_{propulsion} \tag{3.9}$$

<u>Maximum Speed</u>: The maximum speed directly effects the scoring of M2 and must be high enough for the aircraft to complete three 2,500 ft. lap lengths within five minutes with the assumed wind conditions. The maximum speed was calculated using simple power-required calculations that stem from the drag polar and the power available from the propulsion system, as seen in Equation 3.10, below.

$$P_{req} - P_{av} = \left(\frac{1}{2}\rho V_{max}^3 S C_{D,0} + \frac{2W}{\rho V_{max} S \pi ARe}\right) - P_{electric}\eta_{prop} = 0 \tag{3.10}$$

<u>Takeoff</u>: The aircraft must be hand launched, constraining the wing area and power requirement. The hand launch was modeled as a short takeoff into a headwind. The governing relation for takeoff is shown in Equation 3.11, below, and determined the minimum required power to weight ratio.

$$\left(\frac{P}{W}\right) = \frac{(V_{LO}-V_{stall})^3}{2gS_g} \tag{3.11}$$

<u>Tube Weight and Dimensions</u>: The weight of the tube can be estimated as being proportional to the aircraft MTOW because the tube must support any increase in aircraft weight with more structure. In addition, the dimensions of the tube are estimated as a proportion of the wing area. The wing is the largest single component of the aircraft so any increase in wing size must be matched by an increase in the tube dimensions.

The relationships discussed above can be used to determine the RAC as a fallout of the aircraft speed and payload capacity for a conventional configuration. To isolate the effect of speed and payload, these parameters are analyzed independently. The scoring sensitivity in Figure 3.2 below shows the estimated flight score for a combination of wing area and battery cell counts. The plot represents a physics-based tradeoff between speed and aircraft weight, as governed battery count and wing area. The white area represents configurations that cannot meet the speed requirements. The M3 score is assumed to be fixed.
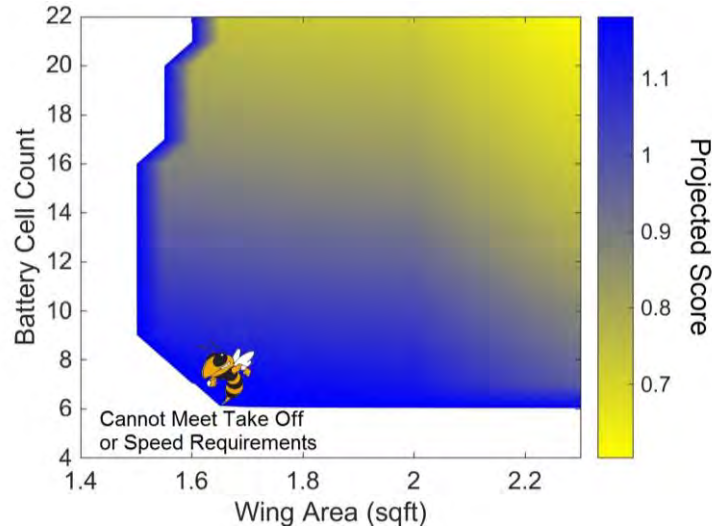
Figure 3.2: A physics-based scoring analysis of the design space. The team's chosen conceptual design point is noted by Buzz's stinger

The maximum score occurs when the battery cell count is minimized. However, increasing the battery size increases top speed. A top speed increase improves the M2 score, but this effect is outweighed by the increase in RAC caused by the additional battery weight. For constant battery size, the wing area should be minimized to reduce the size of the storage tube and increase the maximum speed. The optimal design point is marked with Buzz at a battery cell count of six and wing area of ~1.65 ft^2. This is the optimal design point for a conventional aircraft and will be compared against the design of the Rogallo aircraft.

The effect of hockey pucks carried during M3 was analyzed independently. The baseline aircraft carries three hockey pucks for M2 and M3 and flies three laps for both M2 and M3. Figure 3.3, below, shows the effect on score of carrying a different number of hockey pucks for M3 for a fixed number of laps. From the scoring analysis, carrying three pucks is optimal for the relative flight score of the aircraft. Carrying more hockey pucks for Mission 3 requires a higher propulsion and structural weight, which will cause RAC to increase. Since Mission 2 requires the aircraft to carry three pucks, three pucks were carried for Mission 3.
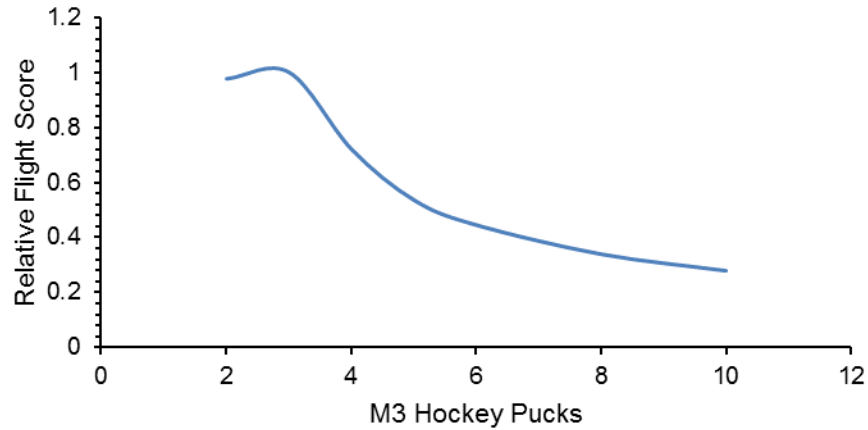
Figure 3.3: Relative flight score vs. Number of hockey pucks carried in M3

3.2 Translation into Design Requirements

The scoring analysis revealed that the overall flight score is driven principally by the RAC. Several aspects were of particular importance:

Tube Size: The scoring sensitivity analysis shows that the tube size has a strong effect on score. Because the RAC is a direct function of the tube length and circumference, creating the smallest possible tube will maximize the score. It is therefore imperative that the aircraft, in storage position, be as compact as possible, with a slender, prolate tube being the first geometry configuration investigated.

Empty Weight: Empty weight has an effect similar to tube size on the score. Any configuration that fails to be as light as possible will not be competitive. Effort must be made to reduce the aircraft empty weight. However, the structure must be able to withstand the expected loads. Such considerations must be carefully balanced to secure the payload and decrease empty weight.

Speed: As per Mission 2, the aircraft top speed has a significant impact on the mission score. Mission 2 score is dependent on the time the aircraft takes to finish three laps. The faster the aircraft finishes three laps, the higher the Mission 2 score will be. However, increasing top speed increases propulsion system weight and must be balanced against the Empty Weight requirement.

Payload: As per Mission 3, the number of hockey pucks carried by the aircraft has a significant impact on the mission score. Mission 3 score is dependent on the number of puck-laps the team is able to achieve. Increasing pucks carried implies increasing score. However, increasing pucks requires more propulsion system weight. As shown in the scoring sensitivity analysis, three pucks for three laps in Mission 3 balances the requirements of all missions in order to maximize the final score.

The analysis conducted in Sections 3.1 and 3.2 were translated into qualitative design metrics that were used to evaluate and select an aircraft configuration, summarized in Table 3.3, below.

Table 3.3: Rules and requirements translated into design requirements

Mission/Scoring Requirement	Design Requirement
Small Tube Size	Compact, collapsible design
Low Empty Weight	Robust, efficient Structure
High Top Speed	Powerful propulsion system
Payload	Sufficient interior volume

3.3   Configurations Considered

3.3.1   Aircraft Configuration

Since the aircraft had to be packed into a tube, selection criteria hinged on the complexity of breaking the aircraft down by closed hinge mechanisms. As a result, several design possibilities were eliminated, but three choices emerged as possible configurations. Each of these configurations were thoroughly analyzed, as detailed below.

Figure 3.4, below, shows a clipped delta configuration examined by the team. The clipped delta presented several unique advantages. An aspect ratio of less than one gave the clipped delta configuration an advantage in packing. The relatively thin cross-sectional area of the configuration's wing enabled a significant speed advantage over other configurations. However, the clipped delta has historically demonstrated significant sensitivity in roll, which potentially would disqualify the aircraft from consideration.

Figure 3.4: Clipped delta configuration

Figure 3.5, below, shows a conventional configuration examined by the team. The conventional configuration is a well understood and oft-examined design that is very robust. In order to fit within the smallest possible tube, a conventional aircraft would require some mechanism to fold both the wing and the tail, introducing significant complexity. Figure 3.6, below, below shows a prototype conventional configuration with its wing folded (left) and fully deployed (right).
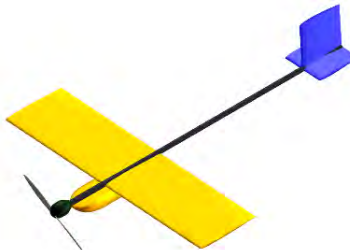

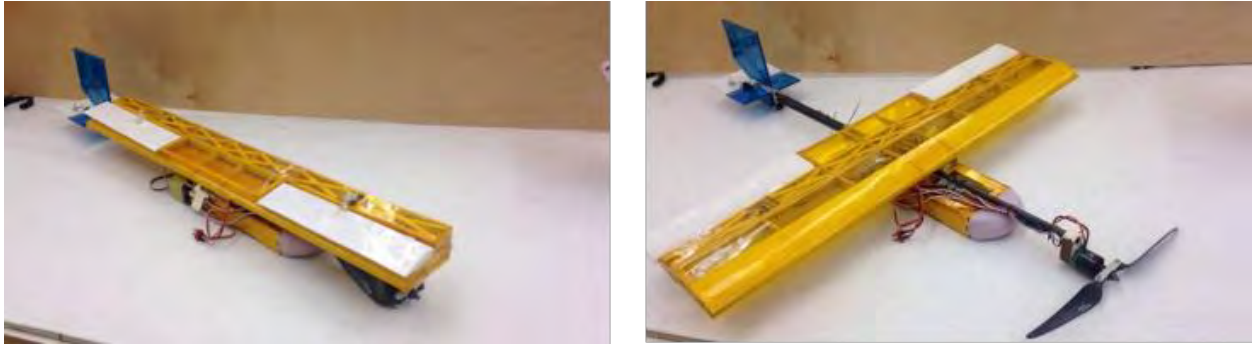*Figure 3.5: Conventional configuration*

Figure 3.6: Conventional wing folded (left) and fully deployed (right)

Figure 3.7, below, shows a Rogallo configuration examined by the team. The Rogallo configuration has the unique advantage of having a wing planform made of fabric which does not require a rigid structure in order to make a lifting surface. As a result, it has the potential to pack very tightly and minimize tube dimensions. This ability to fold is shown in Figure 3.8, below. However, the team's experience with Rogallo wings has shown that the design top speed is inversely coupled with wing area, and that the Rogallo's sensitivity to roll increases rapidly with wing loading. Overall, this makes the Rogallo configuration less robust and riskier than the conventional.
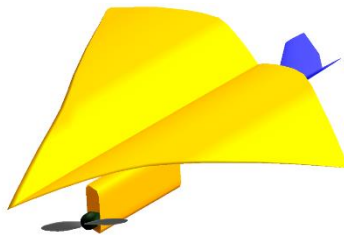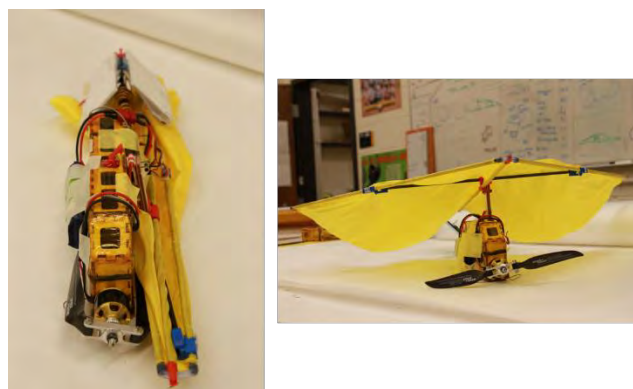

Figure 3.7: Rogallo wing configuration

Figure 3.8: Rogallo wing folded (left) and deployed (right)

3.4 Component Weighting and Selecting Process

In order to asses each configuration from a quantitative standpoint, Figures of Merit (FOM) were created based on the most important configuration factors. The FOM are shown in Table 3.4. Each FOM was assigned an importance of 0 through 5, with 5 being the most important factor and 0 being a non-factor in design.

Table 3.4: Figures of Merit

Figure of Merit	0	1	2	3	4	5
Packing Efficiency						5
Stability				3		
Weight				3		
Speed			2			

Packing efficiency is defined as the ability for a configuration to reduce its size with minimal impact on the primary load bearing structure. As a result of the scoring, the packing efficiency of a given configuration was the most critical design factor. The stability of the aircraft was a significant design factor due to the need to reliably complete all three flight missions. An unstable aircraft would not be able to finish all three missions and achieve a competitive score. Weight of the aircraft was equally as important as stability, due to the strong effect of weight on the RAC. Due to the Mission 2 scoring equation, speed was the final, least important consideration. All configurations could be manufactured in a way to carry three hockey pucks, and as a result payload capacity is not a key figure of merit.

For final selection, each configuration was given a scoring value for each figure of merit, and that rating was then multiplied by the FOM value. The scoring values are shown in Table 3.5, below. The configuration with the highest total quality was then selected for further analysis in the design process.

Table 3.5: Configuration Scoring Values

Score	Value
1	Inferior
3	Average
5	Superior

The three configurations discussed previously are shown in Table 3.6, below, with their respective scores for each of the relevant FOM. These results, combined with those from the qualitative analysis, lead to the team's choice of configuration for the *Buzzooka* aircraft system.

Table 3.6: Aircraft configurations' Figures of Merit

		Aircraft Configurations		
FOM	Value	Rogallo	Conventional	Clipped Delta
Packing Eff.	5	5	3	4
Stability	3	3	5	1
Weight	3	4	3	4
Speed	2	2	5	5
Value	N/A	50	49	45

Table 3.6 shows that while the Rogallo has the highest FOM Score, all three aircraft are closely matched, with each conferring unique advantages. The Rogallo has the greatest packing efficiency and the lowest weight, but suffers from high drag and is known to have roll stability issues, especially in windy conditions. The conventional has the most complex packing scheme, but is also the most stable and has very low drag. Finally, the clipped delta has a simple packing scheme and high speed potential, but suffers in roll stability due to its low span.

Due to the close scores, the team decided to prototype all three aircraft and engage in an internal fly-off. Over the course of development, the Clipped Delta's inherent instability on this scale meant that it was not reliable enough to be a competition aircraft. The conventional configuration and Rogallo configuration each went through multiple iterations and were developed more fully. As expected, the conventional configuration had a substantial advantage in stability and general reliability, demonstrating consistent ability to fly all missions and land safely. Stability and control of the Rogallo configuration was improved substantially over the course of the prototyping process, detailed subsequently in this report, enabling it to compete with the conventional configuration. Initially, the Rogallo had issues with reliable landings, but demonstrated an order of magnitude better scoring potential due to its simple, tightly packing design. Ultimately, the team collectively decided that the higher scoring potential of the Rogallo was worth a concerted effort to enable it to land reliably. This was achieved, and Rogallo configuration was selected as the final configuration.

3.5   Final Conceptual Design Configuration

The final configuration is a Rogallo wing aircraft with a V-tail and a single-engine tractor propulsion system, as shown in Figure 3.9, below. This configuration offers maximum packing efficiency and intrinsically low weight when compared to the conventional aircraft. Issues with stability and reliable mission completion were mitigated over the course of a rapid prototyping process that is discussed later in this report.
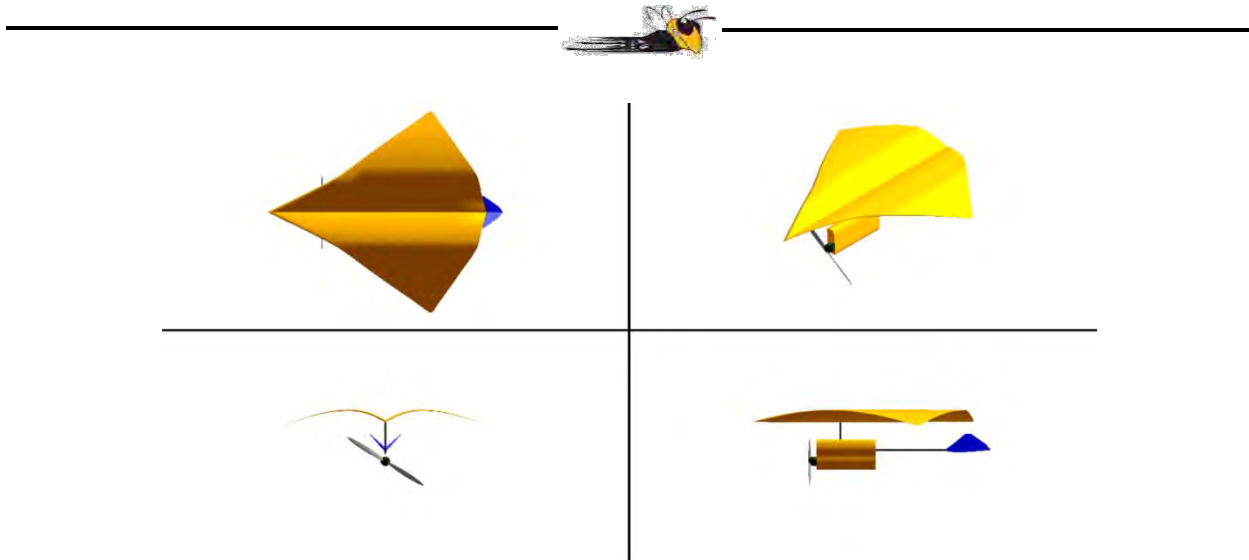
Figure 3.9: Final Rogallo configuration

4 PRELIMINARY DESIGN

The objective of the preliminary design phase was to further narrow the design space. To do this, design and sizing trades for the system were evaluated by examining propulsion system options and wing area sizing for takeoff distance. The weight, drag, motor, propeller data, battery data, and aerodynamic coefficients were calculated and combined to estimate mission performance for all three flight missions.

4.1 Design Methodology

The *Buzzooka* team designed the aircraft using an iterative, performance-focused, multidisciplinary analysis. The team used constraint sizing to select a weight-normalized design point that could satisfy objectives for all three missions. From these design points, the team analyzed possible propulsion systems, system aerodynamic characteristics, built mission models, and compared them to estimates generated as part of the sizing process. After this analysis, the mission performance and stability of the sized aircraft configurations were computed. The design process detailed in sections below is written as sequential, but iterations occurred throughout, as seen in Figure 4.1, below. An example of iteration would be updating wing area at a constant wing-loading if propulsion weight is found to be lower, re-evaluating stability and mission performance, and re-adjusting the wing or propulsion system if needed. All iterations were performed with the ultimate goal of maximizing overall score. Therefore, the design shown in this report is the final product of a more complex, iterative procedure.
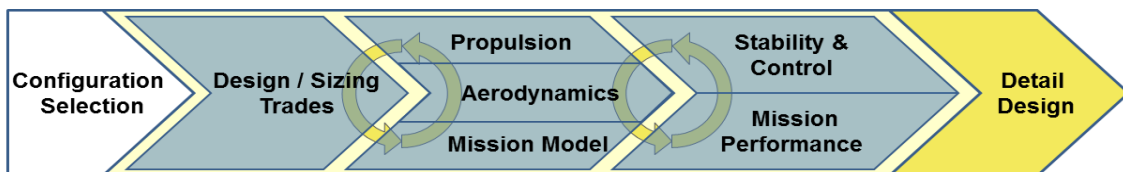

Figure 4.1: The team's preliminary design methodology highlighting the multidisciplinary iterations

4.2   Design Trades

4.2.1   Constraint Sizing

A constraint sizing analysis was conducted to examine the effect of wing loading and power to weight ratio on the performance and scoring potential of each aircraft. Since the maximum aircraft empty weight is a critical part of the RAC, and therefore the overall score as outlined in Section 3.1.1, it is important to keep the weight of the aircraft down by reducing the size of the aircraft and the size of the propulsion system. Since battery weight is roughly proportional to the power available, the lowest power to weight ratio possible will lead to the highest score. Figure 4.2, below, shows that the minimum sustainable power to weight ratio for cruising and turning exhibits diminishing returns, converging asymptotically with increased wing loading. Due to the inherent risks with a Rogallo wing design, the team chose a more conservative design point as designated in Figure 4.2.
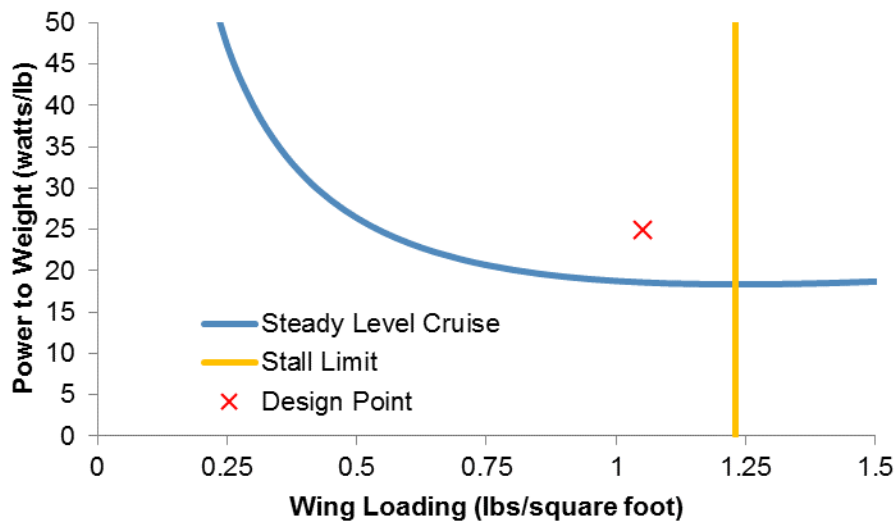

Figure 4.2: Buzzooka constraint sizing design point selection

The constraint sizing process, along with an empirical weight estimate allowed a preliminary determination of power and wing area summarized in Table 4.1, below.

Table 4.1: Preliminary power and wing area

Parameter	Preliminary value
Wing loading (psf)	1.05
Power loading (watts/lb)	25
Estimated weight (lb)	2.13
Wing surface area (ft^2)	2.02
Power required (watts)	53.13

4.2.2 Propulsion System Selection

A fixed pitch propeller was selected to reduce complexity and weight. A system efficiency of 50% is empirically assumed leading to a power requirement of around 106 watts for the propulsion system. From the analysis performed in section 3.1.3, a 6-cell 1500 mAh battery maximizes RAC. The team wanted a direct-drive brushless out-runner motor with a high motor constant, Kv, to draw more power out of a 6-Cell battery. The team researched motors that fit these criteria and created a database containing over 50 motors from various companies, including Hacker, Tiger, Scorpion, Cobra and AXI.

A propeller database was also generated based on the size of the airplane and speed. The propellers tested were Aeronaut folding propellers 9x6, 9x7, 9.5x5, 9.5x6, 10x5, and 10x6 propellers. MotoCalc, a commercially available motor analysis tool, was then used to estimate the motor efficiency, static thrust, and thrust at 30 mph for each motor and propeller combinations, feasible combinations were selected for further analysis and sorted by weight.

The top motor-battery-propeller combinations were analyzed and their variation with speed was graphed. Allowing the team to evaluate the most effective combination to meet the takeoff and max speed requirement. Three motor combinations were chosen to purchase and tested, as shown in Table 4.2, below. Section 8.1.1 will go into further detail regarding these tests.

Table 4.2: Motor specifications

Motor	Kv	Battery (Cells)	Current (Amps)	Best Propeller	Static Thrust (lb.)	Propulsion System Weight (lb.)
Scorpion SII-2212-18	1850	6 (1,500 mAh)	19	9x6	1.32	0.15
Cobra 2814/12	1390	7 (1,500 mAh)	19.0	12x8	1.89	0.20
Hacker A30-22S	1440	7 (1,500 mAh)	17.0	11x8	1.37	0.24

4.3 Mission Model

4.3.1 Description and Capabilities

The three missions were simulated via a set of first order differential equations (Equations 4.1-4.3, below) defining the position and orientation of the vehicle throughout the flight. By integrating these equations over time using a 4th Order Runge-Kutta approach in MATLAB and simple logic defining each of the required mission segments, it is possible to define the position, velocity, and orientation of the vehicle over time. The thrust (T) was defined as a function of velocity, with the relationship defined by MotoCalc, the analysis tool used in the propulsion system selection. The drag (D) was represented via a parabolic drag relationship.

The load factor was explicitly defined for each turn segment, but if it exceeded the estimated maximum lift coefficient, it was limited to that value.

$$\dot{x} = V \tag{4.1}$$

$$\dot{V} = \frac{T-D}{m} \tag{4.2}$$

$$\dot{\psi} = \frac{g\sqrt{n^2-1}}{V} \tag{4.3}$$

4.3.2 Uncertainties

The approach described above has specific limitations and uncertainties. The lack of a vertical dimension means that it cannot capture any aerodynamic effect due to altitude changes, or for the energy required or saved due to climbing or diving. The lack of any wind model discounts any additional drag due to sideslip in flight, or changes in velocity depending on traveling with or against the wind. The flight path defined for each lap assumes an idealized flight path, with the pilot turning perfectly after each 1000 ft. leg and the turns being optimal turns. Finally, there are additional uncertainties in the mission predictions due to any errors or inaccuracies in the thrust and drag predictions.

4.4 Aerodynamic Characteristics

The unconventional planform of the Rogallo wing falls outside the scope of conventional potential flow modeling tools for aircraft aerodynamics. The team compared experimental wind tunnel data (NASA, 1963) against two computer-based tools. The first tool is Athena Vortex Lattice (Youngren & Drela, 2008), or AVL. The team has used this tool with great success for conventional aircraft in the past. The second tool is VORSTAB (Lan, 1987), which is a quasi-vortex lattice program that uses Polhamus' Suction Analogy to determine total lift from potential flow. VORSTAB is capable of analyzing vortex lift which results from leading edge vortices reattaching to the top of the wing and generating more lift than potential flow predictions alone. This is important because low aspect ratio and high sweep planforms such as the Rogallo wing are more likely to generate significant vortex lift. The planform from the NASA paper was modeled with the results shown in Figure 4.3.
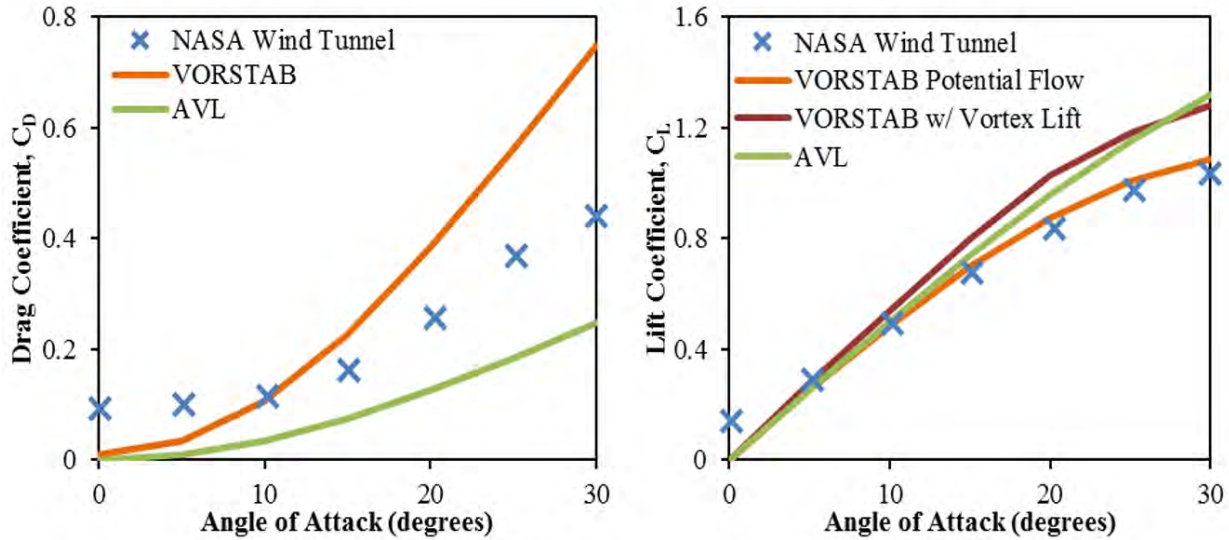
Figure 4.3: Comparison of NASA wind tunnel data to AVL and VORSTAB [NASA, 1963]

4.4.1 Lifting Surface Analysis

VORSTAB results were compared against the NASA wind tunnel results and results from the Georgia Tech wind tunnel. The model was further compared against the final Rogallo wing to ensure scaling and construction techniques do not change the performance. Figure 4.4, below, shows the comparison between VORSTAB results and experimental wind tunnel data of the 2 ft^2 Rogallo wing. Section 7.2 details the setup of the wind tunnel tests.
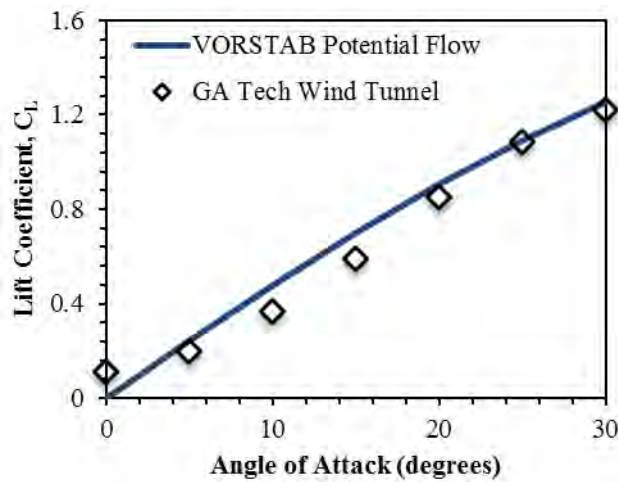

Figure 4.4: Comparison of lift coefficients

4.4.2 Drag Analysis

A preliminary parasitic drag estimate was obtained by summing each component's drag contributions, computed using the semi-empirical methods from Hoerner's *Fluid Dynamic Drag*, and then normalizing each component according to the wing reference area. Table 4.3, below, shows the contributions of the major aircraft components, with Figure 4.5, below, showing the same data as a percentage breakdown.

Table 4.3: Breakdown of various sources of drag

Component	$C_{D,0}$
Wing	0.036
Mast	0.0027
Fuselage	0.0614
Empennage	0.00652
Total	**0.106**

6.12%

33.76%

57.56%

2.57%

- Wing
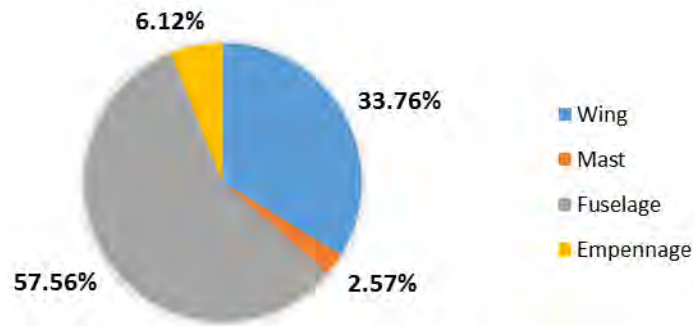- Mast
- Fuselage
- Empennage

Figure 4.5: Breakdown of various sources of drag

Wing: The drag coefficient for the wing was calculated using a linear regression of wind tunnel data, published by the Ohio State University (Warchol, 2009). Data for zero-lift drag ($C_{D,0}$) and Oswald's efficiency factor (e) were both provided as a function of wing sweep angle. These are presented in Figure 4.6 for zero-lift drag (left) and Oswald's efficiency (right).
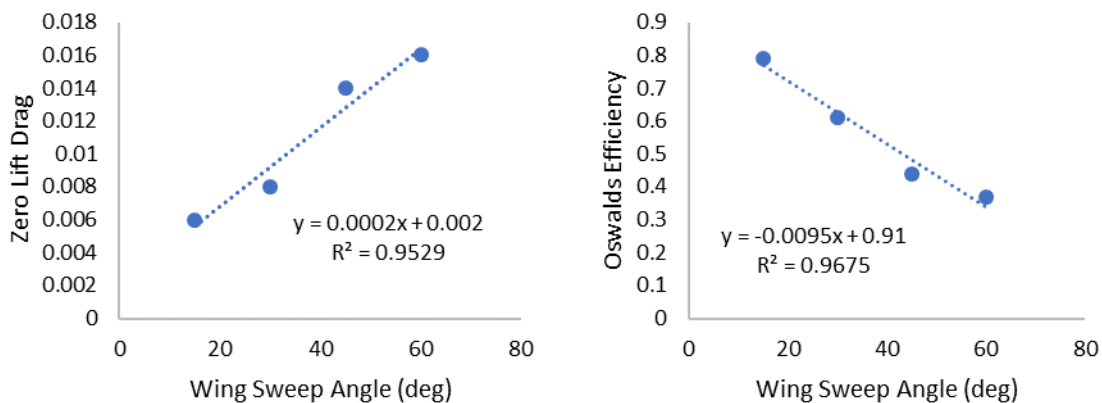

$y = 0.0002x + 0.002$
$R^2 = 0.9529$

$y = -0.0095x + 0.91$
$R^2 = 0.9675$

Figure 4.6: Zero lift drag (left) and Oswald's efficiency factor (right) [Warchol, 2009]

Based on previous experience, the team preliminarily selected a wing sweep angle of 50 degrees, which provided a good margin of safety against deflation. An intrinsic zero-lift drag and Oswald's efficiency of 0.012 and 0.435 were found based on the regressions described in Figure 4.6. The zero-lift drag was then multiplied by a form factor to account for the particular assembly scheme used by *Buzzooka*, resulting in a final wing zero-lift drag of 0.036.

Fuselage: The drag coefficient for the fuselage was determined using Hoerner's method, which computes drag as a function of the body fineness ratio, the Reynold-adjusted skin friction coefficient, and lifting-surface/fuselage interference. The total $C_{D,0}$ contribution of the fuselage was 0.0454 and contributes 44.86% of the total zero-lift drag, which represents the largest portion of zero-lift drag.

Battery The drag coefficient for the battery was determined using Hoerner's method. The externally carried battery had a zero-lift drag of 0.00654 and contributed 6.47% of the zero-lift drag.

Empennage: The empennage was modeled as a pair of flat plates, and their drag was determined using Hoerner's method. A total zero-lift drag of 0.003255 was found. Overall, the contribution of the tail to drag was 4.82%.

The drag polar was calculated using Equation 4.4. $C_{D,0}$ and e were set to the value calculated from the regression in Figure 4.6. C_L values were selected from team wind-tunnel data. Due to the sweep angle of 50° described earlier, the aspect ratio (AR) was 2.88. Figure 4.7, below, shows the resulting drag polar.

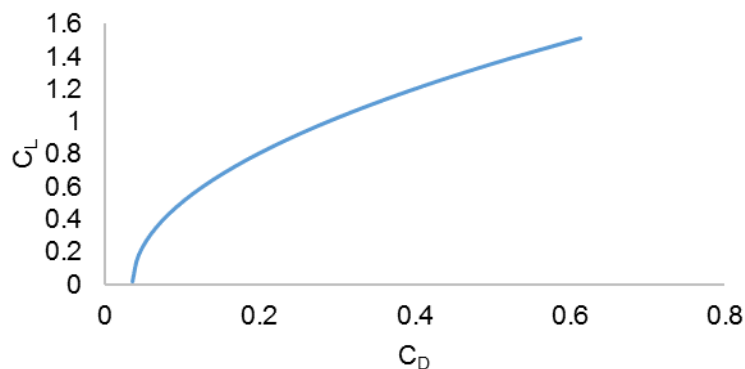$$C_D = C_{D_0} + \frac{C_L^2}{\pi A R e} \tag{4.4}$$

Figure 4.7: Drag coefficient prediction for the Rogallo wing platform

The wing exhibits a very shallow lift-curve slope due to the aspect ratio of 2.88. The wing revealed no stall characteristics in the range of angles of attack that were tested. The maximum angle of attack and maximum lift coefficient were therefore defined using the drag polar in Figure 4.7, above. No distinct upper limit on angle of attack was found analytically. However, flight test results and post-hoc analysis of camera footage showed that angles of attack above ~30° and below ~5° resulted in unpredictable wing deflation behavior. As a result, the aircraft flight envelope was limited to angles of attack between 5° and 30°. While the maximum lift to drag ratio and $C_{L,max}$ of the Rogallo wing are poor when compared to conventional wings, this tradeoff is justified by the compact storage of the wing.

4.5   Stability and Control

Static and dynamic stability were analyzed to ensure that the aircraft would be able to successfully complete the flight missions. The fastest speeds, slowest speeds, heaviest weights, lightest weights, cruise, climbs, and turns were all considered, with results presented only for the critical flight condition.

4.5.1   Static Stability Analysis

The stability of the Rogallo cannot be modeled with VORSTAB alone due to two phenomena: the wing-mast offset from the CG and the prop-wash increasing dynamic pressure over the empennage. The V-tail was projected onto the horizontal plane to define a horizontal tail area and onto a vertical plane to define a vertical tail area. The team used Equation 4.5. to find the true aerodynamic center of the aircraft ($\bar{x}_{ac_A}$) while accounting for the dynamic pressure ratio of the horizontal tail component (η_h, estimated as 1.5). VORSTAB was used to model the Rogallo wing and output wing stability parameters (seen as $C_{L_{\alpha_w}}$ and $\bar{x}_{ac_w}$). Classical potential flow theory was used to compute the tail's stability parameters (seen as $C_{L_{\alpha_h}}$ and $\bar{x}_{ac_h}$). As shown on the right side of Figure 4.8, below, there is a backward shift in the aerodynamic center location of both the wing and tail relative to the center of gravity when the angle of attack changes. This indicates that the effect of the wing-mast offset (denoted h_{mast}) is stabilizing. These shifts are accounted for using trigonometry, as shown in Equations 4.6 and 4.7.

$$\bar{x}_{ac_A} = \left(\bar{x}_{ac_w} + \frac{C_{L_{\alpha_h}}}{C_{L_{\alpha_w}}} \eta_h \frac{S_h}{S} \bar{x}_{ac_h} \right) \left(1 + \frac{C_{L_{\alpha_h}}}{C_{L_{\alpha_w}}} \eta_h \frac{S_h}{S} \bar{x}_{ac_h} \right)^{-1} \tag{4.5}$$

$$\Delta\bar{x}_{ac_{wing}} = \frac{h_{mast}}{\bar{c}} \sin\alpha \tag{4.6}$$

$$\Delta\bar{x}_{ac_{tail}} = \frac{l_{tail}}{\bar{c}} (1 - \cos\alpha) \tag{4.7}$$
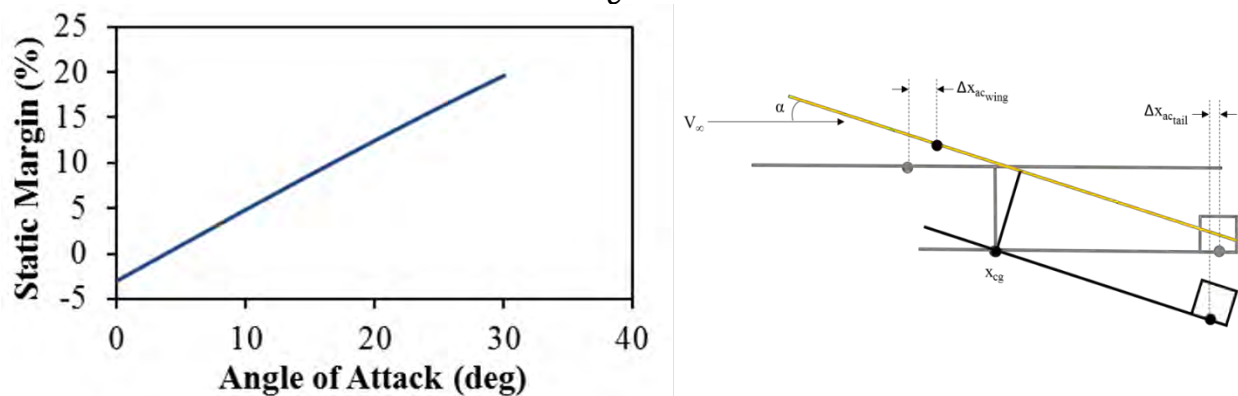

Figure 4.8: Static pitch stability as a function of angle of attack (left) and aerodynamic center shift relative to the CG as a function of angle of attack (right)

An aircraft is longitudinally statically stable if the CG is located in front of the aerodynamic center. This distance is referred to as the static margin if it has been normalized by the mean chord. The aerodynamic center is shifted backward, in the stabilizing direction, by both the shift in aerodynamic center due to an increase in angle of attack and the increase in tail effectiveness due to prop wash. The static margin is shown as a function of angle of attack on the left side of Figure 4.8, above. The aircraft is pitch stable at its target CG location at angles of attack over 5 degrees. This is acceptable because the Rogallo wing must always be flown at an angle of attack over 5 degrees to ensure the wing is inflated.

The most demanding flight condition for trim was at the highest weight and lowest speed. Stability derivatives are given for these flight condition in Table 4.4, below. The aircraft are trimmed at this condition with a small elevator deflection, and no extreme deflections were required for any of the cases analyzed. All cases indicate the aircraft are longitudinally, statically stable with a static margin of 10.2%. All pitch, roll, and yaw derivatives are stable and within the acceptable range based on previous years' pilot feedback.

Table 4.4: Relevant stability coefficients and derivatives for static stability

Parameter		Aircraft
Inputs	W_{total} *(lbs.)*	2.005
	V (ft/s)	43.2
Aerodynamic Parameters	C_L	0.75
	α (deg.)	15°
	β (deg.)	0.0
Deflections	$\delta_{elevator}$ *(deg)*	-5.0
	$\delta_{aileron}$ *(deg)*	N/A
Stability Derivatives	$C_{l,\beta}$ *(rad⁻¹)*	-0.27
	$C_{L,\alpha}$ *(rad⁻¹)*	2.51
	$C_{m,\alpha}$ *(rad⁻¹)*	-0.93
	$C_{n,\beta}$ *(rad⁻¹)*	0.21
Damping Derivatives	$C_{l,p}$ *(rad⁻¹)*	-0.35
	$C_{m,q}$ *(rad⁻¹)*	-2.64
Static Margin	*% Chord*	10.2

4.5.2   Dynamic Stability Analysis

The stability and control derivatives were obtained again using VORSTAB, the mass properties were obtained from the CAD file, and the stability characteristics were calculated using the six degrees of freedom linearized differential equation matrix found in Phillips' *Mechanics of Flight (2nd ed.)*, Section 9.8. Using MATLAB, the eigenvalues and eigenvectors of the matrix revealed that the aircraft is stable in the Short Period, Dutch Roll, and Roll modes, unstable in Spiral mode, and neutrally stable in Phugoid mode. The Spiral modes have a doubling time on the order of three seconds, which is in line with past years' aircraft that flew without issue. The flight conditions used for this calculation were the same ones used in the static stability section, listed in Table 4.4. The dynamic stability characteristics are tabulated in Table 4.5, below.

Table 4.5: Dynamic stability analysis for the least stable case

	Mode	Longitudinal Modes		Lateral Modes		
		Short Period	Phugoid	Dutch Roll	Roll	Spiral
Production Aircraft	Damping Rate (s^{-1})	8.12	0.074	0.81	1.21	0.21
	Time to double/half (s)	0.094	11.12	0.86	0.58	3.16
	Damping Ratio (~)	0.65	0.08	0.10	-	-
	Damped Natural Frequency (s^{-1})	8.47	0.46	8.29	-	-
	Undamped Natural Frequency (s^{-1})	12.26	0.436	8.3	-	-

4.6   Mission Performance

The mission is flown with the aircraft at MTOW, involving a full payload of 3 hockey pucks. Predicting the performance of the aircraft, especially in turning, is key to predicting mission success. Lap trajectories were estimated using the mission simulation described in Section 4.3, propulsion characteristics from MotoCalc, and aerodynamic characteristics of the airplane which were obtained experimentally and semi-empirically. Calculations for *Buzzooka* were performed assuming a 9x6 propeller, a Scorpion SII 2212-18 motor, and a 6S 1500 mAh NiMH battery pack. As per the flight scoring analysis in Section 3.1.3, Missions 2 and 3 will both be conducted with a 3-puck payload and therefore identically simulated. The estimated velocity profile for a single lap of these missions is shown below in Figure 4.9. The maximum velocity is estimated to be 29.89 mph with an estimated lap time of 65.73 seconds, leading to an estimated completion of 3 laps in less than 5 minutes for Missions 2 and 3. Therefore, because Missions 2 and 3 can be completed within the time limit at full loading, the performance targets for Mission 1 should be easily met at a lighter loading. Because the aircraft is hand launched, ground takeoff roll is not considered.
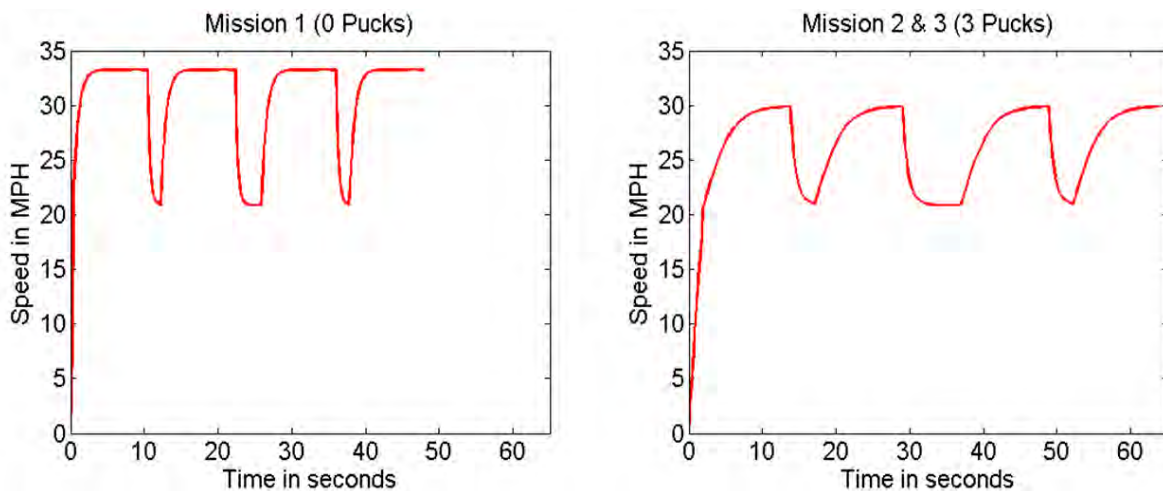

Figure 4.9: Single lap velocity profiles for all missions

5 DETAIL DESIGN

5.1 Final Design – Aircraft

The primary variation between the preliminary and detailed design stages was in the size and layout of the wing. Testing of initial designs of the wing showed fluttering in the rear third of the wing. Different sizes of the Rogallo wing were tested to reduce the fluttering and offer a more efficient lifting surface. Generally, structural analysis and layout, component selection and weight-balance calculations did not indicate major changes were required. With the sizing completed, the final dimensional parameters are listed in Table 5.1, below. Control surfaces were designed to allow for embedded servos, integration of the system, and sized to provide stability at the constant derived wing area. Empennage dimensions are shown in Table 5.2, below. The final aircraft was designed for flight stability, simplicity, and structural efficiency.

Table 5.1: Final aircraft dimensions

Overall Aircraft Dimensions		Aircraft Wing Dimensions	
Length	25.13 in	Span	27.18 in
Width	27.18 in	Mean Chord	21.5 in
Height	5.75 in	Aspect Ratio	2.88
LE Sweep Angle	50°	Wing Area	2 ft^2
CG X-Location	3.94 in		

Table 5.2: Empennage dimensions

Empennage Dimensions	
Chord	5 in
Span	9 in
Dihedral angle	45°
Ruddervator chord	3 in
Ruddervator span	4.5 in

5.2 Structural Characteristics

5.2.1 Layout and Design

The structural layout was created to ensure that all loads were accounted for and have an adequate load path to the major load bearing components. The team divided the loads the aircraft would see into three categories.

Thrust Loads: Includes thrust, torque, and sustained vibrations. Components should be made of harder, quasi-isotropic materials such as plywood, and all fasteners must be locked.

Aerodynamic Loads: Includes wing and control-surface lift, drag, and moment, which translate to bending and torsion. Components can be anisotropic for added strength in the load direction.

Ground Loads: Includes aircraft weight and landing impact. Struts should be metal, which sustains impact by bending, not breaking.

The loads on *Buzzooka* need to transfer to the primary load bearing components, which includes the wing spar and fuselage attachment point. The wing may sustain up to 2.5g load at maximum weight. This requirement is based on the wing tip test. Therefore, all loads from the components not on the wing, such as the payload and empennage, traverse to the spar via the center wing mounting post. The fuselage provides and adequate load path because it is geometrically stiff in order to accommodate the payload. For ground loads, the aircraft assumes a bicycle style landing on the base of the empennage and a point on the fuselage. These loads are shown in Figure 5.1, below.
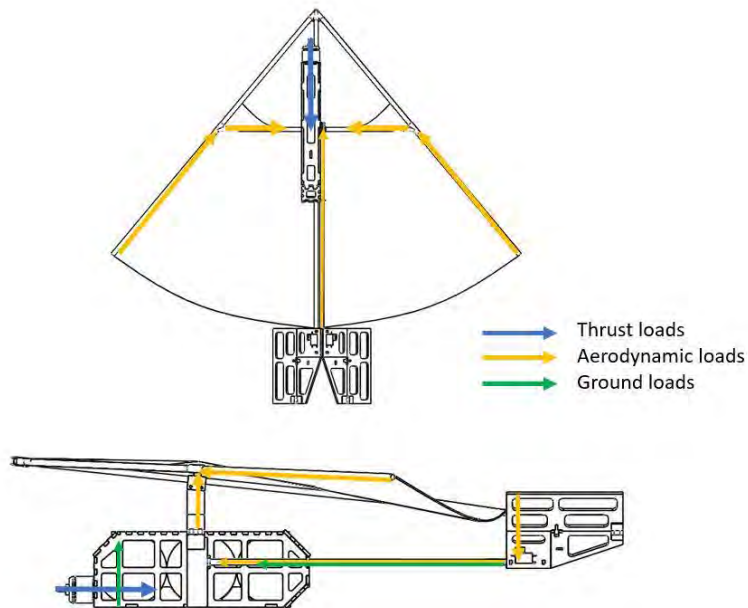
Figure 5.1: Load paths of major forces

5.2.2   Operating Envelope

With the loads mapped and layouts complete, the aircraft structures were designed to withstand the design load of 2.5g at the maximum gross weight of 2.005 lbs. This translates to a 66-degree bank angle for sustained, level turns. The 2.5g design load limit at small deflections was retained as the maximum positive load envelope. Due to the aircraft's Rogallo wing, a negative load envelope was not necessary because the aircraft must fly at a positive angle of attack to keep the wing inflated. The defining structural limits were combined with aerodynamic performance limits to construct a V-n diagram, shown in Figure 5.2, below.
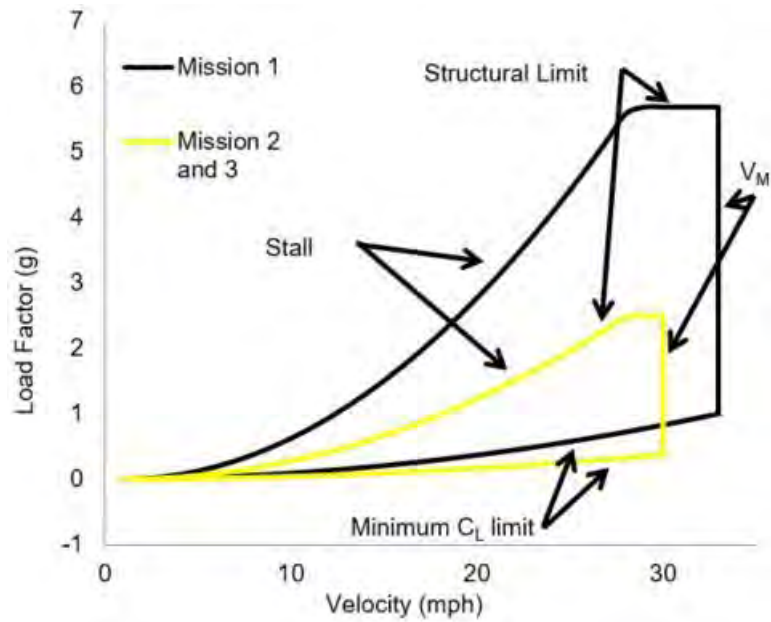
Figure 5.2: V-n diagram showing loading as a function of velocity for all flight missions

5.3 System and Subsystem Design and Implementation

To finalize the aircraft design, the following subsystems were analyzed with greater detail: radio controller, servos, main wing, propulsion system, landing gear, and the structural architecture/assembly for each of these components: fuselage, wing, motor mount, empennage, payload enclosure, receiver and transmitter, propulsion, and servos.

5.3.1 Fuselage

The fuselage is primarily made from 1/8" balsa wood reinforced with carbon fiber tow. Lightening holes were cut to minimize weight. Certain fuselage pieces such as the motor mount, the base for the 3D printed mast connector, and the payload bearing piece at the bottom of the payload bay were made from plywood. A carbon fiber tube was placed at the side of the fuselage. The CAD model (Figure 5.3, below) for the fuselage was designed such that the pieces fit together like a jigsaw puzzle. This method allows for the grain direction of the balsa to be appropriate for load transfer while decreasing manufacturing time and improving consistency.
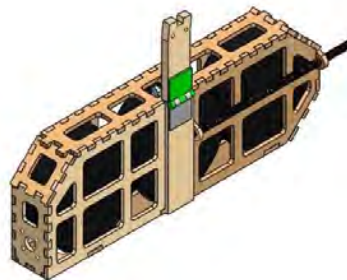

Figure 5.3: Rogallo fuselage CAD

5.3.2 Wing

Buzzooka's Rogallo wing is supported by four carbon fiber tubes which form a triangular planform. The highest loads the wing structure experiences occur during the wingtip test. Euler-Bernoulli beam bending equations and the manufacturer's data were used to determine the maximum acceptable normal stress in the tubes. Equation 5.1, below, gives the area moment of inertia for the beam in terms of the outer diameter (d_o) and the inner diameter (d_i). Since the team knew the aircraft weight and was able to measure the moment arm during the wingtip test, the maximum allowable shear was calculated using Equation 5.2, where y is the overall radius of the tubes. Using rigid body analysis, the team was able to determine that a 0.198" outer diameter, 0.176" inner diameter carbon fiber tube was adequate for the wing structure without adding unnecessary weight.

$$I = \frac{\pi (d_o{}^4 - d_i{}^4)}{64} \tag{5.1}$$

$$\sigma_{xx} = \frac{My}{I} \tag{5.2}$$

The structural elements of the wing are covered by fabric. Rip stop nylon was used because it is inexpensive, strong, and easy to work with. Rip stop nylon was laser cut into the appropriate shapes and hand sewn around the carbon fiber structure.

5.3.3 Motor Mount

The motor mount is attached to the front of the payload bay. Three pieces of 1/8" thick plywood were glued together as a structure capable of withstanding motor thrust and torque loads. Four bolt holes were cut into the plywood to mount the motor. This is shown in Figure 5.4, below.
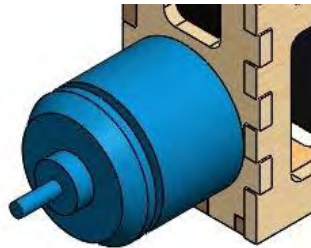

Figure 5.4: Motor mount

5.3.4 Empennage

A 0.198" outer diameter, 0.176" inner diameter carbon fiber tube was used as the tail boom. The carbon fiber tube weighs 0.0092 lbs.

The empennage (Figure 5.5, below) was designed in CAD to minimize size. Flat balsa sheets with lightening holes were used as flat plate airfoils, which decreased control surface effectiveness. The decrease in control authority was corrected by increasing available deflection. A V-tail configuration was chosen because of its ability to fold together and pack compactly. A custom 3D printed joint was used to secure the two ruddervators in place during flight. Servos and actuators were embedded within the surfaces while

minimizing control arm length, size and weight. The two halves of the V-tail and their respective control surfaces were attached with hinge tape to minimize weight and ensure reliable control surface operation. The entire empennage, including control surfaces, was cut out of 1/8" balsa wood with lightening holes.
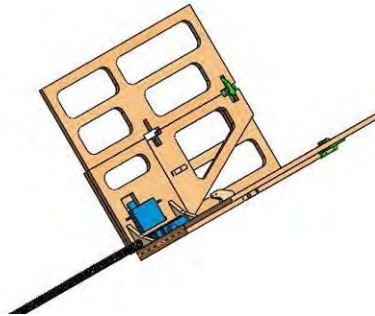

Figure 5.5: Empennage assembly

5.3.5   Payload Enclosure

The payload enclosure (Figure 5.6, below, left) was designed to hold the payload of three hockey pucks for Missions 2 and 3 as shown with minimal weight and overall volume. By positioning the pucks to reduce their wind facing cross section, the cross section of the payload bay was minimized to reduce drag. Each piece of the payload enclosure was made by laser cutting balsa and plywood pieces. Each puck within the payload enclosure was separated by separator tabs (Figure 5.6, below, right). The payload is loaded from the bottom of the enclosure by removing the bottom plate with the puck separators.
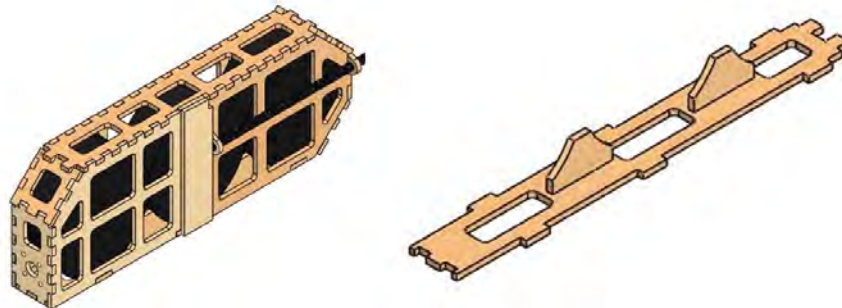

Figure 5.6: Payload enclosure with pucks and puck separator

5.3.6   Receiver and Transmitter Selection

The receiver selected for *Buzzooka* is the FrSky TPR6, as it provides the required failsafe mechanism with minimum weight.

5.3.7   Propulsion System

A 6S1P-Elite 1500 mAh NiMH battery pack was selected to minimize weight while maintaining enough voltage to achieve mission requirements. A variety of motors and propellers were analyzed using the MotoCalc program, as described in Section 4.2.2. Two were selected for further testing, as described in Section 8.2. The Scorpion SII-2212-1850KV motor was chosen for its weight, size and static thrust. The

Aeronaut 9x6 propeller was chosen for its desired ratio between thrust required for cruise speed and thrust required for takeoff. The final selected propulsion system consists of a Scorpion SII-2212-1850KV motor, 6S1P-Elite 1500 mAH NiMH battery pack, a Phoenix 25 speed controller with the Aeronaut 9x6 propeller.

5.3.8 Servo Selection and Integration

The HiTec HS35HD was selected as the tail servos. These servos were selected by analyzing hinge-moments for each control surface using AVL and then finding servos that had sufficient control power to handle the calculated moments, with the lightest weight possible. The selected components are tabulated in Table 5.3 below.

Table 5.3: Selected components.

Components	Description
Motor	Scorpion SII-2212-1850KV
Battery	6S1P ELITE 1500
Speed Controller	Phoenix 25
Receiver	FrSky TPR6
Transmitter	Futaba T8FG
Tail Servos	HiTec HS35HD

5.4 Weight and Balances

An important aspect of stability is correct center of gravity (C.G.) location. To estimate the C.G., a simple calculator was created that consisted of a list of all components, their weights, and their locations along the x-axis and z-axis. Component weights were first estimated using the CAD model and then confirmed with the physical vehicle. The predicted C.G. locations from the CAD of the aircraft are shown in Figure 5.7, below.
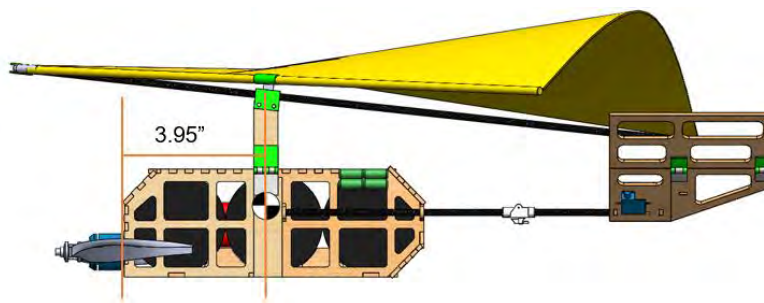

Figure 5.7: CAD predicated CG location

Table 5.4, below, shows the weights and balances of *Buzzooka*. The x-axis was measured positive aft of the nose of the aircraft and the z-axis was measured positive above the chord-line of the wing. The aircraft X-C.G. location shifts less than 0.2 inches between when it is not loaded and fully loaded and is within the mast region of the aircraft. Therefore, the aircraft is within the safe limits for flight.

Table 5.4: Weights and balances chart - Aircraft

Empty Weight					
Component	Weight (lb)	C.G. loc.(in, x-axis)	Moment (in-lbs, y-axis)	C.G. loc. (in, z-axis)	Moment (in-lbs, x-axis)
Fuselage	*0.06*	*1.00*	*0.06*	*0.00*	*0.00*
Empennage	0.03	17.34	0.52	0.00	0.00
Speed Controller	*0.05*	*6.82*	*0.34*	*0.67*	*0.03*
Receiver	0.04	2.70	0.11	0.67	0.03
Propeller	*0.03*	*-1.68*	*-0.05*	*0.67*	*0.02*
Wing	0.10	4.38	0.44	0.67	0.07
Carbon Fiber Tubes	*0.01*	*9.54*	*0.10*	*0.00*	*0.00*
Tail Servo 1	0.01	16.76	0.17	0.30	0.00
Tail Servo 2	*0.01*	*16.76*	*0.17*	*0.30*	*0.00*
Motor	0.15	-0.95	-0.14	0.00	0.00
Fabric	*0.02*	*4.38*	*0.09*	*0.67*	*0.01*
Mast	0.01	4.38	0.04	0.67	0.01
Battery	*0.31*	*2.70*	*0.84*	*-0.67*	*-0.56*
Receiver Battery	0.05	6.31	0.32	0.67	0.03
Aircraft Totals	*0.88*	*3.40*	*2.99*	*-0.40*	*-0.35*
Payload	1.125	4.38	4.93	0.00	0.00
Aircraft Totals	*2.005*	*3.94*	*7.92*	*-0.18*	*-0.35*

5.5   Performance

5.5.1   Flight Performance

The flight performance of the aircraft may be described by the point performance of the vehicle. Key aspects include the velocity envelope, turn performance, and stall speed. Takeoff distance is not considered because the aircraft is hand launched. These parameters are given below in Table 5.5.

Table 5.5: System flight performance parameters for each mission

Parameter	Mission 1	Mission 2 & 3
Weight (lbs)	0.88	2.005
W/S (psf)	0.436	0.993
V_{stall} (ft/sec)	20.62	29.16
V_{max} (ft/sec)	49.50	49.31
Turn Load Factor	2.0	2.0
Turn Radius (ft)	120.94	188.97
Time for 360 (s)	8.41	17.15

Weight represents the gross take-off weights for all of the missions. Both wing loading and stall speed are calculated at 1g assuming steady level flight while using an estimation of C_{Lmax} obtained via wind tunnel load cell experiments. Load factor for each mission is the maximum allowable based on the results from the V-n diagram. In all cases, the load factor is intended to represent a maximum design value of 2g's. Flight-test data indicates that in-flight loads will be lower. The turn radius and time to complete a 360-degree turn were calculated for each mission using the mission's expected maximum velocity and allowable load factor. The maximum velocity of the aircraft occurs at the point when the thrust required is equal to the thrust available. Thrust required is calculated using Equation 5.3, below, where $C_{D,0}$ and e are calculated in Section 4.4.

$$T_R = \frac{1}{2}\rho V^2 S C_{D,0} + \frac{2W}{\rho V^2 S \pi ARe}$$

(5.3)

Thrust available as a function of velocity was computed using MotoCalc for both propellers considered and plotted in Figure 5.8, below, along with the thrust required curves in steady-level flight.
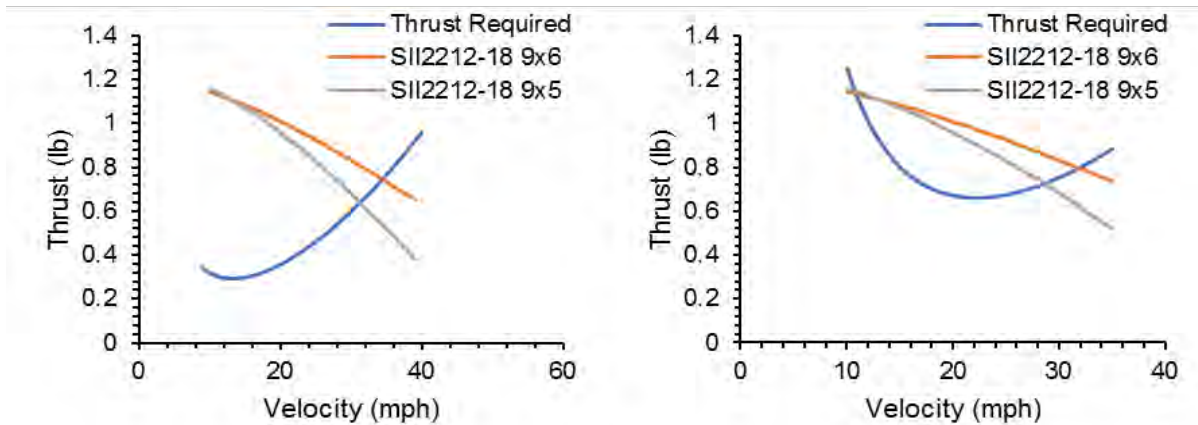
Figure 5.8: Thrust available and thrust required versus velocity

5.5.2   Mission Performance

The mission model described in Section 4.3 was used to estimate the final mission performance of the aircraft. The computed lap times represent an estimate that combines aerodynamic analysis, power and current characteristics from MotoCalc, and the physics of the mission model as described in Section 4.3. Figure 5.9, below, displays the projected first lap trajectories for Missions 1, 2 and 3, with an initial ramp-up following takeoff and dips in velocity occurring at the turns. The remaining laps for Missions 1 and 3 are faster because they do not include takeoff.
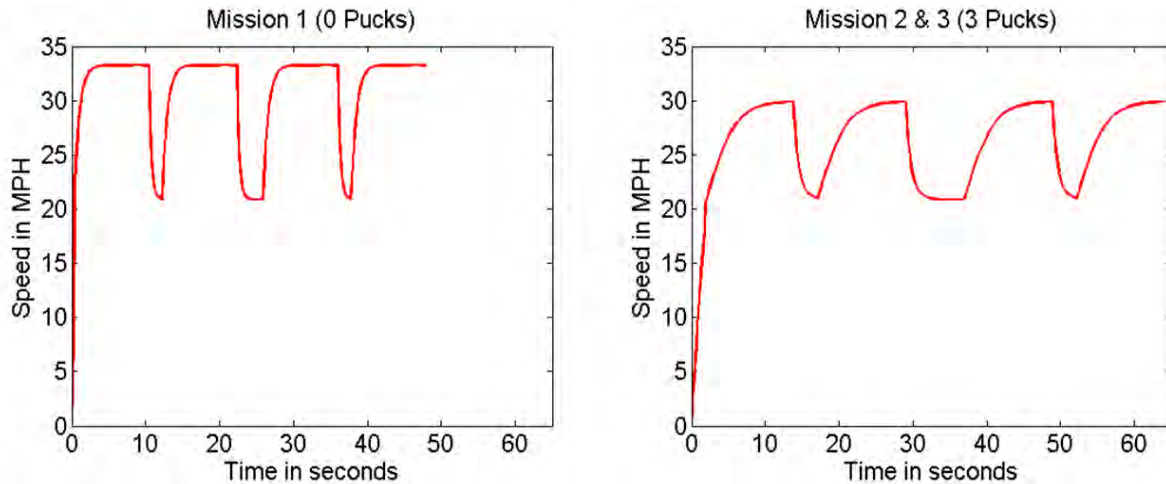
Figure 5.9: Simulation of lap trajectories for all missions

Table 5.6, below, shows the resulting estimated performance for each of the three missions with the selected propellers. The table also includes scoring estimates based on the updated analysis. Because Missions 2 and 3 are scaled to the minimum time and maximum puck number respectively, it is not possible to determine the upper bound possible for mission scoring.

Table 5.6: Aircraft mission performance parameters

Mission Parameter	Mission 1	Mission 2	Mission 3
W/S (psf)	0.4366	0.993	0.993
Propeller Selection	9x6	9x6	9x6
Max Current (Amp)	19	19	19
Static Thrust (lbs)	1.28	1.28	1.28
1st Lap Time (sec)	49.71	65.73	65.73
Mission Performance	3 laps in 5 minutes	3 laps in 5 minutes	3 laps in 5 minutes
Mission Score	1.0	1.0	3.2
RAC	26.53	26.53	26.53

5.6   Final Design – Carrying tube

The carrying tube is designed to safely and securely contain the aircraft while protecting it from a drop of 1 foot in any direction. The outer skin of the tube is made from fiberglass. Circular foam inserts are used to hold the aircraft from moving transversely while a circular plywood base and a plywood structure is used to hold the motor in place so the aircraft does not move longitudinally in the tube. The tube's overall length is 18.6 inches and the overall diameter is 4.25 inches with a total weight of 0.28 lbs, which includes all structure and internal support for the aircraft. This fits the requirement that the tube's length is at least 4 times the outer diameter. Figure 5.10, below, shows an exploded view of the carrying tube displaying the foam inserts, motor mount and cap.
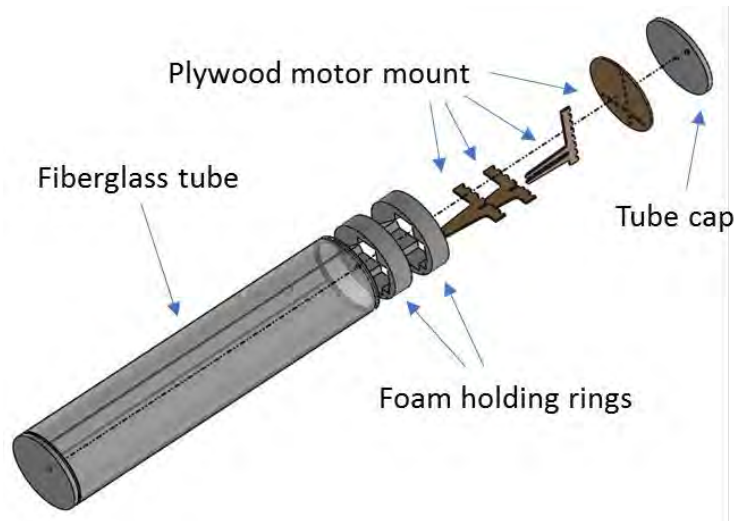
Figure 5.10: Exploded view of the carrying tube

Figure 5.11, below, shows the aircraft secured in the carrying tube (left) and the aircraft being extracted from the tube (right). Note the plywood structure used the secure the motor.
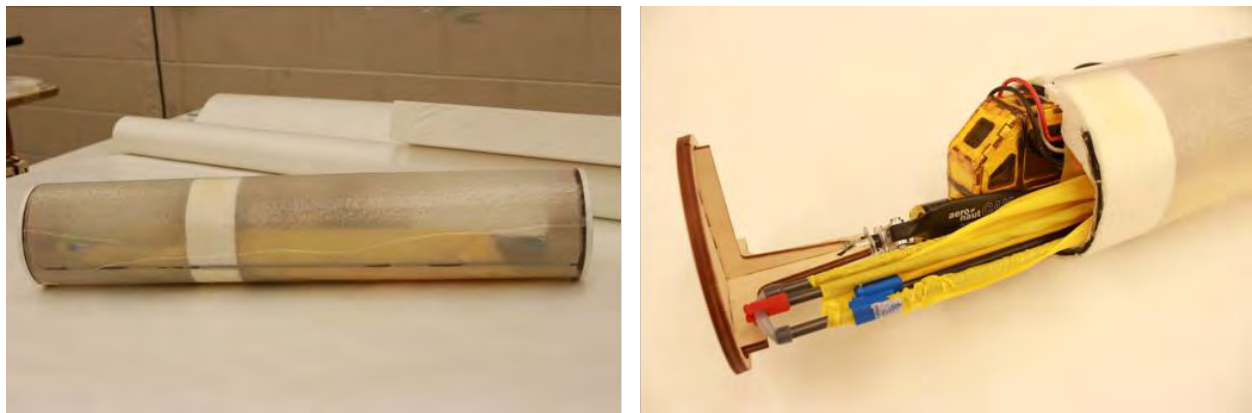

Figure 5.11: Aircraft secured in tube (left) and Aircraft being extracted from tube (right)

5.7   Drawing Package

The following four pages illustrate the detailed CAD of *Buzzooka* system. The first sheet contains the three-view diagram with relevant dimensions. The second and third sheets show the structural arrangement of all major components and the systems layout. The fourth sheet displays the payload arrangements for both aircraft.

26.13

27.18

ISO SCALE: 1:4

5.75

DRAWN Yusuf Ogun Kargin	**Georgia Institute of Technology**		
CHECKED George P. Burdell	**Buzzooka**		
2/19/2017	SIZE **B**	DWG	Aircraft Three View Drawing With Dimensions
SCALE 1:5			All Dimensions in Inches

SHEET 1 OF 4

PARTS LIST

Item	Qty.	Item Name	Description
1	1	Fuselage	Balsa
2	1	Nose Connector	ABS and Silicon
3	4	Wing Rods	Carbon Fiber
4	1	Wing Swivel	ABS
5	2	Wing Side Slide	ABS
6	2	Tail Surfaces	Balsa
7	4	Control Surface Extension Hinge	ABS
8	1	Empennage Lock	ABS
9	1	Tail Boom	ABS
10	1	Mast	Plywood
11	1	Mast Hinge	ABS
12	1	Wing Fabric	Rip Stop Nylon

Wing fabric has been removed for better structural view.

SCALE: 1:5

SOLIDWORKS Educational Product. For Instructional Use Only

DRAWN
Yusuf Ogun Kargin

CHECKED
George P. Burdell

2/19/2017

Georgia Institute of Technology

Buzzooka

SIZE **B** DWG

Structural Arrangement Drawing

SCALE 1:2

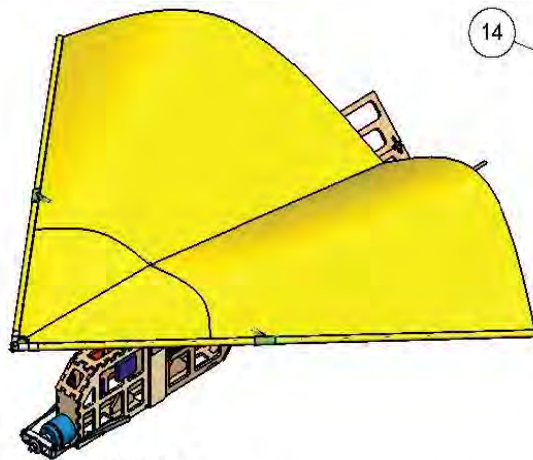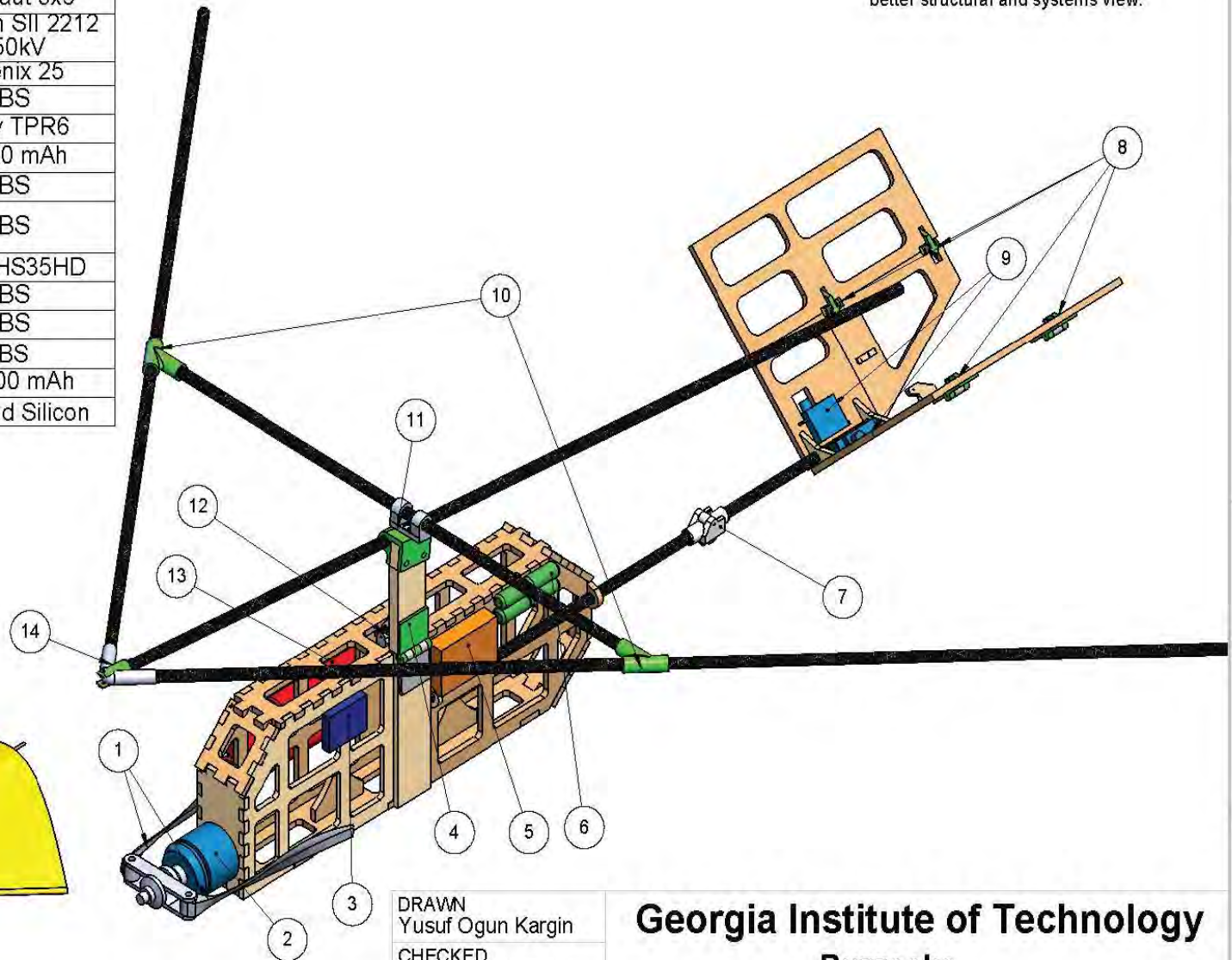All Dimensions in Inches

SHEET 2 OF 4

SYSTEMS LIST

Item	Qty.	Item Name	Description
1	1	Propeller	Aeronaut 9x6
2	1	Motor	Scorpion SII 2212 1850kV
3	1	Speed Controller	Phoenix 25
4	1	Mast Hinge	ABS
5	1	Receiver	FrSky TPR6
6	1	Receiver Battery Pack	4s 400 mAh
7	1	Empennage Fold Hinge	ABS
8	4	Control Surface Extension Hinge	ABS
9	2	Tail Servo	HiTec HS35HD
10	1	Wing Side Slide	ABS
11	1	Wing Swivel	ABS
12	1	Mast Lock	ABS
13	1	Main Battery Pack	6s 1500 mAh
14	1	Nose Connector	ABS and Silicon

Wing fabric has been removed for better structural and systems view.

SCALE: 1:5

SOLIDWORKS Educational Product. For Instructional Use Only

DRAWN Yusuf Ogun Kargin	**Georgia Institute of Technology**
CHECKED George P. Burdell	**Buzzooka**
2/19/2017	SIZE **B** DWG

	Systems Layout Drawing
SCALE 1:2	All Dimensions in Inches

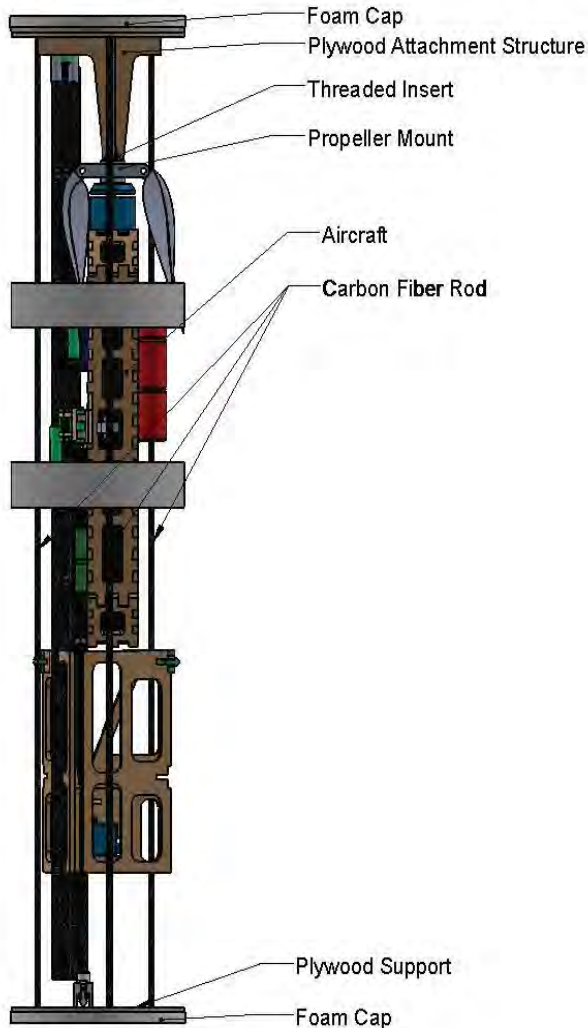SHEET 3 OF 4

Exploded view shows how the folded aircraft fits into the tube.

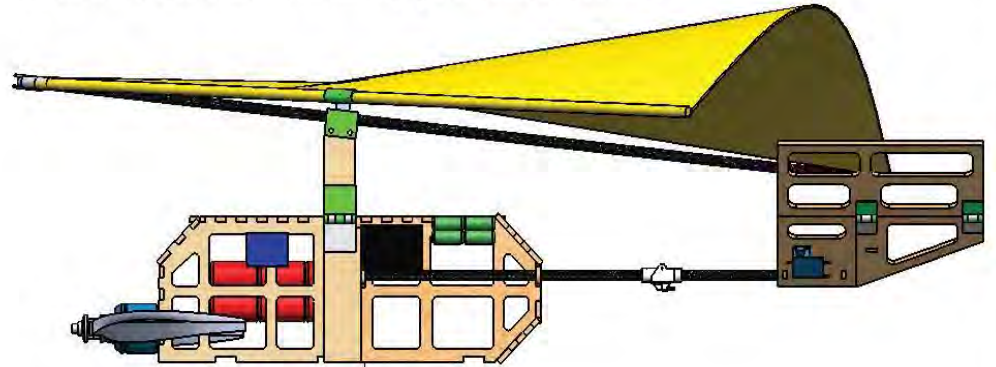Exploded view shows how the maximum payload fits inside the aircraft.

Foam Cap
Plywood Attachment Structure
Threaded Insert
Propeller Mount
Aircraft
Carbon Fiber Rod

Plywood Support
Foam Cap
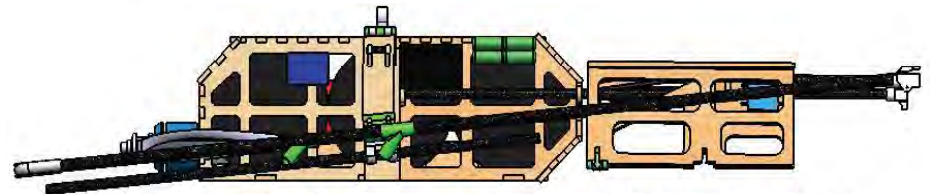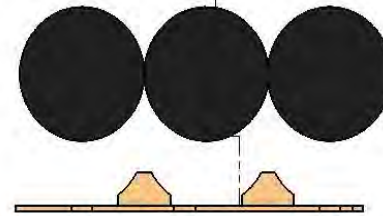
Fully loaded and folded aircraft configuration, ready to be loaded into the tube.

SCALE: 1:6

Fiberglass Cover is hidden for better structural view.

SOLIDWORKS Educational Product. For Instructional Use Only

DRAWN Yusuf Ogun Kargin	**Georgia Institute of Technology**		
CHECKED George P. Burdell	**Buzzooka**		
2/19/2017	SIZE **B**	DWG	Payload Accomodation Drawing
	SCALE 1:3		All Dimensions in Inches	SHEET 4 OF 4

6   MANUFACTURING

The team considered various manufacturing processes and materials to design the aircraft and carrying tube. The manufacturing process selected represented the best combination of weight, reparability, ease of manufacturing, team experience with the process, and cost.

6.1.1   Processes Investigated

The team had a wealth of experience using the built-up balsa wood manufacturing technique. However, there were other viable manufacturing processes that could be superior. These processes were considered and qualitatively compared to the built-up balsa technique using Figures of Merit, detailed below and summarized in Table 6.1, below. Figures of Merit descriptions can be found in Section 3.4.

Weight: As with conceptual design, weight is still the most important factor for any design decision, and is assigned a FOM of 5.

Reparability: With ever-present unknown factors, the reparability of the aircraft and the tube in case of an accident or a crash has to be accounted for, and was assigned a FOM of 2.

Ease of Manufacture: The ability to produce the aircraft to specification is critical to meet expected performance, and is directly related to Ease of Manufacture. It was therefore assigned a FOM of 3.

Experience: The team's knowledge was given some weighting because it relates to the ability of team members to produce quality results, as well as to refine existing techniques. However, since the team is always willing to learn new techniques, experience was only assigned a FOM of 2.

Cost: Keeping in mind that the team had limited resources, cost was inevitably added as a FOM. However, since the team emphasizes winning above all, cost was assigned a FOM of 1.

Table 6.1: Manufacturing FOM Weighting

Figure of Merit	0	1	2	3	4	5
Weight						5
Ease of Manufacture				3		
Reparability			2			
Experience			2			
Cost		1				

These Figures of Merit were used to investigate the manufacturing processes and materials common to remote control aircraft construction. The processes to manufacture the fuselage of the aircraft were investigated in detail below.

Built-up Balsa: Pieces made of competition grade balsa wood are laser cut from CAD models and glued together using cyanoacrylate (CA) adhesive to form the fuselage and the tail surfaces of the aircraft. This process can also be used for lid and aircraft attachment structures for the tube. Additional balsa is then used for additional reinforcement in key areas. The aircraft components are then coated with Ultracote heat shrink film.

Fiber Reinforced Plastic (FRP): Foam molds are created based on the outer-mold line of the aircraft. A fiberglass-epoxy layup or carbon fiber-epoxy layup is then made within a vacuum bag, and the system sealed for 24 hours to allow for a full cure. The molds are then removed and the reinforced plastic acts as the primary structure.

3D Printed ABS: CAD models are printed using professional grade 3D printers. Print time increases proportionally with the volume of the aircraft. Complex joints and connectors are integrated directly into the main aircraft structure, allowing for a maximally efficient design.

Nylon Carbon-Fiber: Rip stop nylon is a common fabric used in lightweight aerospace applications that has the unique property of being able to be precisely cut with the laser cutter. The fabric is purchased in bulk and cut to the desired shape using a laser cutter. This is then stitched together around a minimal structure of carbon fiber tubes lashed together with nylon and fused with epoxy.

The processes were evaluated against each other by assigning each one a FOM score, with a score of five indicating a superior choice, three an average choice, and one equaling an inferior choice. All methods were assumed to result in an aircraft designed for an identical load. The results of the comparison are summarized in Table 6.2, below.

Table 6.2: Example fuselage manufacturing process selection

FOM	Value	Manufacturing Process			
		Built-up Balsa	Fiberglass	3D Printing	Nylon Fabric
Weight	5	5	4	5	5
Ease of Manufacture	3	3	2	4	2
Reparability	2	3	4	1	4
Experience	2	5	2	4	1
Cost	1	5	3	2	5
Total	13	55	41	49	46

Based on the Figures of Merit, built-up balsa was considered the best method for the major fuselage and empennage structure. However, due to the nonconventional nature of the configuration, the team determined that different elements of the design could use different manufacturing processes to create a more harmonious whole. These findings are detailed in Section 6.1.2.

6.1.2   Processes Selected

The team used the above comparison to optimize the built-up balsa technique to achieve the most competitive aircraft by having the lightest structure possible in accordance with competition rules without sacrificing structural integrity. The team saw potential in using other investigated manufacturing processes for specific uses. These optimized techniques are detailed in Table 6.3, below:

Table 6.3: Manufacturing techniques utilized

Manufacturing Component	Material or Technique
Principal fuselage material	Competition grade balsa wood
Principal wing material	Nylon fabric, Carbon fiber structure
Other materials	Local fiber reinforcements, ABS
Adhesive	Cyanoacrylate
Coating	Ultracote
Part manufacture	CAD laser cutting and 3D Printing
Part assembly	Designed-to-fit jigsaw pieces

Of the many different ways to apply built-up balsa, the team chose specific techniques and materials that would minimize the aircraft structure's weight without compromising its strength. These strategies are as follows.

Selective Material Use: Since balsa wood can vary significantly in density and strength, the team sorted its entire stock of balsa by weight. The lightest pieces were selected for construction and were cut using the team's laser cutter, with the lightest of the cut parts reserved for the final competition aircraft.

Local Reinforcements: Due to the very low density of balsa used, several inherently problematic locations could potentially fracture during normal operations. Rather than compensate by over-building the entire aircraft, these locations were reinforced with composite or additional balsa, increasing strength with minimal penalty in weight.

Lightening Holes: An efficient structural design eliminated significant loading from most structural members. Lightening holes were integrated into the fuselage and control surfaces to reduce weight without reducing the overall stiffness and strength of the aircraft.

Covering: Most balsa aircraft are coated with a heat shrink adhesive infused plastic covering material called Monokote, which is durable and easy to handle. However, the team chose to use a more delicate plastic covering, Ultracote, because it is significantly lighter.

In addition to Built-up Balsa, the team determined that the Rogallo Wing and all folding mechanisms would benefit substantially from the other three processes investigated in Section 6.1.1.

Hinges: High-accuracy 3D printers such as Stratasys Fortus 250mc and U-Print SE FDM were used to create hinges to fit the aircraft into the smallest diameter tube. 3D printing allowed all parts to have specific tolerances for exact fits.

Nylon Carbon-fiber: Rip stop nylon was chosen as the primary material of the wing. The need for a flexible material that can inflate during flight drove this choice, and carbon fiber spars to resist flight loads presented the best combination of strength for weight.

FRP: Fiberglass and carbon fiber reinforcements were found to be useful for the motor mount and certain hinges. A carbon fiber tube was selected as the primary tail boom structure for both its high strength to weight ratio and its relative durability compared to built-up balsa. This was important for a region of the aircraft judged to be the subject of frequent impact loads during landing.

6.1.3 Manufacturing Milestones

A milestone chart was established at the beginning of aircraft manufacturing to ensure a logical, consistent order was followed during construction. Progress was recorded and monitored by the team leader to ensure all major milestones were met. The milestone chart is shown in Figure 6.1, below, capturing the planned and actual timing of major events.
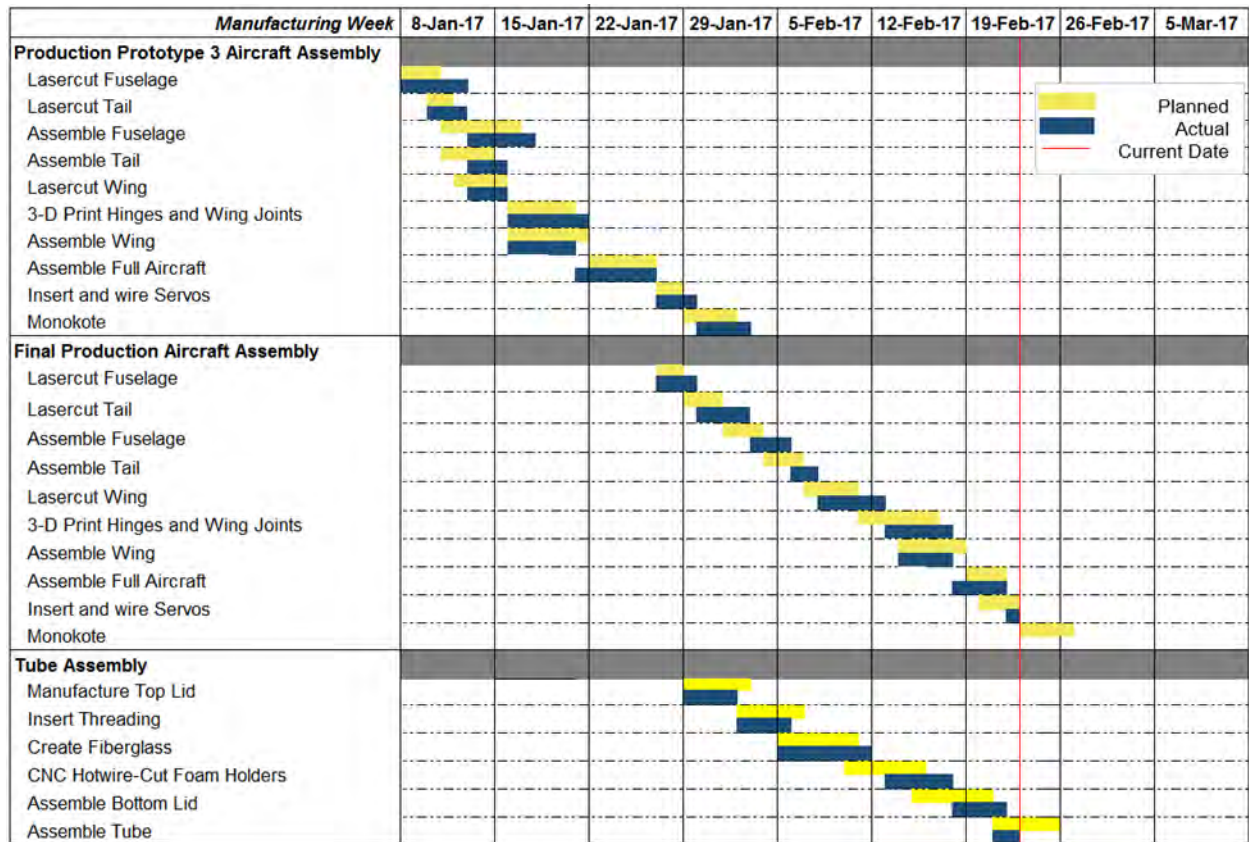
Figure 6.1: Aircraft manufacturing milestone chart showing planned and actual timing of objectives

7   TESTING PLAN

A plan for an extensive testing campaign to validate the aircraft, and its components, was created to determine what configurations and subsystems would be the most capable. Testing culminates in test flying a full round of competition flights on the final competition airframe.

7.1   Objectives and Schedules

The testing was broken up into three main categories: propulsion, structures, and performance. The propulsion and structures subsystems were tested before flying the whole aircraft to gain knowledge and set realistic and useful objectives at each test flight. A breakdown of the testing schedule is displayed in the following Gantt chart, shown in Figure 7.1, below:

Design Month	Sep-16	Oct-16	Nov-16	Dec-16	Jan-17	Feb-17	Mar-17	Apr-17
Subsystem Testing								
Battery Testing	██							
Aircraft Motor/Propeller Testing		██						
Wing Wind Tunnel Testing			██					
Aircraft Structural Testing				██				
Prototype Aircraft Assembly								
Proof of Concept				██				
Mission 3 Performance Empty					██			
Mission 3 Performance w/ Payload						██		
Landing & Takeoff Stability						██		
Final Aircraft Flight Testing								
Competition Mission 1 Performance							██	
Competition Mission 2 Performance							██	
Competition Mission 3 Performance								██

Legend: Planned, Actual, Current Date

Figure 7.1: Aircraft and subsystem testing milestone chart with planned and actual timing of objectives.

The objectives for the propulsion testing were to determine which motors would work best for the aircraft. The motors and propellers tested were based on MotoCalc predictions as expressed in Section 8.1.1. Thrust versus velocity for vehicle performance and power draw for motor performance for each motor propeller combination were determined using measurements of thrust, torque, RPM, voltage, and current draw. Using data obtained from testing, the team was able to compare the actual performance of the motors to the MotoCalc predictions in order to gather a better estimate of actual performance. This information allowed the team to select the best propulsion system to achieve the best score possible.

A rig that included load cells to calculate thrust and torque as well as an electric motor measurement system was constructed for the wind tunnel testing, and is shown in Figure 7.2, below. The team used the rig to perform static thrust tests and used the data to compare it with MotoCalc predictions. The electric motor parameters were monitored with an EagleTree system that records the RPM, voltage, and current draw of the motor. Custom written software was used to collect the torque and thrust values as well as to remotely control the motor for 30-second intervals with 10-second full thrust intervals and 10-second acceleration and deceleration intervals.
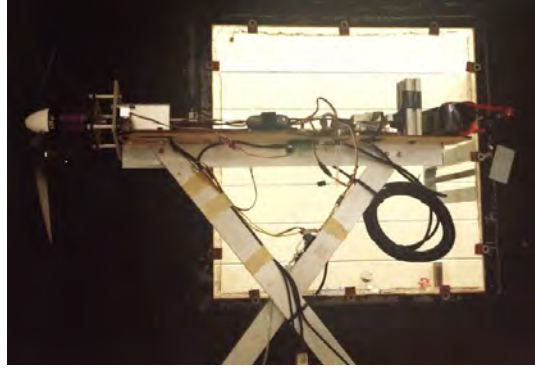
Figure 7.2: Thrust test rig in the wind tunnel

The team used the Georgia Tech Low Turbulence Wind Tunnel to conduct its wind tunnel tests. The wind tunnel is powered by a fan which forces air through a series of honeycombed grates creating a smooth, even flow of air. The fan creates airflow with a maximum airspeed of about 52 feet per second. The wind tunnel creates an environment closely resembling actual flight conditions and thus providing accurate motor and propeller efficiencies. The results of the static thrust tests are described in Section 8.1.1.

7.2   Wing Wind Tunnel Testing

When conducting the early aerodynamic analysis of *Buzzooka*'s fabric Rogallo wing, a combination of VORSTAB and NASA wind tunnel tests were initially used to approximate the lift slope curve and derive the maximum lift coefficient. However, due to the small scale of *Buzzooka* in comparison to these sources, a full-scale wind tunnel test was conducted on the wing to measure the lift produced and verify the lift curve trends with the VORSTAB and NASA results. These tests were conducted in the Georgia Tech Low Turbulence Wind Tunnel, with the experimental set up shown in Figure 7.3, below.
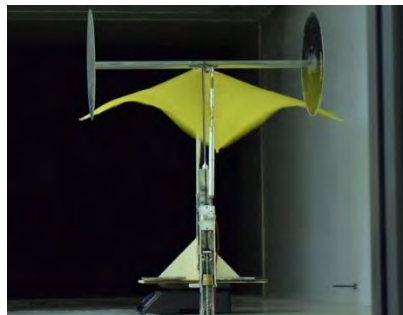
Figure 7.3: Full-scale Rogallo wing wind tunnel test

The test was conducted with full scale wing geometry at the expected flight speed of 30 mph and similar atmospheric conditions at full scale testing (Re: 425,100), removing the need to Reynolds match the testing model. Because the size of the tunnel test section (4ft. by 4ft.) was nearly twice the Rogallo wingspan, a full-scale test without concern for wall-effect pressure changes was justified. In the testing rig, the wing was mounted directly to a load cell sending raw voltage readings to a computer for each of the seven angles of attack that were measured.

7.3 Tube Fit Testing

Tube fit tests were conducted with every major aircraft revision to ensure physical interferences did not occur. This type of testing occurred with every revision and is implicit within each scheduled iteration.

7.4 Structural Testing

Wingtip tests were conducted to validate the structural integrity of the design. A wingtip test simulates the maximum loading the wings would experience in flight by loading the payload bay with the maximum weight and lifting the plane by the wing tip, which simulates a root bending moment of 2.5g. Figure 8.3 shows the test setup used to validate the wingtip test. Two sets of blocks were used to support the wing, which was taped to the edge of the blocks at the wingtips. Since the wing planform resembles that of a delta wing, the wingtip itself is not the location where the center of gravity resides. Therefore, the plane tips forward if no countering moment is applied at the back to balance the plane.

In addition, the aircraft was drop tested in accordance with the regulations from a height of 12 inches. This was done to simulate the test that will be a part of the preliminary validation in the competition to locate weak-points in the structure.

7.5 Flight Testing

Flight testing was conducted across two iterations, with a third planned as the final competition design. Initial iterations were used to determine the flying qualities of the aircraft designs. Verification of structural layouts and load estimates were also conducted. Missions were simulated and the necessary design modifications tabulated.

The second iterations are currently being used as testing platforms. Changes were made to the design based on pilot and manufacturing feedback. This included adding lateral landing gear supports to prevent tip-over during harsh landings, wing sizing modifications to increase roll stability, and stronger wing attachments to resist high speed gusts encountered during testing.

Currently, the second iteration of *Buzzooka* is being used to verify the required battery size to complete M3. Experience and data gained from all iterations of airframes will be used to improve the designs for a third iteration of a final airframe that will go to competition. The third iteration will fly simulations of its respective flight missions for proofing. The schedule and flight order is displayed in Table 7.1, below.

Table 7.1: Flight test goals and order

Flight Test	Aircraft	Goal
1	First Iteration	Maiden flight
2	First Iteration	Mission runs
3	Second Iteration	Maiden flight
4	Second Iteration	Mission runs
5	Second Iteration	Performance optimization
6	Final Iteration	Maiden flight
7	Final Iteration	Mission runs

7.6 Checklists

Various tests have specific procedures which must be followed accurately to produce the desired objectives and ensure safety. This section lists the checklists utilized by *Buzzooka* while conducting tests that required a significant number of steps, such as propulsion and flight testing.

7.6.1   Propulsion Test Checklist

The checklist in Table 7.2, below, was created to ensure safety while dealing with propellers and electrical equipment, and to make sure the test is not wasted due to some mistake in preparation. This checklist was used in the testing of all motor, battery and propeller combinations.

Table 7.2: Propulsion testing checklist

Propulsion Test Checklist					
1. Propeller secured?	☐	2. Motor mount secured?	☐	3. All plugs secured?	☐
4. Batteries peaked?	☐	5. Throttle down?	☐	6. Data system on?	☐
7. Custom code running?	☐	8. All clear of testing rig?	☐	9. Wind tunnel closed?	☐

7.6.2   Flight Test Checklist

The checklist in Table 7.3, below, was created with the important goal of preventing any system from malfunctioning in mid-air, which could lead to the aircraft crashing; its thorough execution is paramount to the team's success, and it will be used at the DBF event as well.

Table 7.3: Pre-flight checklist

General System Checks							
Structural Integrity		Center of Gravity Location				Time	Date
	X			Y			

Payload					
Laterally Secure?		Connections Secure?	Battery Pack	Receiver Pack	Payload Secure?
Attachment secure?			Pins locked?		Clear of Jams?	

Control Surfaces								
Ailerons			Rudder			Elevator		
Deflects?	Glued?	Slop?	Deflects?	Glued?	Slop?	Deflects?	Glued?	Slop?

Electronics and Propulsion						
Receiver Battery Charged?	Primary Battery Charged?	Receiver/ Transmitter Go?	Wires secure?	Battery hot?	Prop secure?	Prop direction?

Weather					
V_{wind}		Θ_{wind}		Temperature	

Initials for Approval					
Chief Engineer		Pilot		Advisor	

8 PERFORMANCE RESULTS

8.1 Component and Subsystem Performance

8.1.1 Propulsion

<u>Batteries</u>: A 6-cell, 1500 mAh NiMH battery pack was discharged at 5 amps (3.3 times its capacity) and at 15 amps (10 times its capacity) to characterize the discharge capabilities of the NiMH batteries. The resulting data is shown in Figure 8.1 on a per cell basis. NiMH battery cells have a nominal voltage of 1.2V, and the 5-amp discharge curve is capable of maintaining this voltage. At 15 amps, the cell voltage continuously drops, resulting in a small decrease in the available effective power. The higher current draw of the 15-amp discharge is necessary to achieve the power required for the aircraft.
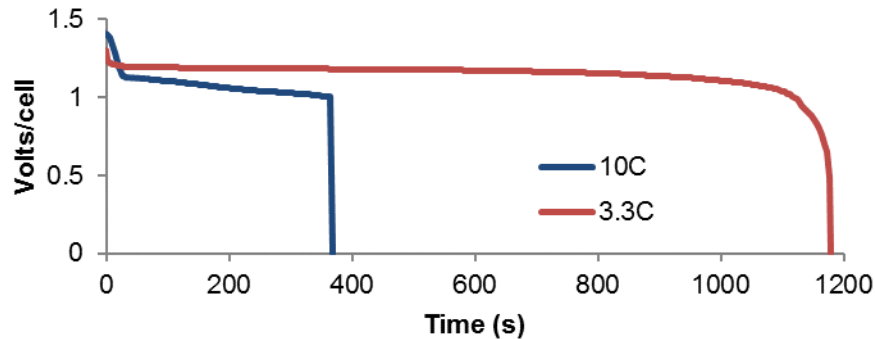
Figure 8.1: Battery discharge rates

<u>Motors and Propellers</u>**:** Using MotoCalc software, several motor and propeller combinations were theoretically computed. The Scorpion SII-2212-18 and Scorpion SII-2213-12 motors provided the best combination of thrust and performance at different aircraft velocities, as well as a realistic current draw to reduce the size of the battery pack. The team tested the motors and propellers using the test stand shown in Section 7.1 in static conditions. Figure 8.2, below, shows the difference between the actual results and the theoretical results posed by the MotoCalc program for the best two propellers tested with regards to their thrust. Though the SII-2213-12 motor provided higher thrust, it was heavier compared to the SII-2212-18 and the current draw was deemed too high and would require a heavier propulsion system overall. Both the 9x5 and 9x6 propellers were tested in flight. The 9x6 propeller was chosen because it had better performance at higher velocities and was adequate for the hand launch of the aircraft.
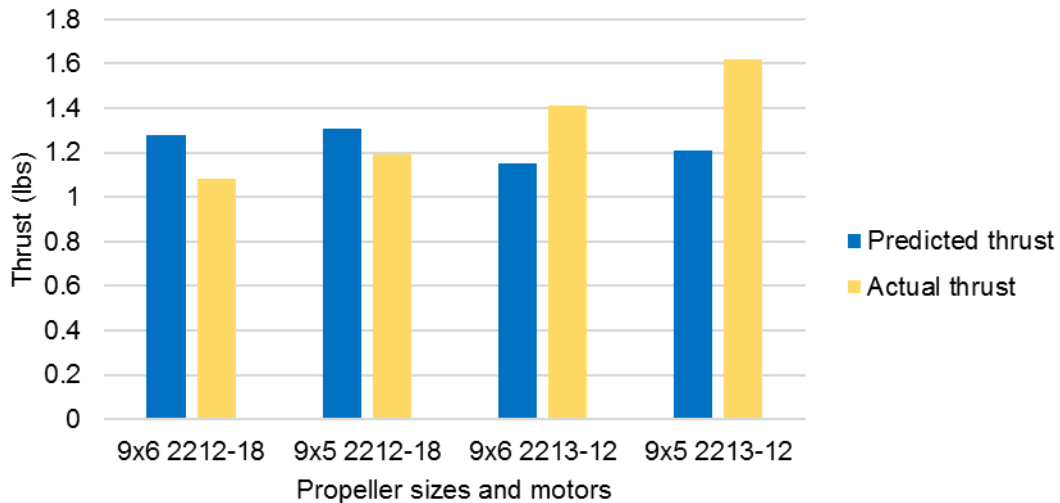
Figure 8.2: Difference between predicted and actual thrust for different propellers

8.1.2   Structural Tests

<u>Wing Testing Results:</u> The full-size airplane was subjected to the required wing tip testing specified in the rules as part of the technical inspection process. This was done by loading the full internal Mission 2 payload of three hockey pucks into the payload bay, then lifting the airplane by the wing tips. Figure 8.3, below, shows the successful wingtip test.
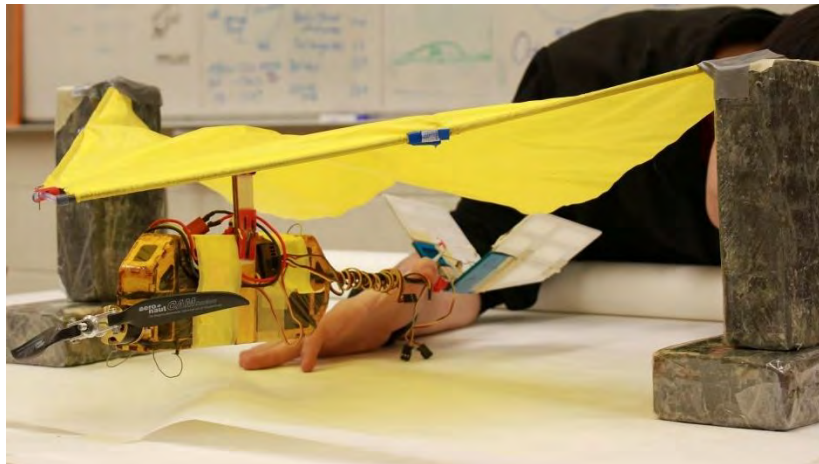
Figure 8.3: Wingtip test using two blocks to support the wing

<u>Carrying tube drop test</u>: The airplane in its folded configuration was placed inside the carrying tube and dropped in accordance to the regulations outlined in the competition rules. The tube was dropped from a height of 12 inches from both ends as well as several drops from the side at different rotations. The aircraft survived all the impacts per the requirements and proved flyable after the impact tests. An example of the drop tests performed can be seen in Figure 8.4.
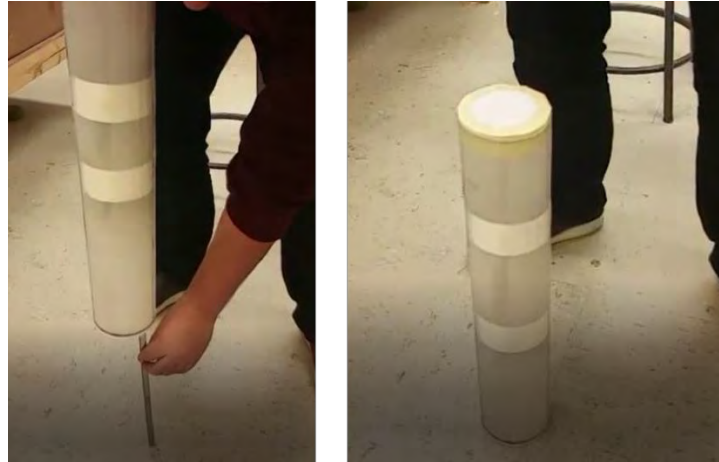
Figure 8.4: Setting up a drop from 12 inches (left) and after impact (right)

8.2   System Performance

Flight tests of *Buzzooka* were performed to evaluate the performance of the aircraft and validate the performance predictions. The first requirement for flight is that the aircraft must be hand launched. Figure 8.5, below, shows the aircraft successfully being hand launched.

Figure 8.5: Aircraft being hand launched

To evaluate system performance during flight testing beyond simple lap timing, the team equipped the aircraft with a data collection system that could be used to compare to the estimated mission performance in Section 4.6. The team purpose-built an Arduino-based telemetry system with a live data feed. On a number of test flights, the Arduino was mounted to the aircraft and recorded GPS at 1 Hz to yield trajectory data. An example of a full lap trajectory is displayed in Figure 8.6 superimposed on satellite imagery using Google Earth.

Figure 8.6: Trajectory of aircraft during competition laps from GPS data

The results of flight testing are shown in Table 8.1, below. They indicate the performance predictions were optimistic. Further optimization and increasing pilot familiarity with the system should improve system performance to meet or exceed the predicted performance.

Table 8.1: Comparison of predicted and actual performance averages

	1st Lap Time (s)		Time for 360 (s)		Laps Flown		Max. Speed (mph)	
	Pred.	Act.	Pred.	Act.	Pred.	Act.	Pred.	Act.
M1	49.7	48.6	8.4	8.5	3	3	33	31
M2/M3	65.7	61.1	15.2	14.1	3	3	30	28
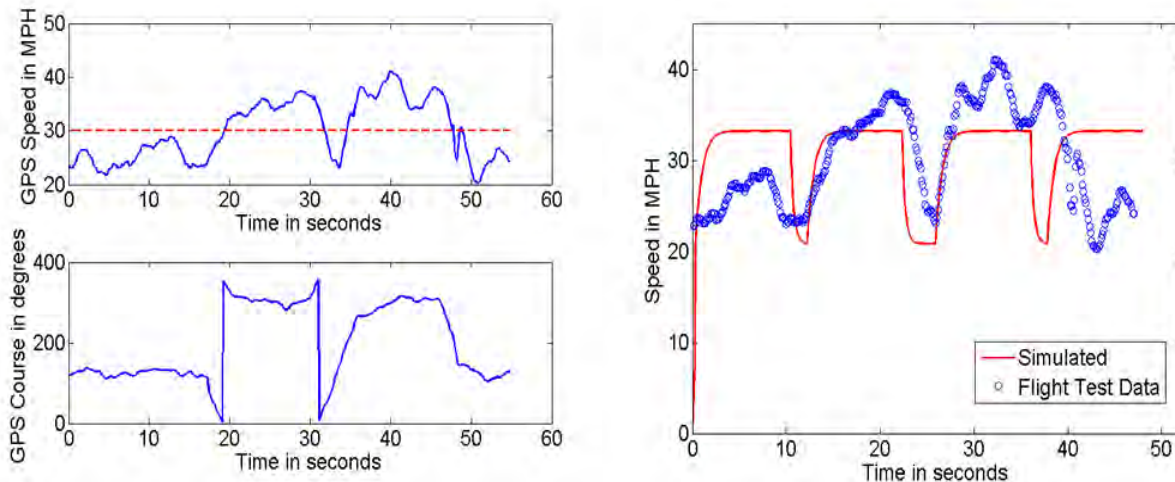
Figure 8.7: Mission 1 aircraft velocity and course from GPS data (left) compared to simulated velocity predictions (right)

The lap times and metrics for M1 and M2/M3 shown in Table 8.1 match very well between the predicted and tested values. However, as shown in Figure 8.7, above, the flight test data does not match perfectly compared to the simulated trajectory. These differences are explained by the uncertainties in the predictions as described in Section 4.3.2. Namely, the mathematical models lack a vertical dimension and any wind

model. When turning, the model assumes the aircraft will drop speed to maintain altitude, an assumption that appears to correspond well with the flight data as shown in Figure 8.7, above, right. The offset for when the turns are initiated can be explained due to pilot variations as the Rogallo attempts to fight the winds as it switches from being in a headwind to a tailwind and vice-versa.

The impact of wind on the test data can be clearly seen in Figure 8.7, above, left, where the aircraft experiences a ~5mph headwind leading into the lap, with an equivalent tailwind after it completes the initial turn. By splitting the difference between the airspeeds in headwind and tailwind, an average airspeed of 31 mph is observed (denoted in red in Figure 8.7, above, left), corresponding well with the predicted maximum airspeed of 33.25 mph. The discrepancy in speeds can be accounted for due to the models assuming an ideal flight path, with the aircraft pushed to their performance limits during turns. In reality, the performance target of 3 laps in 5 minutes does not mandate flying the aircraft at the edge of their performance boundaries.

Predicted and actual times for a 360-degree turn are fairly variable, again due to pilot behavior. In all cases, time for a 360-degree turn was predicted assuming maximum velocity. However, during testing, the pilot tended to reduce speed significantly when going into a turn, which reduced the turn radius. Regardless, the turning performance obtained from the test data exists within the envelope predicted by the simulations, verifying that the aircraft is operating as expected by its design.

In summary, as of the time of this report, there were 28 flight tests of three different prototypes of *Buzzooka*. The research, component selection, and testing that fed into the design process resulted in a lightweight aircraft capable of successfully flying the demonstration flight, speed flight, and range flight as detailed in Missions 1, 2, and 3, respectively. The concept of a single engine, Rogallo wing system carried in a tube proved successful in completing the carrying durability requirements along with the flight missions. The development of this design can be seen below in Figure 8.8.
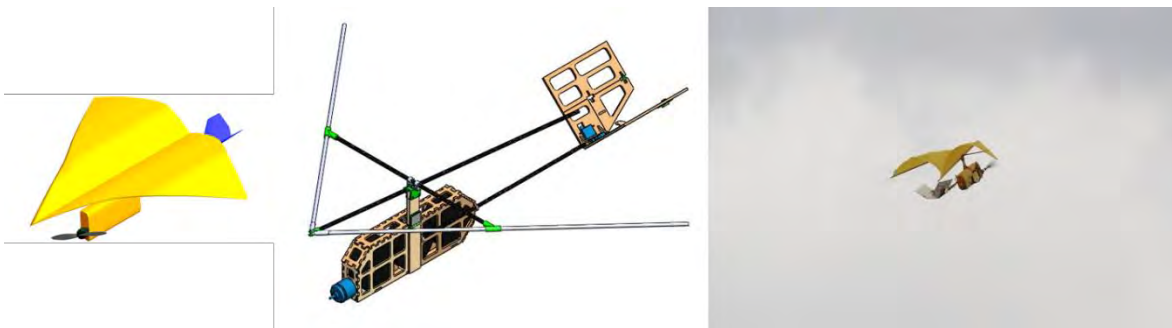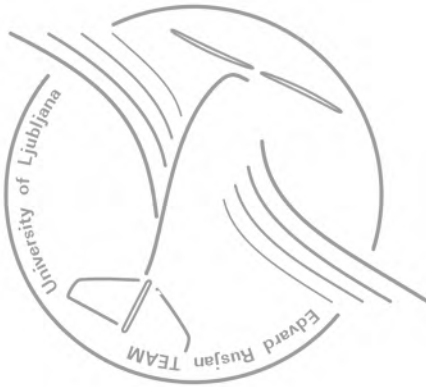

Figure 8.8: Buzzooka, from ideation to reality

9 REFERENCES

Anderson. J. D. *Fundamentals of Aerodynamics,* 4th edition, McGraw Hill.

Bauchau, O. A., & Craig, J. I. (January 7, 2009). *Aerospace Structural Analysis.* Springer.

Drela, M., & Youngren, H. (2008, 08 04). *AVL.* Retrieved 01 10, 2009, from [http://web.mit.edu/drela/Public/web/avl/].

Drela, M., & Youngren, H. (2008, 04 07). *XFOIL.* Retrieved 10 01 2008, from Subsonic Airfoil Development System: [http://web.mit.edu/drela/Public/web/xfoil/].

Hoerner, Sighard F. *Fluid Dynamic Drag*. 2nd. Published by author, 1965.

Johnson, Joseph L. and Hassel, James L. *"Full-Scale Wind-Tunnel Investigation of a Flexible-Wing Manned Test Vehicle." NASA,* Washington D.C., 1963

Katz, Joseph & Maskew, Brian. "Unsteady low-speed aerodynamic model for complete aircraft configurations," *Journal of Aircraft.* Vol. 25, pp. 302-310. Apr. 1988.

Lan, C. Edward. *"VORSTAB – A Computer Program for Calculating Lateral-Directional Stability Derivatives With Vortex Flow Effect," NASA Langley Research Center,* Hampton, Virginia, 1987

McDaniel, Katie et al. (2008). *Georgia Institute of Technology Team Buzzed*. Editor: Johnson, Carl.

Phillips, Warren F. *Mechanics of Flight*. 1st. Hoboken, NJ: Wiley, 2004.

Roskam, Jan. *Airplane Design Part VI*. DARcorp, 2000.

Roskam, Jan. *Airplane Flight Dynamics and Automatic Flight Controls Part I*. DARcorp, 2007.

Selig, M. (2008, 02 19). *UIUC Airfoil Data Site*. Retrieved 10 01, 2008, from [www.ae.uiuc.edu/m-selig/ads.html].

Warchol, Matthew L. "*An Investigation of Flexible Rogallo Type Wing Aerodynamics and the Applications to UAVs," The Ohio State University*, Ohio, 2009

University of Ljubljana

Faculty of Mechanical Engineering

DESIGN – BUILD – FLY COMPETITION

2017

Design report

Contents

Acronyms and nomenclature

CG	-	Center of Gravity	SAS	-	Score Analysis Simulation	A	-	Area
GM	-	Ground Mission	L	-	Lift	R_e	-	Reynolds Number
M1	-	Mission One	D	-	Drag	λ	-	Aspect Ratio
M2	-	Mission Two	FoM	-	Figure of Merit	m	-	Mass
M3	-	Mission Three	n	-	Loading	Ni-MH	-	Nickel-Metal Hydride
TMS	-	Total Mission Score	C_L	-	Lift Coefficient	Ni-Cd	-	Nickel Cadmium
RAC	-	Rated Aircraft Cost	$Cd,0$	-	Zero-Lift Drag Coefficient			
EW	-	Empty Weight	v	-	Velocity			
TW	-	Tube Weight	P	-	Power			

1. Executive summary

This report details the design, testing and manufacturing of Edvard Rusjan Slovenian Team's (EDA) in the 2016-2017 AIAA Design/Build/Fly (DBF) competition. Theme of this year's competition is Tube Launched UAV. The goal is to construct the aircraft which is able to fit inside a tube and is able to carry at least three regulation hockey pucks internally. Competition consists of three flight missions and ground mission all of which must be completed successfully in order to win the competition.

1.1   Design process

The aircraft was designed to achieve the highest possible score in the competition. Intensive studies of parameters showed that RAC has greater effect on final score than flight missions themselves. The team therefore strove to optimize RAC to its minimum while still achieving maximal possible TMS. Design process consisted of three consecutive stages with the first being conceptual design. After brainstorming various ideas, the team decided on high wing monoplane with a pod and boom type fuselage and conventional tail. In the preliminary design stage followed in depth study of aircraft characteristics, e.g., aerofoil, motor, battery cells, etc. After running tests and simulations, the optimal configuration was determined. The last stage of the design process was detail design, where all of previously chosen features were designed for the actual aircraft. Simultaneously several testing procedures were carried out to confirm or assist the designing process.

1.2   Key mission requirements

During conceptual design phase several key mission requirements were recognized. The team realized that next requirements must be met in order to achieve highest score:

Tube dimensions: Final score is highly influenced by tube size. In order for the aircraft to be competitive the tube has to be as small as possible. To achieve small tube dimensions the aircraft must be able to fold into an elongated shape.

Empty weight: Empty weight is a large factor in final score calculation. The entire aircraft must be designed to be as light as possible, while still achieving required performance. In order to minimize total weight of the aircraft, a great amount of effort was put into choosing the most optimal manufacturing processes, materials and propulsion system with best power-to-weight ratio.

Optimal speed cargo ratio: Score of Mission 2 and Mission 3 is largely determined by speed of the aircraft. Mission 3 score is also influenced by the number of carried pucks. In order to achieve the highest score the team must decide on the best speed-to-cargo ratio.

1.3   Aircraft performance

The design process of final aircraft resulted into aircraft with the following performance capabilities:

- Aircraft empty weight of 1.83 lbs

- Tube weight of 0.55 lbs

- Maximal speed of 98 ft/s

- Payload of three pucks can be carried

- Aircraft with overall dimensions of 31.4" in length and wingspan 31.5" can be stored into a tube with length of 19.5" and diameter of 4.5"

- Aircraft can complete 7 laps in five minute window

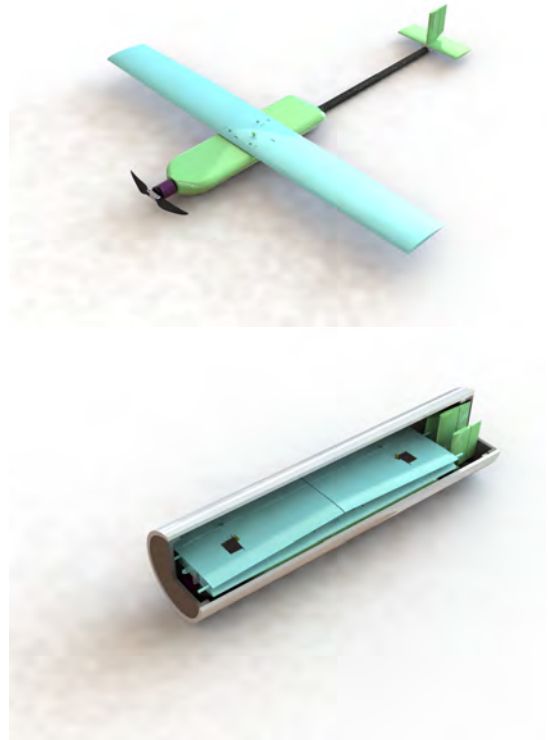- RAC of 79.97 and TMS of 3.84 was estimated

Figure 1: Final aircraft design

2.   Management summary

At the beginning of academic year 2016/17 team had its first meeting. A good amount of new students, freshmen and sophomores in particular, showed up and all of them were extremely motivated to take a part in this year's competition. They all underwent a short interview in which they were asked about their skills and expectations about competition. While the team's primary focus was on the competition, the educational role was not neglected. The number of team members varied for the first two months but remained constant at 18 members after then. With great variety of old and new members our team had a good amount of creative ideas and experience.

2.1   Team organisation

Shortly after first meeting the team split up into several subgroups led by older members: aerodynamics, propulsion, manufacturing, report, documentation & multimedia, funding, project manager, CAD. Younger members were divided according to their skill sets and wishes. Activity across more than one group was also encouraged.

2.2   Organisation chart

To ensure proper communication and development team established a hierarchical structure shown in figure 2.
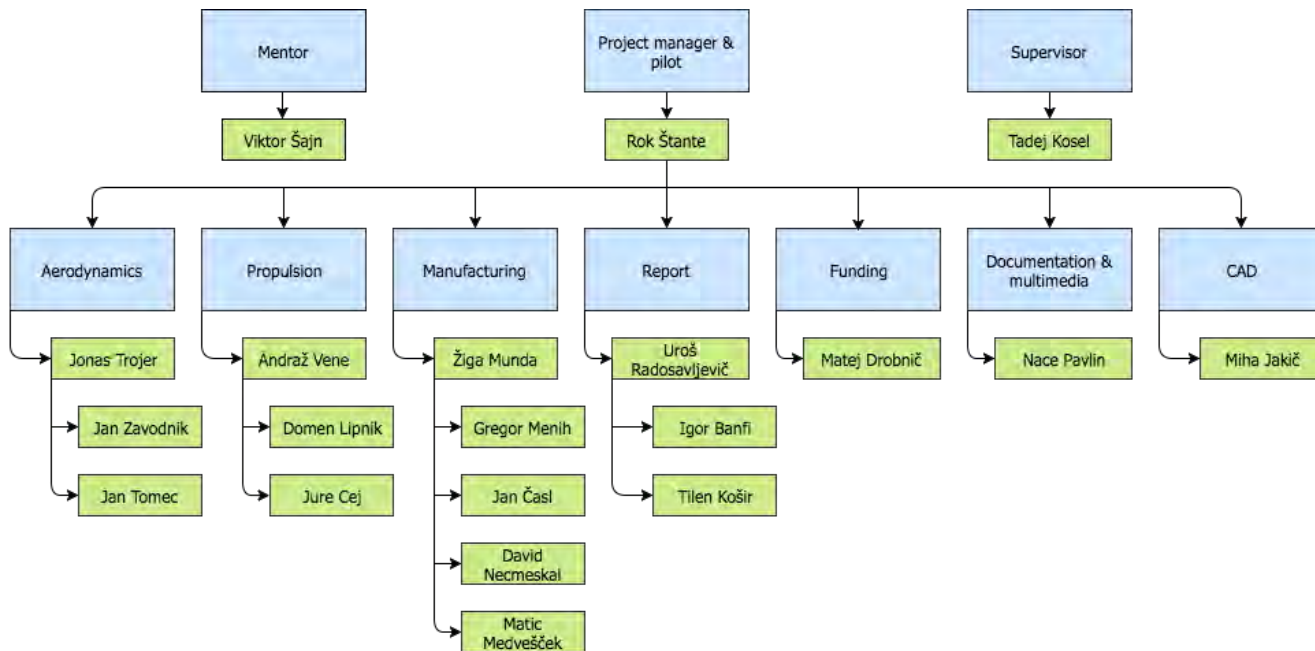

Figure 2: Edvard Rusjan Team organisation chart

Although the structure may seem to have boundary lines between different groups, some members contributed their part in more than one area, especially in brainstorming part that took places in weekly meetings. Members are therefore placed in the subgroups to which they contributed the most.

2.3   Milestone chart

Amount of required work forced the team to establish milestone chart to meet the final deadline. Milestone chart also contained internally set deadlines, which ensured work to be evenly divided throughout the whole year. Although set internally, meeting the deadlines was considered crucial to team's success as all aspects of design parameters and manufacture could be studied in detail. Team's project manager made sure all the deadlines are met. Figure 3 shows our actual work flow compared to the set deadlines.
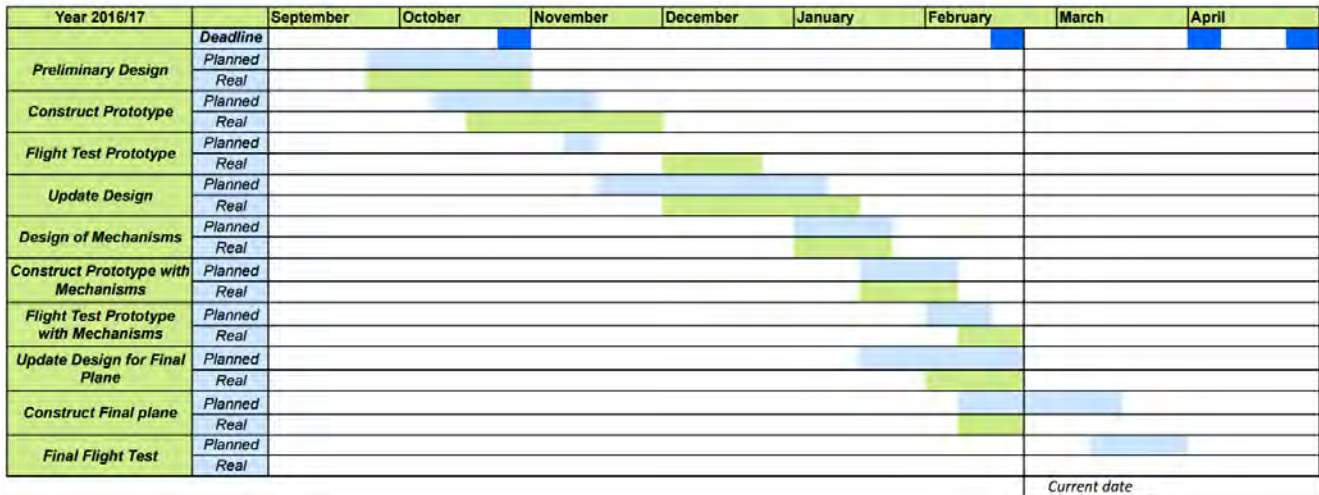
Figure 3: Milestone chart

3. Conceptual design

In the first stage of the design process a detailed analysis of competition rules was conducted. The team extracted key competition parameters and conducted a preliminary scoring analysis. Key parameters and scoring analysis were employed to evaluate possible design configurations. The high wing monoplane with pod and boom type fuselage along with conventional tail configuration was chosen for the final aircraft.

3.1 Mission Requirements

3.1.1 Score Summary

The 2017 Design/Build/Fly competition consists of three flight missions and a ground mission. Final score is calculated by Equation 1.

$$FinalScore = WrittenReportScore \cdot \frac{TMS}{RAC} \tag{1}$$

Total Mission Score (TMS) is calculated by summing the score obtained in flight missions.

$$TMS = M1 + M2 + M3 \tag{2}$$

Rated Aircraft Cost (RAC) is determined by Equation 3.

$$RAC = (EW_{max} + TW) \cdot (L + C) \tag{3}$$

RAC is determined by aircraft's empty weight (EW_{max}), weight of the tube with caps and all internal supports (TW) and size of the tube. Size of the tube is determined by tube length (L) and tube circumference (C). The $\frac{L}{C}$ ratio must exceed a minimum value of 4.

3.1.2 Mission Summary

All flight missions are flown on predesignated course shown in Figure 4.
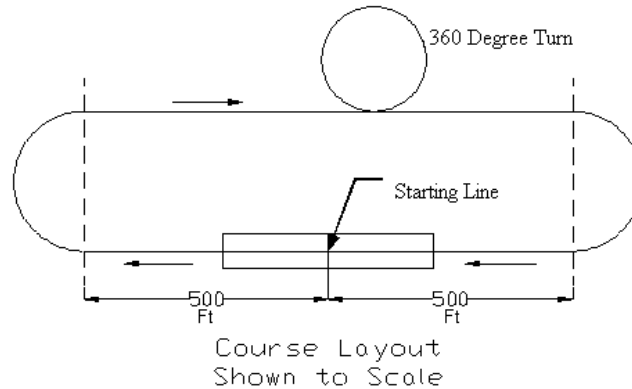

Figure 4: Flight Mission Course

Protest Procedure:

Each lap is 2500 ft long and consists of five individual sections: climb, 180° turn, 1000 ft straight flight, 360° turn and landing. A lap is completed when the aircraft finishes the course by crossing the start line while still in the air.

3.1.3 Flight missions

Flight missions will be completed in order from 1 to 3. New mission cannot be attempted unless the team has successfully completed the preceding mission. M2 can be flown after the team completed M1 and GM. The Aircraft will arrive at the staging area in stowed condition with payload already installed for all flight missions. During all flight missions the aircraft will be hand launched, held by the fuselage during the throw. There is no runway length limit during launch. The teams will have three launch attempts at their disposal, but the clock starts with the first attempt. After each successful flight mission the empty weight of the aircraft will be recorded[6]

Mission 1: Demonstration Flight

The Aircraft must complete three laps in five minute window and perform a successful landing in order to receive a maximum of 1 point.

Mission 2: Speed Flight

The aircraft will fly three laps while carrying three regulation hockey pucks in five minute window and must preform a successful landing in order to receive the score calculated by Equation 4. t_{min} is the time of the fastest team to complete 3 laps. t_{team} stands for the time needed by our team to complete 3 laps.

$$M2 = 2 \times \left(\frac{t_{min}}{t_{team}} \right) \tag{4}$$

Mission 3: Range Flight

The aircraft will fly the course by carrying the number of hockey pucks determined by each team and attempt to complete as many laps as possible in a five minute window. A successful landing must be performed to receive score calculated by equation 5. $N_{laps \times pucks}$ is the number of laps flown by our team multiplied by the number of pucks carried. $N_{laps \times pucks,max}$ is the maximum number of laps multiplied by pucks achieved by any team.

$$M3 = 4 \times \left(\frac{N_{laps \times pucks}}{N_{laps \times pucks,max}} \right) + 2 \tag{5}$$

Ground Mission

Ground mission must be completed before attempting M2. The folded aircraft inserted into the tube will be dropped three times from a height of 12" onto a hard surface. One flat drop and two end drops will be performed. After the mission the aircraft and the tube must not suffer any major damage and the tube caps must remain in place. After completion of three drops, the aircraft will be transitioned into flight condition. All flight systems will be inspected and a wingtip test will be conducted.

3.1.4 Additional constraints

Propulsion system

The aircraft has to be powered by means of electricity and driven by propeller. All propulsion and other parts, that is speed controllers, receivers, batteries, propeller and motor, have to be commercially available. Battery type is limited to Ni-Cd or Ni-Mh. There is no restriction on cell count, capacity or voltage.

3.1.5 RAC and Mission Score Sensitivity Analysis

In order to translate mission requirements into design of an aircraft properly, the impact of *TMS* and *RAC* on final score must be analyzed. The final score is calculated by Equation 1. The total differential of Final score, excluding written report score, is shown below in Equation 6

$$d(FinalScore) = -\frac{TMS}{RAC^2} d(RAC) + \frac{1}{RAC} d(TMS) \tag{6}$$

Dividing equation 6 by score, equation 7 is obtained.

$$\frac{d(FinalScore)}{FinalScore} = -\frac{d(RAC)}{RAC} + \frac{d(TMS)}{TMS} \tag{7}$$

Equation 7 shows that RAC and TMS have the same relative impact on final scoring, therefore in the case where RAC and TMS are increased for the same amount, the final score remains unchanged. An obvious but significant conclusion is that RAC should be increased only to a point where $d(RAC)/RAC = d(TMS)/TMS$.
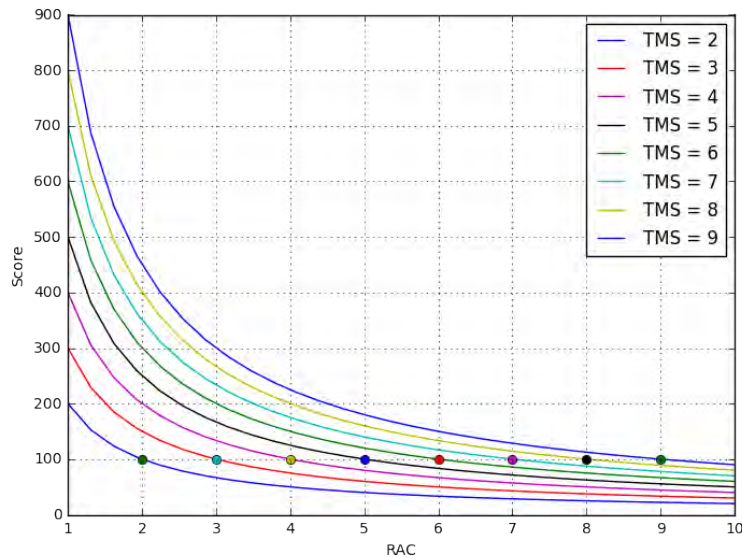
Figure 5: RAC and TMS sensitivity analysis

Intervals of greater RAC importance (Figure 5) are left of the plotted points on each curve. There are numbers of different factors that affect both RAC and TMS. For an example electric motor affects the velocity which increases TMS and total weight of the aircraft which increases RAC. Similar factors are discussed in detail under 3.2.

3.2   Transformation of Mission Requirements into Design Requirements

Based on scoring analysis several design requirements were set.

3.2.1   Pucks

According to sensitivity analysis increasing number of pucks is not necessary beneficial. There is an optimal number of pucks carried in M3 that maximize the final score.

3.2.2   Empty Weight

In order for our aircraft to be competitive it has to be as light as possible. Airplane must be stripped of all unnecessary material to achieve smallest possible weight.

3.2.3   Aircraft and Tube Size

RAC is largely influenced by tube size which is further influenced by aircraft size in folded condition. Folded aircraft shape must be as close to an elongated cylindrical shape as possible in order to maximize tube's effective volume and minimize RAC.

3.2.4 Propulsion

Propulsion influences on RAC and TMS. Primary goal is to choose propulsion system that will be beneficial on the final score, meaning it has to be optimized to increase TMS as much as possible, while keeping RAC as low as possible. This method will be applied to the batteries (capacity, number of cells, weight of each cell) and motor (weight, power). Propulsion will therefore be chosen based on best power to weight ratio.

3.2.5 Landing Gear

Since aircraft has to be hand launched, there will be no landing gear as it only reduces the aerodynamics of the aircraft. The fuselage will however be reinforced to cope with the wear due to landing on asphalt.
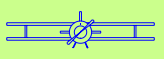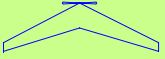
3.3 Review of considered solution of concepts and configurations

Multiple aircraft configurations were objectively evaluated to meet the mission and design requirements. Configurations were considered based on different Figures of Merit (FoM) which were weighted with values 0, 1 or 2. Additionally score of each FoM was multiplied by values of importance (1 - 5).

3.3.1 Aircraft Configuration

Aircraft configuration was decided by evaluating configurations on four FoMs: weight, manufacturability, aerodynamics (C_D in particular) and foldability. Weight and foldability were prioritized. Weight has a significant impact on RAC as well as speed. On the other hand RAC is also greatly influenced by foldability, since the aircraft has to fit a cylindrical shape with the lowest dimensions possible.

Table 1: Aircraft configuration Figure of Merit

Figure of Merit	FoM value of importance	Monoplane	Biplane	Flying wing
Weight	5	1	2	1
Manufacturability	3	2	2	0
Aerodynamics	4	1	0	2
Foldability	5	2	0	2
Total	/	25	16	23

Monoplane: Due to its simplistic design conventional monoplane has an advantage when considering manufacturability and foldability (great variety of folding mechanisms) but is average in areas, where other configurations excel.

Flying wing: Flying wing configuration offered best L/D ratio but was heavily handicapped in other areas like manufacturing due to its complex design process.

Biplane: Wing area per wing span was greater for biplane configuration. Main problem with biplane configuration was folding process of two wings instead of one.

Based on FoM, scoring *monoplane* was chosen as best aircraft configuration.

3.3.2 Wing Configuration

FoMs for choosing the best wing configuration were the following: manufacturability, stability, and foldability. Main priority was given to foldability, because of its impact on tube size and complexity of design.

Table 2: Wing configuration Figure of Merit

Figure of Merit	FoM value of importance	Low wing	Mid wing	High wing
Manufacturability	3	2	0	2
Stability	4	0	1	2
Foldability	5	1	0	2
Total	/	11	4	24

Low wing: Low wing configuration has an advantage when considering manufacturing effort and the ability to fold. The idea was to fold the wings below the fuselage. Low wing configuration was considered to be too unstable. Another disadvantage of such wing configuration is landing, since there will be no conventional landing gear. This increases the danger of wing being damaged during the competition

Mid wing: Mid wing design has a significant disadvantage when it comes to manufacturability, since it requires two separate fixing points for each wing part. Mid wing design can be also difficult to fold, especially if the length of the wings has to be longer than tube dimensions.

High wing: High wing configuration is easy to manufacture and excels in stability. The wing could be folded by simply rotating it. In case of longer wing dimensions compared to the dimensions of the tube, high wing can be also easily folded in thirds.

Based on considerations mentioned above, *High wing* configuration is chosen as best concept design.

3.3.3 Fuselage Configurations

Three different fuselages were competent as possible configuration. The best configuration was chosen based on five FoMs: manufacturability, aerodynamics (C_D), foldability and size. Because the primary concern was the ability to store the aircraft into a smallest possible tube, the priority was given to foldability and size.

Table 3: Fuselage configuration Figure of Merit

Figure of Merit	FoM value of importance	Airfoil	Conventional	Pod & Boom
Manufacturability	1	0	1	2
Aerodynamics	3	1	2	0
Foldability	4	0	0	2
Size	5	1	2	2
Total	/	8	17	20

Airfoil: Airfoil fuselage was considered primarily because of additional lifting surface. A significant downside is the required size and inability to fold.

Pod & Boom: Because of its simplicity, we considered the Pod & Boom configuration to be the easiest to design and build. Pod & Boom configuration is the best option when it comes to size and foldability, since the boom can be retracted into the pod thus reducing size by half. Main disadvantage of this configuration are the aerodynamic features due to turbulence behind the pod.

Conventional: Conventional fuselage configuration was the first option considered. It is easy enough to manufacture and has adequate aerodynamic characteristics. The configuration however lacked the storing ability.

Objective evaluation of possible configurations showed the *Pod & Boom* configuration to be the best option.

3.3.4 Wing Folding Concepts

At this stage several wing folding concepts were proposed and analyzed. The two most promising are compared below. Concepts were evaluated based on following FoMs: simplicity, size and strength. The main purpose of folding mechanism was to reduce dimensions of the tube. Size FoM was prioritized.

Split wing: The main idea was to split the wing in two pieces and rotate them along the fuselage, thus transforming the aircraft into an elongated shape which is able to fit inside the tube. Flaw of this concept was the compromised strength of the wing. Designing and manufacturing a mechanism which is able to perform this motion would be extremely complicated, because the wings would rotate around two separated axis.

One piece wing: The entire wing could be rotated around its axis and positioned in line with fuselage. Further on the wing could be additionally folded at certain point to fit into smallest possible tube. Mechanism for this concept

was estimated to be easier to design because the wing would rotate around one axis.

Based on FoM scoring, the *One piece wing* concept was chosen as best possible configuration.

Table 4: Wing's folding design Figure of Merit

Figure of Merit	FoM value of importance	Split wing	One piece wing
Simplicity	2	1	2
Size	5	2	2
Strength	3	0	2
Total	/	12	20
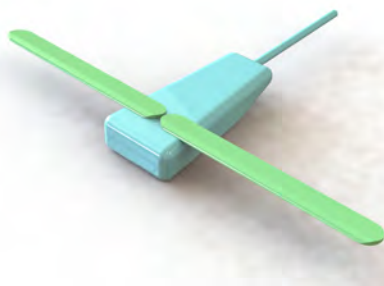
(a)   (b)

Figure 6: Split wing

(a)   (b)   (c)

Figure 7: One piece wing

3.3.5 Empennage Configuration

The only remaining decision regarding configuration is empennage. Several empennage configurations were analyzed and evaluated based on following FoMs: weigh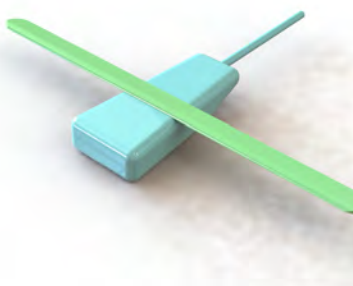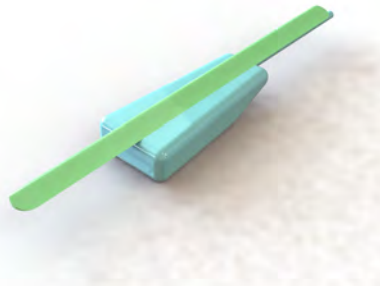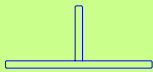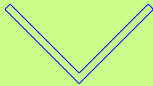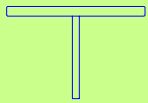t, manufacturability, size and foldability. The team strove for the empennage that does not compromise the tube size. That could be achieved either by choosing a configuration that fits the tube dimensions without folding or choosing configuration with appropriate folding mechanism. The empennage size was therefore given priority.

Table 5: Empennage configuration Figure of Merit

Figure of Merit	FoM value of importance	Conventional	V-tail	T-tail
Weight	1	2	1	0
Manufacturability	2	2	1	1
Size	5	1	2	1
Foldability	5	1	2	1
Stability	4	2	0	1
Total	/	24	23	16

Conventional tail: Conventional tail is reliable and easy to build. In case of strong wind it provides good stability compared to some others empennages considered. The main problem with conventional tail is the space it requires. In case of small tube dimensions the conventional tail has to be folded.

V-tail: V-tail configuration is harder to build, but with some adaptations it can be stored with an ease. A disadvantage of this configuration is strong side wind which causes the aircraft to roll. This represents a certain risk at landing.

T-tail: T-tail configuration was dismissed because of the storing problems.

Although conventional and V-tail configurations' final scores were close, *conventional tail* was chosen as best empennage due to greater stability and control in case of strong wind.

3.4 Final concept

A high wing monoplane with a pod & boom fuselage and conventional tail was chosen as the best configuration for the winning aircraft.
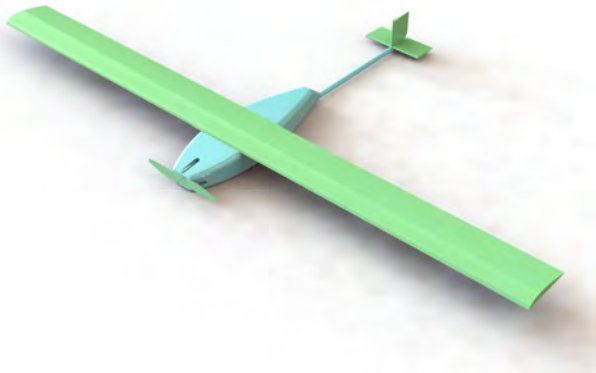
(a) Flight condition
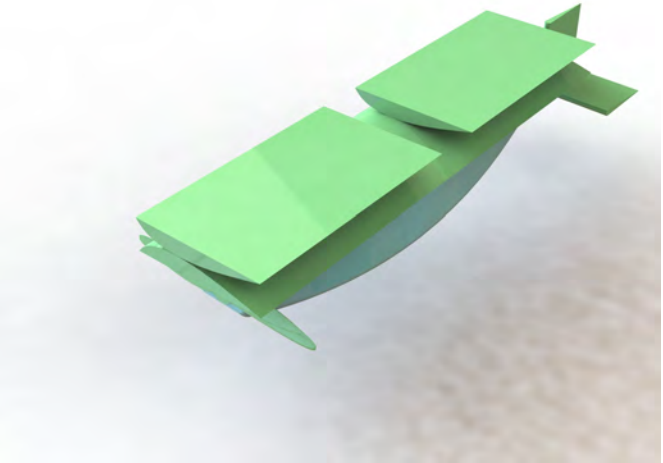
(b) Stowed condition

Figure 8: Final conceptual design

4. Preliminary design

The objective of preliminary design was to determine and further optimize parameters of aircraft's conceptual design to maximize final score. By taking into account RAC, sizing/design trades, aerodynamics and mission model, our score analysis simulation (SAS) managed to calculate the optimal aircraft's parameters and estimated mission performance.

4.1 Design and analysis methodology

The aircraft's preliminary design was carried out by iterating possible parameter combinations in order to extract the one which yields the highest final score. Over the course of the iteration wingspan, airfoils, carried pucks, aspect ratio, and propulsion configuration were alternated. Each iteration included preliminary calculation of aircraft's dimensions, its theoretical performance and consequentially RAC and TMS.
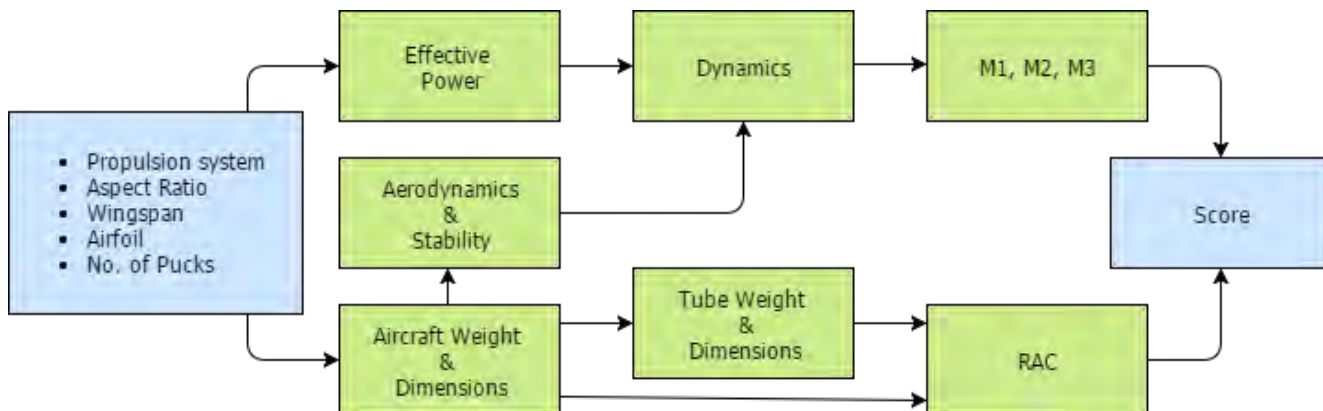
Figure 9: Score Analysis Simulation diagram

TMS is also dependant on success of the competition in M2 and M3. After some testing the team concluded that as long as we assume we are beaten in M2 and M3 their performance can be considered as an arbitrary constant. The team was aware of possible future changes in SAS winning parameters due to unrealistic combination of aircraft's parameters. In order to extract the most influential parameters, a sensitivity analysis of the SAS input parameters was carried out. Each aircraft parameter was individually alternated by 10% and total score change was observed. According to the results shown in Figure 10 wing span and aspect ratio were the parameters with biggest influence on final score. The sensitivity analysis also confirmed the decision the team made about competitors TMS.
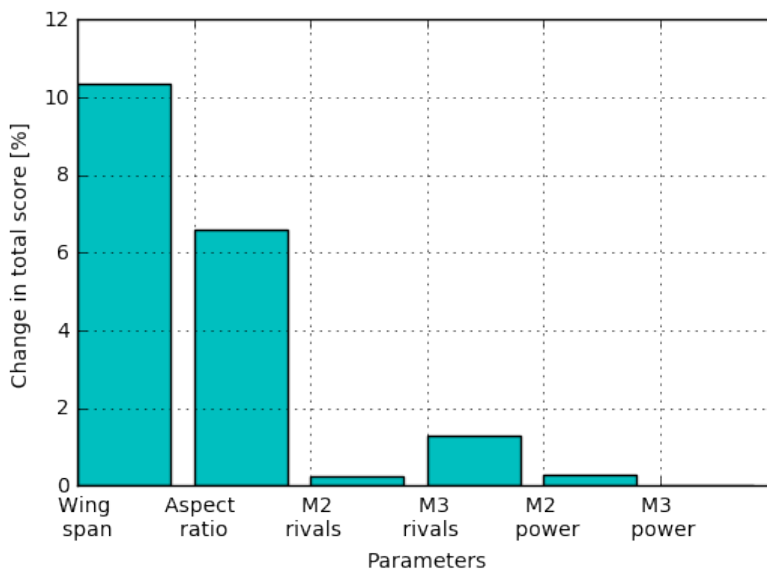
Figure 10: Sensitivity analysis

4.2   Design Trades

4.2.1   Wing span

During iteration procedure the team realised, that choosing optimal wingspan was crucial in order to produce a winning aircraft. Three separate criteria were used to determine the final wingspan: optimum obtained by SAS, dynamic stability and pilot input.

The optimal wingspan determined by SAS was calculated by its effects on aircraft. Greater wingspan meant increase in RAC and lower maximum speed due to increased C_D. On the other hand smaller wingspan results in higher wing loading, higher v_{stall} and consequently greater turn radius. By decreasing wingspan while keeping the chord constant to avoid excessively low Reynolds numbers, the aspect ratio decreases and the wing produces more induced drag. SAS showed the optimal wingspan to be 19.7".

Shorter wingspan also requires smaller tail dimensions for a given tail volume coefficient. Eventually the emmpennage gets small enough to be completely submerged in the prop-wash, decreasing it's effectiveness. To provide necessary dynamic stability the tail volume coefficient needs to increase which produces additional drag.

Lastly pilots input was considered. A testing aircraft was flown several times. With each new flight the wing span was reduced. Pilot determined the 32.5 inch wingspan to be controllable. Testing procedure is described in detail in Section 7.
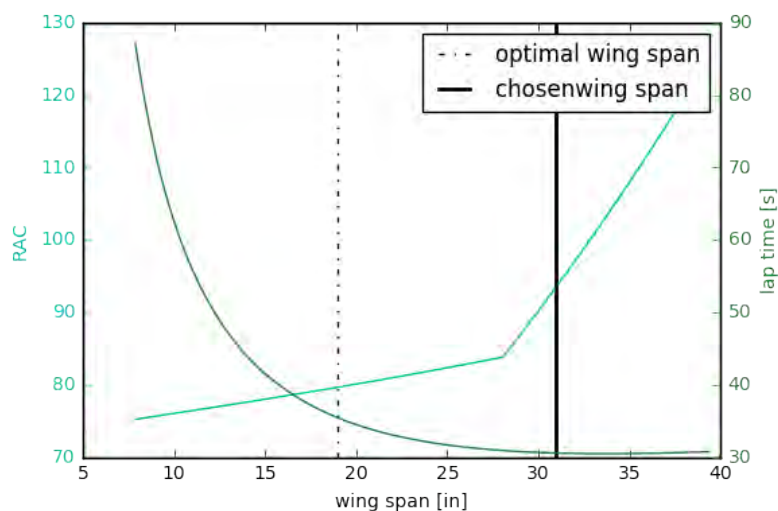

Figure 11: Wingspan effect

4.2.2   Propulsion system selection & number of pucks

Number of carried pucks for M3 and selected propulsion are highly related parameters. Carried payload increases weight and in turn stronger propulsion is needed. Number of carried pucks and propulsion system were deter-

mined simultaneously. Since motor and propeller specifications, number of battery cells as well as number of carried pucks are discrete values, it would be pointless to analyze them as a continuous function. Possible combinations of values were evaluated by SAS.

The propulsion system was determined by parameters: number of battery cells, motor power, propeller size, power consumption during each mission.

Optimal number of battery cells was chosen based on SAS outcome and extensive experiments (described under 8.1.2) in which the exact current and voltage during the discharge was measured. More battery cells could provide greater voltage and capacity but would also significantly increase aircraft's weight thus influencing RAC and speed.

Motor power directly influenced the speed and RAC of the aircraft. Stronger motor increases maximum speed but increases battery consumption and RAC.

Propeller size was determined based on motor used by eCalc and test flights.

SAS outcome showed that three carried pucks for M3 is the most viable option. This result was expected, since SAS anticipated increase in RAC for every additional puck. It turns out that RAC increase makes every additional puck obsolete.

At the end of iterating procedure several promising propulsion systems were presented (Table 6). Power output for M2 and M3 was alternated in order to extract the optimal value. M2 required greater speed, thus power output showed to be most optimal. M3 was therefore treated as endurance mission where selected power output should discharge the whole batteries in five minute window. Concrete values are listed in Table 7.

Table 6: Competent propulsion configurations

Propulsion System Weight [*lbs*]	Motor	Kv	Battery [*mAh*]	Current [*A*]	Power [*W*]	Propeller	Static Thrust [*lbs*]
0.681	Hacker A20-8XL	1500	10x1600 Xcell	31.6	307	8x6	3.06
0.589	Hacker A20-8XL	1500	8x1600 Xcell	24.2	189	8x7	2.31
0.688	Scorpion HKII-2221-2010	2010	10x1600 Xcell	28.6	279	7x5	2.5
0.595	Scorpion HKII-2221-2010	2010	8x1600 Xcell	22.3	174	7x6	1.94

Table 7: Power output

	Throttle [%]	Power [W]	Charge Remaining [%]
M2	100	84W	52,78
M3	57	48W	26.31

4.3 Mission Model

Missions were simulated by calculating time needed to complete each lap. Single lap was simplified to turns and straight flights. Each mission was analysed by its own parameters.

$$t_{lap}(P, \lambda, m, A, C_l) = \frac{2 \cdot l}{v_0(P, m, A, \lambda)} + \frac{4 \cdot \pi \cdot R(P, m, n, C_{lmax}, \lambda)}{v} + 2 \tag{8}$$

Lap time was increased by 2 seconds in order to compensate for time needed to position the aircraft for turning maneuver.

4.3.1 Uncertainties

By using this mission model certain variables were disregarded. We completely disregarded takeoff and landing, since it's effect on aircraft design was minimal. In this mission model our pilot was considered unmistakable. Further on the model disregards the weather conditions in which the aircraft will fly. It also assumes that the aircraft will be flown at constant altitude. This assumption increases uncertainty especially in turning maneuver where constant altitude at $C_{L,max}$ is difficult to achieve.

4.4 Aerodynamic Characteristics

4.4.1 Aerofoil selection

Choosing the correct aerofoil was crucial for a fast and stable aircraft. Aerofoil was chosen based on C_L, C_D, pitching moment and by operating point being near the maximal speed of aircraft achieved during M2. Based on this criteria a low angle of attack was assumed. The aerofoil should produce as little pitching moment as possible in straight flight in order to avoid a high longitudinal dihedral and prevent unnecessary drag. During iteration procedure several different aerofoils were considered. They were compared at Reynolds number of 200 000. High lift aerofoils, such as Eppler 423, were considered unsuitable. Although they produce a higher C_{lmax} the drag during a turn is higher, resulting in increased lap time. High lift aerofoils are significantly better when considering high Reynolds numbers, but were out of aircraft's operating envelope. Therefore it seemed logical to sacrifice C_{lmax} for higher speed. In the last stage of selection MH32, AG24 and S9000 aerofoils were considered. Data for individual aerofoil was obtained by Airfoiltools.com.

Table 8: Aerofoil parameters comparison

Parameter	MH 32	AG 24	S 9000
Thickness [%]	8.7	8.4	9
Max. Thickness @ [%]	30.2	26	28.2
Camber [%]	2.3	2.2	2.1
Max. Camber @ [%]	45.7	46.9	44.8
Max. Lift Coefficient	1.16	1.95	1.29
Critical Angle of Attack [°]	10.5	10	12
Max. Lift-to-Drag Ratio	79.32	70.12	71.01
Angle of attack for Max. L/D [°]	4.75	4.75	4.5

MH32 aerofoil was selected as the most suitable aerofoil. The decision was based on C_L/C_D ratio, which is high enough to ensure adequate turning maneuvers. MH32 will only be advantageous as long as the flow is laminar. In order to achieve such a flow, the upper surface should be as smooth as possible. Manufacturing methods used to achieve necessary characteristics are described in Section 6.
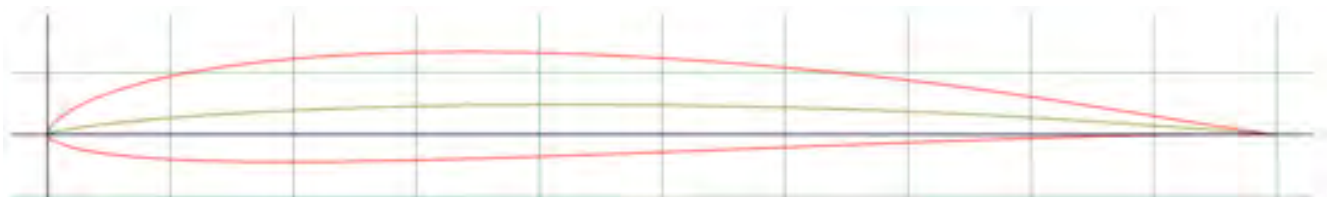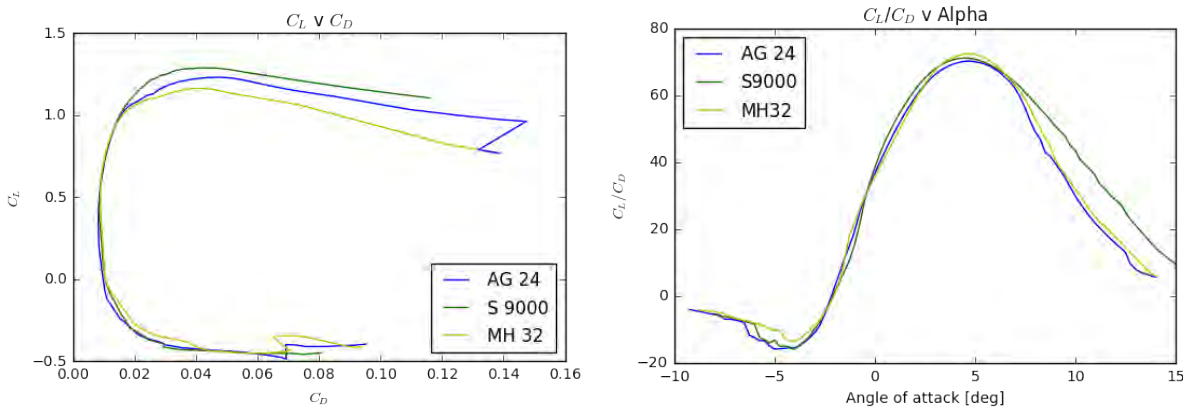

Figure 12: MH32 aerofoil

Figure 13: Airfoil polars

4.4.2 Lift analysis

Lifting surfaces were analysed with Athena Vortex Lattice (AVL) developed by Dr. Mark Drela at MIT. Software calculates aerodynamic characteristics of the aircraft by modeling lifting surfaces as an infinitely thin sheet of discrete vortices and computing their interactions. AVL was used to calculate static stability and trim characteristics of the aircraft's wing and empennage configuration. Beside that the team was able to determine the optimal longitudinal dihedral (wing = $0.6°$ and empennage = $-0.9°$), to ensure straight flight of the aircraft at its maximal velocity of 108.25 ft/s. In other words at maximal velocity the fuselage and the boom are going to be at zero angle of attack, resulting in the lowest drag coefficient. AVL software also confirmed the results of score analysis simulation regarding turning radius, n and C_L of the complete aircraft. There are however some deviations regarding C_{di} which most certainly resulted from linear approximation of polar of the flight obtained in one of the test flights. Figure 14 shows the distribution of panels and strips that were used in drag calculations. Lift and induced angle of attack are shown in the Trefftz plot for cruise flight in equilibrium state.

(a) AVL geometry of simulation with wingspan of 31.50 inch   (b) Trefftz plot of lift and induced angle of attack
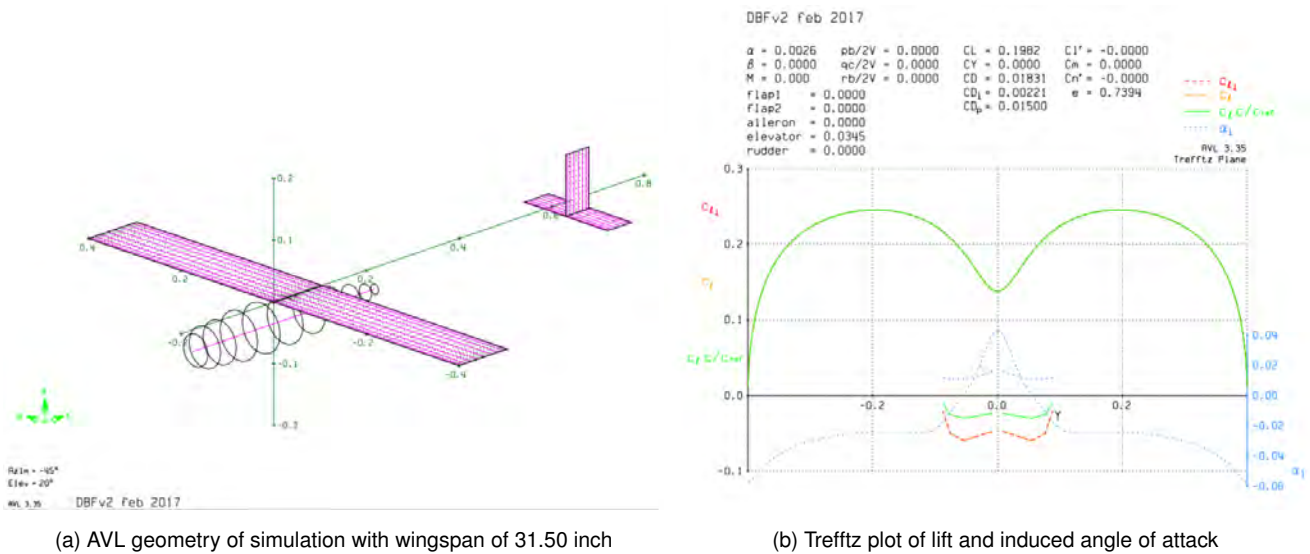
Figure 14: Final conceptual design

Table 9: Result comparison of AVL and SAS

	$n[/]$	Turn Radius [ft]	$C_l[/]$	$C_{di}[/]$
SAS	3.12	70.54	1.100	0.011
AVL	3.07	71.85	1.065	0.003

4.4.3 Drag analysis

Drag reduction was one of the team's main focus. Drag coefficients of various aircraft components were estimated based on strip theory, where lifting surfaces are divided into a number of discrete elements that are treated as two dimensional aerofoils. Aerofoil polars were determined using Xfoil which included viscosity effects. Finite wing effects were taken into account by including the distribution of induced angle of attack obtained via AVL. Fuselage drag was estimated using slender body with the same cross section distribution along the aircraft as the actual fuselage. Table 10 shows drag buildup for each mission and additional situation, where the angle of attack equals to $-1.2°$, since the total drag at that value is minimal. Maximal lift-to-drag ratio of 10.1 is obtained at angle of attack equal to $3°$ ($C_L = 0.37$). The aircraft will therefore be flown in M3 at 82.02 ft/s.
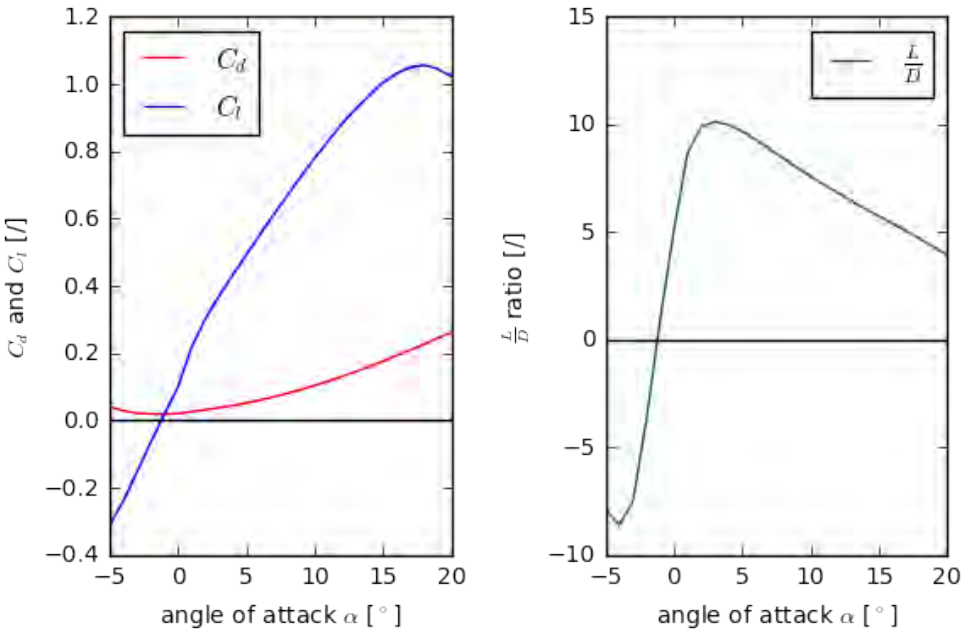
Figure 15: C_l, C_d and lift-to-drag ratio in relation to angle of attack

Table 10: Representation of Drag coefficients for each described situation

Situation		
Zero total lift: fuselage angle of attack $\alpha = -1.2°$ $R_e = 230000$	<table><tr><td>**Component**</td><td>C_d</td></tr><tr><td>Wing</td><td>0.0083</td></tr><tr><td>Horizontal tail</td><td>0.0004</td></tr><tr><td>Vertical tail</td><td>0.0002</td></tr><tr><td>Fuselage</td><td>0.0088</td></tr><tr><td>**Total**</td><td>0.0177</td></tr></table>	
M2: equilibrium fuselage angle of attack $\alpha = 0°$, $v = 108.25 ft/s$, $Re = 180000$	<table><tr><td>**Component**</td><td>C_d</td></tr><tr><td>Wing</td><td>0.0149</td></tr><tr><td>Horizontal tail</td><td>0.0005</td></tr><tr><td>Vertical tail</td><td>0.0002</td></tr><tr><td>Fuselage</td><td>0.0089</td></tr><tr><td>**Total**</td><td>0.0244</td></tr><tr><td></td><td>$C_{d,ind}$</td></tr><tr><td>**Total**</td><td>0.0033</td></tr></table>	
M1 and M3: equilibrium fuselage angle of attack $\alpha = 3°$, $v = 82.02 ft/s$, $Re = 230000$	<table><tr><td>**Component**</td><td>C_d</td></tr><tr><td>Wing</td><td>0.0262</td></tr><tr><td>Horizontal tail</td><td>0.0012</td></tr><tr><td>Vertical tail</td><td>0.0002</td></tr><tr><td>Fuselage</td><td>0.0092</td></tr><tr><td>**Total**</td><td>0.0368</td></tr><tr><td></td><td>$C_{d,ind}$</td></tr><tr><td>**Total**</td><td>0.0109</td></tr></table>	
Legend: ■ Wing ■ Horizontal tail ■ Vertical tail ■ Fuselage		

4.5 Stability and control

Static and dynamic stability was tested in AVL environment. Stability analysis showed the landing phase at velocity $v = 1, 2 \cdot v_{stall} = 55.62$ ft/s is the most critical flight scenario. Stability derivatives of that scenario are shown in Table 11. Trimmed equilibrium flight at that situation can be sustained without extreme elevator deflections. Static margin of 18.5% was found to be enough for sufficient longitudinal static stability. Dynamic stability analysis was carried out considering stability coefficients and aircraft's moments of inertia obtained via CAD model. All poles of the system matrix lie in the left half plane (shown in Figure 16) which indicates stable modes.

Table 11: Static stability coefficients and derivatives

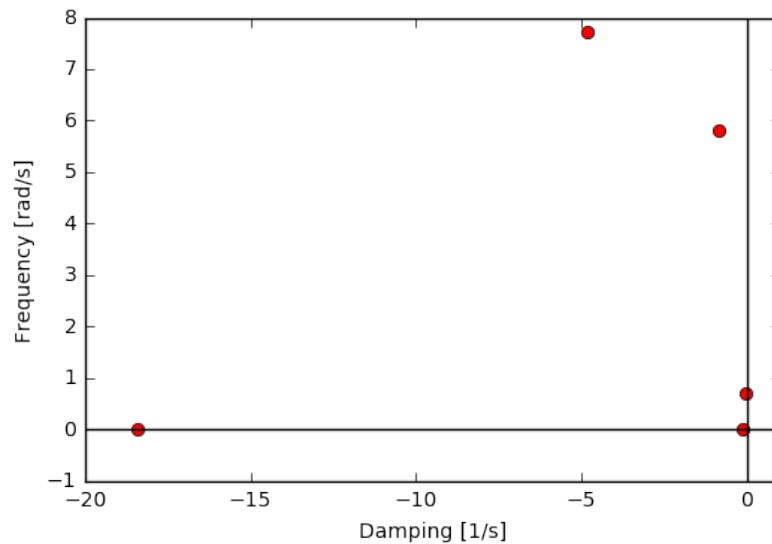| Parameter		Values
Inputs	$W_{total}[lbs]$	2.58
	$v[ft/s]$	55.6
Aerodynamic Parameters	$C_L[/]$	0.75
	$\alpha[°]$	0.33
	$\beta[°]$	0.00
Deflections	$\delta_{aileron}[°]$	0.00
	$\delta_{elevator}[°]$	7.68
Stability Derivatives	$C_{l,\beta}[rad^{-1}]$	-0.18
	$C_{L,\alpha}[rad^{-1}]$	4.74
	$C_{n,\beta}[rad^{-1}]$	0.07
	$C_{m,\alpha}[rad^{-1}]$	-0.88
Damping Derivatives	$C_{l,p}[rad^{-1}]$	-0.50
	$C_{m,q}[rad^{-1}]$	-26.8
	$C_{n,p}[rad^{-1}]$	-0.04
Static Margin	Chord [%]	18.5

Figure 16: System matrix roots

Table 12: Dynamic stability analysis for aircraft's least stable case

Longitudinal Modes	Eigenvalue	Damping ratio	Damped frequency $[1/s]$
Short Period	-4.81 +- 7.73i	0.529	1.45
Phugoid	-0.06 +- 0.71i	0.082	0.11
Lateral Modes			
Dutch Roll	-0.84 +- 5.80i	0.143	0.93
Rolling	-18.4	/	/
Spiral	-0.137	/	/

Possible stability issues can be expected in the dutch roll mode because of its relatively low degree of damping [1]. Team also pointed out some concerns about directional flight stability at lower velocities and greater deflection angles of flaps because of high wing loading and butterfly configuration. The concerns were tested in one of the test flights, where wing loading was optimized to the pilot's zone of comfort.

4.6   Estimates of the airplane mission performance

Based on design decisions and changes score analysis simulation was updated to obtain realistic final score estimates. M1 was assumed to be completed successfully, thus rewarding a score of 1. M2 and M3 scores were estimated by calculating the lap times based on Equation 8. Aircraft will be flown in M2 at its maximal velocity of 108 ft/s at average discharge current of 21 A, whereas in M3 Aircraft will be flown at velocity of 82 ft/s and average

discharge current of 12 A in order to complete as many laps as possible with three pucks given battery capacity. SAS estimates 26% charge will be left after completing M3. In Figure 17 we can see the actual speed over time and the speed used in SAS. Flight tests confirmed that the assumption did not cause any serious deviations between predicted and actual performance.

Table 13: Predicted performance for M1, M2 and M3

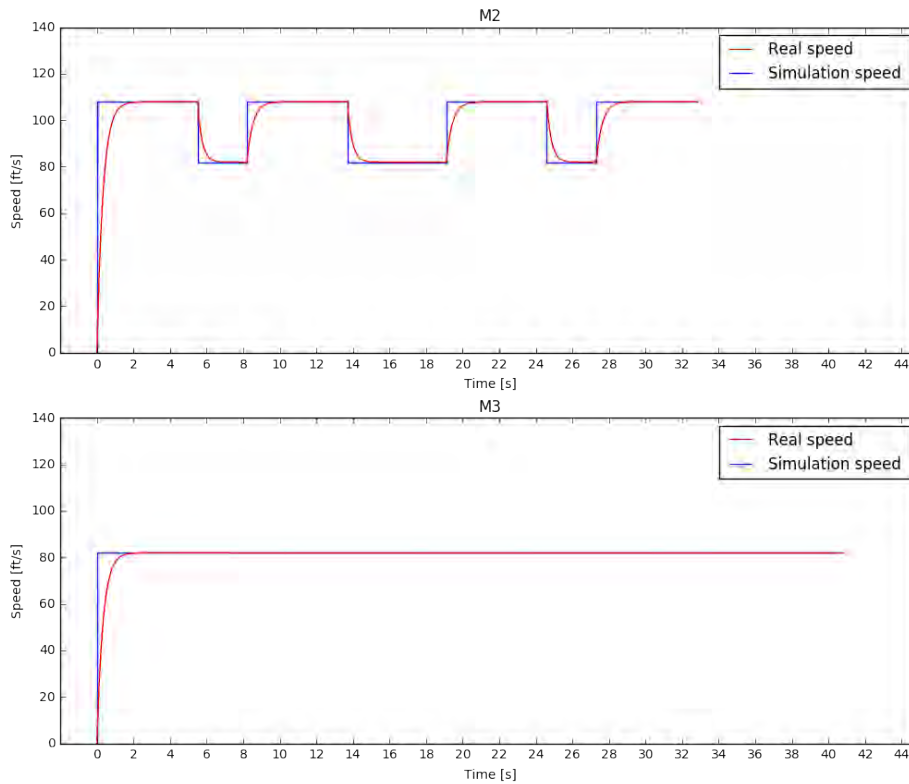|	Mission 1	Mission 2	Mission 3
Carried Pucks	0	3	3
Weight [*lbs*]	1.46	2.58	2.58
Velocity [*ft/s*]	82	108	82
Lap time [*s*]	40.15	32.81	40.15
Number of Laps	3	3	7

Figure 17: Speed for M2 and M3

5. Detail design

On basis of preliminary design final aircraft was designed. Note that final aircraft features slightly deviate from ones chosen in preliminary design.

5.1 Dimensional parameters of the final design

Final aircraft dimensions were chosen based on values determined in preliminary design stage. The aircraft consists of five major components: fuselage, wing, propulsion system, emmpennage, control systems. Aircraft basic dimensions and tube dimensions are listed in Table 14.

Table 14: Final aircraft dimensions

Overall dimensions		Wing		Empennage		Tube dimensions	
Length [*in*]	32	Wing span [*in*]	31.42	Vertical tail span [*in*]	3.29	Tube circumference [*in*]	14.8
Pod length [*in*]	14.25	Chord [*in*]	4.1	Vertical tail chord [*in*]	2.36	Tube length [*in*]	19.7
Boom length [*in*]	14.84	Area [in^2]	111.5	Vertical tail area [in^2]	7.76		
Wing l.e X[*in*]	7.32	Middle part [*in*]	15.71	Horizontal tail span [*in*]	6.3		
		Wingtip part [*in*]	7.86	Horizontal tail chord [*in*]	2.36		
				Horizontal tail area [in^2]	14.47		

5.2 Structural Characteristics

In order to assure necessary structural rigidity to withstand stresses on the aircraft during flight missions the stresses on the wing during the turning maneuver in M2 were calculated and represented in Figure 18. Calculated moments were the baseline in the wing design described in 5.3.2.
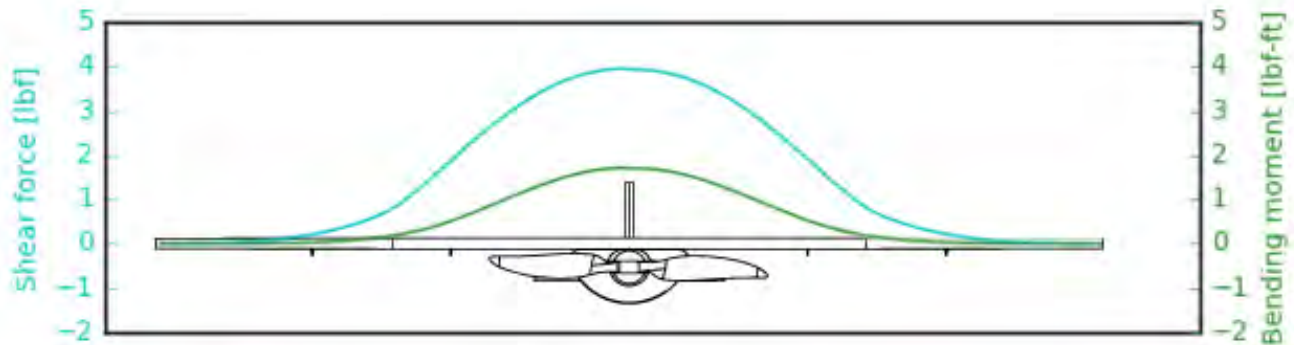
Figure 18: Shear force and moment on wing

To assure the aircraft is going to pass GM, drop test analysis was conducted in SolidWorks environment. Figure 19 shows concentration of stress during drop test. Highest stress of $1.2kpsi$ was calculated and is concentrated on the contact point between tube and ground. Stresses on the aircraft were estimated well within safe limits.
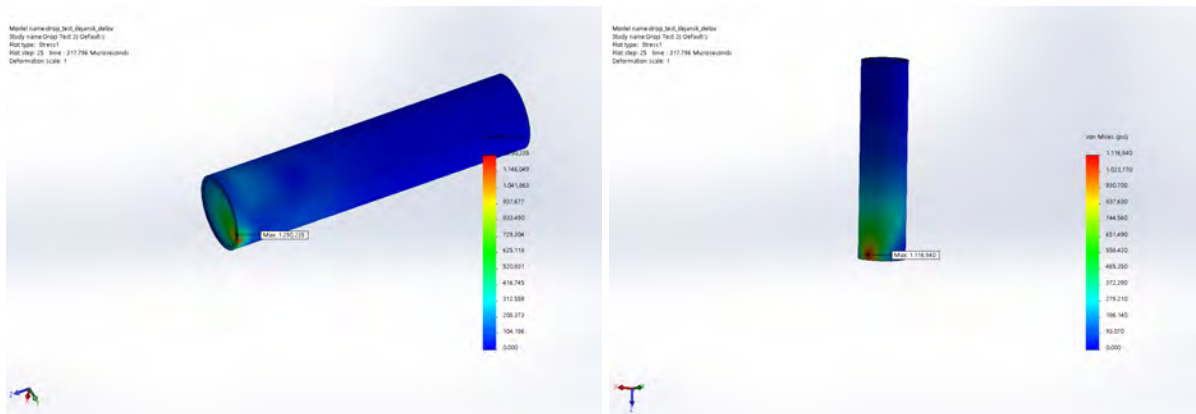

Figure 19: Simulated GM

5.3   System and subsystem

5.3.1   Fuselage

Fuselage is of pod and boom configuration. Size of the fuselage was constructed around needed payload size. Skin-former design was used for the pod. Formers are placed in between carried pucks. Both formers and skin were constructed from carbon fiber composite. Motor is mounted directly on the pod. Anchorage flanges and positioning pin are located on top of the pod (paragraph 5.3.2.1). Payload can be accessed through a hatch located on one side of the pod.

Boom will be constructed as a telescopic tube that can be retracted inside a pod and is manufactured from carbon fiber rod. Its task is to withstand bending moments inflicted by emmpennage. After second Q&A the team realised that radial motion is not restricted by current boom. This will be solved by placing a concentric square profile inside the boom that restricts rotation.
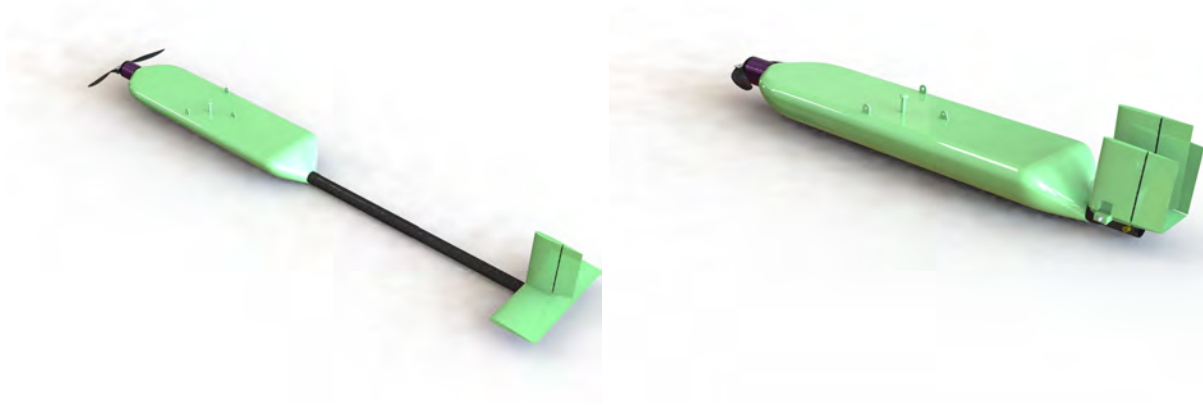

Figure 20: Fuselage in flight and folded condition

5.3.2 Wing

Sandwich-structure composite is used for the wing with styrodur being the core material. Skin material is carbon fiber from 200tex roving positioned in $[-45°, 45°]$ orientation. Thickness of skin layer varies, the thickest being at the fuselage and the thinnest at the wing tip.

Cutouts are made on bottom of the wing where servos are located.

5.3.2.1 **Folding mechanism**

Rotation: Wing is attached to the pod via positioning pin located at top of the pod. Wing is rotated into flight position in three steps: rising, $90°$ rotation, lowering. Rotation over $90°$ is restricted by the pin.

In folded position wing is positioned along the pod. Rotation is restricted by three anchorage flanges located inside the wing. Wing is risen above anchorage flanges and rotated for $90°$ about a pin connecting wing and fuselage. Wing is lowered on anchorage flanges and locked into place via canapy lock. Canapy lock's are spring loaded and can be seen in Figure 22.

Folding wingtips: Wing will be split into three parts. Wingtip parts will fold on the central part as seen in Figure 23. Parts of the wing are moved into flight position in two steps: alignment of wing, unification. Wings are connected via a double hinge (Figure 24). This double hinge restricts rotation and can only be moved to an aligned position of wing portions. Wing is assembled by pushing wingtip portion towards central portion. In the

process wing is connected by locking flange (Figure 24). Wings are reinforced by two wing jigs made from carbon fiber.
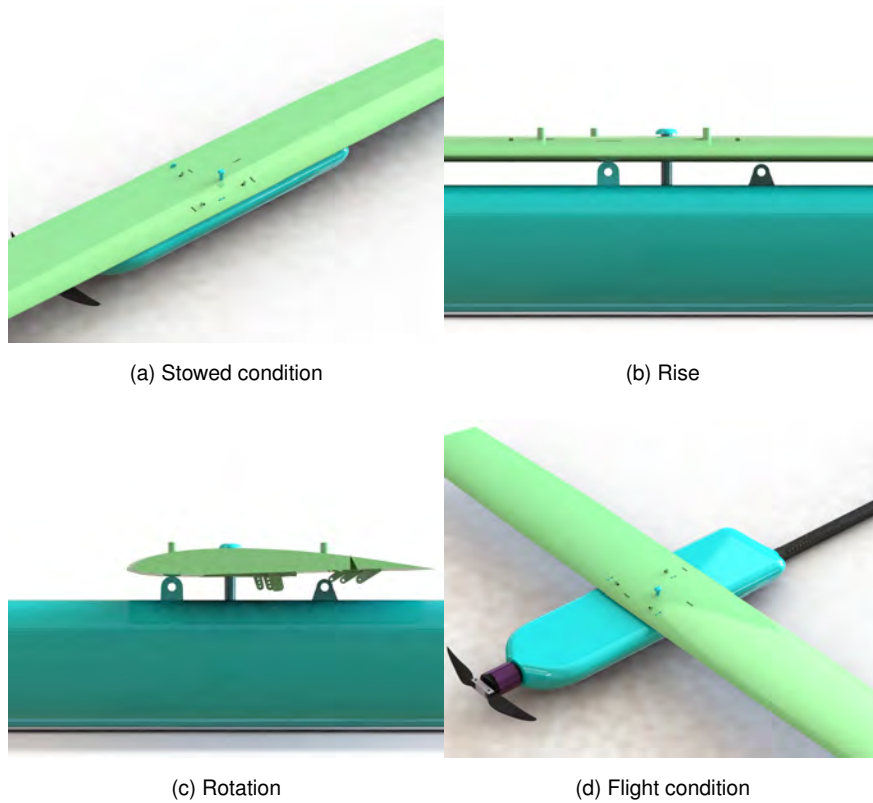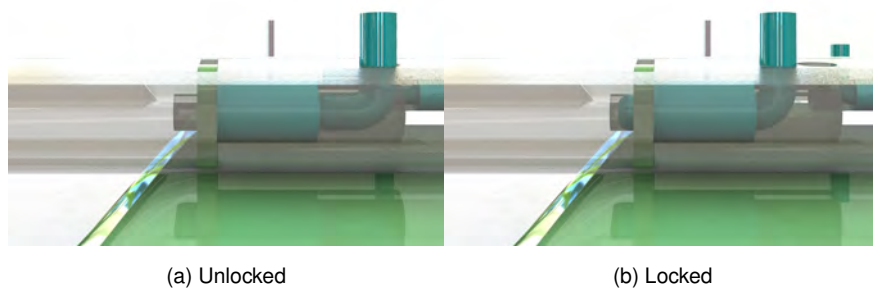

(a) Stowed condition

(b) Rise

(c) Rotation

(d) Flight condition

Figure 21: Transformation into flight condition

(a) Unlocked

(b) Locked

Figure 22: Canapy lock

(a) Folded   (b) Rotated into colinear position   (c) Unification
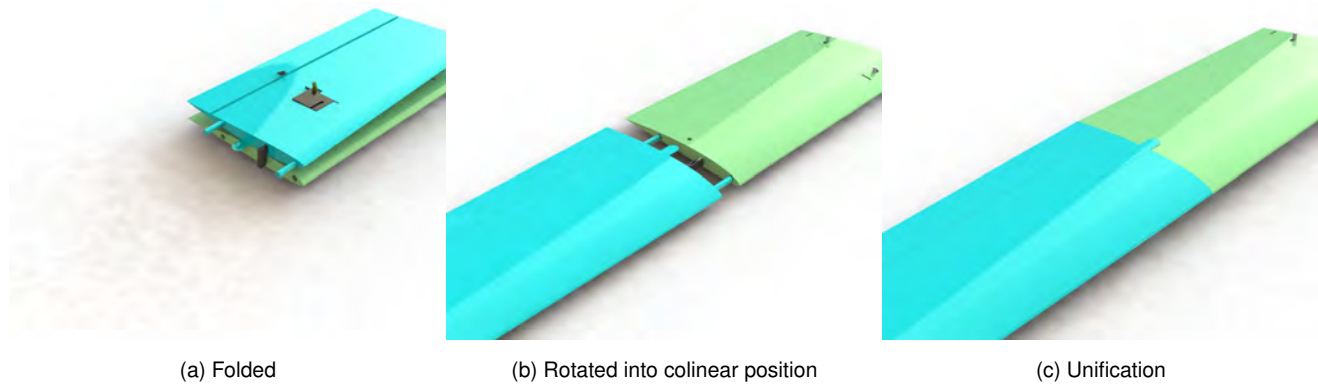
Figure 23: Transformation into flight condition
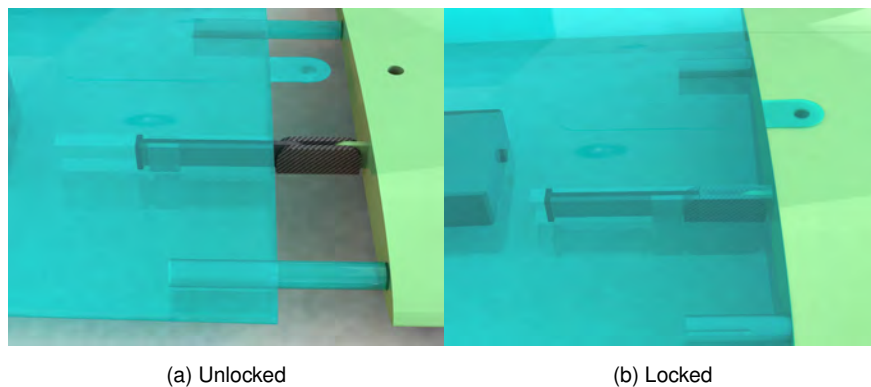

(a) Unlocked   (b) Locked

Figure 24: Locking mechanism

5.3.3 Propulsion system

Several different configurations of propulsion systems were analysed in section 4.2.2 and tested as described in section 7.2.2. Hacker A20-8XL motor was chosen for the final aircraft with a combination of 8x7 foldable propeller. The whole propulsion system is powered by ten 1600 NiMh Xcells which are able to output 30A current. This configuration can produce 2.31 lb of static trust.

5.3.4 Empennage

Conventional Empennage is made by using sandwich structure composite. Core material is depron sanded into symmetrical aerofoil. Skin material is carbon fiber composite. Emmpennage can be folded into the shape shown in Figure 25 to fit inside a tube. Movable parts are connected by a hinge and positioned into flight condition by rotating them and locking into place by spring loaded Canapy lock. Locking procedure is presented in Figure 26.
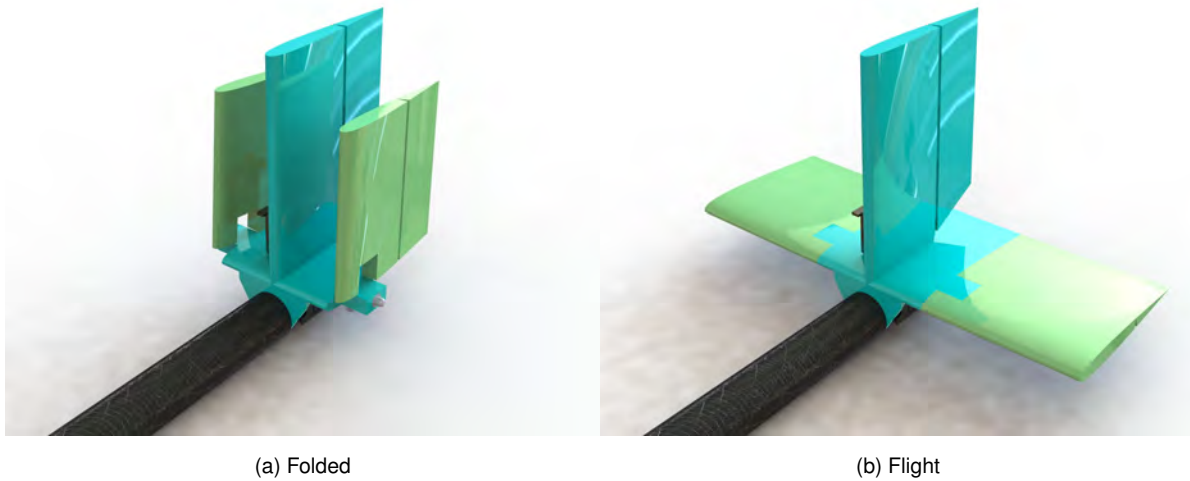
(a) Folded

(b) Flight

Figure 25: Folding procedure

(a) Locked

(b) Unlocked

Figure 26: Locking mechanism

5.3.5 Receiver and Transmitter

Spektrum DX7 is used as a transmitter and Spektrum AR8000 with 2.4 GHz antennas as a receiver. Receiver and antennas are positioned in the rear of the pod. Because large portion of the aircraft is constructed from carbon fiber that blocks 2.4 GHz signals the antennas have to be positioned outside the fuselage. Three antennas are positioned at different angles relative to each other in order to ensure stable connection.

5.3.6 Servos

Dymond D47 servos are used on the aircraft. Servos were selected based on needed torque, size and ability to operate at high voltages. A total of six servos are used on the aircraft: two ailerons, two flaps, an elevator and a rudder.

5.3.7 Tube

Tube is constructed as a sandwich-structure composite, skin layers being made from carbon fiber and core from styrodur. This method was selected because the carbon fiber skin provides necessary rigidity for the casing, styrodur absorbs the impact from the drop test and the whole structure is lightweight. Caps are created by using 3D printing technology.

5.4 Weight and balance

Correct Center of Gravity (CG) location is crucial to achieve aircraft stability during the flight. CG was determined by considering weight of all aircraft components and their location on X and Y axis. Components weight was estimated via CAD model. Aircraft was designed to be in equilibrium during straight flight while carrying payload (M2 & M3). CG of empty aircraft was calculated to be 8.88" relative to X axis and is considered within operating limits.
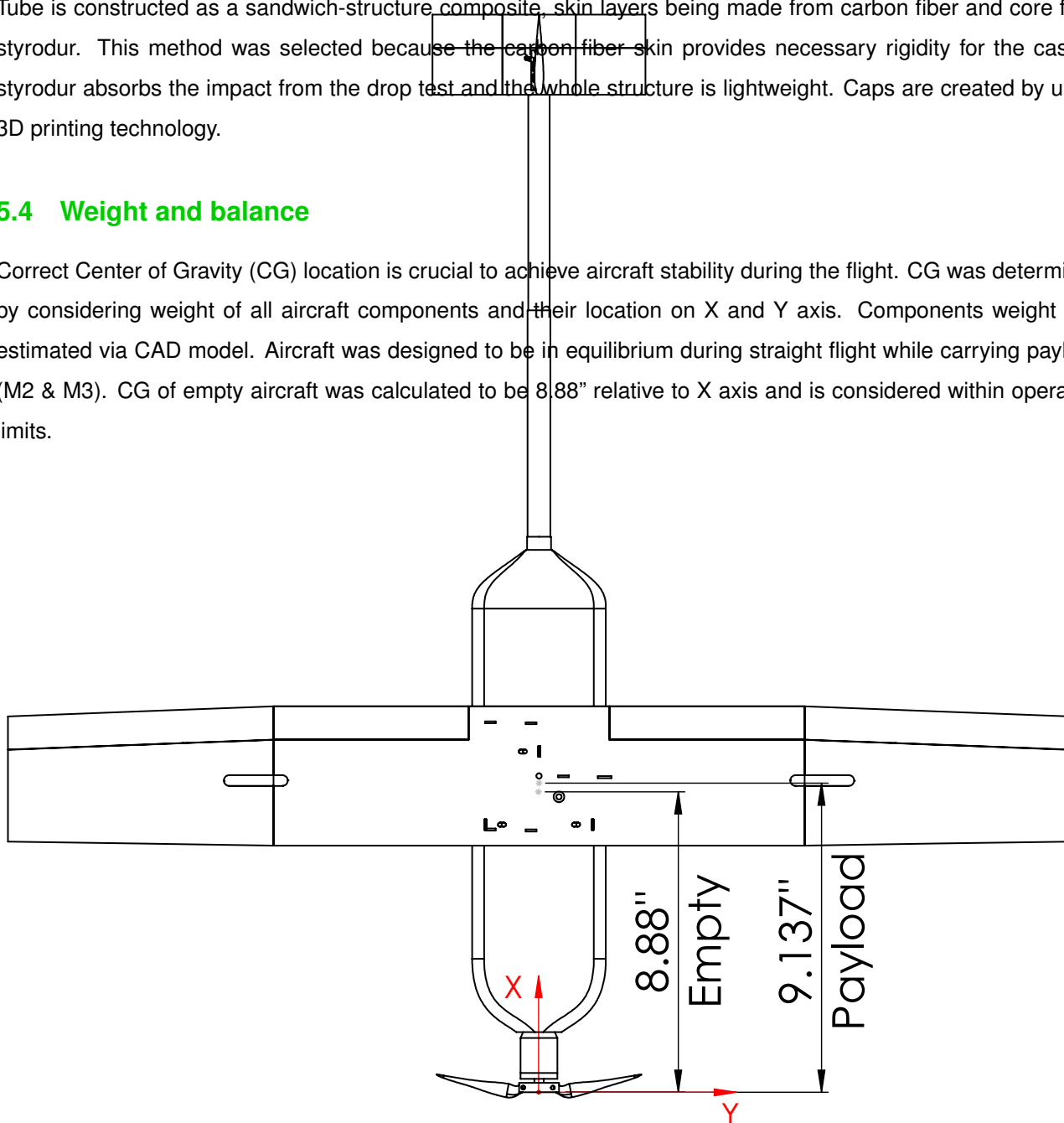
Figure 27: Center of Gravity

Table 15: Weight and balance

Component	weight [lbs]	X [in]	Moment X [lbs in]	Y [in]	Moment Y [lbs in]
Empty aircraft (M1)					
Wing	0.58	9.03	5.2374	0	0
Pod	0.26	8.29	2.155	0	0
Propulsion batteries	0.48	3.98	1.9104	-0.01	-0.0048
Reciever batteries	0.06	9.28	0.557	-0.65	-0.039
Reciever system	0.04	14.83	0.5932	0	0
Controller	0.05	2.47	0.1729	0	0
Electric motor	0.13	1.08	0.1404	0	0
Propeller	0.01	0.17	0.0017	0	0
Boom	0.06	20.48	1.23	0	0
Emmpennage	0.14	30.44	4.2616	0	0
Aircraft	1.83	8.88	16.25	-0.02	-0.057
Loaded aircraft (M2 &M3)					
Payload	1.12	9.55	10.696	0	0
Aircraft \w payload	2.95	9.137	27	-0.01	-0.0402

5.5   Performance of final design

Based on aircraft features described above, aircraft performance was estimated and tested. Estimated mission performance is gathered in Table 16. Testing procedure is described in Section 7.2.3. Mission performance estimation was based on mission model (Section 4.3). Team's victory was largely based on low RAC, which was calculated by Equation 3. A final value of 79.97 was obtained.
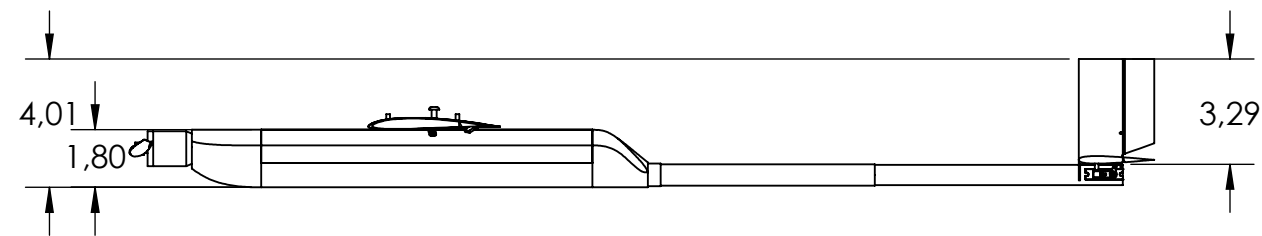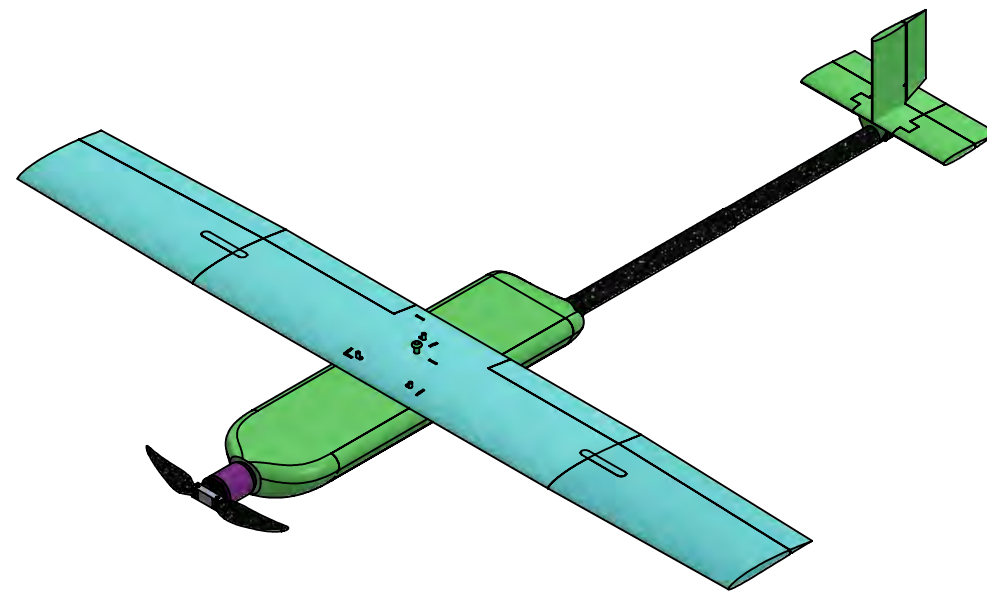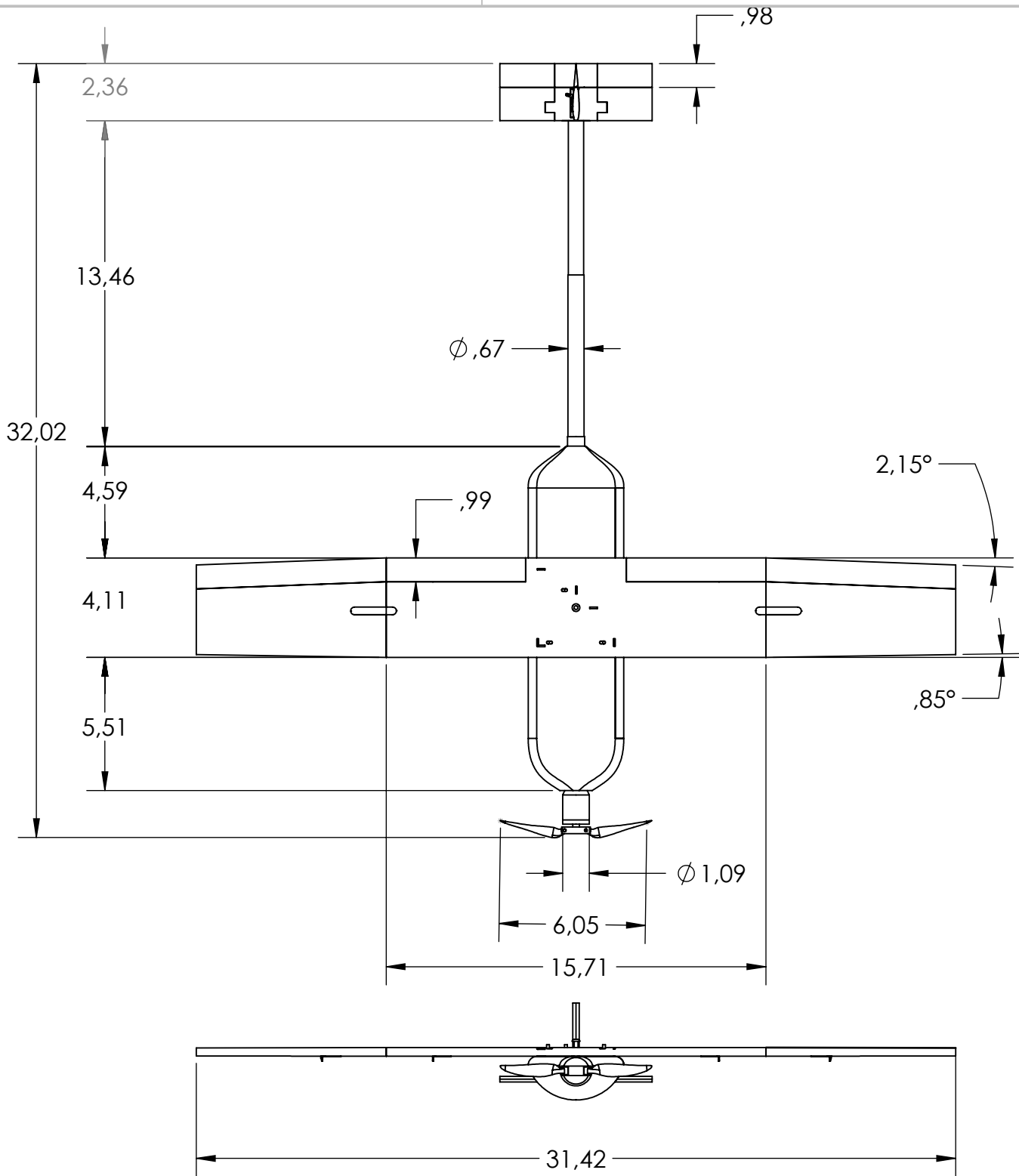
Table 16: Predicted performance for M1, M2 and M3 of final aircraft design

	M1	M2	M3
Carried Pucks	0	3	3
Weight [*lbs*]	1.83	3.09	3.09
Tube Weight Straight speed [*ft*/*s*]	78	98	78
Turn speed [*ft*/*s*]	61	81.86	61
Turn radius [*ft*]	59	70.44	59
Lap time [*s*]	38	30	38
Number of Laps	3	3	7
Max Current [*A*]	24.2	24.2	24.2
Battery charge left [%]	61.34	52.78	26.31
Best team	/	12.5	37.5
Mission score	1	0.284	2.56
Tube Weight [*lbs*]	0.55		
RAC	79.97		
TMS/RAC	0.048		

5.6 Drawing package

Drawing package includes: 3-view drawing, structural arrangement drawing, systems layout drawing, payload accommodation drawing and stowed arrangement drawing.

,98

2,36

13,46

Ø ,67

32,02

4,59

2,15°

,99

4,11

,85°

5,51

Ø 1,09

6,05

15,71

31,42

4,01

1,80

3,29

38

No.	PART	MATERIAL	QTY
1	Hull	Carbon fiber	1
2	Hatch	Carbon fiber	1
3	Middle wing	Styrodur + Carbon fiber	1
4	Right wingtip	Styrodur + Carbon fiber	1
5	Left wingtip	Styrodur + Carbon fiber	1
6	Fixed boom	Carbon fiber	1
7	Retractable boom 1	Carbon fiber	1
8	Retractable boom 2	Carbon fiber	1
9	Middle elevetor	Depron + Carbon fiber	1
10	Left elevator	Depron + Carbon fiber	1
11	Right elevator	Depron + Carbon fiber	1
12	Rudder	Depron + Carbon fiber	1
13	Former rear	Carbon fiber	1
14	Former middle 1	Carbon fiber	1
15	Former middle 2	Carbon fiber	1
16	Former front	Carbon fiber	1
17	Hinge 1	Carbon fiber	2
18	Hinge 2	Carbon fiber	2
19	Wing jig	Carbon fiber	4
20	Positioning pin	Carbon fiber	1
21	Canapy lock	/	5

DETAIL A
SCALE 2 : 5

DETAIL C
SCALE 2 : 5

DETAIL B
SCALE 2 : 5

TITLE:
Structural arrangement

SIZE DWG. NO.
B DBF 2017 - 2

SCALE 1:5

No.	Qty.	PART	DESCRIPTION
1	1	Motor	Hacker A20-8XL
2	1	Propeller	Folding 8x7
3	1	Controller	YGE brushless
4	10	Propulsion battery	1600 NiMh XCell
5	1	Reciver battery	6x120mAh
6	2	Flaperon servo	Dymond D47 s
7	2	Aileron servo	Dymond D47 s
8	1	Reciever	Spektrum AR8000
9	1	Satellite reciever	Spektrum AR8000 - sattelite reciever
10	1	Elevator servo	Dymond D47 s
11	1	Rudder servo	Dymond D47 s

DETAIL A
SCALE 2 : 5

DETAIL B
SCALE 2 : 5

UNLESS OTHERWISE SPECIFIED:

DIMENSIONS ARE IN INCHES
TOLERANCES:
FRACTIONAL ±
ANGULAR: BEND ± .05
TWO PLACE DECIMAL ±.030
THREE PLACE DECIMAL ±.005

	NAME	DATE
DRAWN	I. BANFI	2.17.2017
CHECKED	V. ŠAJN	2.21.2017

TITLE:

Systems layout

UNIVERSITY OF LJUBLJANA
FACULTY OF MECHANICAL ENGINEERING
Edvard Rusjan Slovenian Team

SIZE: B

DWG. NO.
DBF 2017 - 3

SCALE 1:5

40

PUCK
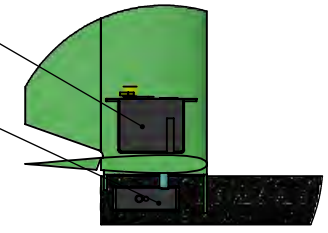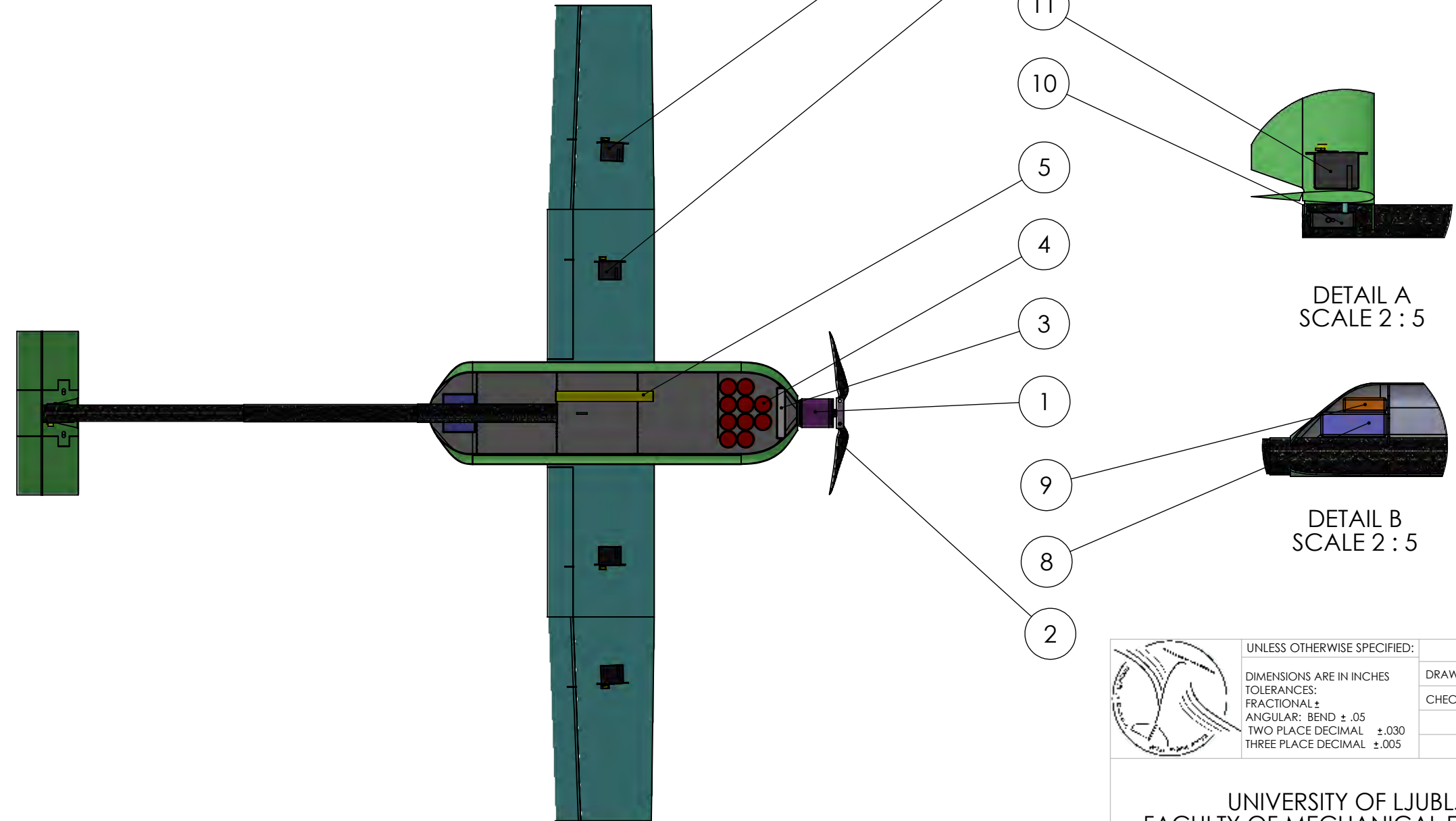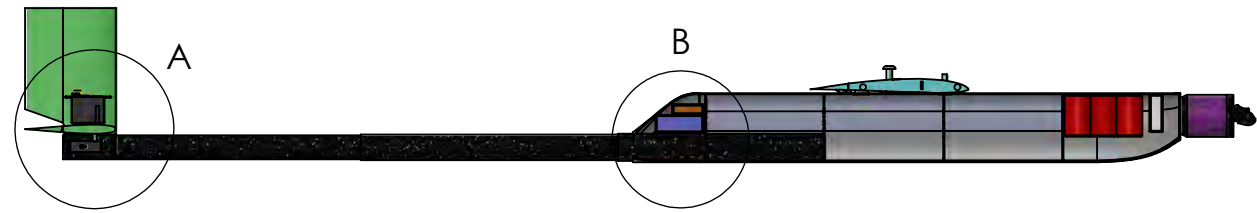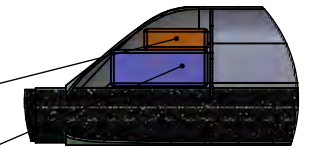
SCALE 1:2

B

SCALE 1:5

HATCH

PUCKS

1,00

$\varnothing$ 3,00

UNLESS OTHERWISE SPECIFIED:		NAME	DATE		
DIMENSIONS ARE IN INCHES TOLERANCES: FRACTIONAL± ANGULAR: BEND ± .05 TWO PLACE DECIMAL ±.030 THREE PLACE DECIMAL ±.005	DRAWN	I. BANFI	2.17.2017	TITLE:	
	CHECKED	V. ŠAJN	2.21.2017		

UNIVERSITY OF LJUBLJANA
FACULTY OF MECHANICAL ENGINEERING
Edvard Rusjan Slovenian Team

TITLE:
Payload accommodation

SIZE B DWG. NO. DBF 2017 - 4

SCALE 1:5

B

STOWED ARRANGEMENT

SCALE 1:5

⌀ 4,72

19,72
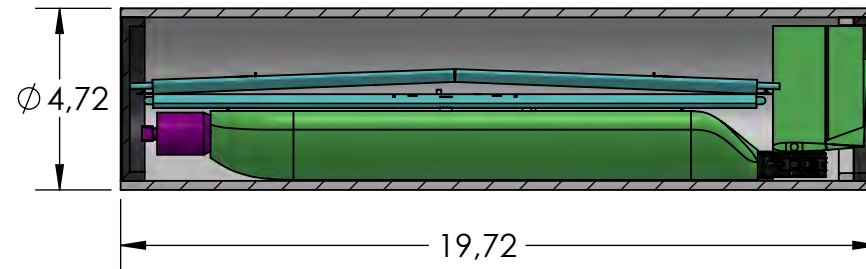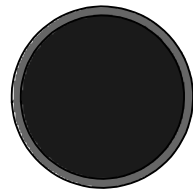
TRANSITION TO FLIGHT CONDITION

SCALE 1:10

A
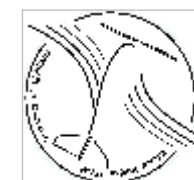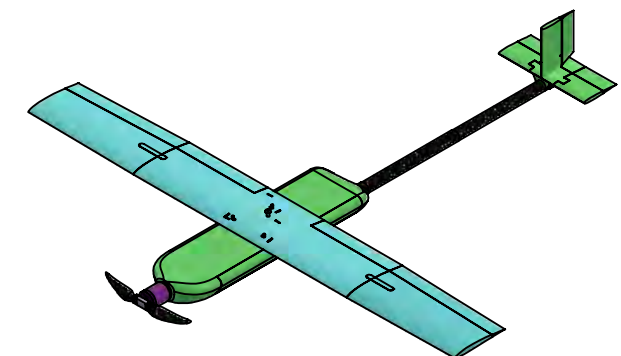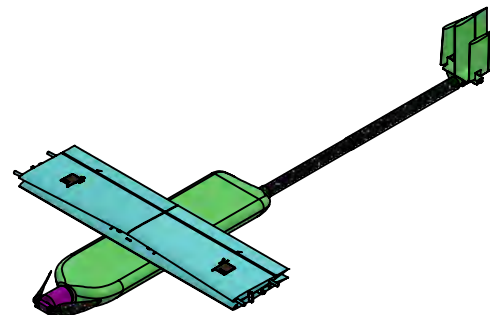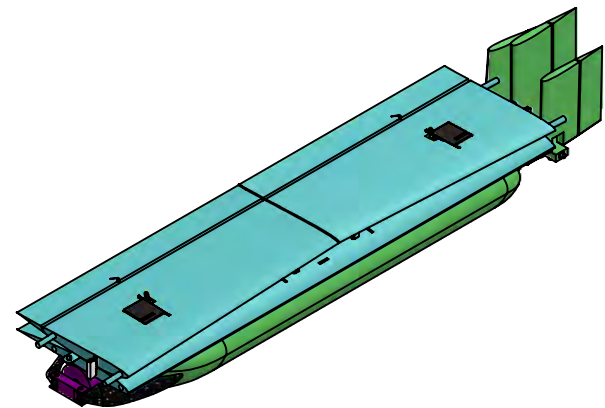
UNLESS OTHERWISE SPECIFIED:		NAME	DATE
DIMENSIONS ARE IN INCHES TOLERANCES: FRACTIONAL± ANGULAR: BEND ± .05 TWO PLACE DECIMAL ±.030 THREE PLACE DECIMAL ±.005	DRAWN	I. BANFI	17.2.2017
	CHECKED	V. ŠAJN	21.2.2017

TITLE:

Stowed arrangement

UNIVERSITY OF LJUBLJANA
FACULTY OF MECHANICAL ENGINEERING
Edvard Rusjan Slovenian Team

SIZE	DWG. NO.
B	DBF 2017 - 5

6. Manufacturing plan and processes

The final goal was to build a competitive aircraft which would be lightweight, easy to manufacture and cost efficient as financial resources were limited. All of the above were achieved by considering several manufacturing processes and materials.

6.1 Investigated manufacturing processes

Selection of the best manufacturing method was carried out by evaluating different methods by Figures of Merit (FoM) which were weighted with values 0, 1, 2. Additionally score of each FoM was multiplied by values of importance (1 - 5). Figures of Merit were: weight, size, manufacturability, reparability and cost.

Weight of the aircraft was key factor in our manufacturing process, since it increased RAC and decreased maximal speed. Because of its major negative impact on scoring it was weighted with an importance factor of 5. Second considered factor was **size** of the model. Size FoM was valued as 4 because of its important impact on RAC. **Manufacturability** factor was concerned mostly with time required to produce the aircraft and team's experience with the technique. Several aircraft were planned to be built and short time period had to be considered when choosing manufacturing process. Team's experience with certain method directly influences the quality of the aircraft. Manufacturability was assigned the value of 2. **Cost** of required manufacturing materials was also considered, as team had limited resources. A value of importance of 2 was given to that FoM.

It should be pointed out, that testing aircraft were built by different manufacturing methods than the competition aircraft. The reasons lie in cost and manufacturability.

6.1.1 Evaluation

- *Foam model*: One of evaluated manufacturing processes was foam construction technique. It was favored when considering weight, because of foam's low density. The technique also offers simple, straight forward manufacture and most of the manufacturing team was already familiar with this method. However this technique would produce larger aircraft, due to low elastic modulus of the foam. The necessary materials for manufacture were also not obtainable from our sponsors so price FoM was considered low.

- *Balsa construction*: Constructing the airplane from balsa wood and covering it with foil was considered. This method has advantages when considering weight and size. It was however handicapped mainly in manufacturing because construction was considered time consuming and the team was not familiar with it. Price of balsa construction is high and team's sponsors could not provide the necessary materials.

- *Sandwich structure*: Sandwich-structure composite with foam filling and carbon fiber skin was one of proposed methods. This method allowed construction of small lightweight aircraft. A great part of manufacturing team was already familiar with the process and needed materials were provided by sponsors. On the other side such technique rises the level of possible errors in manufacture.

- *Molded composite materials*: This method could produce a small, lightweight and rigid aircraft, consisting of carbon fibers and a matrix. However the manufacturing process would be time consuming and the aircraft would be harder to repair. Costs of this method were high, since necessary molds needed to be bought or constructed and the smallest alteration of the design would require an entirely different mold.

Objective evaluation of presented methods is visible in Table 17. Sandwich structure is selected for the best manufacturing method.

Table 17: Manufacturing methods Figure of Merit

Figure of Merit	Value of Importance	Foam	Balsa	Sandwich	Composite
Weight	5	2	2	2	2
Size	4	0	2	2	2
Manufacturability	2	2	1	1	0
Cost	2	0	0	2	0
Total	/	14	20	24	18

6.2 Manufacturing processes selected

Several different approaches were used in order to produce a quality aircraft.

- 3D printing: Tube caps were 3D printed.

- Lightening holes: Wherever possible, unnecessary material was removed. Holes in fuselage formers reduced overall weight but did not compromise safety of the aircraft.

- Hot wire cutting: Wings were cut with hot wire technique.

- Lamination: Lamination was used to construct a sandwich-structure overlay. The method was used on wings, fuselage and emmpennage. Several layers of carbon fiber in $[-45°, +45°]$ orientation assured the necessary rigidity of object. Additional layers of carbon fiber were added in places of critical stresses.

- CNC cutting: More complex pieces such as parts of rotational mechanism, fuselage formers and airfoil shape guides were cut by CNC machine. This assured the necessary precision.

Figure 28: An example of lamination of the wing

6.3   Manufacturing plan

Manufacturing schedule and milestones are shown in Figure 29.

Year 2016/17		January	Februar	March
	Deadline			
Prototype with mechanism				
CNC Foam Core Cutting	Planned			
	Real			
Lamination of Parts	Planned			
	Real			
Cutting and Finishing Laminated Parts	Planned			
	Real			
Making of Mechanisms	Planned			
	Real			
Assembly of Aircraft	Planned			
	Real			
Inserting Servos, Motor etc.	Planned			
	Real			
Final Plane				
CNC Foam Core Cutting	Planned			
	Real			
Lamination of Parts	Planned			
	Real			
Cutting and Finishing Laminated Parts	Planned			
	Real			
Making of Mechanisms	Planned			
	Real			
Assembly of Aircraft	Planned			
	Real			
Inserting Servos, Motor etc.	Planned			
	Real			

Current Date

Figure 29: Manufacturing timeline

7. Testing plan

In order to achieve maximum score, testing of the key components is crucial to success. It enables the team to compare theoretical predictions with real life situations. The strong point of testing is the fact, that it quickly points out possible errors in decision making regarding all kinds of aircraft components. Therefore team proposed detailed and extensive testing objectives followed by a tight schedule.

7.1 Schedule

The testing was divided in three main categories: subsystem testing, testing of prototype with mechanism and final aircraft testing. In order to test all of the above a schedule seen in Figure 30 was proposed.

Figure 30: Testing Schedule

7.2 Detail testing objectives

There were two reasons for running various tests. The purpose of the initial tests was to improve accuracy of the simulation and further testing was then conducted regarding the actual aircraft prototype and final design.

7.2.1 Initial throwing velocity test

Since the aircraft will be hand launched, we needed to determine the approximate velocity with which we can initially propel the aircraft. The test was carried out by picking several team members and have them throw an improvised aircraft of mass similar to the one of final aircraft. Based on measured data approximate initial velocity was calculated.

7.2.2 Propulsion testing

Battery testing was conducted to get proper characteristics of batteries, use the results to improve simulation outcome and choose the best propulsion configuration, as propulsion team believed that NiMH batteries represents the major constraint on the propulsion performance. The aim was to get actual capacity, its internal resistance, precise times of battery discharge at different currents and maximal momentary power output of chosen batteries. Based on the obtained battery characteristics propulsion team was able to find optimal propulsion configuration for the aircraft. On top of that score analysis simulation also required maximum discharge current that batteries can withstand.

Motor and propeller testing Chosen propulsion configuration described in 5.3.3 was tested in the final test flights in order to determine its actual performance. At that point the team was not exactly determined about propeller type so the test were conducted with 8x7 and 8x6 respectively.

7.2.3 Flight testing

Initial flight tests were performed in order to achieve more accurate simulation outcome. SAS lacked actual maximum velocity - mass relationship at the same power output of the motor. At this stage the actual configuration of the plane wasn't chosen yet, therefore tests were performed on a rapid prototyped aircraft with 3D printed fuselage and balsa wing.

Further flight tests were carried out on current configuration of the plane. The main foci here were to compare theoretical results of the simulation to the real life situation, validate the selection of the correct propulsion system and check the structural integrity of aircraft folding mechanisms.

Table 18 includes all flight tests performed and their goals. Note that "prototype 1" is the rapid prototyped aircraft and "prototype 2" is the final prototype containing folding mechanisms, final propulsion system and holds the shape of final aircraft.

Table 18: Order and goals of performed test flights

Flight Test	Aircraft	Goal
1	prototype 1	velocity - mass relationship
		battery consumption
2	prototype 1	velocity - mass relationship
		battery consumption
3	prototype 2	validation and comparison of simulation outcome - mission runs
		validation of propulsion system
4	prototype 2	validation of mechanisms' structural integrity
		Directional flight stability
5	final aircraft	mission runs
6	final aircraft	mission runs

7.2.4 Structural testing

Structural tests were conducted in order to assure structural integrity of the aircraft during flight and ground missions.

Wing bending test was carried out to simulate wing tip test. The wing was fixed at wing tips and load was placed in the middle. If the failure stress was considered high enough for the plane to be viable the test was successful.

Tube test: One of the main objectives of the ground mission was to test structural strength of the tube containing the aircraft. Due to tight education and testing schedules of team members the tube test has not been carried out yet. However to assure tube and aircraft configuration will pass the ground mission, drop test is going to be performed under the conditions described in the mission details (one flat drop and 2 side drops from 12 inches). The test is going to be rendered successful, if the tube and the aircraft remain undamaged.

To be on the safe side, team managed to simulate the drop test in the SolidWorks environment. The results can be seen in Figure 19.

7.3   Check list

Table 19: Pre flight checklist table

General system check

Structural integrity	Wings locked?	Tail locked?	Propeller secured?	Throttle down?	Data system on?	Runaway clear?	Batteries filled?

Payload

Laterally secured	Connections secure?	Battery pack?	Receiver pack?	Payload secure?	Attachment secure?	Pins locked?	Payload secure?

Control surfaces

Ailerons		Rudder	Elevator	Flaps
Defects?	Glued?	Defects? Glued?	Defects?	Glued?

Electronics and propulsion

Receiver battery charged?	Primary battery charged?	Receiver/ transmitter ok?	Wires secure?	Battery hot?	Prop secure?	Prop direction?

Weather

Speed		Angle	Temperature

Initials for approval

Chief engineer	Pilot	Advisor

8. Performance results

8.1 Demonstrated performance of key subsystems

8.1.1 Initial throwing velocity test

Initial throwing velocity was determined using speed camera. Each throw was recorded and then analyzed frame by frame to obtain initial velocity of the improvised aircraft. Results showed that the strongest team member threw the aircraft of mass equal to 3,30 lbs with initial velocity of 49.21 ft/s. By taking into the account the static thrust of the aircraft, the team concluded that 80% of maximal measured initial velocity was enough for the aircraft to take off without any problems.

Figure 31: an example of the strongest team member throwing improvised aircraft

8.1.2 Propulsion testing

Battery testing: In order to better understand the capabilities of NiMH cells that are going to be used in the competition, several discharge cycles were preformed on single cells while measuring voltage and current. Measurements were made with a custom electronic circuit (Figure 32 consisting of a current shunt resistor, a simple amplifier, an Arduino Uno, running custom code preforming analog to digital conversion, some basic calculations and communication to a PC and an array of resistors as a variable load as shown in figure below.
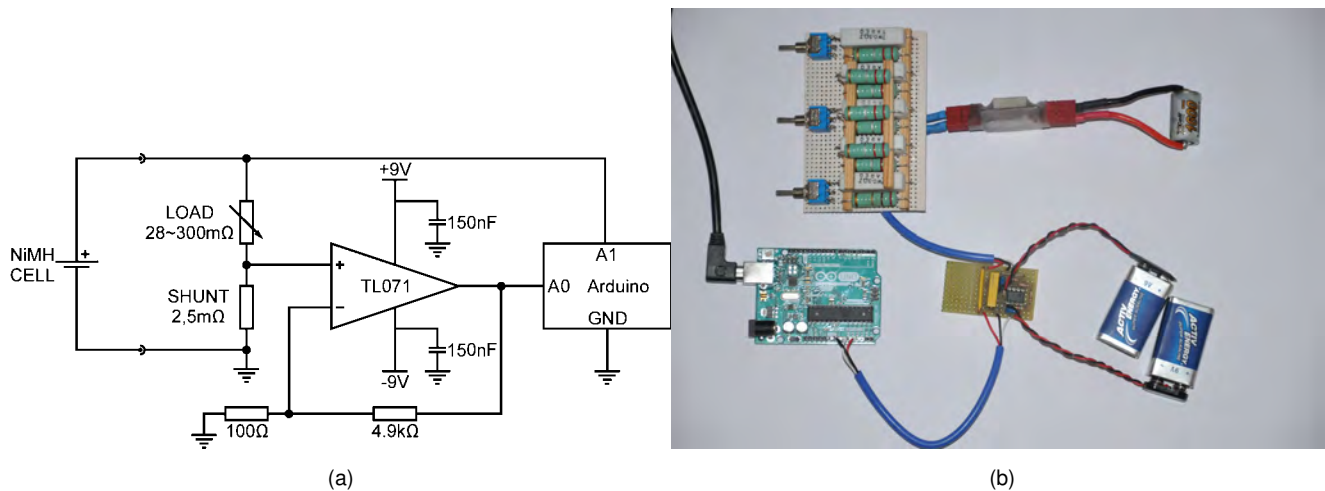
Figure 32: Electric circuit

Simulation showed that 1600 mAh batteries were the most promising, so therefore extensive tests were performed on them. Based on previous competitions the team decided to use XCell NiMH batteries. Initial experiment included testing of its actual capacity. Before each discharge cycle a cell was charged with a current of 1,6A or 1C. Discharge cycles were preformed at different constant resistance loads (0.3 Ω, 0.22 Ω, 0.15 Ω, 0.1 Ω, 0.073 Ω, 0.55 Ω and 0.032 Ω) simulating a constant throttle scenario. Discharge cycles were terminated when cell voltage dropped under 0,88V in order to prevent over discharge. Measured data was then used to calculate battery capacity through approximation by the least square method using derived equation 9. Figure 33 shows approximated relation between time of discharge and average current.
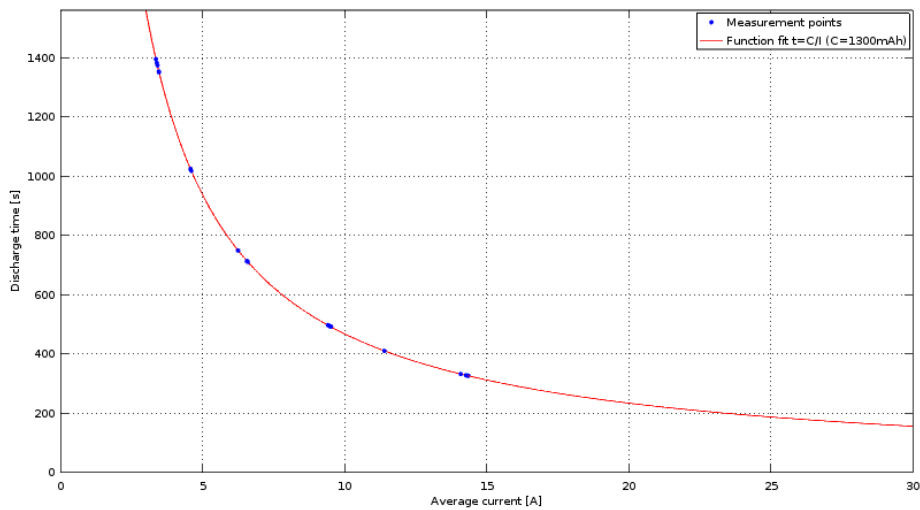

Figure 33: Relationship between time of discharge and average current

$$C = \frac{\sum i \frac{t_i}{I_{i,avg}}}{\sum i \frac{1}{I_{i,avg}^2}} \qquad (9)$$

Results showed that discharge capacity of each battery cell equals to roughly 1300 mAh, although they were properly charged to 1600 mAh. These kind of results were expected as companies tend to address higher capacity values.

Further testing was conducted to obtain actual values of battery internal resistance, unloaded voltage and consequentially maximal theoretical power output in relation to the different discharge capacities. Internal resistance was determined based on voltage and current changes at 100 mAh discharge intervals, when the load element in the circuit was switched off for five seconds and then turned back on. That way measures were taken, when there was no external load. The experiment was carried out at different loads of 0.3 Ω, 0.22 Ω, 0.15 Ω, 0.1 Ω, 0.073 Ω, 0.55 Ω and 0.032 Ω on just one battery cell wired into the electric circuit. Unloaded battery voltage at different discharge capacities was recorded as voltage right after the load was switched off. Results are shown in the Figure 34.

$$R_{int}(C_{discharge}) = \frac{\Delta V(C_{discharge})}{\Delta I(C_{discharge})} \qquad (10)$$

(a)   (b)
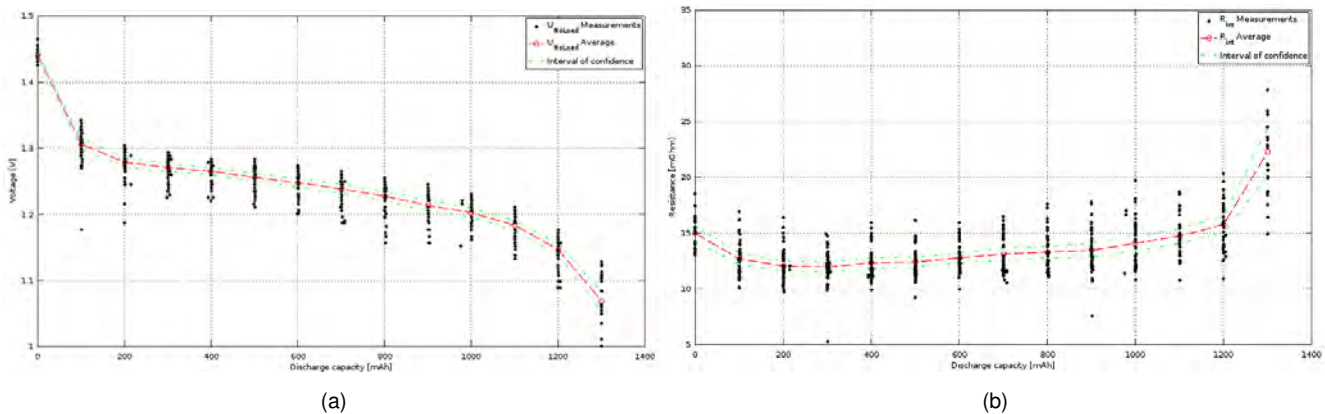
Figure 34: Voltage and Internal Resistance in relation to Discharge capacity

The reason for deviation of the collected data at each discharge capacity (black dots) lies mostly in contact resistance of connectors and load selection switches, since at low voltages (cca. 1,2V) changes in resistance of degree $10^{-3}\Omega$ can greatly impact the measured results. Another factor to consider at this point were heat losses due to increase of temperature, especially at higher currents.

Obtained voltages and internal resistances were further used to model theoretical relation between load power and load current at different discharge capacities (Equation 11 and Figure 35). This theoretical model was validated in one of the test flights. Current, voltage, discharge capacity and power were measured during flight on configuration of ten battery cells wired in series. Based on measured discharge capacity during the flight the propulsion team calculated corresponding internal resistance and voltage at no load in each time frame. By dividing Equation 11 by current team obtained Equation 12 that was used to calculate expected value of the voltage during the flight (note that n stands for number of battery cells). Figure 35 shows comparison between calculated and measured voltage values.

$$P_{Load} = U_{NoLoad} \cdot I - R_{Int} \cdot I^2 \tag{11}$$

$$U_{load,expected}(C_{discharge}) = (U_{NoLoad}(C_{discharge}) - R_{Int}(C_{discharge}) \cdot I(C_{discharge})) \cdot n \tag{12}$$
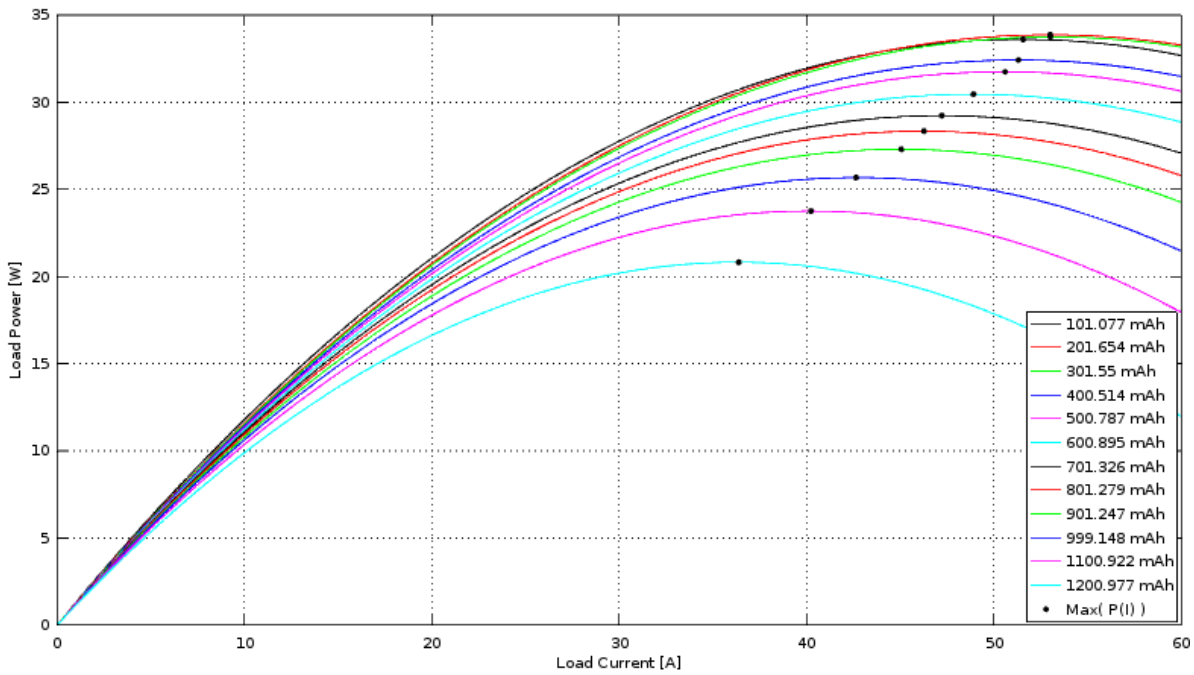

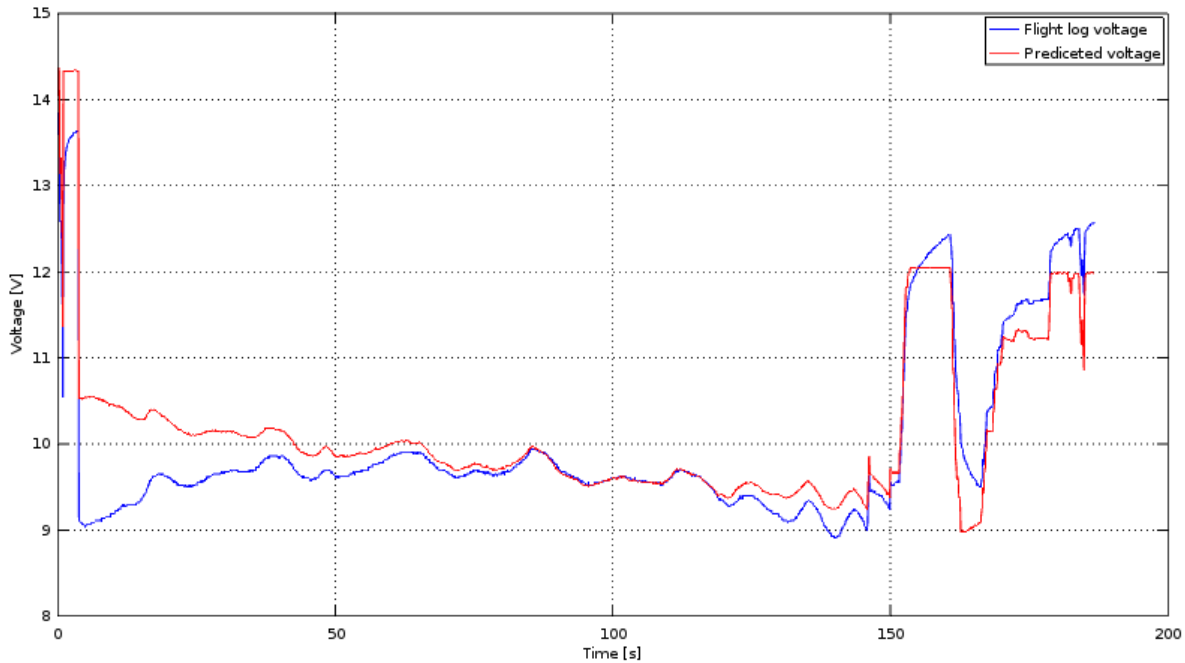Figure 35: Relation between load power and load current

Figure 36: Comparison between calculated and measured voltage values

Calculated and measured voltage curves correspond surprisingly well with each other, although there are some deviations. Initial deviation of the curves (from $t_0 = 0$ s to approximately $t_1 = 53$ s) appear due to the fact that battery cells were not warmed up before the flight, whereas lab tested cell was constantly warm. The trend of rise in temperature of battery cells can be seen as decrease in voltage difference between the curves from t_0 to t_1. Deviations appears again from approx. $t_2 = 125$ s to $t_3 = 180$ s. The reason for that lies in testing of battery's internal resistance and unloaded voltage. That test did not take into the account the way voltage varies over time (for an example at the moment the load was switched off measuring device recorded increase of voltage in the next time interval, although voltage actually increased a bit more after that moment). Considering all the deviations that were discussed the theoretical model was still confirmed as valid.

Motor and propeller testing: Propulsion configuration shown in Table 20 was tested for its actual performance. Current, power and maximal speed was measured at maximal throttle during the flight and results were compared to the ones from eCalc. Based on results seen in Table 21 and observation during the test flight, the team concluded 8x7 is the optimal propeller configuration as it best compensates the voltage drop during battery discharge.

Table 20: Tested propulsion configuration

Propulsion System Weight	Motor	Kv	ESC	Battery	Propeler
0,681 [*lb.*]	Hacker A20-8XL	1500	YGE 30	Xcell: 10x1600 *mAh*	8x6 and 8x7

Table 21: Propulsion performance results

	Propeller	Current [A]	Power [W]	Speed [ft/s]
eCalc	8x6	31,6	307	106.6
test		25,8	235	104,9
eCalc	8x7	35	337	122,2
test		29,7	270	118,5

8.1.3 Flight testing

Test of determining the dependency of the aircraft's velocity on aircraft's mass yielded results shown in Table 23. Prototype aircraft (its parameters are shown in Table 22) was loaded with different load masses and was flown five circuits containing straight lines of approximately 820 ft in length and constant radius of approximately 160 ft. Aircraft was equipped with EagleTree telemetry system with live data feed recorded at 10 Hz to get the trajectory of the flight, which was then further processed to obtain needed velocities. Current and voltage were also measured and recorded using EagleTree to obtain actual power output of the motor.

Table 22: Aircraft testing parameters

Parameter	Value
Aircraft Weight [lbs]	2.64
Wing Surface [ft^2]	3.55
Chord Length [ft]	0.64
Wingspan [ft]	5.54
Wing Aspect Ratio	8.68

Table 23: Test flight results

Measurement number	1	2	3	4	5
Number of pucks	0	1	2	3.18	4.24
Speed [ft/s]	66.43	63.15	63.77	59.43	60.33
Average Power [W]	133.5	122.2	129.3	118.0	112.5

Batteries were recharged only after third flight so therefore voltage and current needed to be normalized. Graph in Figure 37 has a falling tendency due to the voltage drop and not due to the increase of mass. Motor power

output should therefore be greater for increasing number of pucks to ensure the velocity of the aircraft increases or remains the same. C_d was calculated for each particular run (each puck configuration). The values were then used to calculate the velocities at desired power output. Calculations of C_d and velocities are done by using Equation 13 and 14 (Note that n represents number of pucks). That way velocity - number of pucks relation was obtained.

$$C_{d,run} = \frac{P_{run}}{\frac{1}{2} \cdot A \cdot \rho \cdot v^3} \tag{13}$$

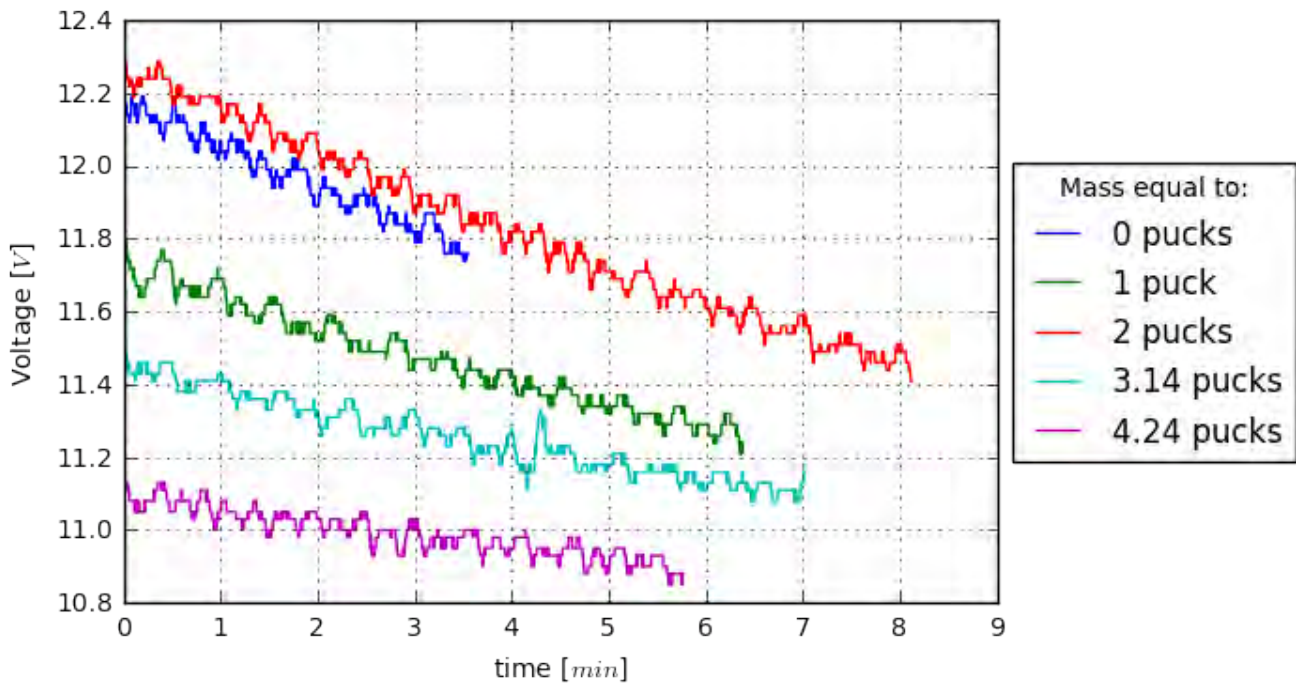$$v(n) = \sqrt[3]{\frac{P_{desired}}{\frac{1}{2} \cdot \rho \cdot A \cdot C_d(n)}} \tag{14}$$

Figure 37: $V(t)$ relationship for all five runs

(a)   (b)
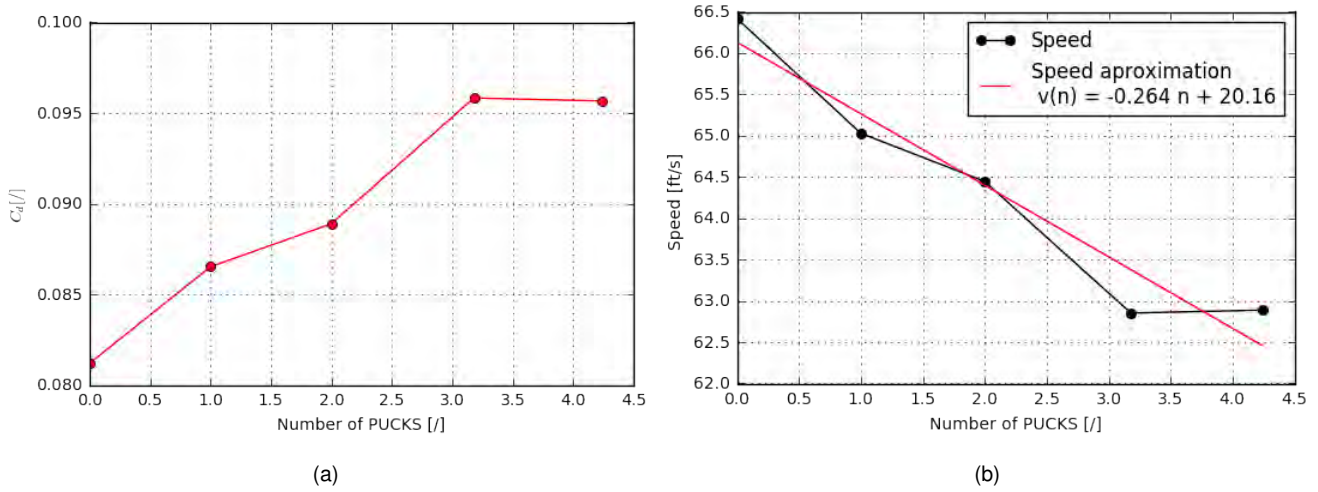
Figure 38: C_d and speed in relation to number of pucks at $P_{desired} = 133.5\,W$

The relation needed to be included to the score analysis simulation indirectly as polar of the flight, so therefore C_l was calculated for each mass by Equation 15. The $C_d - C_l$ relationship is shown in Figure 39.

$$C_l = \frac{(m_{plane} + n \cdot m_{paka}) \cdot g}{\frac{1}{2} \cdot \rho \cdot A \cdot v^2}$$
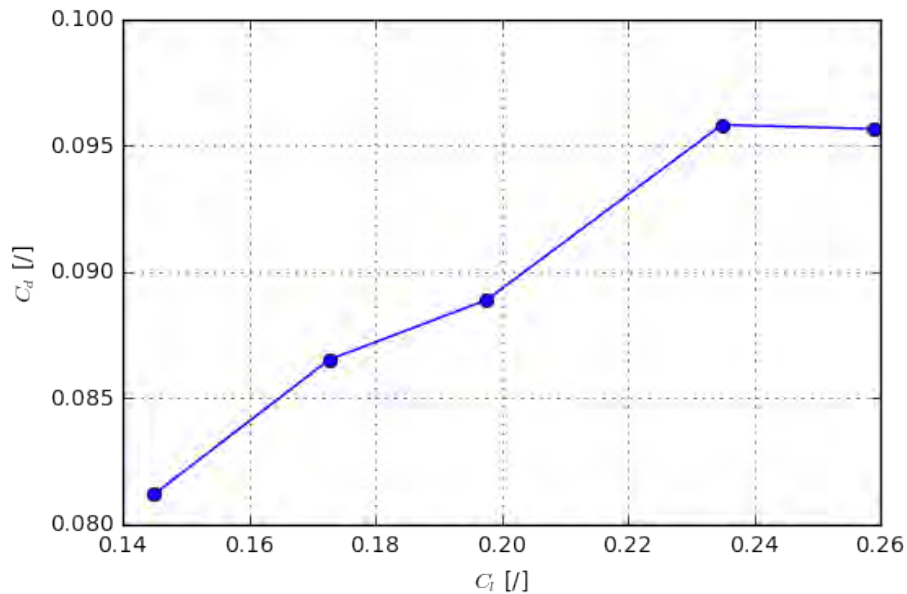
(15)

Figure 39: Relationship between C_d and C_l

There were several factors which may affect the results. First factor was the propulsion which performed badly because of weak electric motor. With increasing mass, the needed lift force increased as well and since the aircraft was flown at maximal power, increasing lift coefficient was the only way to provide enough lift force. By doing that the angle of attack starts to rapidly increase. Increase in mass causes greater wing loading. Thus the aircraft's minimal velocity increases to sustain flight. This issue could be improved by choosing a more powerful propulsion configuration as the mass increase would have a smaller impact on aircraft's velocity. That way more data could be sampled leading to more precise and accurate results. Second factor is the aircraft's trajectory which was not a straight line at constant height. Third factor are the aircraft's dimensions and parameters (aspect ratio, wing loading and span, fuselage, envelope etc.) which differ from the team's final aircraft design. That means the polars of the flight are slightly different which affects maximal velocity of the aircraft in its equilibrium state at each mass change. Fourth factor are flight conditions in which the test was carried out. Wind is a variable that cannot be controlled thus it causes noise on measured data.. Lastly the fifth factor could also be systematic errors of measurement devices, especially standard GPS+EGNOS which tracked aircraft location and velocity. These could be improved by using RTK GPS system or Pitot tube (for velocity measurements).

8.1.4 Structural testing

Wing test: Wing tip test was conducted by placing nine pucks on the middle of the wing and measuring its maximal deflection. Supports are placed 31.5" apart as this was the final wingspan of the aircraft design. Nine pucks equal to 3.38 lbs and since the final aircraft design with included payload weighs 2.58 lbs the team concluded the aircraft is going to pass the wing tip test without any issues.

Figure 40: Wing tip test

8.2   Performance demonstration of the complete airplane

There were three aims in the last three flight tests: *checking structural integrity of mechanisms, finding minimal possible wing loading with which the pilot is still able to fly, actual mission performance.* Final aircraft design was equipped with EagleTree telemetry system with live data feed recorded at 10 Hz. Current and voltage were also measured and recorded using EagleTree which enabled the team to study possible errors in greater details.

The final aircraft initially contained wings with wingspan of 41.5". After 6 standard laps described in 4, the pilot assessed aircraft's control. Wingspan was then reduced by 1" after each flight run until aircraft's control became unmanageable. Based on his current skills the pilot concluded the final wingspan to be 31.5". Although SAS showed 19.69" to be optimal wingspan size, final wingspan was increased to 31.5". The pilot however is extremely motivated to improve his flying skills. Wingspan of the final aircraft may therefore also be reduced before the actual competition takes place, since according to sensitivity parameter analysis described in 4.1 it is the most influential factor in maximizing final score. During the same test flights structural integrity of mechanisms was also confirmed as there were no observed issues.

After determining the wingspan, mission performance of the final aircraft design was tested. The main information the team wanted to get from the tests were times of M2 and M3 along with transition time of the aircraft to the flight condition. M2 and M3 results are shown and compared to predicted values in Table 24. Aircraft's transition time was measured to be 52 seconds which satisfies mission requirements.

Table 24: Comparison between predicted and average actual aircraft performance

	Lap Time [s]		$360°$ Turn [s]		Laps Flown		Straight Speed [ft/s]		Turn Speed [ft/s]		Battery Charge Left [%]	
	Pred.	Act.	Pred.	Act.	Pred.	Act.	Pred.	Act.	Pred.	Act.	Pred.	Act.
M2	32.81	33.56	5.41	5.81	3	7	108.24	107.95	81.86	79.74	52.8	48.2
M3	40.15	42.15	5.41	6.32	3	7	81.99	80.04	81.86	79.05	26.3	20.7

The results shown in Table 24 deviate from the predicted values because of several reasons. The main factor affecting results was the total drag of the aircraft which was greater than specified in Section 4.4.3, due to manufacturing constrains. It was nearly impossible to reach precise relative angles of attack between the wing and empennage, which certainly caused additional drag, resulting into greater power consumption. There are additional reasons for deviation of actual times of $360°$ and $180°$ turns from predicted times. The pilot had difficulties keeping constant turn radius in M2 and M3. He also tended to slow down before turning although the aircraft was capable initiating the turn with its maximal speed. Another factor causing the deviation is the aircraft's turn

model in SAS, which was simplified to be executed at constant speed. Speed was therefore not modelled as continuous function but rather as two discrete values as seen in Figure 17. SAS also neglects altitude changes during the flights which caused even greater deviations in M2 and M3 lap times. Another factor are weather conditions. Wind speed and temperature have a major impact on aircraft aerodynamics in terms of angles of attack and air density [2] . Lastly systematic errors of measurement devices could also cause distortion in data sampling.

SAS was found to be a sufficient model especially in analysing and predicting maximal and minimal speed of the aircraft. Actual aircraft performance exceeded initial expectations, however there is still room for improvements. Beside the wingspan, tail volume coefficient and steering surfaces could be further optimized. The team also pointed out concerns about aircraft's landing. Rough landing field could severely damage the aircraft without landing gear. Therefore fuselage bottom will possibly be reinforced with aramid fibers in order to sustain the wear.

Overall the team is extremely satisfied with the work invested into the process that led to final aircraft design and is confident that the aircraft will perform well when the competition takes place.

Figure 41: Prototype during the flight

9. References

[1] Phillips, W. F., *Mechanics of flight*, John Wiley & Sons, 1st ed., 2010.

[2] Anderson, Jr., J. D., *Fundamentals of Aerodynamics*, McGraw-Hill, 5th ed., 2011.

13 March 2017

American Institute of Aeronautics and Astronautics
1801 Alexander Bell Drive
Suite 500
Reston, VA 20191
703-264-7536

Mr. Meltem Şahin:

This letter recognizes that the team from University of Turkish Aeronautical Association has successfully completed their entry form for the 2017 AIAA Foundation/Cessna/Raytheon Student Design/Build/Fly competition and passed the Proposal phase of the competition.

As such, the team qualifies to participate in the Design Report phase of the competition. If the report is submitted in the required format by the specified submission date, you will be allowed to bring your aircraft and compete in the contest fly-off weekend. Teams who do not complete and submit the Design Report as required will not be allowed to compete at the fly off.

This important event offers the opportunity for yourself and the listed competing team members to demonstrate the performance of their aircraft design and to participate in formal and informal technical interchange with members of the other competing teams. The event is scheduled to be in **Tucson, AZ, USA from 20-23 April 2017**.

We look forward to your team meeting all the contest requirements and competing in the fly-off in Tucson.

Please note that it is your responsibility to share this letter with team members for the purposes of obtaining a visa, if necessary.

Members of the University of Turkish Aeronautical Association Team

Anıl Ali Yalçın
Serdar Artun
Köksal Mert Danışan
Meltem Şahin
Süleyman Murat Köroğlu
Damla Durmuş
Furkan Burak Arslan
Gürkan Sertsoy
Mehmet Selman Okal
Uğur Mermer
Gialtsin Nteli Chousein Tsolak
İbrahim Can Özcan
Seda Namal
Mehmet Yasin Danış
Ayce Dilara Koçak
Nagehan Önder
Emre Zengin
Arif Can Başıbüyük
Burak Dündar
Mehmet Ekim
Ege Konuk

Sincerely,

 Russ Althof for DBF Organizing Committee and

 Karen Thomas – Managing Director, Member Services